Tectonic evolution of Tian Shan and Kunlun Shan belts constrained by magnetostratigraphic and thermochronologic analyses

Wei Yang

THÈSE / UNIVERSITÉ DE RENNES 1
sous le sceau de l'Université Européenne de Bretagne

En Cotutelle Internationale avec
L' Université de Pékin, Chine

pour le grade de

DOCTEUR DE L'UNIVERSITÉ DE RENNES 1

Mention : Sciences de la Terre

Ecole doctorale Scicences de la Matière Rennes

présentée par

Wei YANG

Préparée à l'unité de recherche 6118 CNRS-
Géosciences Rennes
Observatories des Sciences de l'Univers de Rennes (OSUR)

L'évolution tectonique des chaines du Tian Shan et Kunlun Shan occidentale contrainte par analyses magnéto-stratigraphiques et thermochonologiques

Thèse soutenue à Rennes
le 2 juin 2014

devant le jury composé de :

Yan CHEN
Professeur à l'Université d'Orléans / *rapporteur*

Johan De Grave
Professeur Ghent University / *rapporteur*

Jean-Noël PROUST
Directeur de recherche CNRS – Université de Rennes 1 / *examinateur*

Laurie BARRIER
Maitresse de conférence à l'Université Paris 7 - IPGP / *examinatrice*

Guillaume DUPONT-NIVET
Chargé de recherche CNRS – Université de Rennes 1 / *directeur de thèse*

Marc JOLIVET
Chargé de recherche CNRS – Université de Rennes 1 / *co-directeur de thèse*

Résumé

Le Tian Shan constituant une partie importante de la Ceinture Orogénique d'Asie Centrale (Central Asian Orogenic Belt) - une des plus grandes et persistante orogènes d'accrétion Phanérozoïque dans le monde - mérite une attention particulière de la communauté des sciences de la Terre. La plupart des études précédentes impliquant le Tian Shan ont porté soit sur les accrétions Paléozoïque soit sur l'orogenèse intracontinentales à la fin du Cénozoïque. Il en résulte la nécessité urgente, adressée dans cette thèse, de contraindre l'évolution tectonique entre le Mésozoïque et le Cénozoïque précoce afin de comprendre le couplage entre la chaine et les bassins d'avant-pays du Tian Shan et des régions adjacentes. L'excellente conservation des séquences sédimentaires du Mésozoïque au Cénozoïque précoce dans les piémonts du Tian Shan est la garantie d'un laboratoire idéal pour comprendre les relations entre l'évolution de la chaine et les bassins d'avant-pays durant la période ciblée. Ce travail suit les réalisations exceptionnelles publiées récemment à propos des piémonts du Tian Shan (par exemple la Thèse de Gloria Heilbronn, Université de Rennes 1, 2014) en utilisant la sédimentologie, la thermochronologie, les méthodes magnétostratigraphiques, paléontologiques et paléoécologiques qui ont révélé les questions en suspens qui restent à résoudre. Deux questions scientifiques critiques sont adressées dans cette thèse présentées comme suit. (1) L'évolution mésozoïque du bassin d'avant-pays dans les piémonts nord et sud du Tian Shan. (2) L'évolution au Cénozoïque précoce du soulèvement du Tian Shan. Comme indiqué dans les chapitres suivants de cette thèse, ce travail fournit des informations détaillées sur l'évolution tectonique mésozoïque à cénozoïque et les relations entre les bassin d'avant-pays préservés dans les piémonts du Tian Shan, en utilisant la magnétostratigraphie, les analyses géochronologiques U-Pb sur zircons détritiques et trace de fission sur apatites détritiques. Ceci à la fois dans les piémonts du nord Tian Shan (région de Manasi) et dans les piémonts du sud Tian Shan (région d'Ulugqat),

qui constituent des laboratoires idéaux encore mal contraints qui seront comparées aux enregistrements existants dans les sous-bassins adjacents .

Dans le chapitre 1, l'évolution du nord Tian Shan est étudiée par datation U/Pb (LA-ICP-MS) de zircons détritiques sur 14 échantillons de grès d'une série continue d'âge fin Paléozoïque à Quaternaire dans la marge sud du bassin de Junggar (région de Manasi). L'objectif est de suivre les changements dans la provenance des sédiments à travers le temps et de corréler ces changements avec les phases tectoniques majeures de la chaine. Les échantillons ont été systématiquement recueillis le long de deux sections sédimentaires voisines du bassin d'avant-pays. Les résultats montrent que les zircons détritiques sont pour la plupart d'origine magmatique, avec une légère influence de zircons métamorphiques. Les âges U-Pb de zircons détritiques varient considérablement entre 127 et 2856 Ma et peuvent être divisés en quatre groupes principaux: 127-197 Ma (sous-pics à 159 Ma) , 250-379 Ma (sous-pics à 318 Ma) , 381-538 Ma (sous-pic à 406 Ma) et de 543 à 2856 Ma (sous-pic à 912 Ma) . Ces groupes indiquent que les zircons ont été en grande partie tirés de la zone du Tian Shan plus au sud depuis une initiation du bassin au Carbonifère. Les variations de provenance indiquent que le l'évolution de la chaine avec la marge sud du bassin de Junggar peut généralement être divisé en quatre étapes : (1) Fin Carbonifère - Trias évolution du bassin dans un contexte d'extension en demi-graben ou post- orogénique; (2) Du Trias moyen au Jurassique supérieur, le sud de Junggar est devenu un bassin subsidant passivement jusqu'à ce que (3) il soit inversée au cours du Crétacé inférieur - Paléogène ; (4) Au cours du Néogène , le piémont développé le long de la marge nord du bloc Nord Tian Shan Nord et le bassin de Junggar est devenu un véritable bassin d'avant-pays.

Dans le chapitre 2, l'évolution encore mal contrainte entre le Mésozoïque et le début du Cénozoïque de la marge sud-ouest du Tian Shan est étudiée en utilisant les datations U/Pb (LA- ICP-MS) sur zircons détritiques et les traces de fission sur

apatites détritiques. Les changements dans la provenance des sédiments à travers le temps sont obtenus à partir des séries Jurassique à Cénozoïque exceptionnellement bien exposées dans la zone d'Ulugqat. Les âges U/Pb sur zircons détritiques varient considérablement de 222 à 3179 Ma et peuvent être statistiquement séparés en quatre groupes principaux : 240-320 Ma, 400-540 Ma, Ma 550-1600 et 1640-2800 Ma. Ces zircons sont issus de la région Tian Shan plus au nord et du recyclage de la marge paléozoïque Nord Tarim. Les âges des traces de fission sur apatites détritiques incluent des sources dont l'âge mésozoïque a été conservé ainsi que des sources beaucoup plus jeunes exhumées pendant les périodes du Miocène inférieur à moyen. La combinaison de ces données implique l'évolution suivante. L'érosion générale de la chaine du Jurassique moyen au Crétacé supérieur est associée à un système de drainage large. La diminution progressive de la variété des sources pendant le Mésozoïque est compatible avec l'enfouissement progressive du socle par les sédiments. Les données U/Pb sur zircons détritiques et de traces de fission sur apatites indiquent la survenue d'un événement dans le piémont sud du Tian Shan à la fin du Crétacé - Tertiaire précoce et une activation de chevauchements entre 18 et 16 Ma qui pourrait être liée à la faille de Talas Ferghana.

Dans le chapitre 3 , nous présentons une étude magnétostratigraphique détaillée de la zone Ulugqat au sud-ouest du Tian Shan, dans le but d'améliorer la compréhension de son soulèvement et de l'histoire de la déformation de la région au cours du Cénozoïque. La section d'une épaisseur de 1700 mètres a été déposée entre ~ 20,8 et 13,3 Ma d'après la corrélation la plus probable à l'échelle de références des âges des inversions de polarité géomagnétique. Une discordance entre l'apparition de dépôts continentaux d'avant-pays de la formation Kezilouyi et les derniers dépôts marins de la formation éocène Bashibulake est ainsi datée à 20,8 Ma. Ceci indique un hiatus de sédimentation important (entre 38,5-35,5 à 20,8 Ma) correspondant à l'absence de dépôts d'avant-pays dans le nord-ouest du Tarim à l'Oligocène. Cela contraste avec le sud-ouest bassin du Tarim où les dépôts marins éocènes sont recouvertes de manière

continue par des dépôts d'avant-pays continentaux oligocène. Ceci suggère que la formation d'un bassin d'avant-pays a commencé plus tôt dans le sud du bassin du Tarim en réponse à l'activation Eocène - Oligocène du Kunlun Shan au sud. Le long de la marge sud du Tian Shan, toutefois, l'activité tectonique significative ne commencerait qu'au début du Miocène comme le montre les études thermochronologiques. De plus , les données magnétostratigraphiques indiquent une augmentation importantes des taux d'accumulation de sédiments entre 19 et 18 Ma, en même temps que l'exhumation dans la zone d'Ulugqat indiquée par les analyses de trace de fission sur apatites détritiques de deux échantillons à 18,5 ± 5,2 et 16,6 ± 2,8 Ma respectivement. Régionalement, cet âge correspond aussi à la propagation vers le sud de la déformation du Tian Shan dans le bassin du Tarim. Ce changement de régime tectonique est aussi contemporain de l'activation tectonique d'un système de décrochement majeur séparant le bassin du Tarim du saillant du Pamir à l'ouest. Ceci suggère que ce système a permis à partir de 20-18 Ma de transférer la déformation compressive de la collision Inde-Asie vers le Tian Shan et peut-être la faille de Talas Ferghana.

En conclusion, ce travail à permis de montrer que l'érosion du paléo- Tian Shan commencée au Trias moyen s'est traduite par le pénéplanation générale au Mésozoïque du Tian Shan qui était dominé par un système de drainage large pendant une longue période de quiescence tectonique. Le piémont nord du Tian Shan était caractérisé par un bassin en subsidence thermique post- extensive avec peu d'activité tectonique, et le piémont sud a également connu un aplanissement général de la topographie. Au cours du début du Jurassique, du Crétacé inférieur et du Crétacé supérieur, trois inversions tectoniques mineures sont identifiées avec des ajustements du bassin d'avant-pays du Tian Shan. Ces inversions peuvent correspondre respectivement à l'accrétion des terrains Cimmérien, de Lhassa, et du Kohistan - Dras à la limite sud de la plaque eurasienne.

Les données U-Pb sur zircons détritiques et les données traces de fission sur apatite indiquent une première réorganisation du bassin à la fin du Crétacé - début du tertiaire, contemporaine d'une réactivation de l'érosion le long du piémont sud du Tian Shan. Nous avons interprété cette réactivation fin Crétacé – début Paléogène du Tian Shan sud à la réponse initiale des effets lointains de la collision Inde - Eurasie.

Pendant le reste du Cénozoïque, la principale réactivation du Tian Shan est initiée fin Oligocène – début Miocène. Cela est attesté dans le piémont nord du Tian Shan par nos données U-Pb sur zircons détritiques et dans le piémont sud du Tian Shan par les données traces de fission sur apatite suggérant des chevauchements entre 18 et 16 Ma, par les résultats magnétostratigraphiques révélant une importante lacune de sédimentation oligocène ainsi que l'augmentation des taux d'accumulation à ~ 18,5 Ma.

Cependant, il y reste encore beaucoup de questions scientifiques importantes connexes non résolues. Des recherches complémentaires doivent être menées dans le piémont nord du Tian Shan, en particulier pour les série Cénozoïques qui sont encore peu contraintes en termes de thérmochronologie bien qu'elles soient déjà assez bien datés par magnétostratigraphie. Cela permettrait d'obtenir plus de connaissances sur l'histoire encore mal connue de l'exhumation du Tian Shan nord au cours du début du Cénozoïque. Le long de la marge sud Tian Shan il serait important d'étendre à l'Ouest et à l'Est des études corrélatives au sein des unités stratigraphiques semblables en utilisant des approches géochronologiques similaires. Cela donnerait l'occasion d'explorer les possibles propagations latérales du raccourcissement crustal le long de la chaine du Tian Shan et de mieux comprendre les différences potentielles entre la déformation tectonique du Tian Shan oriental avec le Tian Shan occidental, de part et d'autre de la faille de Talas Ferghana vers l'Est et les interaction avec l'activation du saillant du Pamir vers l'Ouest.

Abstract

The Tian Shan as a major part of the Central Asian Orogenic Belt (CAOB), one of the largest and long-lasting Phanerozoic accretionary orogens in the world, deserves the broad attention of geologists. Most previous studies involving the Tian Shan focused on either its Late Paleozoic amalgamations or the Late Cenozoic intracontinental orogenesis. This results in the necessity and urgency adressed in this thesis to further constraint the Mesozoic to Early Cenozoic tectonic evolution and basin-range coupling in the Tian Shan and adjacent regions. The excellent preservation of the Mesozoic-Early Cenozoic depositional sequences in Tian Shan piedmonts provides an ideal existing laboratories to understand the basin-range relation and depositional setting during the targeted time frame. Our work is following recently published outstanding achievements from the piedmonts of the present-day Tian Shan (e.g. Thesis of Gloria Heilbronn, Université de Rennes 1, 2014) using sedimentological, tectonic chronological, magnetostratigraphic, paleontological and paleoecological methods that have revealed outstanding issues that remain to be solved. Two critical scientific issues are adressed in the présent thesis as follows. (1) Mesozoic basin-range relationship in the northern and southern piedmonts of the Tian Shan. (2) Spatio-temporal differences in the Early Cenozoic uplift of the Tian Shan. As detailed in the following chapters of this thesis, we aim to provide detailed information on the Mesozoic-Cenozoic tectonic evolution and basin-range relations of piedmonts of the Tian Shan, by using magnetstratigraphy, detrital zircon U-Pb geochronology and detrital apatite fission-track analyses both in the northern Tian Shan peidmont (Manasi area) and in the southern Tian Shan piedmont (Ulugqat area), which are ideal laboratories still poorly constrained that will be compared to existing records in the adjacent subbasins.

In chapter 1, the évolution of the northern Tian Shan is investigated through U/Pb (LA-ICP-MS) dating of detrital zircons from 14 sandstone samples from a continuous

series ranging in age from latest Palaeozoic to Quaternary in the southern margin of the Junggar Basin (Manasi area). The aim is to trace changes in sediment provenance through time and to correlate them with major tectonic phases in the range. Samples were systematically collected along two nearby sections in the foreland basin. The results show that the detrital zircons are mostly magmatic in origin, with some minor input from metamorphic zircons. The U-Pb detrital zircon ages range widely from 127 to 2856 Ma and can be divided into four main groups: 127-197 (sub-peak at 159 Ma), 250-379 (sub-peak at 318 Ma), 381-538 (sub-peak at 406 Ma) and 543-2856 Ma (sub-peak at 912 Ma). These groups indicate that the zircons were largely derived from the Tian Shan area to the south since a Late Carboniferous basin initiation. The provenance and basin-range pattern evolution of the southern margin of Junggar Basin can be generally divided into four stages: (1) Late Carboniferous-Early Triassic basin evolution in a half-graben or post-orogenic extensional context; (2) From Middle Triassic to Upper Jurassic times, the southern Junggar became a passively subsiding basin until (3) being inverted during Lower Cretaceous-Palaeogene; (4) During the Neogene, a piedmont developed along the northern margin of the North Tian Shan block and Junggar Basin became a true foreland basin.

In chapter 2, the still poorly constrained Mezosoic to early Cenozoic evolution of the southwestern Tian Shan piedmont is investigated using U/Pb (LA-ICP-MS) dating of detrital zircons and fission track analysis on detrital apatites. Changes in sediment provenance through time are obtained from the exceptionally well-exposed Jurassic to Cenozoic sédiment at the Ulugqat area. The U/Pb detrital zircon ages range widely from 222 to 3179 Ma and can be statistically separated in four main groups: 240–320 Ma, 400–540 Ma, 550–1600 Ma and 1640–2800 Ma. These zircons were derived from the Tian Shan area to the north and from recycling of the Paleozoic North Tarim margin. The detrital apatite fission track ages encompass sources with preserved Mesozoic ages as well as much younger sources exhumed during middle Miocene times. Combined together those data show a general planation of the range from

Middle Jurassic to Late Cretaceous associated to a wide drainage system. The progressive decrease in the variety of sources through the Mesozoic is consistent with burying of the basement exposures by sediments. Detrital zircon U/Pb data indicate an late Cretaceous – Early Tertiary event within the southern Tian Shan piedmont and a possible activation of the Talas Fergana Fault between 18 and 16 Ma.

In chapter 3, we present a detailed magnetostratigraphic study from the Ulugqat area in piedmont of the Southwest Tian Shan, in order to improve understanding of the uplift and deformation history of the Southwest Tian Shan during the Cenozoic. The 1700-m-thick section comprises an age span from ~ 20.8 to 13.3 Ma according to the most likely correlation to the geomagnetic polarity time scale. An unconformity between the onset of continental deposits of the Keziluoyi Formation and the last marine deposits of the Bashibulake Formation is detected around 20.8 Ma. This major depositional hiatus spreading from the 38.5-35.5 to 20.8 Ma corresponds to the absence of Oligocene foreland deposits in the northwestern Tarim. This contrasts with the southwestern Tarim basin where Eocene marine records are overlain continuously by continental foreland deposits through the Oligocene. This suggests foreland deformation initiated earlier in the southern Tarim basin in response to Eocene-Oligocene activation of the Kunlun Shan to the south. Along the southern Tian Shan, however, significant tectonic activity only initiated in the early Miocene as supported by thermochronologic studies. There sediment accumulation rates increase conspicuously at ~ 18.5 Ma, concurrent with the previous detrital apatite fission-track analysis from the Ulugqat area, yielding totally reset central ages respectively at 18.5 ± 5.2 and 16.6 ± 2.8 Ma. This age corresponds to the southward propagation of deformation of the Tian Shan piedmont into the Tarim basin. This change of tectonic regime is also coeval with the tectonic activation of a major strike-slip system separating the Tarim basin from the Pamir salient to the west. This together suggests that this system enabled from 20-18 Ma onwards to transfer compressional

deformation from the India-Asia collision to the Tian Shan and possibly the Talas Ferghana Fault.

In conclusion, this worl enabled to show that erosion of the Paleo-Tian Shan initiated in the Middle Triassic results in the general peneplanation of the Mesozoic Tian Shan dominated by a wide drainage system and long-lasting tectonic quiescence. The northern piedmont of the Tian Shan was characterized by a post-extensional thermally subsiding basin without much tectonic activity, and the southern piedmont also experienced a general flattening of topography. During the Early Jurassic, Early Cretaceous and Late Cretaceous, three identified minor tectonic inversions and adjustments of basin-range pattern in the Tian Shan, may potentially correspond respectively to the accretions of Cimmerian, Lhasa, and Kohistan-Dras in the southern margin of the Eurasian plate.

Detrital zircon U-Pb and apatite fission-track data indicate an initial late Cretaceous – Early Tertiary basin reorganization and coeval renewed erosion along the southern Tian Shan piedmont. We interpreted this late Cretacesou to Paleogene activity in STS as the initial response of the distant effects of India-Eurasia collision as previously argued.

During the Late Cenozoic, the major reactivation of the Tian Shan initiated around the Late Oligocene-Early Miocene times. This is evidenced mainly from the detrital zircon U-Pb geochronology in the northern piedmont of the Tian Shan, the apatite fission-track data suggesting a possible activation of the Talas Fergana Fault between 18 and 16 Ma, the major Oligocene depositional hiatus and conspicuous increase in accumulation rates at ~ 18.5 Ma revealed by the magnetostratigraphic results in the southern piedmont of the Tian Shan. Cenozoic uplift of the Tian Shan propagated northwards and evolved from local to regional effects during the late Cretaceous to Miocene times. This is also consistent with the northward propagation of far-field effects of the Indo-Asia collision.

However, there is still plenty of unresolved related important scientific issues. Further research ought to be carried out in the northern piedmont of the Tian Shan in terms of low temperature thermochronology, especially for the Cenozoic series that are still constrained poorly in that aspect although they are already fairly well dated using magnetostratigraphy. This would enable to gain more insights on the exhumation history of NTS during the Early Cenozoic period. Along the southern Tian Shan piedmont it would be important to extend to the West and East correlative studies within the similar lithostratigraphic units by using similar geochronological approaches. This would provide opportunities to explore possible lateral propagation of the crustal shortening along the Tian Shan and understand further potential difference in tectonic deformation between the ETS and WST, across the Talas Ferghana Fault to the East, towards the Pamir salient to the West.

Preface

My PhD thesis, titled "Mesozoic-Cenozoic tectonic evolution and basin-range relations of the northern and southern piedmonts of the Tian Shan" is constructed around three topics of research, of which two have already published, and the third one close to be submitted. The three papers are presented in my thesis as different chapters, respectively for the Latest Palaeozoic-Cenozoic detrital zircon U-Pb geochronology in the northern margin of the Tian Shan, the Mesozoic-Cenozoic detrital zircon U-Pb and apatite fission track analysis, and the Late Cenozoic magnetostratigraphy in the piedmont of the southwestern Tian Shan. Although I show all the achievements as my work, all of my co-authors will be thanked here. The fruits result also from their great efforts and contributions.

Acknowlegements

Over the years of my PhD thesis between the Université de Rennes 1 and the Peking University, a close relationship beween my life and geosiences has been established. This is also resulted from my own interest on touring in well-known mountains and rivers in the western China. I was lucky enough beyond all doubt to choose the Junggar and Tarim Basins as the laboratories to conduct the researches for my PhD topic. Therefore, I would like to thank the western China firstly, a magical land where I was brought up.

I would like to start acknowledging my three supervisors Guillaume Dupont-Nivet, Marc Jolivet and Zhaojie Guo, for your sincere confidence and support, and the opportunities to me to work with the friendly French research teams.

In fact I have been to Xinjiang for field work for four times during the last few years. In all I spend almost five months there and so many lovely minorities left deep memories for me. An excellent novel can be even composed based on plenty funny stories when getting along with them. So many Uyghur, Kazak, Kirgiz, Tadjik and Mongolian guys provided assistance to us when we were struggling to find the target areas, trying to get our trapped car out from the mud, or hard working on collecting samples under the burning sun. I will never forget the fresh horse milk freely supplied by the Kirgiz people in Wuqia, and the golden apricots picked up by the dusty small hands of the Tadjik boys in Kusilaf. The drivers Duan, Wang, Yuming Qi and Jilin Huang displayed their outstanding talent on driving Toyota 4500 on the bumpy roads in Xinjiang. Besides, Bruno is still missing from the above list. This strong man has been so important to the field work in Tarim in 2012, and assisted us so much with collecting and packing up the samples, especially during working at temperatures close to 40 ℃ or in the typical storm of northeastern Pamir. Hope I can also invite this guy in the future to join a team for field investigation, which would be still attractive and can be another wonderful vacation to him. I thus have to thank all those people

involved during the fieldwork, definitely including my graduate student brothers Ziya Zhang and Beibei Zhu.

In Université de Rennes 1, I have accomplished most of the necessary experiments including paleomagnetic measurements and apatite fission track analysis. Many colleagues have contributed in various ways to the conduction of the above work, during the processes of sample pre-treatment, experimental installation test, targeted sample measuring, as well as initial data handling. Of course I need to thank the Dutch guy Roderic Bosboom firstly. To him I own most of the skills related with the magnetostratigraphy throughout my PhD, including how to design detail flow for systematic thermal demagnetization, how to perform ChRM analyses, and how to operate the processing software properly. I would also like to thank Chauvin Annick, Roperch Pierrick, Cullerier Philippe, Dufresne Philippe, Garnier Lucie for their great help in the Paleomagnetic laboratory.

Low-temperature thermochronology plays roles of equal importance during the years of my thesis. During the apatite fission track dating in the laboratory managed by Marc Jolivet, my colleagues Poujol Marc and Heilbronn Gloria assisted me a lot with adjusting the delicate electron microscope. It is really an unforgettable experiences to regulate the objective stage when it gets angry. Without conselling from Gloria and her guidance in solving problems, it would have never succeeded to keep the normal efficiency during counting tracks. I have to admit that AFT experiments made me more patient at settling some intractable issues.

Then I am very grateful to Prof. Li Su, graduate students Jiao Li, Hong Yu and Hongyu Zhang of the Geological Lab Center, China University of Geosciences (Beijing), for their great help during detrital zircon LA-ICP-MS dating.

Of course Jean-Noel Proust, Edward Sobel, Yan Chen, Laurie Barrier of the reading committee are all thanked for taking plenty of their precious time to carefully read thourgh my thesis manuscript.

As mentioned above, the condition of my life in Rennes is significantly covariant with the research processes. I thus need to thank all my friends in Rennes, for their accompanying and assistance in daily living. Wentao huang, Yingying Jia, two PhD students also coming from Peking University helped me to take care of my apartment, and I will remember all those days we enjoyed together forever. Of course Laurie Bougeois who gets so excited about fossil oysters would be thanked for her kind explanation to me during the complex procedure for getting my new Carte de residence in Rennes. Then I will have to thank Duprat-Oualid Sylvia, a nice French girl for her great support to help translating some important materials from Université de Rennes 1, as well as the introduction for the amazing and beautiful beach in Brittany. I am sure she is very interested in the Asian, especially the Chinese history and even culture, which also results in the possibility for me to probe deeply into the French traditions. Some similarity in culture between France and China can thus be understood by us. I am looking forward to be a super tour guide when all the young European friends plan to visit North China someday.

Finally, I warmly thank those mentioned above as well as innumerable others for helping and supporting me. Those years of my life have been one of the best so far, and without any of you it would not have been wonderful like this.

Curriculum Vitae

Date of birth: 19 Dec 1986 Born in Lanzhou, China

Education :

●Ph. D. candidate, Geosciences, Université de Rennes 1, 2011

Thesis: Mesozoic-Cenozoic tectonic evolution and basin-range relations of the northern and southern piedmonts of the Tian Shan

●Ph. D. candidate, Geology, Peking University, 2009

Focus: Structural geology

●B. A, Geology, Lanzhou University, 2009

Thesis: Tectonic settings and source characteristics of Ordovician volcanic rocks in Northern Qilian orogenic belt

Research experiences

2009-2013 National 973 project: Continental Dynamics of the Central Asian Orogenic Belt and its Metallogeny-Intracontinental orogenesis and Metallogeny, China (2007CB411305).

2010-2011 National Science and Technology Major Project: Structural analysis of complex petroliferous basins, effects on generation, migration and accumulation of oil/gas-Development associated with structural belts along the northern and southern piedmonts of the Tian Shan (2011ZX05009-001).

2011-2013 Partenariat Hubert Curien avec la Chine Program Cai Yuanpei, Ministère des affaires étrangère - Chinese Scientific Council. Projet nr. 26048TB: CAUSE, AGE ET CONSEQUENCES DU RETRAIT MARIN DE L'ASIE.

Main Publications

Yang, W., Jolivet, M., Dupont-Nivet, G., Guo, Z.J., Zhang, Z.C., Wu, C.D., 2013. Source to sink relations between the Tian Shan Range and Junggar Basin (northwest China) from Late Paleozoic to Quaternary: evidence from detrital U-Pb zircon geochronology. Basin Research 25 (2), 219-240.

Yang, W., Jolivet, M., Dupont-Nivet, G., Guo, Z.J., 2013. Mesozoic-Cenozoic tectonic evolution of southwestern Tian Shan: Evidence from detrial zircon U-Pb and apatite fission track ages of the Ulugqat area, Northwest China. Gondwana Research. http://dx.doi.org/10.1016/j.gr.2013.07.020.

Yang, W., Dupont-Nivet, G., Jolivet, M., Guo, Z.J., submitted. Magnetostratigraphy and apatite fission track ages from Ulugqat area, Northwest China: implications for the Cenozoic tectonic evolution of the Tarim Basin and southwest Tian Shan.

Table of contents

List of Figures

Siltstone; 8 Medium-grained sandstone; 9 Fine sandstone; 10 Pelitic sandstone; 11 Pelitic siltstone; 12 Sandy mudstone; 13 Mudstone; 14 Coal layers, coal streaks; 15 Limestone; 16 Cross bedding; 17 Unconformity.

Fig. 1.4 (a) Volcanic-sedimentary sequences of the Aerbasayi Formation; (b) Characteristic gravels from conglomerates of the volcanic-sedimentary sequences; (c) Typical red gravels and pebbles of the Late Jurassic Qigu Formation (white circles) and brown-reddish conglomerate pebbles of the Kalazha Formation found in the Dushanzi Formation conglomerate (black circles); (d) Late Jurassic tuffaceous sandstone pebbles found in the Dushanzi Formation conglomerate (white circles).

Fig. 1.5 Representative CL images of zircons from the 14 sandstone samples. White circles show the location of U-Pb analysis. Numbers are U-Pb ages in Ma.

Fig. 1.5 (continued).

Fig. 1.6 Relative - age - probability plots and number histograms of U-Pb ages of detrital zircons of Permian to Quaternary sandstone samples in the southern margin of the Junggar Basin.

Fig. 1.7 U-Pb concordia diagrams for zircon grains of the 14 sandstone samples.

Fig. 1.8 Combined relative probability density and histogram plots of the 14 samples. The diagram to the left corresponds to the black box in the first diagram.

Fig. 1.9 Palaeogeographic reconstructions of key periods in the evolution of the Tian Shan Range – Junggar Basin history as described in the text. The map extends roughly between the Bayanbulak basin to the left and the Junggar Basin to the right. Only the major faults are shown such as the Main Tian Shan Shear Zone (MTSZ) or the Nikolaev line (see Jolivet et al., 2010). Question marks indicate possible but not documented movements on the faults. Faults in dotted lines are inactive. The arrow represents sediment provenance deduced from detrital U/Pb zircon ages and various

sedimentology data described in the text. The topography was drawn using both provenance data and low thermochronology data obtained in the range by Dumitru et al. (2001) and Jolivet et al. (2010). Black arrows indicate major sources, dark-grey arrows indicate minor sources. Light-grey arrows indicate possible minor sources. The light-grey shaded areas indicate basins (deposition areas) and dark-grey shaded areas indicate lakes.

Fig. 2.1 General topographic and tectonic map of the Tian Shan belt and adjacent areas. Only the major tectonic structures are indicated. "M.T.S.Z" is the Main Tian Shan Zone (modified from Jolivet et al., 2010). The black square corresponds to the study area detailed in Fig. 2.2.

Fig. 2.2 Geological and tectonic sketch map of the Southwestern Tian Shan crossing northwestern China and Kyrgyzstan with the approximate location of Fig. 2.3 shown with a box and samples locations of KA02 and ZKS01 (modified after BGMRXUAR, 1978). "Z. River" is the Zhuoyoulehansu river.

Fig. 2.3 Simplified geological map of the Ulugqat area with the position of the samples, except samples KA02 and ZKS01which are reported on Fig. 2.2 (modified after BGMRXUAR, 1978).

Fig. 2.4 Generalized stratigraphic column of the Middle Jurassic to Quaternary series of the studied area (modified after Zhang et al., 2011).

Fig. 2.5 (a) Combined relative probability density and histogram plots of the available zircon U/Pb data on basement rocks in South Tian Shan (Brookfield, 2000; Yang et al., 2001; Solomovich et al., 2002; Liu et al., 2004; Yang et al., 2006; Konopelko et al., 2007, 2009, 2012; Wang et al., 2007a; Wang et al., 2007b; Zhang et al., 2007a; Djenchuraeva et al., 2008; Sun et al., 2008; Alekseev et al., 2009; Lin et al., 2009; Yang and Zhou, 2009; Hegner et al., 2010; Li, 2010; Orozbaev et al., 2010; Su et al., 2010; Seltmann et al., 2011; Alexeive et al., 2011; Gao et al., 2011; Han et al., 2011;

Kröner et al., 2012; Long et al., 2011; Gou et al., 2012; Huang et al., 2012). (b) Combined relative probability density and histogram plots of the detrital zircon U/Pb ages of sediments from the South Tian Shan piedmont. A summary plot of all available U/Pb detrital zircon ages (b-1) Summary of the U/Pb detrital zircon ages from Kuqa area (Li and Peng, 2010). (b-2) Summary of the U/Pb detrital zircon ages from Tekes area (Ren et al., 2011).

Fig. 2.6 Summary of detrital apatite fission track ages obtained from the piedmont of Southwest Tian Shan (e.g. Sobel and Dumitru, 1997; Dumitru et al., 2001; Jia et al., 2003; Sobel et al., 2006; Du et al., 2007a, 2007b; De Grave et al., 2012), 50-80 Ma (e.g. Sobel and Dumitru, 1997; Dumitru et al., 2001; Du et al., 2007a, 2007b), and 15-20 Ma (e.g. Sobel and Dumitru, 1997; Dumitru et al., 2001; Sobel et al., 2006; De Grave et al., 2012).

Fig. 2.7 Representative CL images of zircons from the 8 sandstone samples. White circles show location of U/Pb analysis. Numbers are U/Pb ages in Ma**.**

Fig. 2.8 Relative-age-probablity plots and number histograms of U/Pb ages of detrital zircons from Middle Jurassic to Quaternary sandstone samples collected in the Zhuoyoulehansu section.

Fig. 2.9 U/Pb concordia diagrams for zircon grains of the 8 sandstone samples.

Fig. 2.9 (continued).

Fig. 2.10 Combined relative probability density and histogram plots of the 8 samples. The diagram to the left corresponds to the blue box in the first diagram.

Fig. 2.11 Single grain apatite fission track age distributions of the samples presented in age spectra and radial plots. Age spectra (black lines) were created according to Hurford et al. (1984).

Fig. 2.11 (continued).

Fig. 3.1 (a) Location of the studied area shown on large-scale map of Asia. (b) Simplified geological map of the Ulugqat area with location of the Mine (A) and Ulugqat (B) sections.

Fig. 3.2 Generalized stratigraphic column of the Cenozoic series of the studied Ulugqat area (modified after Yang et al., 2013).

Fig. 3.3 Field photographs of formations and sedimentological features at the Mine section. (a) Unconformity between the Bashibulake and Keziluoyi Formation, channel sandstone beds of the Bashibulake Formation indicative of a fluvial depositional environment, and the gravel layer at the bottom of the Keziluoyi Formation. (b) Red mudstones interbedded with thick-bedded sandstones of the upper of Keziluoyi Formation indicative of the fluvio-lacustrine facies. Sinuous-crested ripples are locally developed. (c) Brown-red mudstones interbedded with gray-green mudstones, siltstones and sandstones of the Anjuan Formation indicative of a shallow lacustrine environment. (d) Conglomeratic sandstones, occasional red-brown mudstones and sandy mudstones of the basal unit of the Pakabulake Formation indicative of fluvio – shore shallow lacustrine deposits, with a thin-bedded gravel layer presents at the bottom.

Fig. 3.4 (a) Plots showing typical thermal demagnetization behaviors of representative specimens with quality 1, 2 and 3. Numbers next to symbols indicate temperature of demagnetization steps in ℃. (b) Bulk susceptibility and (c) intensity behavior of representative specimens upon the thermal demagnetization. The starting intensity is given in 10^{-3}/m.

Fig. 3.4 Continued.

Fig. 3.5 ChRM directions, reversals test and fold test. Full symbols are projections on the horizontal plane and open symbols on the vertical plane.

Fig. 3.6 Magnetostratigraphy of the Mine section. (a) Stratigraphic description of the measured section in meters (m). (b) VGP latitude. Full (open) dots are reliable (unreliable) directions. Grey dots are isolated directions that have been discarded. Crossing dots are isolated unreliable directions that have been discarded. (c) The corresponding magnetic polarity zones for the preferred correlation. (d) GPTS 2012: geomagnetic polarity time scale of Gradstein et al. (2012). (e) The corresponding magnetic polarity zones for the alternative correlation.

Fig. 3.7 Correlation of the polarity zones recognized in the Mine section to the GPTS 2012 (Gradstein et al., 2012) with corresponding accumulation rates. The preferred and alternative correlations are shown by the thick black and grey lines, respectively.

List of Tables

Table 3.1 Simplified litho-biostratigraphic correlation of the Kuqa subbasin, Ferghana-Alai and Afghan-Tadjik Basins to the chronological framework recognized in the southwest Tarim Basin. The wavy line represents a gap between the Late Eocene and Oligocene in the western Tarim Basin. The Bashibulake Formation in western Tarim corresponds to the lower Suweiyi Formaiton in northern Tarim (Jia et al., 2004; Bosboom et al., in revision), the Sanglak Formation in Afghan-Tadjik Basin (Dzhalilov et al., 1982), as well as the Rishtan, Isfara, Hanabad, Sumsar, and Shurysay Formations in Ferghana-Alai Basin (Pomazkov, 1972; Bosboom et al., in revision); the Keziluoyi Formation corresponds to the upper Suweiyi and lower Jidike Formations in northern Tarim (Jia et al., 2004), the Massaget Formation in Ferghana-Alai Basin (Pomazkov, 1972), as well as Hissarak, Shurysay, and Baldzhua complex/Kamoli Formations in Afghan-Tadjik Basin (Dzhalilov et al., 1982; Bosboom et al., in revision); the Anjuan Formation corresponds to the upper Jidike Formation in northern Tarim (Jia et al., 2004), the Baktry Formation in Ferghana-Alai Basin (Coutand et al., 2002; Bosboom et al., in revision), as well as the Childara and lower Hingou Formaitons in Afghan-Tadjik Basin (Dzhalilov et al., 1982); finally the Pakabulake Formation corresponds to the Kangcun Formation in Northern Tarim (Jia et al., 2004), the Sokh Formation in Ferghana-Alai Basin (Coutand et al., 2002), as well as the upper Hingou and Tavildara Formations in Afghan-Tadjik Basin (Dzhalilov et al., 1982; Bosboom et al., in revision).

Table 3.2 Sedimentation accumulation rates.

* Notes: Level – stratigraphic level from the studied section; Age – age of correlated chron based on GPTS 2012 (Gradstein et al., 2012); Rate – calculated sediment accumulation rate; Av. rate – average rate for longer intervals.

General Introduction

Geologic background

The Tian Shan is a major part of the Central Asian Orogenic Belt (CAOB), as one of the largest and long-lasting Phanerozoic accretionary orogens in the world, deserves the broad attention of geologists (Sengör et al., 1993; Jahn et al., 2004; Windley et al., 2007; Kröner et al., 2008; Rojas-Agramonte et al., 2011). The CAOB extends west-east from Russian Ural Mountains to the west Pacific Ocean as an arcuate zone projecting to the south, with the northern and southern margins respectively meeting the Siberian and Tarim-North China (Sino-Korean) Cratons (e.g. Chen et al., 2013) (Fig. 1a). The tectonic evolution of the CAOB is quite complex and still elusive (Biske and Seltmann, 2010; Windley et al., 2007; Gao et al., 2009; Lamb and Badarch, 1997; Lehmann et al., 2010; Ren et al., 2011, Xiao et al., 2004, 2010). Most scholars support the idea that accretion of the CAOB results from the complicated multipolarity subduction, orocline bending, rotation and collision processes of various magmatic arcs, accretionary complexes, microcontinents and seamounts, sea plateau and pristine oceanic crust. In previous studies, the CAOB is always simplified consisting of the western Kazakhatan-Tian Shan and Altai-Mongolia tectonic domains, respectively characterized by the Kazakhstan and Tuva-Mongol oroclines (Sengör et al., 1993; Sengör and Natal'in, 1996; Buslov et al., 2001; Collins et al., 2003; Abrajevitch et al., 2007; Levashova et al., 2007; Windley et al., 2007; Xiao et al., 2010).

The focus of this thesis is the Tian Shan orogenic belt, which plays a crucial role during all the phases of development of the CAOB, extends east-west for ~ 3000 km through western China, Kazakstan and Kirghizstan with the average elevations about 4 km (Xiao et al., 1990; Şengör et al., 1993; He et al., 1994; Li and Xiao, 1999; Shu et al., 2004; Windley et al., 2007; Jolivet et al., 2010; Yang et al., 2013; Li et al., 2009) (Fig. 1b). As a major part of the CAOB, the lithosphere construction of the Tian Shan

also underwent a complicated process involving the accretions of late Palaeozoic islands and microcontinents (Watson et al., 1987; Coleman, 1989; Gao et al., 1998; Charvet et al., 2004, 2007, 2011; Shu et al., 2004; Li et al., 2009). The Chinese Tian Shan, as the eastern segment of the Tian Shan orogenic belt, extends over 2500 km, and usually divided into the North, Central, South Tian Shan (NTS, CTS, STS), as well as Yili terrane in the western part (Fig. 1.1) (e.g. Gao et al., 1998; Charvet et al., 2011). The present-day North Tian Shan (NTS) is situated north of the northern margin fault of the Central Tian Shan (CTS), which is sandwiched between its northern and southern margin faults, and the South Tian Shan (STS) is located between the southern margin fault of the CTS and the northern Tarim margin fault (e.g. Li et al., 2009; Yang et al., 2013). The Chinese Tian Shan can be also subdivided into the East Tian Shan (ETS) and West Tian Shan (WTS) from the view of latitude roughly along longitude 88 ° E, respectively lying in western China and extending to Kazakstan and Kirghizstan. The eastern segment of WTS seated in China is always referred to as the southwestern Tian Shan (SWTS) (e.g. Gao et al., 2009; Lin et al., 2009; Wang et al., 2011).

During the Late Devonian-Early Carboniferous, the Tarim-STS terrane collide with the CTS block, and the Tarim-CTS terrane successively amalgamated with numerous island arc systems within the present-day NTS until the Early Permian (Huang, 1980; Wang et al., 1990; Allen et al., 1992; Biske and Seltmann, 2010; Han et al., 2010; Charvet et al., 2011). Corresponding to the above accretions, the CTS is mainly composed of widespread Proterozoic metamorphic basements intruded by granites mostly emplaced during 490-380 Ma (e.g. Zhou et al., 2001; Han et al., 2004; Glorie et al., 2010). The final closure time of the North Tian Shan Ocean is still debated, but most authors have argued extensively that the amalgamation between the CTS and NTS occurred during the Late Carboniferous to Early Permian, consistent with the post-collisional A-type granites emplaced between 320 and 280 Ma, which are widely

distributed in CTS and NTS (Zhou et al., 2001; Han et al., 2004; Konopelko et al., 2007; Glorie et al., 2010).

During the Late Cenozoic, the Tian Shan has again reactivated and gradually evolved into the great intracontinental orogenic belt, induced by the far-field effects of the Indo-Asian collision (e.g. Molnar and Tapponnier, 1975; Tapponnier and Molnar, 1977, 1979; Avouac et al., 1993; Lu et al., 1994; Guo et al., 2003). Both piedmonts of the Tian Shan are characterized by development of the rejuvenated foreland basins. Controlled by the intense tectonic compression, the basin-range pattern in the southern margin of the Junggar Basin has been significantly adjusted, and three large-scaled rows of the foreland fold-thrust belts are exposed as the piedmont belt, the Huoerguosi-Manasi-Tugulu belt, and the Dushanzi-Anjihai belt from south to north (e.g. Fang et al., 2006; Li et al., 2007). The piedmont belt, composed of the Kalazha, Changji, and Qigu anticlines was developed during the Late Miocene to Early Pliocene (Avouac et al., 1993; Lu et al., 2010; Li et al., 2010), while the Dushanzi-Anjihai belt during the Late Pliocene to Early Pleistocene. On the southern flank of the Tian Shan, the Kuqa foreland fold-thrust belt, evolved since the Middle Miocene consists of the northern monocline belt, Sidike anticline belt, Keyi structural belt, Baicheng-Yangxia depression belt and Qiulitage anticline belt from north to south (e.g. Liu et al., 2000; Lu et al., 2000). Also a significant fold-thrust belt yielding a width of around 30 km developped at about this time in piedmont of the southwestern Tian Shan. A succession of structures are dominant within this belt, such as the Mutule, Bapanshuimo, Atushi, Talanghe, Kashi, Mingyaole and Mushi anticlines (e.g. Chen et al., 2005; Fu et al., 2010; Li et al., 2011).

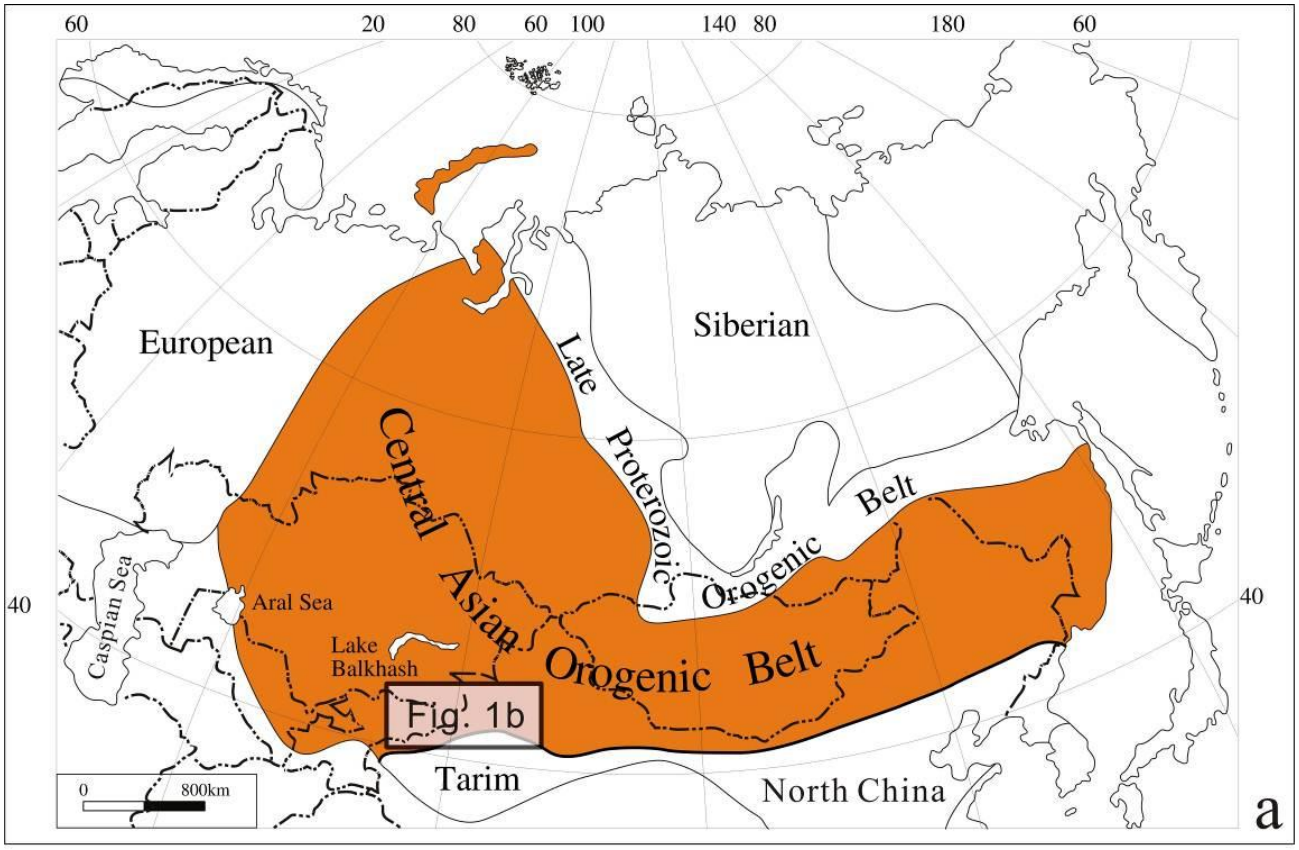
60
20
80
60
100
140
80
180
60
European
Siberian
Late Proterozoic Orogenic Belt
Central Asian Orogenic Belt
Caspian Sea
Aral Sea
Lake Balkhash
Fig. 1b
Tarim
North China
40
40
0
800km
a

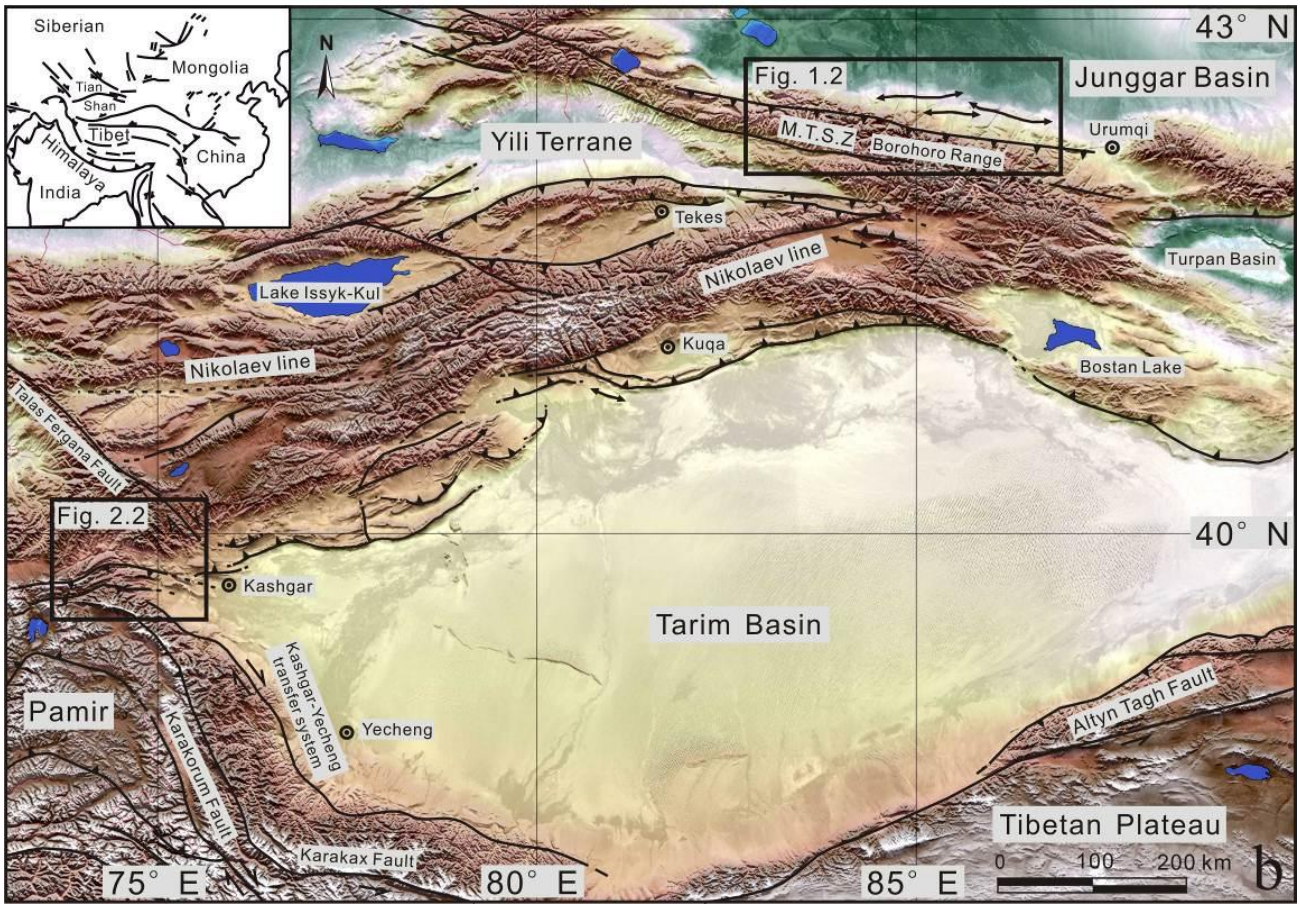
Siberian
Mongolia
Tian Shan
Tibet
China
Himalaya
India
N
43° N
Fig. 1.2
Junggar Basin
M.T.S.Z
Borohoro Range
Urumqi
Yili Terrane
Tekes
Nikolaev line
Turpan Basin
Lake Issyk-Kul
Kuqa
Bostan Lake
Nikolaev line
Talas Fergana Fault
Fig. 2.2
40° N
Kashgar
Tarim Basin
Pamir
Kashgar-Yecheng transfer system
Yecheng
Karakorum Fault
Altyn Tagh Fault
Karakax Fault
Tibetan Plateau
75° E
80° E
85° E
0
100
200 km
b

Fig. 1 (a) Tectonic sketch map of the Central Asain Orogenic Belt (modified after Jiang et al., 2014). (b) General topographic and tectonic map of the Tian Shan orogenic belt and adjacent areas. Only the major tectonic structures are indicated. "M.T.S.Z" is the Main Tian Shan Zone (modified from Jolivet et al., 2010). The black squares correspond to the study areas detailed in Fig. 1.2 and Fig. 2.2.

Critical scientific issues aadressed by this thesis

By far, most previous studies involving the Tian Shan focus on either its Late Paleozoic amalgamations or the Late Cenozoic intracontinental orogenesis, which results in the necessity and urgency adressed in this thesis to further constraint the Mesozoic to Early Cenozoic tectonic evolution and basin-range coupling in the Tian Shan and adjacent regions. The excellent preservation of the Mesozoic-Early Cenozoic depositional sequences in Tian Shan piedmonts results from the rapid input and burying of debris material, and provides the ideal existing laboratories to understand the basin-range relation and depositional setting during the targeted time frame (e.g. Jordan and Gardeweg, 1988; Flemings and Jordan, 1990; Hendrix, 2000). The targeted areas include the Junggar and Kuqa foreland Basins representing some of the most important and promissing hydrocarbon fields in western China, for which the identification and subdivision of potential source and host systems remains to be greatly improved by new constraints on basin-filling processes of the targeted time frame. On the other hand, the global/regional coupling between the Asian paleoclimate evolution and tectonic uplift in this distinctive orogenic systems has long been a puzzling issue, of particular interest to geologists (e.g. Molnar and England, 1990) but its Mesozoic-early Cenozoic history remain poorly contrained depsite the occurrence of major events such as the India-Asia collision. Effective estimations of potential relationships between Asian geodynamics and the Tibetan plateau growth are impaired by the poor age control on Mesozoic-Early Cenozoic sedimentary records. Such records, available on either side of the Tian Shan can promote our

understanding of crustal shortening and tectonic deformation in the adjacent basins. The coeval evolution of paleoenvironment such as the onset and development of monsoonal system and associated continental aridification, for which the Late Cenozoic has been intensely studied (e.g. Ruddiman et al., 1997; Deng et al., 2008) also remains to be revealed by these Mesozoic to early Cenozoic records. Our work is following recently published outstanding achievements from the piedmonts of the present-day Tian Shan (e.g. Thesis of Gloria Heilbronn) using sedimentological, tectonic chronological, magnetostratigraphic, paleontological and paleoecological methods that have revealed outstanding issues that remain to be solved.

The critical scientific issues are summarized as follows.

1. Mesozoic basin-range relationship in the northern and southern piedmonts of the Tian Shan

The Mesozoic topography and tectonic setting of the Tian Shan is enigmatic, and most researchers consider that the Tian Shan is dominated by an extensional setting due to the post-orogenic relaxation, and could not be a towering topography significantly separating paleoclimate patterns (e.g. Hendrix et al., 2000; Shu et al., 2004; Guo et al., 2005, 2006; Fang et al., 2006). Additionally, strong erosion during the Triassic and Early Jurassic initiated general peneplanation of the Tian Shan region, consistent with the long period of tectonic quiescence during the Middle-Late Jurassic in Central Asia (Shu et al., 2004). Whereas some studies showed that the Tian Shan existed as a distinct positive physiographic feature during the Mesozoic (e.g. Hendrix et al., 1992; Dumitru et al., 2001), predominantly evidenced by the Mesozoic sediment deformations and cooling ages from the thermochronological analysis (e.g. Hendrix et al., 1992; Dumitru et al., 2001; Jolivet et al., 2010; Chen et al., 2011). The associated minor uplift has been attributed largely to the accretions in the southern margin of the Eurasian plate (Hendrix et al., 1992). The tectonic driver of basin formation along the southern and northern piedmont of the Tian Shan during the

Mesozoic thus remains debated. For example, Li et al. (1998) and Liu et al. (2000) considered that the southern Junggar Basin has been under an extensional geodynamic setting during the Mesozoic-Paleogene until tectonic inversion commenced in the Neogene. Chen et al. (2002) and Jolivet et al. (2010) considered it as an intracontinental subsiding basin during the Jurassic to Early Tertiary period, consistent with unconformity between the Jurassic and Cretaceous series. Whereas Hendrix et al. (1992) and Zhang et al. (1999) support the idea that the southern Junggar Basin was a foreland basin during the Triassic-Middle Jurassic times, corresponding to the coeval uplift in NTS.

The Mesozoic tectonic setting of the southern margin of the Tian Shan equally remains enigmatic. Seveal studies suggested that the northern Tarim Basin, controlled by the weak compression existed as an intracontinental foreland basin during the Mesozoic (e.g. Tang et al., 2012), whereas many authors considered it as a passively subsiding basin characterized by a diffuse basin-range differentiation, a geographically wider source area and a relatively low topography (e.g. Li et al., 2010; Liu et al., 2013).

A detailed study of tectonic chronology and sedimentology in the basin-range junction belts may thus provide detailed information on the Mesozoic tectonic setting, peneplanation timing, general topographical feature, and basin attributes in both piedmonts of the Tian Shan.

2. Spatio-temporal differences in the Early Cenozoic uplift of the Tian Shan

Although it is now clear that during the Late Cenozoic, the Tian Shan was rejuvenated by the distant effects of the India-Eurasia collision (Monlar and Tapponnier, 1975; Tapponnier and Monlar, 1977, 1979; Burchfiel and Royden, 1991; Avouac et al., 1993; Lu et al., 1994; Yin et al., 1998; Burchfiel et al., 1999; Allen et al., 1999; Guo et al., 2003), the onset of this deformation in the early Cenozoic remain virtually unconstrained (e.g. Wei et al., Tectonics, 2013). In the early Cenozoic, the

cause of the disappearance of marine deposits has been attributed either to the réactivation of tectonic associated with the India-Asia collision or to sea level fluctuation (e.g. Coutand et al., 2001 ; Bosboom et al., 2011). Based on this lack of knowledge many authors have noted the spatio-temporal differences in the Early Cenozoic uplift of the Tian Shan, as another important issue currently debated for its significant implication on tectonic and climate.

Some rare studies suggest a possible tectonic uplift in Tian Shan during the Paleogene. Cooling ages around 46 Ma were extracted from apatite fission-track analysis in the Chinese CTS, SWTS and Kyrgyz Tian Shan (e.g. Dobrestsov et al., 1996; Du and Wang, 2007; Wang et al., 2010). However, there are scarce sedimentary records corroborating this cooling event in both piedmonts of the Tian Shan. The well-developed conglomerates in the Paleogene Kumugeliemu Formation of the northern Tarim Basin probably reflect a near-source sedimentation that may have been induced by the coeval uplift in the Tian Shan (e.g. Li et al., 2004; Du and Wang, 2007). The provenance of the Kuqa basin sediments also significantly changed during the Paleogene, characterized by an increase in detrital heavy minerals leading some authors to infer Paleogene uplift in the CTS and STS as the initial correspondence of the distant effects of India-Eurasia collision (e.g. Du and Wang, 2007). Another intense debate concerns the timing of the initiation of uplift and rejuvenation in the Tian Shan, yielding the contrasted views respectively as Oligocene (e.g.Windley et al., 1990; Hendrix et al., 1994; Dumitru et al., 2001; Sobel et al., 2006) or Middle-Late Miocene (Avouac et a1., 1993; Abdrakhmatov et a1; 1996; Métivier and Gaudemer, 1997; Bullen et a1., 2001). A Pliocene onset of uplift was even proposed (Burchfiel et al., 1999). To be specific, Cenozoic unroofing in the Tian Shan around ca. 26-24 Ma is evidenced respectively by the apatite fission-track data (e.g. Hendrix et al., 1994; Sobel et al., 2006) and the widely distributed transition in sedimentary facies in the northern piedmont from the Paleogene meandering river to Neogene shore-shallow lacustrine, and the conglomerates developed on the top of the Oligocene Shawan

Formation in the northern piedmont (e.g. Deng et al., 2008). Whereas Middle Miocene rapid uplift initiation was concluded from studies on both of the piedmonts of the Tian Shan (e.g. Charreau et al., 2006; Fang et al., 2006; Du and Wang, 2007; Deng et al., 2008) with the amount of tectonic uplift and exhumation in the Tian Shan increasing progressively from west to east.

Besides, the results from detrital zircon U-Pb geochronology conducted in the southern Junggar Basin suggest a stepwise uplift and exhumation propagated from CTS to NTS during the Late Oligocene to Middle-Late Miocene period (e.g. Chen et al., 2012). This is consistent with the northward propagation of far-field effects of the Indo-Asia collision (e.g. Chen et al., 2012). According to the GPS measurements in the Central Asia, rates of the crustal convergence in the Tian Shan decrease gradually from west to east, suggesting a distinct difference in tectonic deformation between the ETS and WST. This is further interpreted to be induced by northward indention of the Pamir salient and clockwise rotation of the Tarim terrane (e.g. Avouac et al., 1993; Reigber et al., 2001; Shen et al., 2001; Niu et al., 2007; Jiang et al., 2009; Zubovich et al., 2010) although Late Miocene wholesale Tarim tectonic rotation is not favored by paleomagnetic studies (Dupont-Nivet et al., 2002; Bosboom et al., in press in tectonics). Clearly, these studies have so far neglected the Early Cenozoic evolution of the Tian Shan. In this thesis we therefore aim to bridge this gap by providing time constraints on both the deposition and exhumation in this critical period.

As detailed in the following chapters of this thesis, we aim to provide detailed information on the Mesozoic-Cenozoic tectonic evolution and basin-range relations of piedmonts of the Tian Shan, by using magnetstratigraphy, detrital zircon U-Pb geochronology and detrital apatite fission-track analyses both in the northern Tian Shan peidmont (Manasi area) and in the southern Tian Shan piedmont (Ulugqat area), which are ideal laboratories still poorly constrained that will be compared to existing records in the adjacent Kuqa subbasin.

CHAPTER 1

Source to sink relations between the Tian Shan Range and Junggar Basin (northwest China) from Late Paleozoic to Quaternary: evidences from detrital U-Pb zircon geochronology

Wei YANG[a], Marc JOLIVET[b], Guillaume DUPONT-NIVET[a,b,c], Zhaojie GUO[a]*, Zhicheng ZHANG[a], Chaodong WU[a]

[a] *Key Laboratory of Orogenic Belts and Crustal Evolution, Ministry of Education, School of Earth and Space Sciences, Peking University, Beijing, China 100871*

[b] *Géosciences Rennes, Université Rennes 1, UMR 6118,CNRS/INSU, Rennes, France*

[c] *Faculty of Geosciences, Utrecht University, The Netherlands*

** Corresponding author. Tel.: + 86-10-62753545; fax: + 86-10-62758610. E-mail address: zjguo@pku.edu.cn (Z. Guo).*

Abstract

The tectonic evolution of the Tian Shan range, as for most ranges in continental Asia is dominated by north-south compression since the Cenozoic India-Asia collision. However, pre-collision governing tectonic processes remain enigmatic. An excellent record is provided by thick Paleozoic – Cenozoic lacustrine to fluvial depositional sequences that are well preserved in the southern margin of the Junggar Basin and exposed along a foreland basin associated to the Late Cenozoic rejuvenation of the Tian Shan ranges. U/Pb (LA-ICP-MS) dating of detrital zircons from fourteen

sandstone samples from a continuous series ranging in age from latest Paleozoic to Quaternary is used to investigate changes in sediment provenance through time and to correlate them with major tectonic phases in the range. Samples were systematically collected along two nearby sections in the foreland basin. The results show that the detrital zircons are mostly magmatic in origin, with some minor input from metamorphic zircons. The U-Pb detrital zircon ages range widely from 127 to 2856 Ma and can be divided into four main groups: 127-197 Ma (sub-peak at 159 Ma), 250-379 Ma (sub-peak at 318 Ma), 381-538 Ma (sub-peak at 406 Ma) and 543-2856 Ma (sub-peak at 912 Ma). These groups indicate that the zircons were largely derived from the Tian Shan area to the south since a Late Carboniferous basin initiation. The provenance and basin-range pattern evolution of the southern margin of Junggar Basin can be generally divided into four stages: (1) Late Carboniferous – Early Triassic basin evolution in a half-graben or post-orogenic extensional context; (2) From Middle Triassic to Upper Jurassic times, the southern Junggar became a passively subsiding basin until (3) being inverted during Lower Cretaceous – Paleogene; (4) During the Neogene, a piedmont developed along the northern margin of the North Tian Shan block and Junggar Basin became a true foreland basin.

Keywords: Detrital zircon, U-Pb, Provenance, Asia, Tian Shan, Junggar Basin

1.1 Introduction

The Junggar Basin, situated north of the Tian Shan ranges (Fig. 1.1), holds sub-continuous record of the still controversial tectonic evolution of this part of continental Asia. While continental detrital sedimentation initiated in late Paleozoic time, the basin has been rejuvenated as a foreland basin since the late Cenozoic period due to north-south compression induced in this region by the effects of the India-Asia

collision (Burchfiel and Royden, 1991; Avouac et al., 1993; Lu et al., 1994; Yin et al., 1998). Thick accumulations of sediments derived mostly from the Tian Shan range area form the Mesozoic to Quaternary lacustrine to fluvial depositional sequences that are well preserved and exposed in the southern margin of the Junggar Basin (Hendrix, 2000; Fang et al., 2005; Fang et al., 2006a; Wu et al., 2006; Charreau et al., 2009a). The tectonic evolution of the Junggar Basin underwent different stages since the latest Paleozoic, and this evolution is still largely debated. The first divergence between authors concerns the tectonic setting at the basin initiation generally attributed to be Permian in age. Some studies support the idea that the Permian basin was a foreland basin (Carrol et al., 1995; Liu et al., 1994, 2000; Chen et al., 2001; Jia et al., 2003; He et al., 2004), while others considered it as a transtensional basin (Allen et al., 1995; Cai et al., 2000; Chen et al., 2005). Finally Fang et al. (2006c) considered that the Junggar Basin formed as a fault-controlled depression during a Permian extensional tectonic episode. Another important, and still enigmatic issue is the Mesozoic setting of the Junggar Basin with contrasting hypothesis involving: an extensional basin (Li and Chen, 1998; Liu et al., 2000), a continental depression basin (Xu et al., 1997a, 1997b; Chen et al., 2002; Jolivet et al., 2010), or a foreland basin associated to the collision of the Qiangtang terrane to the south (Hendrix et al., 1992; Zhang et al., 1999; Chen et al., 2002). Several studies showed that the Tian Shan ranges existed as a positive physiographic feature during the Mesozoic (Hendrix et al., 1992; Dumitru et al., 2001; Jolivet et al., 2010; Chen et al., 2011). However, Hendrix (2000) suggested that during the Early-Middle Jurassic, the range could not be considered as a towering topography significantly separating climate patterns. This suggests that the Mesozoic Tian Shan, together with its adjacent regions, may have been under an extensional tectonic setting resulting from post-orogenic relaxation after the Permian collision (Guo et al., 2005, 2006; Fang et al., 2006a). These contrasting hypotheses put forward the necessity to look for more effective evidences in order to correctly

understand the tectonic setting of the Junggar Basin at different stages since its late Paleozoic inception.

Detrital zircon U-Pb chronology has become a powerful tool for provenance and geodynamic studies (e.g. Fedo et al., 2003; Gehrels et al., 2003; Prokopiev et al., 2008). The systematic study of variations through time of characteristic detrital zircon ages populations obtained from sedimentary sequences in basins can reflect the changes in basin-range relationship. The complete (or near complete) late Paleozoic to Quaternary lacustrine to alluvial fan sedimentary series are exposed along the southern margin of the Junggar Basin. A detailed study of the U-Pb detrital zircon age populations in those series may thus provide detailed information on the evolution of the sediment sources and the palaeo-drainage system. In this study, 14 sandstone samples (Fig. 1.2) from upper Paleozoic to Quaternary strata were collected along two sections on the southern margin of the Junggar Basin in order to perform U-Pb (LA-ICP-MS) dating of detrital zircons. The results are used to discuss the behavior of the Junggar Basin through time, as well as the characteristic phases of interaction between the basin and the Tian Shan range.

1.2 Geological setting

1.2.1 General evolution of the Tian Shan range

The present-day Tian Shan range extends through western China, Kazakhstan and Kyrgyzstan and represents an important part of the Central Asian Orogenic Belt (CAOB) (see for example Windley et al., 2007 for a complete synthesis of the evolution of the CAOB). The lithosphere of the Tian Shan orogenic belt results from complex accretions of island arcs and amalgamation of continental lithospheric blocks during the late Paleozoic (Watson et al., 1987; Coleman, 1989; Gao et al., 1998; Carroll et al., 1990, 1992, 1995; Allen et al., 1992; Windley et al., 1990, 2007; Shu et

al., 2002; Xiao et al., 1992, 2004; Charvet et al., 2004, 2007, 2011; Glorie et al., 2010). The following summary of the geological history of Tian Shan, is supported by a review of available U/Pb ages on zircons obtained for various granitoids and host rocks presented on Fig. 1.1.

The Tarim – South Tian Shan (STS) and Central Tian Shan blocks (CTS) collided during Late Devonian – Early Carboniferous. This accretion was followed during Late Carboniferous – Early Permian by the collision of the newly formed Tarim – Central Tian Shan terrane with a series of late Paleozoic island arcs now forming the Northern Tian Shan (NTS) (e.g. Huang et al., 1980; Wang et al., 1990; Allen et al., 1992; Biske and Seltmann, 2010; Han et al., 2010; Charvet et al., 2011). The CTS basement is mainly composed of metamorphic Proterozoic series extensively intruded by granitic plutons ranging in age between 380 and 490 Ma (Zhou et al., 2001; Han et al., 2004; Glorie et al., 2010). The second accretion episode is marked in CTS and NTS by the occurrence of numerous Early Permian (295 – 280 Ma from U/Pb on zircons) postcollisional A-type granites that cross-cut the Paleozoic structures (e.g. Konopelko et al., 2007; Gao et al., 2009; Wang et al., 2009; Glorie et al., 2010). Zircon (U-Th)/He ages from the CTS confirm the occurrence of a major cooling phase in Early Permian (Jolivet et al., 2010). The compressive structures that formed during those various episodes of accretion were then reworked by late Paleozoic strike-slip shear zones such as the Main Tian Shan Shear Zone (MTSZ) that separates the CTS from the NTS (e.g. Laurent-Charvet et al., 2002, 2003; Allen et al., 1995). Numerous Permian 40Ar/39Ar and K-Ar ages on muscovite and biotite from the MTSZ or similar major structures indicate that this shearing phase probably ended in Late Permian or Early Triassic (e.g. Shu et al., 1999; Chen et al., 1999; Laurent-Charvet et al., 2002).

The Tian Shan area was then reactivated by the successive terrane collision onto the south Asian margin during the Early Mesozoic (Hendrix et al., 1992; Dumitru et al.,

2001; Greene et al., 2005; Lu et al., 2010; Jolivet et al., 2010). Apatite fission track and (U-Th)/He data from the CTS and the southern edge of the NTS demonstrate that the Permian exhumation phase has been subsequently overprinted by an Early Jurassic cooling phase (Dumitru et al., 2001; Jolivet et al., 2010) probably related to the far-field effects of the final collision between the Qiantang and Kunlun blocks (e.g. Jolivet et al., 2001; Roger et al., 2010, 2011).

Strong erosion during the Triassic and Early Jurassic initiated a phase of general peneplanation of the Paleo-Tian Shan range that was probably already well evolved by Early-Middle Jurassic times (Shu et al., 2004). This Mesozoic erosion phase has been widely recognized throughout Central Asia (e.g. Jolivet et al., 2007, 2009, 2010, 2011; Vassallo et al., 2007). However, apatite fission track data from the NTS as well as the occurrence of coarse sediments in the surrounding basins (Yili and Junggar) suggest that recurrent, small magnitude vertical movements occurred in the range during Late Jurassic and Early Cretaceous (Dumitru et al., 2001; Jolivet et al., 2010) implying that peneplanation of the range was probably not complete. De Grave et al. (2004, 2007) and Glorie et al. (2010) report similar observations in the Kyrgyz Tian Shan. Sedimentological data within the surrounding basins indicate that by Late Jurassic - Cretaceous, and possibly onward, the largely peneplaned Tian Shan region may have been affected by an extensional tectonic setting induced by post-orogenic relaxation (Shu et al., 2004; Guo et al., 2005, 2006; Fang et al., 2006a). This was associated with the renewed development of the adjacent basins.

Finally, during late Cenozoic, the Tian Shan area has again been reactivated by the distant effects of the India-Eurasia collision, leading to the formation of the actual intracontinental orogenic belt (Molnar and Tapponnier, 1975; Tapponnier and Molnar, 1977, 1979; Burchfiel and Royden, 1991; Avouac et al., 1993; Lu et al., 1994; Yin et al., 1998; Burchfiel et al., 1999; Allen et al., 1999; Dumitru et al., 2001; Guo et al., 2003; Buslov et al., 2004, 2007; Jolivet et al., 2010).

1.2.2 General evolution of the Junggar Basin

The Junggar Basin is divided in six structural units (e.g. Li, 1993; Qiu et al., 2008). The deepest one, lying along the northern edge of the Tian Shan range, is the Southern depression that collected about 16 km of sediments since Permian time. Its basement is mainly composed of Carboniferous volcanic rocks. The Permian magmatism occurring in the Junggar Basin and its adjacent regions is generally attributed to a tensional and continental rift tectonic setting (Kovalenko et al., 1996; Han et al., 1997; Jahn et al., 2000a, 2000b; Jahn, 2004) for which clear evidence is reported from the Bogda region, the eastern Junggar Basin and the Turpan-Hamin Basin (Han et al., 1999; Wartes et al., 2002; Shu et al., 2004). However, as already exposed in the introduction, the initiation of the Junggar basin is still largely discussed both in terms of timing and initiating mechanism. If most of the authors agree that the basin initiated during the Permian, some studies consider that it could be have evolved as a half-graben during Late Carboniferous (e.g. Qiu et al., 2005).

Following inception, many authors consider the Mesozoic Junggar Basin as a foreland basin (Hendrix et al., 1992; Graham et al., 1993; Zhang et al., 1999; Chen et al., 2002), with the Tian Shan ranges existing as a positive physiographic feature at least during Triassic and Jurassic times (Hendrix et al., 1992; Dumitru et al., 2001). However, based on the widespread Lower and Middle Jurassic series including well developed coal strata and concentrated thick coal seams, many others consider the tectonic setting as a thermally subsiding basin associated to a paleo-range which was progressively eroded away without much tectonic activity (Dumitru et al., 2001; Fang et al., 2005; Vassallo et al., 2007; Jolivet et al., 2007, 2010; Glorie et al., 2010).

The present-day southern margin of the Junggar Basin exposes three rows of late Cenozoic fault-propagation folds formed successively towards the north in the foreland (Avouac et al., 1993; Burchfiel et al., 1999; Deng et al., 2000; Lu et al., 2010; Li et al., 2010, 2011). These folds are referred from south to north as the piedmont

belt, the Huoerguosi-Manas-Tugulu belt and the Dushanzi-Anjihai belt (Fig. 1.2). The southernmost piedmont belt consists of several anticlines formed during Late Miocene to Pliocene, such as the Qigu anticline (Avouac, 1993; Lu et al., 2010; Li et al., 2010). The northernmost Dushanzi-Anjihai anticlines evolved during the Late Pliocene-Early Pleistocene (Avouac et al., 1993). This Neogene tectonic activity induced uplift and erosion of the Mesozoic sedimentary series along the southern edge of the Junggar Basin (Fig. 1.2).

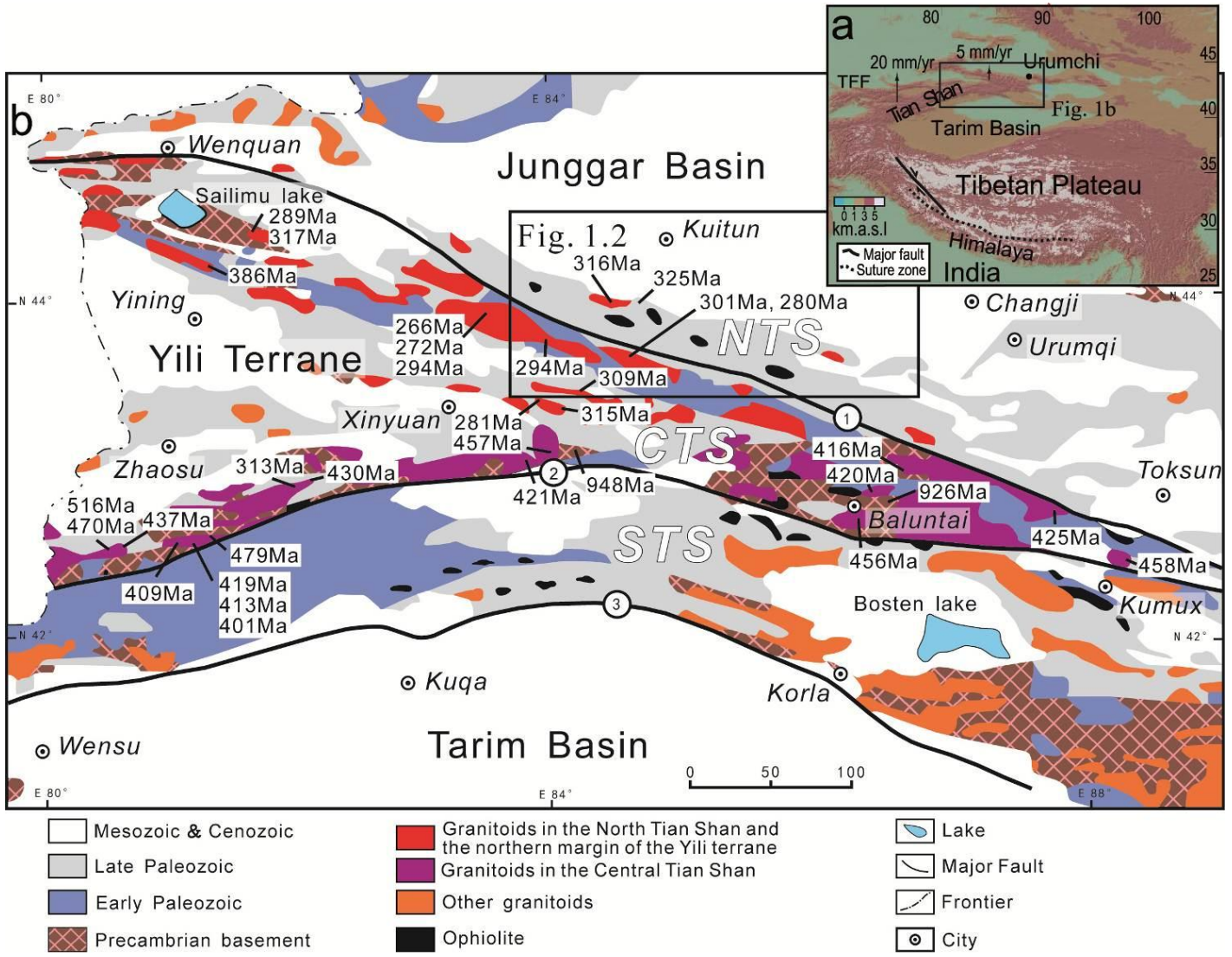
a
80
90
100
45
40
35
30
25
20 mm/yr
5 mm/yr
Urumchi
TFF
Tian Shan
Fig. 1b
Tarim Basin
Tibetan Plateau
0 1 3 5
km.a.s.l
Himalaya
Major fault
Suture zone
India
b
E 80°
E 84°
E 88°
N 44°
N 42°
Wenquan
Junggar Basin
Sailimu lake
289Ma
317Ma
386Ma
Fig. 1.2
Kuitun
316Ma
325Ma
301Ma, 280Ma
Changji
Urumqi
Yining
Yili Terrane
266Ma
272Ma
294Ma
294Ma
309Ma
315Ma
NTS
Xinyuan
281Ma
457Ma
CTS
416Ma
420Ma
926Ma
Toksun
Zhaosu
313Ma
430Ma
421Ma
948Ma
Baluntai
516Ma
470Ma
437Ma
479Ma
419Ma
413Ma
401Ma
409Ma
STS
425Ma
456Ma
458Ma
Bosten lake
Kumux
Kuqa
Korla
Wensu
Tarim Basin
0
50
100
1
2
3
Mesozoic & Cenozoic
Late Paleozoic
Early Paleozoic
Precambrian basement
Granitoids in the North Tian Shan and the northern margin of the Yili terrane
Granitoids in the Central Tian Shan
Other granitoids
Ophiolite
Lake
Major Fault
Frontier
City

Fig. 1.1 (a) Digital elevation model (GTOPO90) of the Indo-Asia collision zone. Arrows indicate GPS-derived shortening estimates. TFF: Talas Fergana Fault (modified from Li et al., 2011). (b) Geological and tectonic sketch map of the southern margin of Junggar Basin and adjacent regions with the approximate location of Fig. 2 shown with a box. ① The northern margin fault of central Tianshan Mountains ② The southern margin fault of central Tianshan Mountains ③ The northern Tarim margin fault. NTS = Northern Tian Shan; MTS = Middle Tian Shan; STS = Southern Tian Shan (modified from CHARVET, J. et al., 2011). The age data obtained in NTS and the northern margin of the Yili terrane come from Xu et al. 2005 and 2006, Li et al. 2007, Wang et al. 2007, Tang et al. 2008, Chen et al. 2010a and 2010b, Han et al. 2010, Tong et al. 2010, Gao et al. 2011 and Li et al. 2011; the age data obtained in CTS come from Han et al. 2004, Yang et al. 2006, Long et al. 2007, Su et al. 2008, Hu et al. 2010, Tong et al. 2010 and Long et al. 2011.

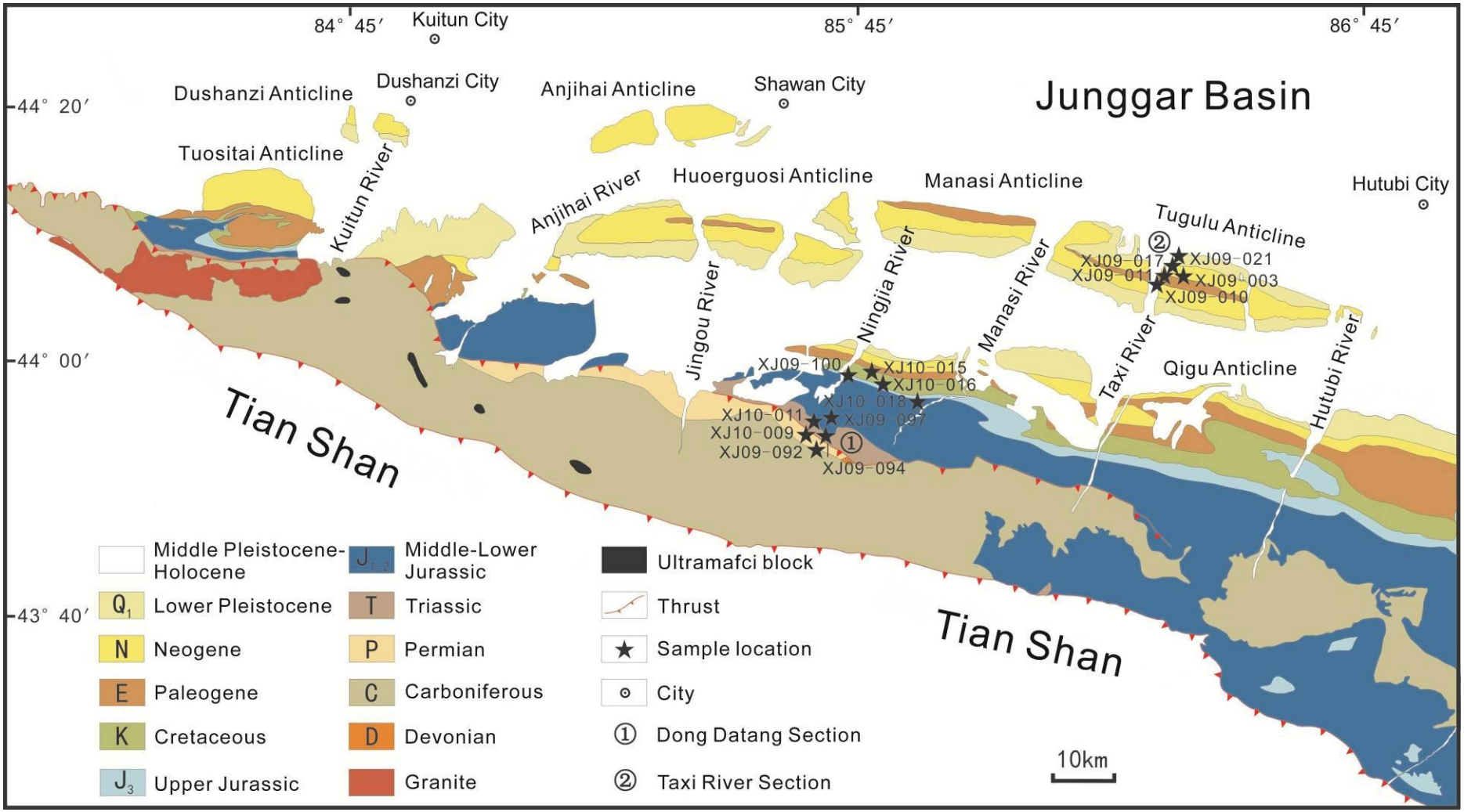
84° 45′
Kuitun City
85° 45′
86° 45′
Junggar Basin
Dushanzi Anticline
Dushanzi City
Anjihai Anticline
Shawan City
44° 20′
Tuositai Anticline
Kuitun River
Anjihai River
Huoerguosi Anticline
Manasi Anticline
Hutubi City
Tugulu Anticline
②
XJ09-017
XJ09-021
XJ09-011
XJ09-003
XJ09-010
Jingou River
Ningjia River
Manasi River
Taxi River
Hutubi River
Qigu Anticline
44° 00′
XJ09-100
XJ10-015
XJ10-016
XJ10-018
XJ10-011
XJ09-097
XJ10-009
①
XJ09-092
XJ09-094
Tian Shan
Tian Shan
43° 40′
Middle Pleistocene-Holocene
Q1 Lower Pleistocene
N Neogene
E Paleogene
K Cretaceous
J3 Upper Jurassic
J1-2 Middle-Lower Jurassic
T Triassic
P Permian
C Carboniferous
D Devonian
Granite
Ultramafci block
Thrust
Sample location
City
① Dong Datang Section
② Taxi River Section
10km

Fig. 1.2 Geological setting of the southern margin of the Junggar Basin with samples locations (map modified from Li et al., 2011).

1.3 Stratigraphy and sedimentary characteristics

The studied Dong Datang and Taxi He sections (Fig. 1.2) have been chosen for their exceptional preservation and exposure of the Permian to Quaternary sedimentary series along the southern margin of the Junggar Basin (Fang et al., 2007). For a comprehensive understanding of the basin evolution, a summary of the observed and published descriptions of lithologies, depositional systems, paleocurrent measurements and general environmental cycles through time is presented (Fig. 1.3).

The Permian series consist of the Aerbasayi Formation, the Quanzijie Formation and the Wutonggou Formation, which are mainly composed of tuffaceous conglomerates, breccia, andesite porphyry and pebbly coarse-grained sandstones. The depositional environments evolved from an alluvial fan – braided river system in the Aerbasayi Formation to a braided river and delta system in the Upper Permian Wutonggou Formation indicating a slight retrogradation phase (note that in this study, as the Junggar basin is not connected to the sea, we use the terms progradation and retrogradation with respect to the position of the lacustrine environment. For example, a complete progradation sequence will correspond to a progressive shift in depositional environment from lake sediments towards coarse alluvial fan sediments).

The Triassic series can be divided into the Shangcangfanggou Group and the Xiaoquangou Group. The sediments are brown-grey-coloured mudstones, argillaceous siltstones, litharenites, and sandy mudstones. The Lowermost Shangcangfanggou Group is characterized by typical braided river to deltaic sandy

conglomerates (Wu et al., 2006) while the Xiaoquangou Formation was deposited in an alluvial plain to shallow lacustrine system. The facies evolution towards a lacustrine environment reinforces the general retrogradation phase initiated in the Permian. However, Hendrix et al. (1992) report alluvial and braided river facies in the Upper Triassic series of the nearby Manas section which suggesting lateral facies variations probably due to local topography. Paleocurrent measurements (Hendrix et al., 1992) indicate an E-W drainage system in the Upper Triassic (Fig. 1.3).

The Jurassic series, showing a maximum thickness over 4000 m, are broadly distributed with both the local depocenter and subsidence center located next to the Changji area (Fig. 1.1) (Fang et al., 2005). The sequence consists of the Lower Jurassic Badaowan Formation and Sangonghe Formation, the Middle Jurassic Xishanyao Formation and Toutunhe Formation, and finally the Upper Jurassic Qigu Formation and Kalazha Formation (Wu et al., 2006; Fang et al., 2005, 2006a, 2007).

The Badaowan Formation, lying uncomformably on the Triassic series, is composed of mudstones interbedded with gray sandstones in the lower part and interbedding of sandy mudstones and sandstones (containing thin coal layers or coal streaks) in the upper part. These sediments were deposited in a braided river to shallow lacustrine environment (Fig. 1.3). Paleocurrents are mostly oriented towards the NE but Hendrix et al. (1992) report NNW to W paleocurrent directions in the Manas section.

The following Sangonghe Formation is mainly composed of grey-green mudstones and sandstones, containing thin coal streaks and coal layers. The facies correspond to alluvial plain and lacustrine deposits. Paleocurrents are oriented towards the north in our section and towards the W – NW in the Manas section (Hendrix et al., 1992). During the Lower Jurassic, the Junggar Basin underwent two

large-scale lacustrine transgressions (Fang et al., 2005) which are consistent with the general retrogradation phase observed in our data.

The thickness of the Xishanyao Formation is the largest, and may locally exceed 1000 m. Celadon (pale-grey to green) sandstones and mudstones rich in coal layers and coal streaks which can be regarded as the characteristics of lake swamp deposits are ubiquitous in that formation. Thick coal layers are often found in the middle and lower parts. Paleocurrents are oriented towards the NNW in our section and towards the NNE in the Manas section (Hendrix et al., 1992). The Chepaizi-Mosuowan low uplift, located in the northern side of the southern margin of the Junggar Basin (north of Fig. 1.2), began to develop during the depositional period of the Xishanyao Formation. However, the general northward paleocurrents direction indicates that the source area was still to the south and that the Chepaizi-Mosuowan uplift had little influence on the established drainage system that provided sediments to this area of the basin.

The Middle Jurassic Toutunhe Formation is mainly composed of mottled mudstones, sandy mudstones and sandstones, representing a braided-river sedimentary environment. This shift between a mainly lacustrine environment in the Xishanyao Formation to a braided river environment marks the onset of a progradation phase. The amount of red banded sediment occurring in the Xishanyao formation increases up section, indicating that the climate became gradually dry (Fang et al., 2005). Although the Chepaizi-Mosuowan low uplift developed further during that time, the northwestward directed paleocurrents indicate that this uplift still has little effect on the drainage system in the studied area.

There is an obvious local unconformity between the underlying Toutunhe Formation and the overlying Upper Jurassic Qigu Formation (although this one is not observed by Hendrix et al. (1992) in the Manas section). The Qigu sediments are mostly composed of interbedding of brown-purple mudstones and sandstones, with

the mudstone mainly restricted to the upper part, and thin-bedded limestone interbedded at the bottom. These sediments were deposited in a shallow lacustrine to alluvial plain environment, with paleocurrents still oriented towards the NW in the Manas section where the Qigu Formation reaches its greatest thickness (about 683 m) (Hendrix et al., 1992).

The Upper Jurassic Kalazha Formation is formed by a typical brown-reddish thick-bedded conglomerate, also called the "Kalazha red dyke". This conglomerate corresponds to a large alluvial fan deposit representing the last stage of the progradation event initiated during the Middle Jurassic Xishanyao Formation (Fig. 1.3). Paleocurrents in the Manas section are oriented NW or NE (Hendrix et al., 1992). During the sedimentation of the Qigu and Kalazha formations, the Chepaizi-Mosuowan uplift was still continuously active (Fang et al., 2005). The slight spread in paleocurrents directions (Fig. 1.3) may indicate a possible effect of this growing relief on the drainage pattern. However, the source area of the sediments is still situated toward the south.

The Cretaceous series in the southern margin of the Junggar Basin, consists in the Tugulu Group and the Donggou Formation. The sediments of the Tugulu Group are mainly composed of celadon mudstones interbedded with sandstones deposited in a lacustrine environment. Paleocurrents from the Manas section are again NW or NE directed (Hendrix et al., 1992). However, measurements of paleocurrent directions in lacustrine environments should only be considered as indicative. The Tugulu Group marks the onset of a new progradation phase that initiated from the sharp change between the alluvial fan of the Kalazha Formation and the lacustrine environment of the Lower Tugulu Group. The Donggou Formation is mainly composed of celadon mudstones, sandstones and conglomerates corresponding to alluvial to braided river system. Paleocurrents directions are mainly unchanged.

The Palaeogene series consist of the Ziniquanzi Formation, the Anjihaihe Formation and the Shawan Formation. Unfortunately no paleocurrent measurements are available for the Tertiary section. The Ziniquanzi Formation is mainly characterized by purplish red mudstones and sandstones corresponding to a lacustrine environment. The Anjihaihe Formation is mainly composed of mottled mudstones and sandy mudstones interbedded with sandstones, which are again characteristic of lacustrine environments (Fig. 1.3). The Shawan Formation consists in reddish-brown pelitic siltstones, mudstones and glutenite interlayers deposited in a lacustrine to alluvial plain environment. The lake depth reached its maximum during the sedimentation of the Anjihaihe Formation (Fang et al., 2006b; Charreau et al., 2008). However, this major lacustrine phase seems to represent an isolated event within a general progradation phase that initiated in the Lower Cretaceous. Although we have no constraints on the forces that drive these changes in depositional environments, climate variations associated to a generally low tectonic activity may induce the observed recurrent changes between lacustrine and alluvial plain systems.

The Neogene series are divided into the Taxihe Formation and the Dushanzi Formation, which are both characterized by their great thickness (locally exceed 2000 m). The Taxihe Formation is mainly composed of reddish-brown sandy conglomerates and pelitic sandstones deposited in an alluvial plain environment. The Dushanzi Formation contains brown sandy mudstones, fine graywackes and conglomerates characteristic of a braided river system.

Finally, the Quaternary Xiyu Formation is characterized by a typical conglomerate, interbedded with gray medium-grained litharenite and sandy mudstone (BGMRXUAR, 1978, 1993, 2008; Wang et al., 2000a; Fang et al., 2007; Charreau et al., 2009b). It corresponds to a series of major alluvial fan deposits

which represent the maximum of the general progradation phase that initiated in Early Cretaceous.

1.4 Sampling and analytical methods

Fourteen sandstone samples ranging in age from the latest Paleozoic to the Quaternary were collected from two field sections to the southern Junggar Basin (Fig. 1.3). Nine samples of upper Paleozoic-Mesozoic strata were selected from the western Dong Datang profile, and 5 samples of Cenozoic strata from the eastern Taxi He profile (Fig. 1.2). Due to the short distance separating the two profiles, the sources of the sediments in both of them may generally be considered as similar. The major characteristics of the samples are described in Table 1.

Detrital heavy minerals were separated from sandstone samples by the standard procedures used for mineral separation (Li et al., 2004). This work was conducted by the Chengxin Geology Service Co. Ltd, Langfang, Hebei Province, China. Zircons were specifically extracted using heavy liquids and magnetic techniques and finally purified by hand picking and careful identification under a binocular microscope. A quantity of zircon grains (generally more than 200 grains) were randomly selected with a steel pin and mounted on adhesive tape then enclosed in epoxy resin and polished to yield a smooth flat internal surface (slice). After being photographed under reflected and transmitted light, the samples were prepared for cathodoluminescence (CL) imaging, in order to choose potential internal target sites for U-Pb dating (Yuan et al., 2007; Long et al., 2010).

Cathodoluminescence (CL) imaging was carried out using a HITACHI S3000-N Scanning Electron Microscope at the Institute of Geology, Chinese Academy of Geological Sciences. CL images of typical zircon grains are presented in Figure. 5. LA-ICP-MS (Laser Ablation-Inductively Coupled Plasma-Mass Spectrometer) U-

Pb dating was conducted on an Agilent 7500a ICP-MS connected to a 193nm Excimer laser ablation system of American New Wave UP 193 SS at the China University of Geosciences, Beijing. The operating parameters were as follows: Ar plasma gas flow rate was 1.13l/min, RF (Radio Frequency) power was 1350W, and elemental integral time was 20 ms for U, Th, Pb and 15ms for other elements (Si, Ti and Zr). Helium with a flow rate of 0.7l/min was used as the carrier gas to enhance the transport efficiency of the ablated material. The spot diameter was 36 μm and 25 μm. The analytical laser frequency was 10Hz, and each analysis consisted in 5 s pre-denudation and 45 s signal acquisition. The GLITTER 4.4 software was used to calculate the U-Pb isotope ratios and element contents. Age calculations, plotting of relative probability and concordia diagrams were made using ISOPLOT (version3.0) (Ludwig, 2003). Standard zircon Tomorrow (Black et al., 2003; Qi et al., 2005) was used as an external standard for correction of isotopic ratios to calculate U-Pb ages, while zircons Qinghu and 91500 (Wiedenbeck et al., 1995) were the monitoring standards. For elemental concentration analysis, NIST610 was the external standard, and ^{29}Si was the internal standard. Meanwhile, NIST612 and NIST614 were used as the monitoring standard. The common-Pb correction was performed following the method described by Andersen (2002). A detailed description of the technical procedure is given in Yuan et al. (2004).

For usual U-Pb (LA-ICP-MS) dating of detrital zircons, about 80-120 grains for each sample can meet the requirements of statistical analysis of basic age distribution (Andersen, 2005). In this study, except for sample XJ10-009, 100 grains from each sample were selected randomly for analysis such that, the results should reflect the provenance characteristics. Those ages with discordance degree ＞10% were excluded from analysis (Gehrels et al., 2003; Prokopiev et al., 2008). Isotopic ages with errors and related raw data are listed in full as appendix 1.

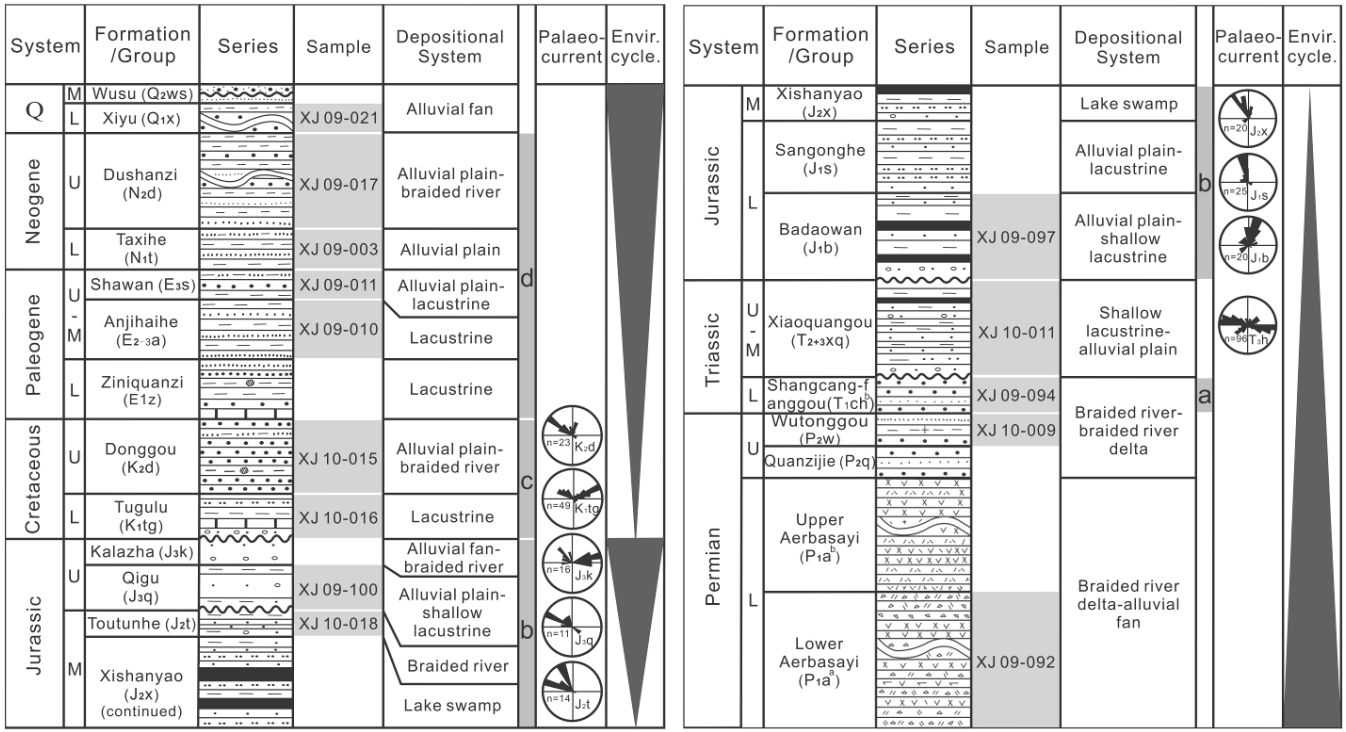
System
Formation /Group
Series
Sample
Depositional System
Palaeo-current
Envir. cycle.
Q
Neogene
Paleogene
Cretaceous
Jurassic
Wusu (Q2ws)
Xiyu (Q1x)
Dushanzi (N2d)
Taxihe (N1t)
Shawan (E3s)
Anjihaihe (E2-3a)
Ziniquanzi (E1z)
Donggou (K2d)
Tugulu (K1tg)
Kalazha (J3k)
Qigu (J3q)
Toutunhe (J2t)
Xishanyao (J2x) (continued)
XJ 09-021
XJ 09-017
XJ 09-003
XJ 09-011
XJ 09-010
XJ 10-015
XJ 10-016
XJ 09-100
XJ 10-018
Alluvial fan
Alluvial plain-braided river
Alluvial plain
Alluvial plain-lacustrine
Lacustrine
Alluvial fan-braided river
Alluvial plain-shallow lacustrine
Braided river
Lake swamp
Xishanyao (J2x)
Sangonghe (J1s)
Badaowan (J1b)
Xiaoquangou (T2+3xq)
Shangcang-fanggou (T1ch)
Wutonggou (P2w)
Quanzijie (P2q)
Upper Aerbasayi (P1a)
Lower Aerbasayi (P1a)
XJ 09-097
XJ 10-011
XJ 09-094
XJ 10-009
XJ 09-092
Lake swamp
Alluvial plain-lacustrine
Alluvial plain-shallow lacustrine
Shallow lacustrine-alluvial plain
Braided river-braided river delta
Braided river delta-alluvial fan

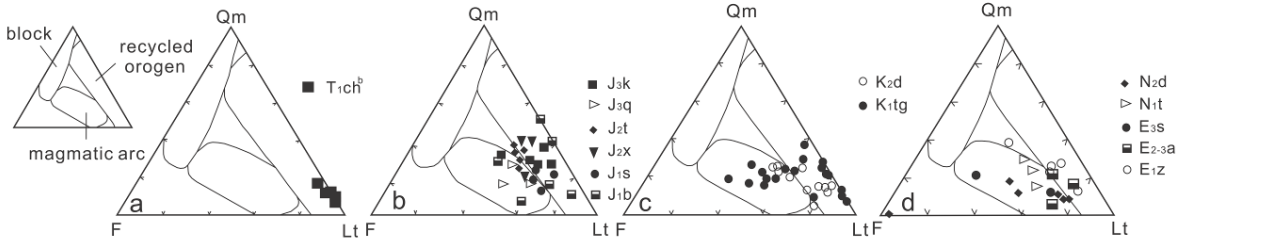
block
recycled orogen
magmatic arc
Qm
F
Lt
a
b
c
d
T1ch
J3k
J3q
J2t
J2x
J1s
J1b
K2d
K1tg
N2d
N1t
E3s
E2-3a
E1z

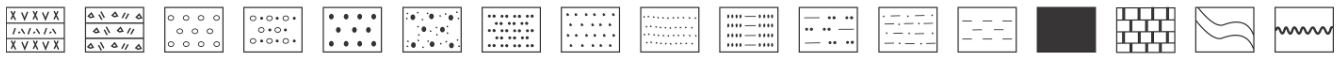
1
2
3
4
5
6
7
8
9
10
11
12
13
14
15
16
17

Fig. 1.3 Generalized stratigraphic column of the studied Permian to Quaternary series (modified after BGMRXUAR, 1978; Fang et al., 2005). See text for series descriptions and depositional environments. Paleocurrents are from Hendrix et al. (1992) and Fang et al. 2005, and sandstone compositional data from Fang et al. 2006a. 1 Andesite porphyry; 2 Tuffaceous conglomerate, breccia; 3 Conglomerate; 4 Litharenite; 5 Coarse-grained sandstone; 6 Alluvial litharenite, sandy conglomerate; 7 Siltstone; 8 Medium-grained sandstone; 9 Fine sandstone; 10 Pelitic sandstone; 11 Pelitic siltstone; 12 Sandy mudstone; 13 Mudstone; 14 Coal layers, coal streaks; 15 Limestone; 16 Cross bedding; 17 Unconformity.

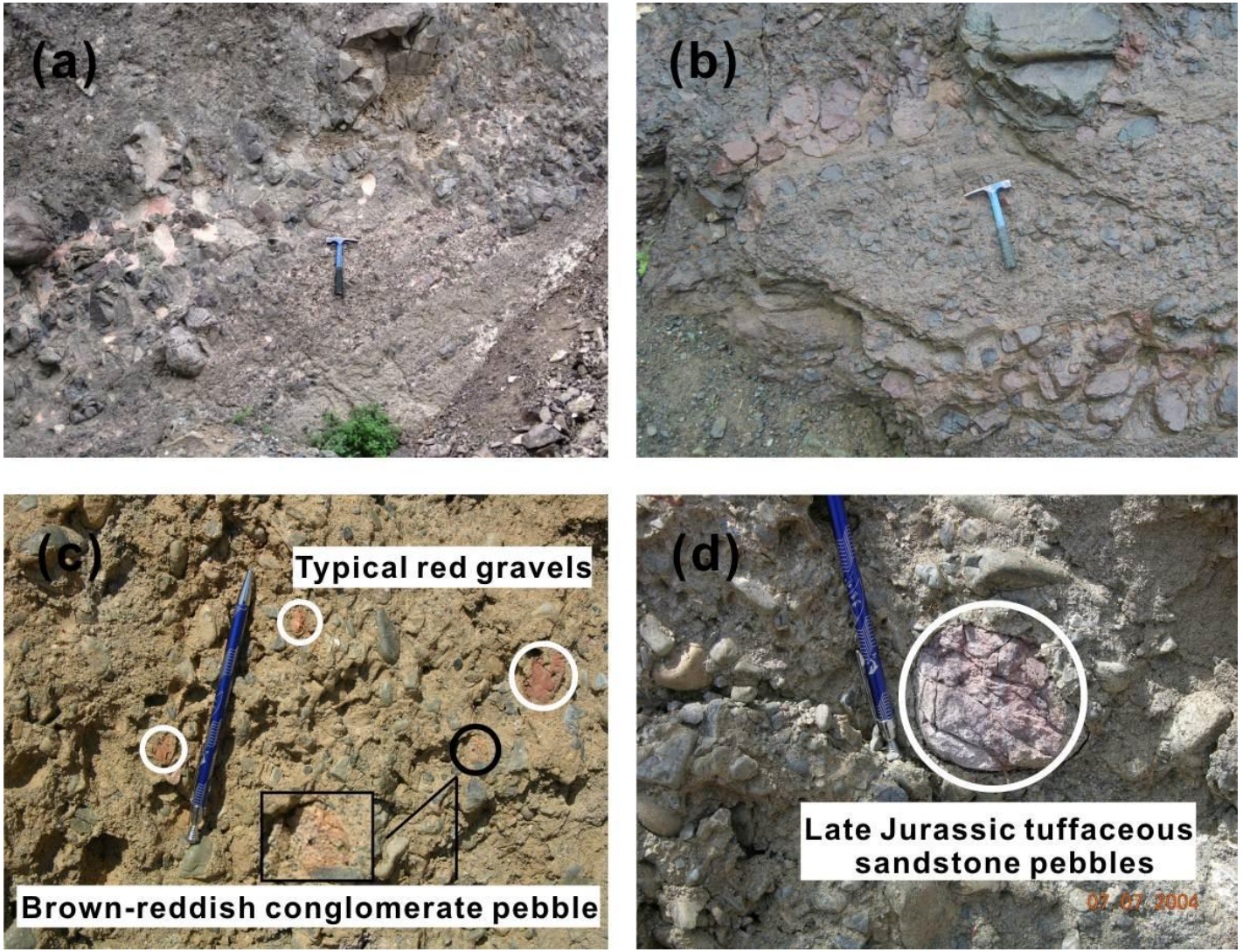
(a)
(b)
(c)
Typical red gravels
Brown-reddish conglomerate pebble
(d)
Late Jurassic tuffaceous sandstone pebbles
07.07.2004

Fig. 1.4 (a) Volcanic-sedimentary sequences of the Aerbasayi Formation; (b) Characteristic gravels from conglomerates of the volcanic-sedimentary sequences; (c) Typical red gravels and pebbles of the Late Jurassic Qigu Formation (white circles) and brown-reddish conglomerate pebbles of the Kalazha Formation found in the Dushanzi Formation conglomerate (black circles); (d) Late Jurassic tuffaceous sandstone pebbles found in the Dushanzi Formation conglomerate (white circles).

Table 1.1 Summary of major characteristics of the samples.

System	Formation/group	Sample code	Lithofacies
Quaternary	Xiyu Fm.	XJ09-021	Medium-grained litharenite contained in sandy conglomerate alternating beds of the Xiyu conglomerate
Neogene	Dushanzi Fm.	XJ09-017	Medium-coarse-grained sandstones contained in a sandstone lens, associated with interbedded sand and gravel, in which the conglomerates are dominant
	Taxihe Fm.	XJ09-003	Grey-green coarse-grained sandstones
Palaeogene	Shawan Fm.	XJ09-011	Grey-green medium-coarse-grained sandstones
	Anjihaihe Fm.	XJ09-010	Khaki medium-grained sandstones
Upper Cretaceous	Donggou Fm.	XJ10-015	Grey-green coarse-grained sandstones
Lower Cretaceous	Qingshuihe Fm.	XJ10-016	Grey-green coarse-grained sandstones
Upper Jurassic	Qigu Fm.	XJ09-100	Reddish-brown coarse-grained sandstones
Middle Jurassic	Toutunhe Fm.	XJ10-018	Grey-green coarse-grained sandstones
Lower Jurassic	Badaowan Fm.	XJ09-097	Yellow-green pebbly coarse-grained sandstones
Middle-Upper Triassic	Xiaoquangou Group	XJ10-011	Grey-green pebbly coarse-grained sandstones
Lower Triassic	Shangcangfanggou Group	XJ09-094	Grey coarse-grained sandstones associated with purplish red medium-grained sandstones
Upper Permian	Wutonggou Fm.	XJ10-009	Mottled pebbly coarse-grained sandstones
Lower Permian	Aerbasayi Fm.	XJ09-092	Mottled pebbly coarse-grained sandstones within volcanic-sedimentary sequences in the lower sub-formation

1.5 Results

The various zircon age groups and the corresponding statistical data for every sample are shown in Table 1.2.

1.5.1 Paleozoic Samples

A total of 100 zircon grains were measured from Lower Permian sample XJ09-092 collected from the Aerbasayi Formation, and 97 effective data points were obtained. U-Pb ages range from 280 to 1500 Ma, with 94 ages ranging from 280 to 373 Ma (Fig. 1.6). Most of these 94 crystals are characterized by relatively distinct oscillatory zoning in CL images (Fig. 1.5), indicative of a magmatic origin, while the rest mostly show faint zoning in CL images, suggesting a metamorphic origin (Hanchar and Rundnick, 1995; Hoskin and Black, 2000; Corfu et al., 2003). The other ages are 456-460 Ma (two grains) and 1500 Ma (one grain), respectively. These zircon grains all show oscillatory zoning indicative of a magmatic origin. The Th/U ratios of the 97 zircon grains range from 0.4 to 2.24, also indicating magmatic zircons (Hoskin and Black, 2000).

Due to the small amount of grains available in sample XJ10-009 (Upper Permian Wutonggou Formation), only 31 zircon grains satisfied the test conditions, and 30 effective data points were obtained. U-Pb ages range from 250 to 2553 Ma, and can be divided into three groups: 250-362 Ma (9 grains), 434-508 Ma (5 grains) and 624-2553 Ma (16 grains). The 14 zircons ranging in age from 250 to 508 Ma are dominantly characterized by oscillatory zoning in CL images (Fig. 1.5), indicative of a magmatic origin. The remaining grains, ranging in age from 624 to 2553 Ma, mostly show the characteristics of metamorphic zircons. The Th/U ratios of the 31 zircon grains vary from 0.16 to 1.32, significant decrease compared to the sample XJ09-092 due to an increase in the proportion of metamorphic zircons. Again, due to the small number of analyzed crystals, the age populations derived from this sample are simply indicative and maybe have no real statistical meaning.

1.5.2 Mesozoic Samples

One hundred zircon grains were randomly selected from each of the 7 samples of Lower Triassic (Shangcangfanggou Group) to Upper Cretaceous (Donggou Formation). Between 100 and 97 effective data points were obtained from these samples (Table 1.2).

Like for the previous Paleozoic samples, the age groups are defined from the age of the series forming the range: the Mesozoic ages; the late Paleozoic ages corresponding to the late Paleozoic magmatic belt (the Upper limit is 250 Ma, the boundary between Permian to Triassic, and the Lower limit is 380 Ma, corresponding to the final emplacement of the granitic plutons in CTS (380-490 Ma); the early and middle Paleozoic ages partly corresponding to the Paleozoic magmatic rocks in the CTS (380 Ma to 542 Ma); and finally the Precambrian ages.

The U-Pb ages from the 7 samples range from 127 to 2852 Ma, and can be mainly divided into 4 groups as follow: 127-183 Ma, 250-379 Ma, 382-538 Ma and 543-2852 Ma. In addition, a minority of ages range from 207 to 249 Ma (24 grains) (Fig. 1.6). The zircons yielding an age between 127 and 183 Ma mainly appear in the samples from the Middle Jurassic Toutunhe Formation, the Upper Jurassic Qigu Formation, the Lower Cretaceous Qingshuihe Formation (Tugulu Group) and the Upper Cretaceous Donggou Formation. Most of these grains show well-zoned crystal textures indicative of a magmatic origin. For all the 7 samples, the dominant population (about 62.2%) in the age spectrum falls within 250-379 Ma, and most of the zircons are of magmatic origin according to their well-developed oscillatory zoning. Metamorphic zircons characterized by no zoning, faint zoning, or relatively typical fan-shaped zonation in CL images, only account for about 8.6%. Within the group 382-538 Ma, the magmatic zircon grains are also dominant (about 82.3%). However, the zircons ranging in the age interval 543-2852 Ma mainly display faint internal zoning, or inherited cores, interpreted to reflect a metamorphic genesis, and very few can be regarded as magmatic zircons. The few grains ranging in age from 207 to 249 Ma also seem to be of metamorphic origin due to their faint internal zoning. Except for two grains with very low values of 0.09 and 0.10, the Th/U ratios of the detrital zircons from the 7 samples vary from 0.12 to 2.09, and are

predominantly higher than 0.10, reflecting that magmatic zircons are in overwhelming majority.

1.5.3 Cenozoic Samples

One hundred zircons crystals were randomly selected from each of the 5 samples collected in the Paleogene (Anjinhaihe Formation) to Quaternary (Xiyu Formation) section (Fig. 1.2 and 1.3). Between 100 and 91 effective data points were obtained from these samples (Table 1.2). The U-Pb ages from the 5 samples range widely from 157 to 2856 Ma, and can be mainly divided into 4 groups: 157-197 Ma, 257-379 Ma, 381-532 Ma and 620-2856 Ma (Fig. 1.6). Besides, there are also several individual ages comprised between 213 and 241 Ma (6 grains). The zircons ranging in age between 157 and 197 Ma mainly appear in samples from the Neogene Taxihe and Dushanzi formations, and almost all the grains show well-developed oscillatory zoning, indicative of a magmatic origin (Fig. 1.5). The population of ages between 257 and 379 Ma is also the most important component in the age spectrum of every sample (Table 1.2 and Fig. 1.6), and the magmatic zircons are dominant (about 80%). Within the group between 381 and 532 Ma, the metamorphic zircons are largely in minority (about 14.9%), while the remaining crystals are all magmatic in origin (Fig. 1.5). However, in the group of zircons dated between 620 and 2856 Ma, most grains are considered to be of metamorphic origin, based on their faint internal zoning or the occurrence of inherited cores. The 6 grains ranging from 213 to 241 Ma are all metamorphic zircons. Except for three grains with very low values of 0.02, 0.03 and 0.09, the Th/U ratios of detrital zircons of the 5 samples vary from 0.11 to 1.98, and are predominantly higher than 0.10, again indicating that overall many of those crystals are of magmatic origin although a non-negligible proportion are of metamorphic origin.

In summary, the U-Pb ages of detrital zircons from the 14 sediment samples ranging in deposition age from the latest Paleozoic to the Quaternary, vary widely from 127 to 2856 Ma and can be mainly divided into four groups: 127-197 Ma, 250-379 Ma, 381-538 Ma and 543-2856 Ma (Fig. 1.6 and 1.7). Based on their morphological characteristics and internal texture, the genetic conditions of the

various types of zircons have been determined. Magmatic zircons are dominant (about 78.9%), and metamorphic zircons are in minority (about 21.1%) (Fig. 1.5).

The age population within 127-197 Ma with a sub-peak at 159 Ma (7.7% of the combined age spectra) is associated to the Mesozoic magmatism and will be discussed further below. The age population within 250-379 Ma (a sub-peak of 318 Ma), accounting for 65.6% of the combined age spectra, is assigned to the late Paleozoic magmatic belt of the NTS block and the northern margin of the Yili terrane (Fig. 1.1). These series can be regarded as the most important source of detrital materials through time. Finally the age populations within 381-538 Ma (a sub-peak of 406 Ma) and 543-2856 Ma (a sub-peak of 912 Ma), accounting for 16.9% and 7.5% of the combined age spectra, may mainly and respectively reflect the early Paleozoic magmatic rocks and Proterozoic basements in Central Tian Shan (Fig. 1.1). While now separated from the Junggar Basin by the North Tian Shan range, these two sources also contributed to the sediment flux to the southern margin of the Junggar Basin.

XJ09-092

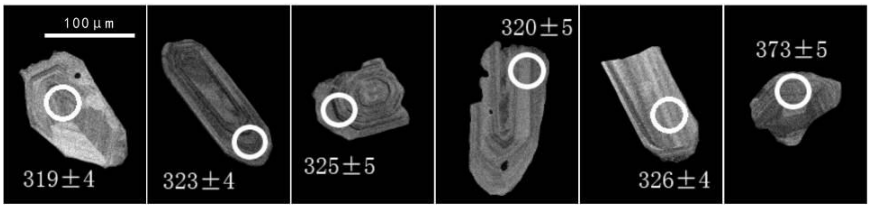

XJ10-009

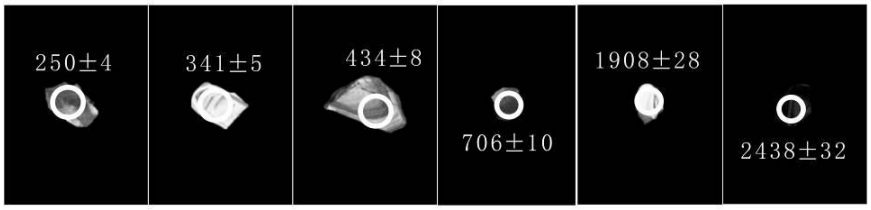

XJ09-094

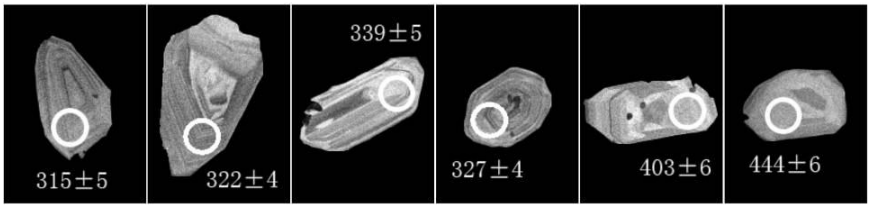

XJ10-011

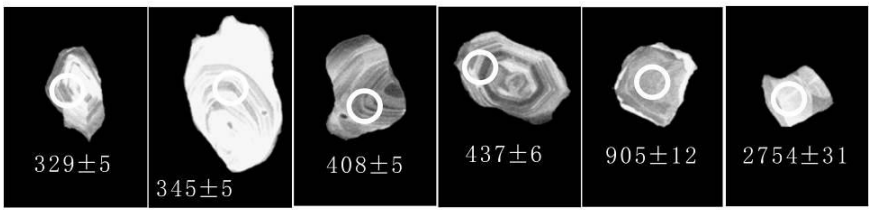

XJ09-097

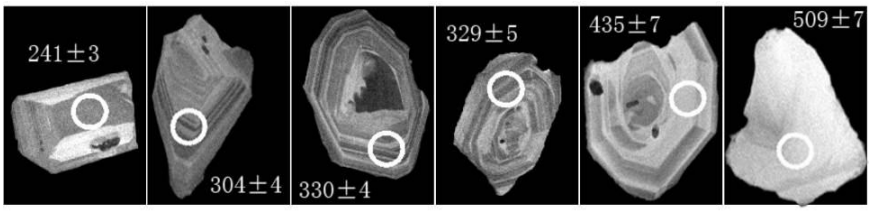

XJ10-018

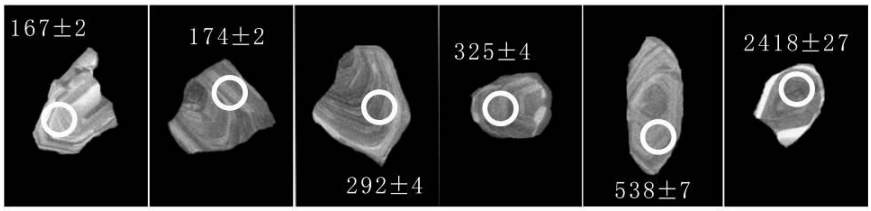

XJ09-100

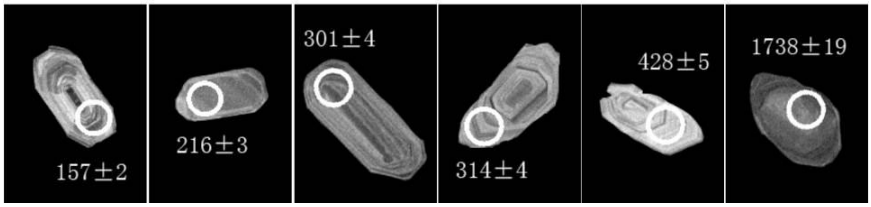

XJ10-016

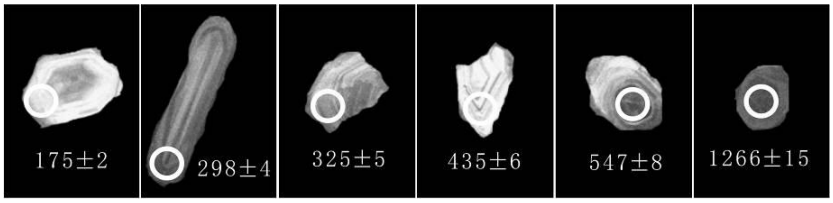

XJ10-015

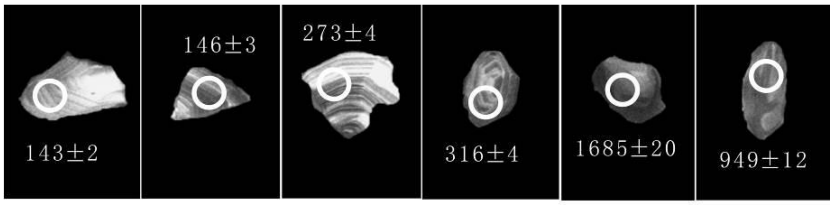

XJ09-010

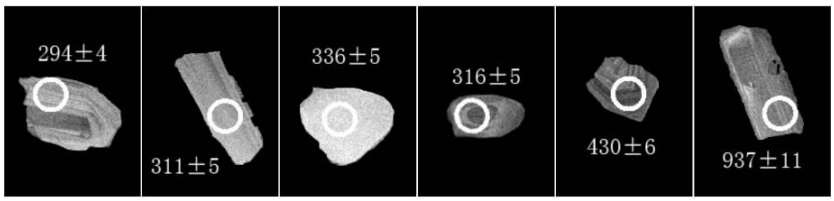

XJ09-011

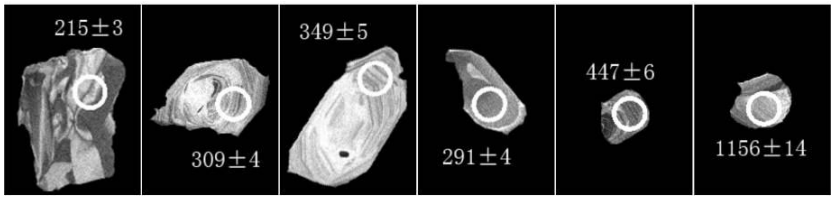

XJ09-003

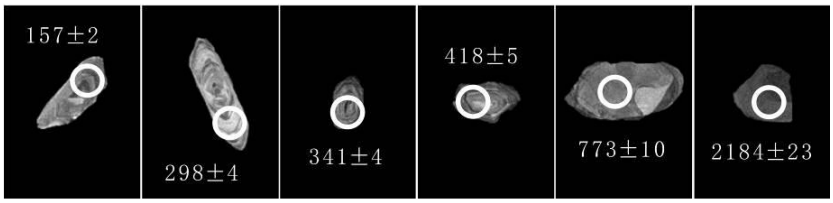

XJ09-017

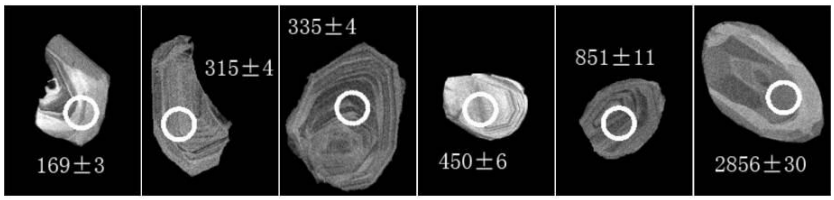

XJ09-021

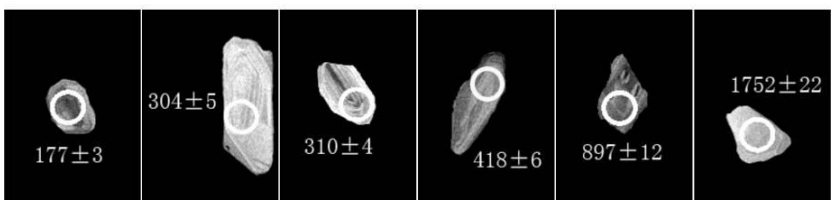

Fig. 1.5 Representative CL images of zircons from the 14 sandstone samples. White circles show the location of U-Pb analysis. Numbers are U-Pb ages in Ma.

Table 1.2 Summary of the various age groups and the corresponding statistical data for the14 samples.

Sample code	Main detrital zircon age groups (Ma)	Number of grains in that group	% of total zircon pop.	Number of effective data points
Paleozoic samples				
XJ09-092	280-373	94	96.9	97
	456-1500	3	3.1	
XJ10-009	250-362	9	30.0	30
	434-508	5	16.7	
	624-2553	16	53.3	
Mesozoic samples				
XJ09-094	303-379	91	92.9	98
	384-455	7	7.1	
XJ10-011	267-379	50	50.5	99
	383-482	35	35.4	
	905-2852	13	13.1	
XJ09-097	253-354	70	71.4	98
	387-519	23	23.5	
	640-1081	2	2.0	
XJ10-018	158-183	28	28.9	97
	261-350	45	46.4	
	382-538	12	12.4	
	567-2418	4	4.1	
XJ09-100	151-179	18	18.0	100
	250-364	61	61.0	
	387-527	6	6.0	
	910-1831	6	6.0	
XJ10-016	163-180	6	6.0	100
	274-367	65	65.0	
	391-470	19	19.0	
	547-2625	7	7.0	
XJ10-015	127-174	30	30.3	99
	273-359	48	48.5	
	390-494	13	13.1	
	543-1685	7	7.1	
Cenozoic samples				
XJ09-010	257-372	73	74.5	98
	392-463	18	18.4	
	735-2607	6	6.1	
XJ09-011	282-375	81	82.7	98
	387-454	12	12.2	
	620-1235	4	4.1	
XJ09-003	157-163	5	5.5	91
	267-371	48	52.7	
	381-501	25	27.5	
	702-2184	11	12.1	
XJ09-017	162-197	8	8.0	100
	265-352	61	61.0	
	382-522	21	21.0	
	813-2856	8	8.0	
XJ09-021	165-177	3	3.0	99
	266-379	59	59.6	
	384-532	23	23.2	
	721-1762	13	13.1	

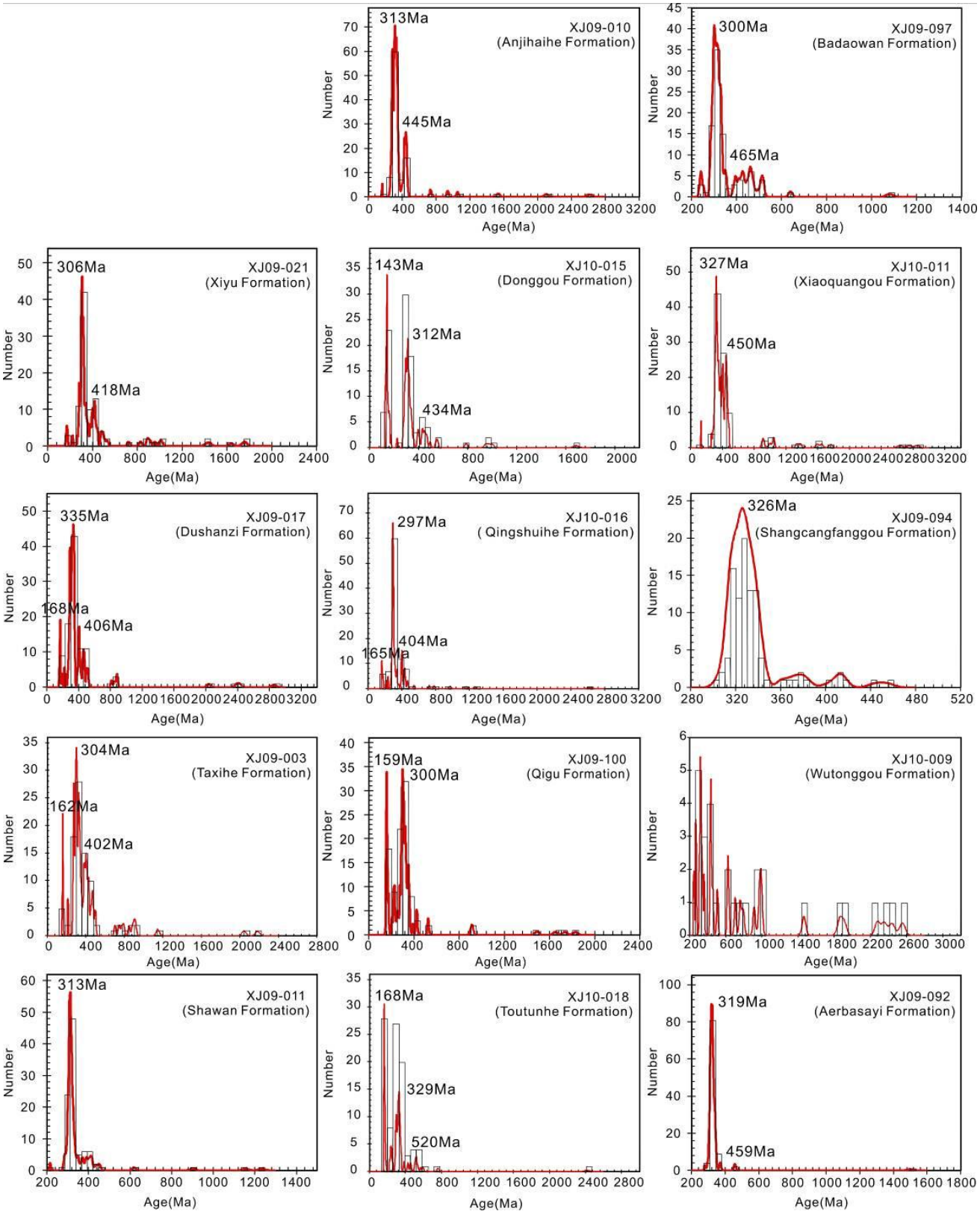

Fig. 1.6 Relative - age - probability plots and number histograms of U-Pb ages of detrital zircons of Permian to Quaternary sandstone samples in the southern margin of the Junggar Basin.

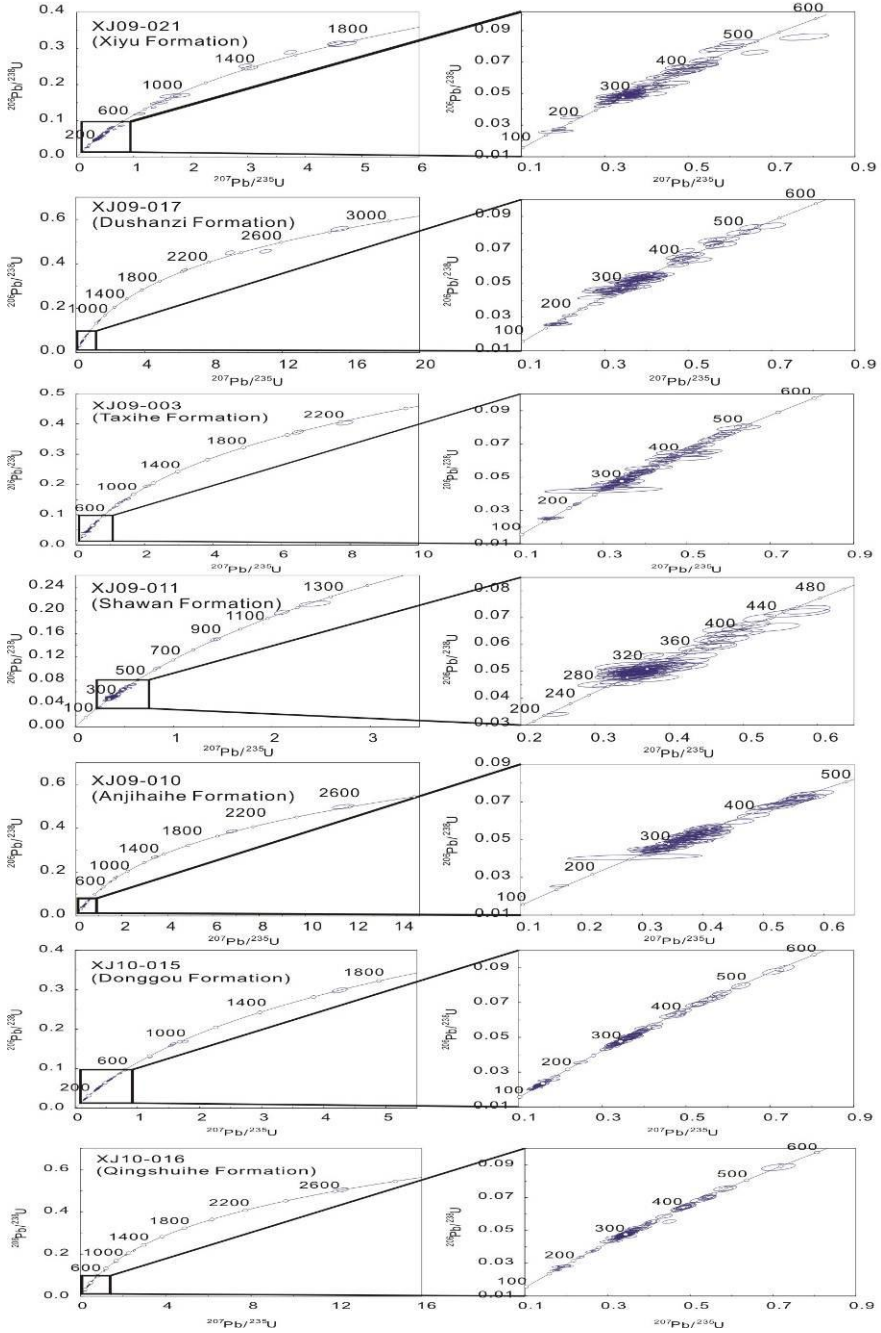
XJ09-021
(Xiyu Formation)
XJ09-017
(Dushanzi Formation)
XJ09-003
(Taxihe Formation)
XJ09-011
(Shawan Formation)
XJ09-010
(Anjihaihe Formation)
XJ10-015
(Donggou Formation)
XJ10-016
(Qingshuihe Formation)
XJ09-100
(Qigu Formation)
XJ10-018
(Toutunhe Formation)
XJ09-097
(Badaowan Formation)
XJ10-011
(Xiaoquangou Formation)
XJ09-094
(Shangcangfanggou Formation)
XJ10-009
(Wutonggou Formation)
XJ09-092
(Aerbasayi Formation)
$^{206}Pb/^{238}U$
$^{207}Pb/^{235}U$

Fig. 1.7 U-Pb concordia diagrams for zircon grains of the 14 sandstone samples.

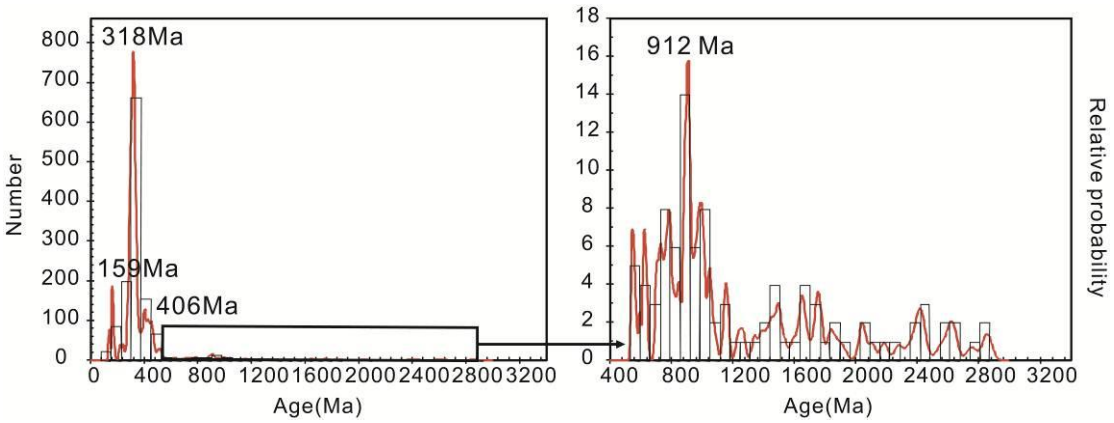

Fig. 1.8 Combined relative probability density and histogram plots of the 14 samples. The diagram to the left corresponds to the black box in the first diagram.

1.6 Discussion

Since latest Paleozoic time, the provenance area of the sediments from the southern margin of the Junggar Basin has been mainly situated to the south in the Tian Shan area (Hendrix, 2000). This is consistent with the continuous northward component of the paleocurrent directions. Even the Middle Jurassic to Lowermost Cretaceous growth of the Chepaizi-Mosuowan uplift, north of the section, seems to have had only a limited effect on the large-scale drainage system. Variations in zircon U-Pb age distribution within individual samples clearly indicate that sediment sources varied in relation with four distinct stages of the geological history of the southern Junggar Basin (Fig. 1.8 and Fig. 1.9). These variations will be discussed below in chronological order to constrain the main stages of the topographic and tectonic evolution of the Tian Shan range as determined by detrital U-Pb geochronology.

1.6.1 Late Carboniferous – Early Triassic phase

The U-Pb age pattern of the detrital zircons from the Aerbasayi Formation (sample XJ09-092) is characterized by magmatic zircons with a single population peak age at 319 Ma (Fig. 1.6), indicating a single source of magmatic rocks. The associated conglomerates were investigated in the field to establish their occurrence, contact relationship and distribution within the Aerbasayi Formation (Fig. 1.4a). This should

be considered as volcanic debris flow deposits (Xie et al., 1994; Di Crescenzo and Santo, 2005; Klubertanz et al., 2009) based on the occurrence of volcanic rocks in the volcanic-sedimentary sequences as well as the poorly sorted and sub-angular characteristics of the gravels in the conglomerate (Fig. 1.4b). Moreover, the mottled pebbly coarse-grained sandstones represent autochthonous sedimentation (Di Crescenzo and Santo, 2005) which implies that the source was very close to the deposition area (Fig. 1.4a and 1.4b). Considering the single magmatic source and the proximal volcano-sedimentary context, we suggest that the real stratigraphic age of sample XJ09-092 is Late Carboniferous instead of Early Permian as previously indicated by the 1:200000 geological map of this area (BGMRXUAR, 1978). It implies a Late Carboniferous, rather than an Early Permian initiation of the Southern Junggar Basin. Field observations as well as published large scale geological sections across the basin (e.g. Qiu et al., 2005, 2008) suggest that Late Carboniferous – Early Permian sedimentation occurred in an extensional setting with normal faults creating substantial topographic differences on localized structures (Fig. 1.9). The single provenance implies that during this period the late Paleozoic magmatic belt in the North Tian Shan and the northern margin of the Yili terrane was the principal provenance area. The Late Carboniferous age of the Aerbasayi Formation contradicts the model of formation of the Junggar Basin as a transtensional basin developing between the Tian Shan shear zones and the Irtysh shear zone (Allen et al., 1994, 1995; Sengör and Natal'in, 1996). Movements on those shear zones, and especially in the Tian Shan, have clearly been dated to the Permian (e.g Wang et al., 2006; de Jong et al., 2009; Charvet et al., 2011). The evidences for extension suggest that the Junggar Basin was neither developing as a foreland basin (Carroll et al., 1992, 1995; Liu et al., 1994, 2000, Chen et al., 2001; Jia et al., 2003; He et al., 2004) but rather in a post-collisional extensional setting (Fang et al., 2006a) or as a half-graben structure (e.g. Qiu et al., 2005, 2008). Wartes et al. (2002) suggested that the Permian extension could have been followed by contraction.

Due to the small amount of available zircon crystals in sample XJ10-009, the detrital U-Pb zircon age composition of the Upper Permian Wutonggou Formation (Fig. 1.6) is only indicative. However, both the Paleozoic magmatic series of the NTS block and the Proterozoic basement of the CTS block contributed to the detrital

material supply. This confirms that the CTS block was accreted to the NTS block at that time (e.g. Huang et al., 1980; Wang et al., 1990; Allen et al., 1992; Biske and Seltmann, 2010; Han et al., 2010; Charvet et al., 2011). It also shows that a limited amount of sediments supplied in the Junggar Basin were issued from the CTS implying a widening of the drainage system towards more distant sources. Erosion of the CTS and NTS blocks is consistent with the zircon (U-Th)/He and apatite fission track data obtained in the range which show a major exhumation episode during that period and thus the development of a strong topography (Dumitru et al., 2001; Jolivet et al., 2010). Finally, the large dextral strike-slip movements observed during the Permian along the main shear zones separating the CTS and NTS blocks confirm the strong tectonic activity during that time (e.g Wang et al., 2006; de Jong et al., 2009; Charvet et al., 2011).

The Lower Triassic Shangcangfanggou Group sample (XJ09-094) shows some similarities with sample XJ09-092 from the Aerbasayi Formation (Fig. 1.6) with one major Carboniferous peak age. However, the slightly older peak age of 326 Ma in sample XJ09-094, associated to several minor middle to early Paleozoic peaks that are only poorly recorded in sample XJ10-009, suggest exhumation of older, probably deeper sources. This exhumation may reflect active erosion during the Permian - Early Triassic in accordance with the low temperature thermochronology data obtained in the range (Dumitru et al., 2001; Jolivet et al., 2010). The Lower Triassic detrital material is interpreted as again mostly derived from the late Paleozoic magmatic belt of the NTS block, while the minor Devonian to Ordovician ages reflect older magmatic series probably derived from the CTS block (Fig. 1.6). Those results suggest that, like in the Upper Permian (Wutonggou Formation), connections existed between the CTS block and the Junggar Basin (Fig. 1.9). Recycling of the Lower Permian sediments may also explain the occurrence of CTS-derived zircons but the age spectrum of those sediments is much larger, weakening that hypothesis.

1.6.2 Middle Triassic – Upper Jurassic phase

A first noticeable change in the distribution of detrital zircon U-Pb ages occurs in sample XJ10-011 from the Middle to Upper Triassic Xiaoquangou Group (Fig. 1.6) with the appearance of a distinct Ordovician peak age and of several Proterozoic to

Archean ages. Those last ages were already expressed in sample XJ10-009 from the Upper Permian Wutonggou Formation. However they were only a minor proportion of an already extremely limited set of zircon ages. Furthermore, those ages completely disappear in the Lower Triassic XJ09-094 sample. While some limited connections between the Junggar Basin and the Precambrian basement of the CTS block existed during the Upper Permian and the Lower Triassic, this connection appears clearly established in the Upper Triassic. The provenance in sample XJ10-011 is thus interpreted as a mixture of three sources: the late Paleozoic magmatic belt in the North Tian Shan and the northern margin of the Yili terrane representing the major zircon population (peak age of 327 Ma), the early Paleozoic magmatic rocks in CTS representing the second major population (peak age of 450 Ma), and finally a significant contribution from the Precambrian basement of the CTS block (Fig. 1.6). Recycling of the upper Paleozoic – lower Mesozoic series could also partially explain apparent increase in Precambrian and early Paleozoic ages. However, the age spectra, and especially the dominant Paleozoic peak cannot be solely attributed to recycling. The increased contribution from the CTS block implies a noticeable evolution of the drainage system and thus of the regional topography. The NTS source being important, positive reliefs were certainly still present in that area. However, this topography was probably smooth enough to allow rivers to cut through and bring material from the CTS block to the south. Sediment transport was then occurring over large distances and clastic sedimentation migrated southward covering surfaces previously in erosion. The major topographic barrier formed by the NTS block since the Early Permian was no more present. This is consistent with the progressive erosion of the topography that resulted from the Permian accretion events as seen by the low temperature data in the range (Dumitru et al., 2001; Jolivet et al., 2010). The extensional setting that was prevailing in the Junggar Basin during the Late Carboniferous – Permian probably ended in the Lower Triassic allowing a progressive decrease of the locally strong topography induced by normal faulting. From Middle Triassic, tectonic subsidence ceased and the southern Junggar Basin clearly became slowly subsiding basin. We have no real argument to discuss the origin of this subsidence but it could be due to relaxation of far-field constrains generated by the Permian accretion events.

The provenance of the Lower Jurassic Baodaowan Formation (sample XJ09-097) (Fig. 1.6) mainly includes the late Paleozoic magmatic belt of the NTS block (peak age of 300 Ma) and the early Paleozoic magmatic rocks of the CTS block (peak age of 465 Ma). Proterozoic ages are nearly absent. The observed unconformity between the Upper Triassic and Lower Jurassic indicates limited vertical tectonic movements and a possible slight reorganization of the drainage pattern. We do not have enough information to fully discuss those changes. However, Dumitru et al. (2001) suggested that the Permian – Triassic exhumation phase had been overprinted by a subsequent Early Jurassic cooling phase. Jolivet et al. (2010) related that episode to the collisions of the Cimmerian blocks to the south (e.g. Jolivet et al., 2001; Roger et al., 2010, 2011). Nonetheless, the widespread Lower and Middle Jurassic series, including the well-developed coal strata and the concentration of thick coal seams in the Middle Jurassic Xishanyao Formation, attest the widening of a passively subsiding Junggar Basin (Fig. 1.2 and 1.3). Fang et al. (2005) suggested that the southern edge of the basin extended at least to the south of the Houxia area (Fig. 1.1).

The age spectrum of the Middle Jurassic Toutunhe Formation (sample XJ10-018) presents a dramatic change, with the first appearance of zircons from sub-contemporaneous Mesozoic magmatic sources (peak age of 168 Ma) (Fig. 1.6). In addition to the occurrence of those zircons of clear magmatic origin, several lines of evidence suggest that magmatism, limited in volume but distributed over a wide area occurred in Central Asia during the Mesozoic (see discussion below). The other two sources of zircons in sample XJ10-018 again correspond to the late Paleozoic magmatic belt of the NTS block (peak age of 329 Ma) and to the early Paleozoic magmatic rocks of the CTS block (peak at 520 Ma) (Fig. 1.9). The Toutunhe Formation also marks the end of the long-lasting general retrogradation phase that initiated in the Late Carboniferous and ended with the lacustrine facies of the Middle Jurassic Xishanyao Formation. While retrogradation was consistent with a progressive erosion of the topography during the late Palaeozoic – early Mesozoic, and the coeval widening of the drainage pattern and of the sedimentation area, the onset of a progradation phase suggests topographic or climatic changes. We have only a limited amount of data to discuss this issue but the suspected tectonic reactivation of the

range that initiated during the Lower Jurassic (see above) could be an explanation for this change between retrogradation and progradation.

The Upper Jurassic Qigu Formation (sample XJ09-100) is very similar to the Middle Jurassic sample XJ10-018. The peak age of 159 Ma again reflects the products of coeval Late Jurassic volcanic activities. The peak age of 300 Ma represents sediments derived from the NTS magmatic belt. The older ages may be either derived from the CTS block or from recycling of the Mesozoic cover deposited on the NTS basement.

1.6.3 Lower Cretaceous – Paleogene phase

The sharp facies variation from the alluvial fan of the Kalazha Formation to the lacustrine deposits of the Lower Tugulu Group marks the end of the Middle to Upper Jurassic progradation phase and the onset of a new progradation. The age population pattern of the Lower Cretaceous Tugulu Group (sample XJ10-016) (Fig. 1.6) still yields Jurassic volcanic zircons attesting for recycling from the underlying sedimentary series. The proportion of the age population with a peak of 297 Ma rose markedly to become predominant (65.0%), suggesting that the contribution of the late Paleozoic NTS magmatic belt further increased as a source. This, associated to the potential recycling of the Jurassic series may indicate renewed erosion of the NTS block. During the Early Cretaceous, the southern margin of the Junggar Basin was thus under erosion. The surface of the basin decreased and its southern boundary shifted northward significantly, near the present day southern Junggar Basin boundary (Fang et al., 2006a).

However, the proportion of the NTS late Paleozoic source decreases to 48.5% in the age populations of the following Upper Cretaceous Donggou Formation (sample XJ10-015) (Fig. 1.6). The peak age of 143 Ma recorded in that sample by magmatic zircons indicates the occurrence of Late Jurassic – Early Cretaceous (up to 127 Ma) magmatism in the region. The decrease in proportion of the late Paleozoic source (peak age of 312 Ma) can be explained by an increased amount of sediment recycling from the underlying upper Paleozoic – lower Mesozoic sequence. Material eroded from the NTS late Paleozoic magmatic belt are simply diluted within the recycled

zircons of various origin. The early Paleozoic age peak of 434 Ma also suggests that either the connections with the CTS block still exist or that, more probably, sediment recycling occurs. While the reactivation of the topography observed during the Lower Jurassic seems to have had no impact on the Junggar Basin (continued widening and possibly reinforced subsidence), the Cretaceous period is clearly marked by inversion of the southern margin of the basin (Fig. 1.9). The geodynamic mechanism that induced this basin inversion remains to be constrained and several hypotheses have been put forward such as the collision of the Lhasa block to the south (Hendrix et al., 1992; Gu, 1996; Fang et al., 2006b). However, except for the occurrence of the Jurassic magmatic sources, the Early Cretaceous detrital zircon ages pattern remains similar to the overall Mesozoic series pattern, and we infer that the modifications in the basin-range relations was a relatively minor internal adjustment compared to the previous estimates. This is consistent with the long period of tectonic quiescence recorded by fission track thermochronology studies in Tian Shan, Mongolia and Northern Tibet during the Cretaceous (Jolivet et al., 2001; Jolivet et al., 2007; Vassallo et al., 2007; Roger et al., 2010). The basic properties and essential characteristics of the basin were preserved.

The age patterns of the two Paleogene samples (XJ09-010 and XJ09-011) are quite similar. The Mesozoic ages have disappeared and the late Paleozoic source now largely dominates. While the late Paleozoic age peaks of 313 Ma are identical to the peak age of 312 Ma of sample XJ10-015, the disappearance of the Mesozoic magmatic zircons clearly excludes direct sediment recycling from the Cretaceous and Jurassic series. For sample XJ09-010 from the Anjihaihe Formation, the peak ages of 313 Ma and 445 Ma approximately correspond to the magmatic events in the Late Carboniferous and Late Ordovician. These respectively correspond to the late Paleozoic magmatic belt and the Late Ordovician granites, which are two important sources widespread in Central Tian Shan. The Precambrian ages reflect the contribution of older basement from the CTS block although they may also be partially recycled from pre-Jurassic Mesozoic series. The Junggar Basin remained in an overall relatively stable basin-range setting during that period (Fang et al., 2004; Jolivet et al., 2010). However, later in the paleogene, uplift probably initiated leading to progressive modifications of the drainage pattern and to the decrease of the

contribution from CTS block sources (especially in the Shawan Formation) and the increased erosion of the sedimentary series now reaching down to pre-Jurassic strata (Fig. 1.6).

In summary, the Middle-Late Triassic to Paleogene basin-range pattern was overall characterized by a large source area and a relatively low topography that was punctually high enough to generate coarse clastic sediments but not to create long-lasting topographic barriers for the sediment supply. This setting is consistent with a post-extensional thermally subsiding basin associated to a paleo-range which has been progressively eroded away without much tectonic activity (Dumitru et al., 2001; Vassallo et al., 2007; Jolivet et al., 2007, 2010; Glorie et al., 2010). Two relatively minor internal adjustments occurred in the Lower Jurassic and in the Earliest Cretaceous probably in relation with the various accretion episodes that occurred along the southern margin of Asia during the Mesozoic.

1.6.4 Neogene to Quaternary phase

From the Neogene Taxihe Formation (samples XJ09-003 and XJ09-017), a relatively important change took place again in the distribution of detrital zircon U-Pb ages reflecting, a new transformation in the source system (Fig. 1.9). In those samples the Jurassic magmatic source, characterized by the peak ages of 162 Ma and 168 Ma is again present (Fig. 1.6). Recycling of the Mesozoic series is further attested by the lithology of the pebbles within the Dushanzi Formation. For example, the red gravels of the Late Jurassic Qigu Formation and the brown-reddish conglomerates of the Kalazha Formation (Fig. 1.4c), as well as the Late Jurassic tuffaceous sandstone pebbles (Fig. 1.4d) are all found in the Dushanzi Formation conglomerates. The zircons from the late Paleozoic NTS magmatic belt are again the major components and are derived both from contemporaneous erosion of the NTS basement and sediment recycling (Fig. 1.6). However, the proportion of zircons derived from the early Paleozoic magmatic rocks (age peaks of 402 Ma and 406 Ma) and the Proterozoic basement of the CTS block obviously increases. Connections between the internal parts of the growing range and the Junggar Basin are unlikely (the topographic barrier formed by the uplift of the NTS was probably already important), and those zircons are most probably recycled from the Mesozoic strata.

The distribution of detrital zircon U-Pb ages in the Quaternary Xiyu Formation (sample XJ09-021) basically retained the characteristics of the Neogene samples XJ09-003 and XJ09-017, indicating similar provenances. The main difference is that during deposition of the Xiyu Formation, the contribution from the Mesozoic magmatism decreased significantly (3.0%), while the older Central Tian Shan basement components were more represented (13.1%). This can be explained by erosion of progressively older cover series. Today, the whole Late Carboniferous to Quaternary series of the northern piedmont are being eroded and recycled. During the Neogene to Quaternary period, the southern margin of the Junggar Basin became a piedmont and the basin a true foreland basin.

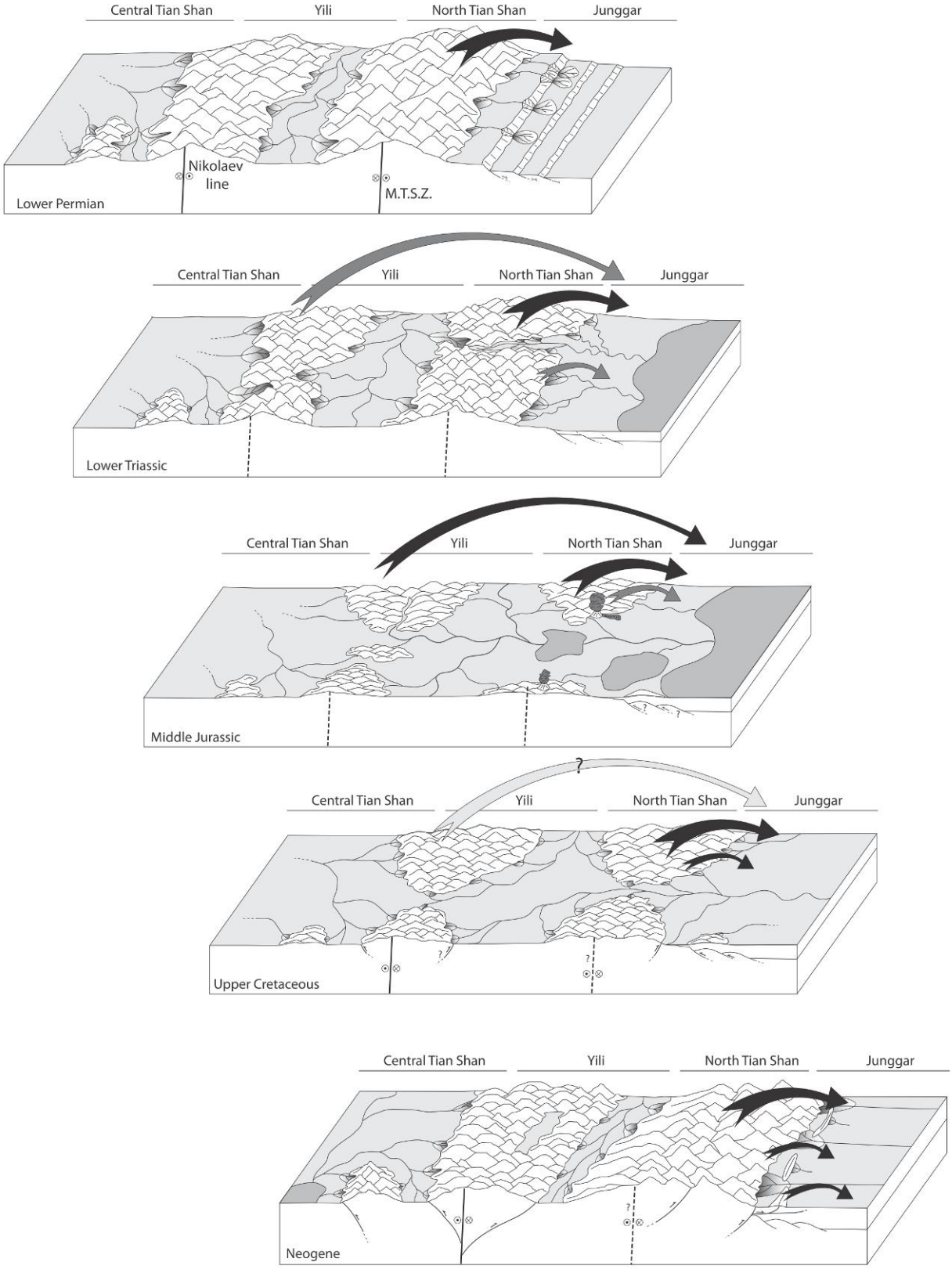
Central Tian Shan
Yili
North Tian Shan
Junggar
Nikolaev
line
M.T.S.Z.
Lower Permian
Central Tian Shan
Yili
North Tian Shan
Junggar
Lower Triassic
Central Tian Shan
Yili
North Tian Shan
Junggar
Middle Jurassic
?
Central Tian Shan
Yili
North Tian Shan
Junggar
Upper Cretaceous
Central Tian Shan
Yili
North Tian Shan
Junggar
Neogene

Fig. 1.9 Palaeogeographic reconstructions of key periods in the evolution of the Tian Shan Range – Junggar Basin history as described in the text. The map extends roughly between the Bayanbulak basin to the left and the Junggar Basin to the right. Only the major faults are shown such as the Main Tian Shan Shear Zone (MTSZ) or the Nikolaev line (see Jolivet et al., 2010). Question marks indicate possible but not documented movements on the faults. Faults in dotted lines are inactive. The arrow represents sediment provenance deduced from detrital U/Pb zircon ages and various sedimentology data described in the text. The topography was drawn using both provenance data and low thermochronology data obtained in the range by Dumitru et al. (2001) and Jolivet et al. (2010). Black arrows indicate major sources, dark-grey arrows indicate minor sources. Light-grey arrows indicate possible minor sources. The light-grey shaded areas indicate basins (deposition areas) and dark-grey shaded areas indicate lakes.

1.7 Notes on the Mesozoic volcanism

There are relatively few direct field evidences of Mesozoic magmatic activity in the southern margin area of the Junggar Basin. However, near the Manas River and slightly further east, thin tuffaceous sandstone intercalations have been reported in the Lower part of the Qigu Formation (BGMRXUAR, 1978). In addition, numerous studies indicated that Mesozoic volcanism was extensively distributed both in northern Xinjiang and in the surrounding regions (Han et al., 1999; Sobel and Arnaud, 2000; Ji et al., 2006; Jolivet et al., 2007; Xu et al., 2008; Guo et al., 2010). For example, a whole rock $^{40}Ar/^{39}Ar$ age of 192 Ma has been obtain on a basalt flow from the Karamay region in western Junggar (Xu et al., 2008). Similar ages were reported on volcanoes in the nearby Gobi Altay, Mongolia (Jolivet et al., 2007). In NE Tibet, several layers of volcanic rocks are interbedded in the sequences of Middle Jurassic continental clastic rocks of the Tuoge, Duobagou and Lucaogou area of the Dunhuang basin (Zhang et al., 1998).

Volcanism is not restricted to the Jurassic and ages of 100 Ma and 70 Ma have been obtained on olivine basalts and basalts from the Tuyon basin, southwest Tian Shan (Ji

et al., 2006; Wang et al., 2000b). In North Tibet, Early Cretaceous basaltic magmatic activities are reported in the Sanweishan area (Feng et al., 2010). In the Hanxia and Hongliuxia area of the Jiuxi basin, Lower Cretaceous volcanic intercalations and two phases of magmatism were identified at 112-106 Ma and 83 Ma, respectively (Yang et al., 2001; Wang et al., 2004).

Potential sources of this intracontinental volcanism are still elusive. Although it is beyond the scope of this paper to solve this issue, we note nonetheless that in Tian Shan this magmatism occurred slightly after the Lower Jurassic renewed exhumation phase observed in the range (Dumitru et al., 2001; Jolivet et al., 2011) and before the Lower Cretaceous inversion of the southern Junggar Basin. This might suggest that magmatic activity took place during an apparently tectonically quiet period.

1.8 Conclusions

The detrital zircon geochronology and related genetic mineralogy studies show that the detrital zircons from the 14 samples of the latest Paleozoic to Quaternary formations are mostly magmatic in origin, with some minor input from metamorphic sources. The U-Pb detrital zircon ages range widely from 127 to 2856 Ma and can be divided into four main groups: 127-197 Ma (sub-peak at 159 Ma), 250-379 Ma (sub-peak at 318 Ma), 381-538 Ma (sub-peak at 406 Ma) and 543-2856 Ma (sub-peak at 912 Ma). These groups, together with the available measurements of paleocurrent directions indicate that the detrital zircons (and thus probably most of the sediments) were largely derived from the Tian Shan area to the south since the basin initiated in Late Carboniferous time. The 250 - 379 Ma age group, accounting for 65.6% of the combined age spectra, is assigned to the late Paleozoic magmatic belt in the North Tian Shan and the northern margin of the Yili terrane, which can be regarded as the most important source of detrital material through times. The 381 - 538 Ma and 543 - 2856 Ma age groups, accounting respectively for 16.9% and 7.5%, of the combined age spectra mainly reflect the early Paleozoic magmatic rocks and Proterozoic basement of Central Tian Shan. Finally, the 127 - 197 Ma age group, representing 7.7% of all ages, corresponds to Mesozoic volcanism (mainly tuffs). The occurrence

of those Jurassic volcanic zircons within the Neogene sediments highlights the importance of sediment recycling within the evolving piedmont. However, that recycling is not restricted to the Tertiary and occurred regularly throughout the Mesozoic history of the range, especially during the Cretaceous.

The provenance and basin-range pattern evolution of the southern margin of the Junggar Basin can be generally divided into four stages as follows. (1) During the Late Carboniferous to Early Triassic, the provenance is relatively unimodal. The detrital material was almost exclusively derived from the late Paleozoic magmatic belt of the North Tian Shan and the northern margin of the Yili terrane. Only a small amount of sediment was derived from the Central Tian Shan. This is interpreted in terms of near-source sedimentation in basin developing in a post orogenic extensional setting or as a half-graben. Strong topography in the range is suspected. (2) A major change in the history of the Junggar Basin occurred during the Middle-Late Triassic. Until the Upper Jurassic, the southern Junggar Basin progressively extended towards the south reaching beyond the Houxia area and evolved as a passively subsiding basin. The topography resulting from the late Paleozoic – early Mesozoic tectonic movements was progressively eroded and the drainage system reached the CTS block. (3) The following noticeable event corresponds to the Lower Cretaceous - Paleogene inversion of the southern Junggar Basin illustrated by the onset of erosion of the Jurassic sedimentary series and the progressive northward migration of the edge of the basin. However, it seems that while effective, this event remained of limited magnitude and that no major topography developed in the range. (4) Finally, major Neogene reactivation of the Tian Shan range led to the development of a piedmont along the northern edge of the NTS block and the Junggar Basin became a true foreland basin. The increasing amount and diversity of early Paleozoic and Precambrian zircons recalls the strong recycling of sediments from the entire Mesozoic and Tertiary sedimentary sequences of the North Tian Shan piedmont.

CHAPTER 2

Mesozoic-Cenozoic tectonic evolution of southwestern Tian Shan: evidence from detrital zircon U/Pb and apatite fission track ages of the Ulugqat area, Northwest China

Wei Yang[a,b], M. Jolivet[b], G. Dupont-Nivet[a,b,c], Zhaojie Guo[a]*

[a] *Key Laboratory of Orogenic Belts and Crustal Evolution, Ministry of Education, School of Earth and Space Sciences, Peking University, Beijing, China 100871*

[b] *Géosciences Rennes, Université Rennes 1, UMR 6118,CNRS/INSU, Rennes, France*

[c] *Faculty of Geosciences, Utrecht University, The Netherlands*

** Corresponding author. Tel.: + 86-10-62753545; fax: + 86-10-62758610. E-mail address: zjguo@pku.edu.cn (Z. Guo).*

Abstract

The Late Tertiary tectonic and topographic evolution of the Tian Shan Range has been widely studied as it represents a key example of active intra-continental mountain belts. Recent studies have shown that both the general tectonic framework of Tian Shan and some of its actual topographic features were inherited from the still poorly constrained Late Paleozoic – Mesozoic evolution of the range. In addition, better understanding of the tectonic and topographic evolution of the area before the last phases of late Cenozoic deformation is required to constrain the unresolved climatic and paleogeographic reconstructions. We present here U/Pb (LA-ICP-MS) dating of detrital zircons and apatite fission track analysis on detrital apatites from the exceptionally well-exposed Jurassic to Cenozoic sediment series of the still poorly constrained southwestern Tian Shan piedmont to investigate changes in sediment provenance through time. The U/Pb detrital zircon ages range widely from 222 to 3179 Ma and can be statistically separated in four main groups: 240-320 Ma, 400 – 540 Ma, 550 – 1600 Ma and 1640 – 2800 Ma. These zircons were derived from the Tian Shan area to the north and from recycling of the Paleozoic North Tarim margin. The detrital apatite fission track ages encompass sources with preserved Mesozoic

ages as well as much younger sources exhumed during middle Miocene times. Combined together those data show a general planation of the range from Middle Jurassic to Late Cretaceous associated to a wide drainage system. The progressive decrease in the variety of sources through the Mesozoic is consistent with burying of the basement exposures by sediments. Detrital zircons U/Pb data indicate an initial Tertiary uplift of the southern Tian Shan piedmont around Eocene times and a possible activation of the Talas Fergana Fault between 18 and 16 Ma.

Keywords: Southwest Tian Shan; Tarim Basin; Detrital zircon; U-Pb; Apatite fission track

2.1 Introduction

The Tian Shan, up to 7400 m high, is a 2500 Km long range extending through western China, Kazakhstan, and Kyrgyzstan (Fig. 2.1). This range belongs to the larger Central Asian Orogenic Belt (CAOB) extending from the Urals to the Pacific across the East European, Siberian, North China, and Tarim cratons (e.g. Şengör et al., 1993; Windley et al., 2007; Jolivet et al., 2010). The lithosphere of the Tian Shan orogenic belt results from complex accretions of island arcs and amalgamation of continental lithospheric blocks during the Late Paleozoic (Watson et al., 1987; Coleman, 1989; Gao et al., 1998; Carroll et al., 1990, 1992, 1995; Windley et al., 1990, 2007; Allen et al., 1992; Xiao et al., 1992, 1994; Shu et al., 2002; Charvet et al., 2004, 2007, 2011; Glorie et al., 2010). The Tian Shan area was then reactivated by successive terrane collisions onto the south Asian margin during Early Mesozoic time (Hendrix et al., 1992; Dumitru et al., 2001; Greene et al., 2005; Lu et al., 2010; Jolivet et al., 2010). Apatite fission track and (U-Th)/He data from the Central Tian Shan and the southern edge of the North Tian Shan demonstrate that the Permian exhumation phase has been subsequently overprinted by an Early Jurassic cooling phase (Dumitru et al., 2001; Jolivet et al., 2010; Qiu et al., 2012), probably related to the far-field effects of the final collision between the Qiangtang and Kunlun blocks (e.g. Jolivet et al., 2001; Roger et al., 2010, 2011). Strong erosion during Triassic and Early Jurassic

times initiated general peneplanation of the Tian Shan region that was probably well evolved during Early-Middle Jurassic time (Shu et al., 2004; Jolivet et al., 2010; Liu et al., 2013; Yang et al., 2013). Sedimentological data within the surrounding basins also indicate that by Late Jurassic – Cretaceous, and possibly onwards, the largely peneplaned Tian Shan region may have been affected by extension induced by post-orogenic relaxation (Shu et al., 2004; Guo et al., 2005, 2006; Fang et al., 2006). Finally, the Tian Shan experienced a rapid uplift during the Miocene, attested by a series of thermochronological results (e.g. Du and Wang, 2007a; Zhang et al., 2007b; Wang et al., 2010).

Sediment recycling within evolving piedmonts is a first order parameter for basin-range interactions or mass-balance studies. However, this process remains difficult to evaluate using classical sedimentology methods. The occurrence of major Mesozoic and Cenozoic sediment recycling has been recently demonstrated within the evolving piedmont of North Tian Shan using U/Pb dating of detrital zircons (Yang et al., 2013). In the region, the Mesozoic to Cenozoic detrital zircon populations are characterized by the occurrence of Early to Middle Jurassic volcanic zircons recycled into the Cretaceous and Tertiary series. This recycling implies a Late Jurassic – Early Cretaceous tectonic inversion of the southern edge of the Junggar Basin, and coeval modifications in the basin-range relations (Yang et al., 2013).

The present study aims to understand the evolution of the Southwest Tian Shan piedmont over the same period and test whether or not such sediment recycling occurred (Figs. 2.1 and 2.2). The Southwest Tian Shan Range and the westernmost Tarim Basin is intimately linked, study of the sedimentary series in the piedmont of Southwest Tian Shan can thus provide detailed information on the evolution of the sediment sources and basin-range setting of the westernmost Tarim. In order to obtain a tectono-sedimentary history of the piedmont as complete as possible over the Middle Jurassic to Quaternary period, we combined U/Pb dating on detrital zircons with detrital apatite fission track analysis. While the U/Pb results will provide information on the source of the sediments and on the occurrence of sediment recycling, the apatite fission track data will constrain the timing of exhumation and erosion along the piedmont through time.

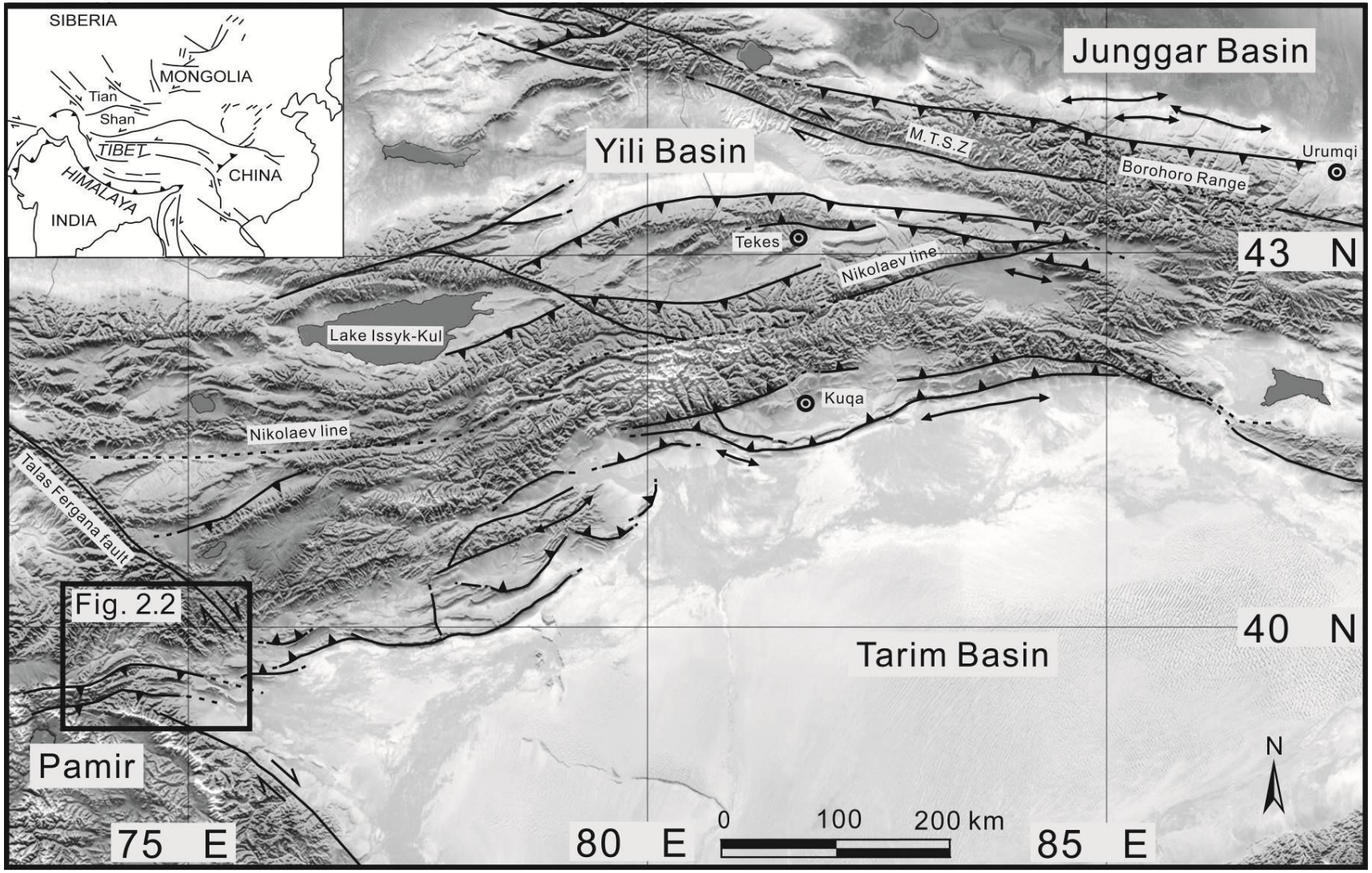
SIBERIA
MONGOLIA
Tian
Shan
TIBET
CHINA
HIMALAYA
INDIA
Junggar Basin
Yili Basin
M.T.S.Z
Urumqi
Borohoro Range
Tekes
Nikolaev line
43 N
Lake Issyk-Kul
Kuqa
Nikolaev line
Talas Fergana fault
Fig. 2.2
40 N
Tarim Basin
Pamir
N
0
100
200 km
75 E
80 E
85 E

Fig. 2.1 General topographic and tectonic map of the Tian Shan belt and adjacent areas. Only the major tectonic structures are indicated. "M.T.S.Z" is the Main Tian Shan Zone (modified from Jolivet et al., 2010). The black square corresponds to the study area detailed in Fig. 2.2.

2.2 Geological setting

The study area is located at the junction of the Southwest Tian Shan, the western Tarim and the western Kunlun/northern Pamir, whose major geological features and tectonic evolution are summarized as follows.

2.2.1 The Tian Shan

The first accretion-collision stage recorded in the Tian Shan basement occurred before the Visean and built the Eo-Tian Shan Mountains (e.g. Windley et al., 1990; Gao et al., 1998; Charvet et al., 2011). A second accretion-collision stage was characterized by the Late Carboniferous- Early Permian collision of the newly formed Tarim – Central Tian Shan terrane with a series of Late Paleozoic island arcs now forming the North Tian Shan (NTS) (e.g. Huang et al., 1980; Wang et al., 1990; Allen et al., 1992; Biske and Seltmann et al., 2010; Han et al., 2010; Gao et al., 1998; Charvet et al., 2011). This Permian accretion in Tian Shan resulted in the North Tian Shan suture that currently marks the geological boundary between the Yili - Central Tian Shan (CTS) plate and the NTS volcanic arc. The collision induced north-directed deformation in NTS and symmetrical south-directed deformation in CTS and South Tian Shan (STS). This phase was followed by Permian post-collisional magmatism and large strike-slip faulting along major fault systems (e.g. Han et al., 1997, 1999, 2010; Charvet et al., 2011). Following the multiple Early Mesozoic reactivation described above, the crustal shortening related to the distant effects of the ongoing Cenozoic India-Eurasia collision finally led to the formation of the actual orogenic belt and the present-day topography of the range (Fig. 2.1) (Molnar and Tapponnier, 1975; Tapponnier and Molnar, 1977, 1979; Burchfiel and Royden, 1991; Avouac et al., 1993; Lu et al., 1994; Yin et al., 1998; Burchfiel et al., 1999; Allen et al., 1999; Dumitru et al., 2001; Guo et al., 2003; Buslov et al., 2004, 2007; Jolivet et al., 2010).

In China, the STS orogen was generally interpreted as a collisional belt between the Yili- Central Tian Shan and Tarim blocks (Fig. 2.1) (e.g. Windley et al., 1990; Allen et al., 1992; Gao et al., 1998, 2009), without participation of island arcs in the orogeny (e.g. Biske and Seltmann, 2010; Burtman, 2008; Gao et al., 2009; Yang and Zhou, 2009). The Southwest Chinese Tian Shan (SWTS), as an important segment of the South Tian Shan orogen, experienced multi-stages accretion involving Early Paleozoic passive margin sediments and fragments of the Tarim craton, remnants of the South Tian Shan oceanic lithosphere, as well as active margin materials of the Kazakhstan-Yili terrane (e.g. Gao et al., 2009, Han et al., 2011). The basement of the Southwest Chinese Tian Shan is characterized by Precambrian granitic gneisses with U-Pb zircon ages ranging between 798 Ma and 969 Ma (e.g. Hu et al., 1986, 1997, 2000; Chen et al., 1999, 2000; Wang et al., 2006; Zhu and Song, 2006; Zhu, 2007; Ma et al., 2012a,b, 2013). These gneisses are covered by Meso-Neoproterozoic carbonates, clastic rocks and minor tillites, together with Cambrian-Early Ordovician siltstones, mudstones, sandstones and volcanics (e.g. Gao et al., 1998, 2009). Precambrian to Middle Ordovician rocks are intruded by granites of Middle Ordovician ages varying from 460 to 470 Ma (Kiselev, 1999; Konopelko et al., 2008) and Early Silurian ages between 435 – 440 Ma (Konopelko et al., 2008). These ages indicate an Ordovician to Middle Silurian magmatic event induced by the oceanic subduction and following accretion of the Tarim and Central Tian Shan (e.g. Gao et al., 1998, 2009; Lin et al., 2009). Widespread Late Carboniferous – Early Permian A-type granites in NTS and STS, characterized by 280-320 Ma zircon U-Pb ages, indicate a post-collisional tectonic setting in North Tian Shan and suggest the final closure of the North Tian Shan Ocean, resulting in the final accretion of the Junggar Block and the NTS volcanic arc (e.g. Han et al., 1999, 2011; Charvet et al., 2007; Konopelko et al., 2007; Gao et al., 2009; Wang et al., 2009; Glorie et al., 2010; Yang et al., 2013). During Triassic and Jurassic times, the Southwest Tian Shan, as well as the adjacent tectonic units apparently underwent a major period of tectonic quiescence (e.g. Dumitru et al., 2001; Jolivet et al., 2010; Han et al., 2011).

2.2.2 The western Tarim

The Tarim craton is one of the largest cratons in China (Fig. 2.1; Zheng et al., 2013). It is characterized by Neoarchean to Palaeoproterozoic metamorphic basement

(granitic gneisses, schists, marbles, quartzites, and stromatolitic limestones) with zircon U-Pb ages varying from 2830 to 1900 Ma (Long et al., 2010, 2011a,b, 2012; Zhao and Guo, 2012; Zhang et al., 2013). This basement is unconformably covered by Mesoproterozoic to Paleozoic marine to non-marine sediments (e.g. Guo et al., 2003; Deng et al., 2008; Lu et al., 2008; Ren et al., 2011; Shu et al., 2011; Zhang et al., 2012; Ge et al., 2012; 2013a,b; Zhao and Cawood, 2012; He et al., 2012). The Silurian and Devonian series exposed along the northern margin of the Tarim Basin corresponds to passive margin sediments composed of clastic rocks and limestones (e.g. Ren et al., 2011). The Middle Devonian limestones unconformably overly the Silurian series (e.g. Zhang et al., 2004; Zhou and Chen 1990), and both Silurian and Devonian sediments were deformed and intensely metamorphosed. The overlying marine Carboniferous sediments (limestones and marine detrital facies) show a total thickness ranging between 2900 and 3400 m (e.g. Zhou and Chen, 1990; Jia et al., 2004). Finally, Permian molasses and continental volcanic rocks are well developed in the northern part of the Tarim craton (e.g. BGMRXUAR, 1993; Shu et al., 2007; Yang et al., 2007; Tian et al., 2010; Zhang et al., 2010a, 2010b).

In the western Tarim Basin, the Upper Triassic series are locally represented in the piedmont of the Southwest Tian Shan, and composed of alluvial to lacustrine clastic rocks interbedded with coal-bearing sandstones. The widespread Lower and Middle Jurassic series are mainly marked by shallow lacustrine deposits, whereas the Upper Jurassic series are formed by alluvial fan deposits. During the Early Cretaceous the lacustrine to alluvial depositional system was still well developed, and marine sedimentary palaeoenvironments are dominant in Upper Cretaceous series (see detailed description below).

The Cenozoic deformation of the Tarim Basin was coupled with mountain building in the surrounding orogenic belts (e.g. Molnar and Tapponnier, 1978; Windley et al., 1990; Yin and Harrison, 2000; Yang and Liu, 2002). This deformation was contemporaneous, and most probably partially responsible for the retreat of the Neotethys Sea from the Tarim Basin towards the West during the Late Eocene (Ramstein et al., 1997; Garzione et al., 2005; Graham et al., 2005; Zhang et al., 2007c; Kent-Corson et al., 2009; Bosboom et al., 2011). This westward retreat of the vast

shallow epicontinental sea that once extended across most of the Eurasian continent is regarded as an important forcing mechanism for the Tertiary aridification and climate change in the Asian continental interior (e.g. Graham et al., 2005; Sun and Wang, 2005; Bosboom et al., 2011).

2.2.3 The western Kunlun and Pamir

The western Kunlun orogenic belt extends from the northern margin of the Tibetan Plateau to the south to the southern margin of the Tarim Basin to the north (Pan, 1990, 1996; Yin and Bian, 1995; Deng, 1996; Matte et al., 1996; Ding et al., 1996; Searle, 1996; Mattern and Schneider, 2000; Wang, 2004). The far-field effects of the India-Eurasia collision induced multi-stages uplift and erosion during the Cenozoic within the range (Sobel and Dumitru, 1997; Jolivet et al., 2001; Cui et al., 2006; Wang et al., 2006; Liu et al., 2010). Based on apatite fission track data, Sobel and Dumitru (1997) suggested that strong exhumation and cooling occurred during Late Oligocene to Middle Miocene. Recent thermochronological results account for a more complex exhumation and deformation pattern, divided into three distinct stages: the Late Oligocene to Early Miocene (Li et al., 2007; Cao et al., 2009; Liu et al., 2010), the Middle to Late Miocene (Wang et al., 1999; Wang et al., 2001; Wang et al., 2002; Cao et al., 2009; Liu et al., 2010) and the Late Miocene to present day (e.g. Li et al., 2005; Li et al., 2007; Cao et al., 2009; Liu et al., 2010). Sedimentation and drainage patterns changed with the uplift of the Kunlun Mountains causing thick accumulations of sediments in the foreland basin in western Tarim (e.g. Zheng et al., 2006).

The Pamir salient, that represents the northwestern continuation of the Tibetan Plateau, evolved during the India-Asia collision (e.g. Burtman and Molnar, 1993; Sobel et al., 2011). The northern Pamir has been interpreted to result from at least 300 km northward shortening with respect to the rest of Eurasia (e.g. Burtman and Molnar, 1993; Cowgill et al., 2010; Fu et al., 2010). On lithospheric scale, this motion can be accommodated by southward continental subduction of the Tarim lithosphere beneath the Pamir (e.g. Burtman and Molnar, 1993; Thomas et al., 1994; Robinson et al., 2007; Fu et al., 2010). Additionally, the deformation in the Pamir propagated towards the Tarim basin during Oligocene to Miocene times, based on provenance changes, sedimentary facies, and thermochronological data from the southwestern Tarim Basin

(Sobel and Dumitru, 1997; Yin et al., 2002; Bershaw et al., 2012). However, according to geometrical and kinematic studies cited above, there was no apparent direct tectonic interaction between the distal northern Pamir and Southwest Tian Shan during the Late Oligocene to Middle Miocene (see also Coutand et al., 2002) such that the provenance data from the Southwest Tian Shan piedmont provided here can be interpreted mainly as derived from a Tian Shan source.

2.2.4 Synthesis of existing geochronology data

2.2.4.1 *U/Pb zircon ages*

In order to assess the potential sources of the detrital zircon age populations in the sediments of the Zhuoyoulehansu section, we compiled the zircon U/Pb data on basement rocks available in South Tian Shan (Fig. 2.5a) (Brookfield, 2000; Yang et al., 2001; Solomovich et al., 2002; Liu et al., 2004; Yang et al., 2006; Konopelko et al., 2007, 2009, 2012; Wang et al., 2007a; Wang et al., 2007b; Zhang et al., 2007a; Djenchuraeva et al., 2008; Sun et al., 2008; Alekseev et al., 2009; Lin et al., 2009; Yang and Zhou, 2009; Hegner et al., 2010; Li, 2010; Orozbaev et al., 2010; Su et al., 2010; Seltmann et al., 2011; Alexeive et al., 2011; Gao et al., 2011; Han et al., 2011; Long et al., 2011; Gou et al., 2012; Huang et al., 2012; Kröner et al., 2012).

The basement U/Pb ages (Fig. 2.5a) can be generally divided into three main groups: 220-390 Ma (sub-peak at 294 Ma), 400-550 Ma (sub-peak at 435 Ma) and 555-1450 Ma (sub-peak at 741 Ma). These groups correspond respectively to the Late Carboniferous – Early Permian post collisional granites of NTS and CTS; The Ordovician to Middle Silurian magmatism of STS and CTS; and finally to the Neo-Proterozoic basement of STS.

Most of the available detrital zircon U/Pb data from sediment series in South Tian Shan were obtained from the Kuqa area to the east and the Tekes area to the west (Figs. 2.1 and 2.5b). These data highlight the previously described major periods of magmatic activity and tectonic movements or quiescence during the Late Paleozoic – Mesozoic. The Cenozoic evolution of the sediments sources is characterized by two variations. A first provenance change in the Lower Paleogene was induced by the uplift and denudation of the South Tian Shan as well as by the coeval rejuvenation of

the basin-range topography. A second major adjustment initiated during the Miocene and resulted from the intense tectonic uplift of South Tian Shan and the corresponding sharp increase in the basin-range topography (e.g. Li and Peng, 2010; Ren et al., 2011).

2.2.4.2 *Apatite fission track ages*

According to the apatite fission track (AFT) ages from the basement, the exhumation history of the Tian Shan Range can be divided into three main stages: a Middle Jurassic to Late Cretaceous erosion phase driven by slow exhumation, mainly characterized by AFT ages ranging between 70 and 160 Ma (e.g. Jia et al., 2003; Glorie et al., 2010; Jolivet et al., 2010); an Early Palaeocene to Late Eocene localized, tectonically driven phase characterized by AFT ages varying from 65 to 35 (e.g. Wang et al., 2009; Glorie et al., 2010; Jolivet et al., 2010); and finally a Late Oligocene to Miocene general exhumation event corresponding to AFT ages ranging from 20 to 25 Ma (e.g. Dumitru et al., 2001; Sobel et al., 2006; Jolivet al., 2010; De Grave et al., 2012). The two last stages correspond to major tectonic uplift and topographic adjustments in South Tian Shan.

The available detrital apatite fission track ages were mostly obtained from the piedmont of Southwest Tian Shan, and generally range between 13 and 197 Ma (Fig. 2.6). Four statistically distinguishable peak ages of 16 Ma, 49 Ma, 98 Ma, and 145 Ma are observed on the detrital age compilation histogram (Fig. 2.6). The peak age of 145 Ma is interpreted as non-reset source ages corresponding to the AFT age of the Mesozoic surface still observed in the range (e.g. Dumitru et al., 2001; Jolivet et al., 2010). The peak age of 16 Ma corresponds to the Late Oligocene – Early Miocene reactivation and strong exhumation of the Tian Shan Range. The two last detrital age groups represented by peak ages of 49 Ma and 98 Ma are more difficult to interpret. Those ages most probably correspond to partially annealed Mesozoic ages although some Late Cretaceous ages have been recorded on basement samples in the range (e.g. Dumitru et al., 2001; Wang et al., 2009; Glorie et al., 2010; Jolivet et al., 2010) and might participate to those detrital ages.

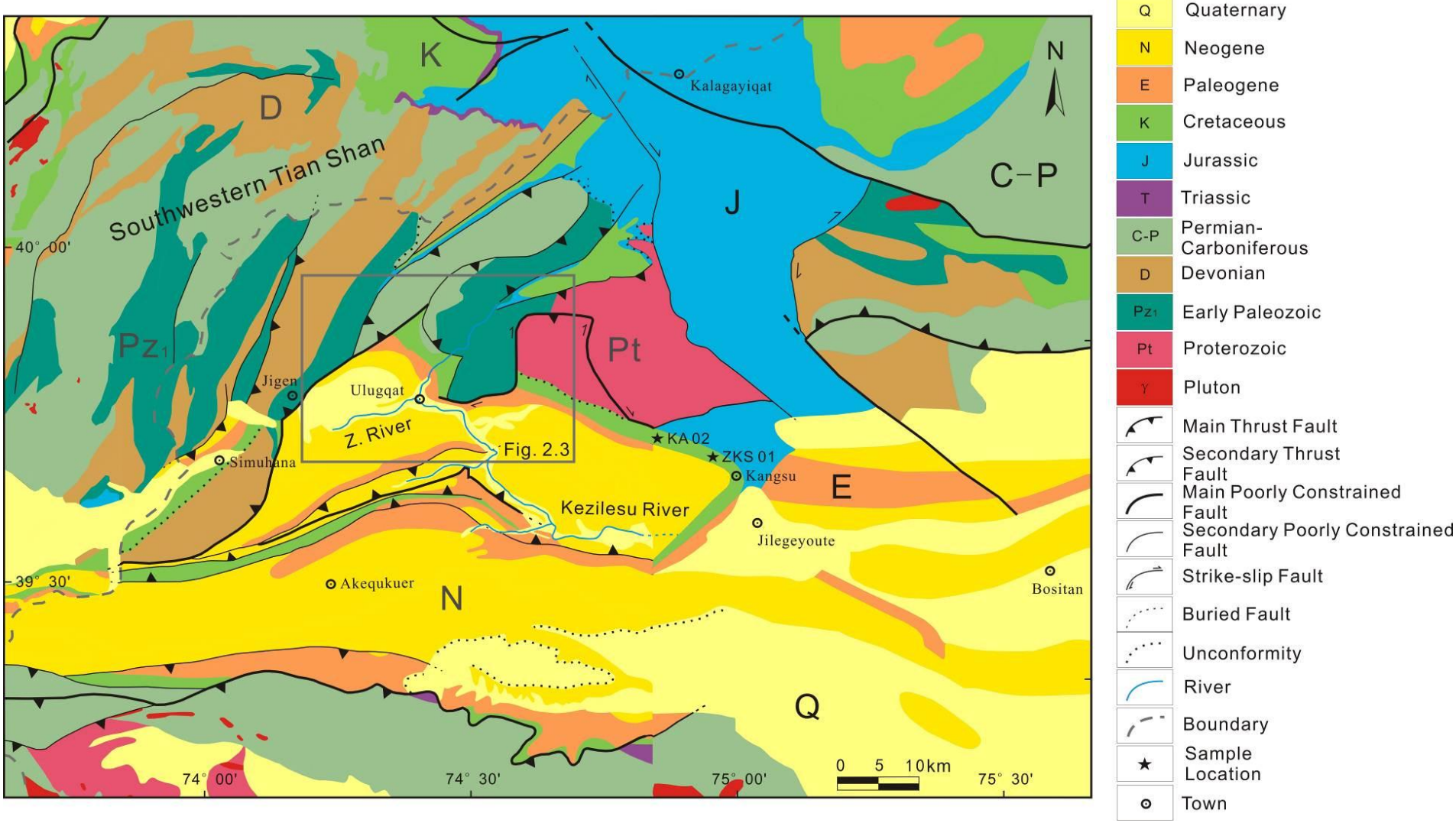
Southwestern Tian Shan
K
D
C–P
J
N
Pz1
Pt
Kalagayiqat
Jigen
Ulugqat
Z. River
Fig. 2.3
Simuhana
KA 02
ZKS 01
Kangsu
E
Kezilesu River
Jilegeyoute
Akequkuer
Bositan
Q
40° 00'
39° 30'
74° 00'
74° 30'
75° 00'
75° 30'
0 5 10km
Quaternary
Neogene
Paleogene
Cretaceous
Jurassic
Triassic
Permian-Carboniferous
Devonian
Early Paleozoic
Proterozoic
Pluton
Main Thrust Fault
Secondary Thrust Fault
Main Poorly Constrained Fault
Secondary Poorly Constrained Fault
Strike-slip Fault
Buried Fault
Unconformity
River
Boundary
Sample Location
Town

Fig. 2.2 Geological and tectonic sketch map of the Southwestern Tian Shan crossing northwestern China and Kyrgyzstan with the approximate location of Fig. 2.3 shown with a box and samples locations of KA02 and ZKS01 (modified after BGMRXUAR, 1978). "Z. River" is the Zhuoyoulehansu river.

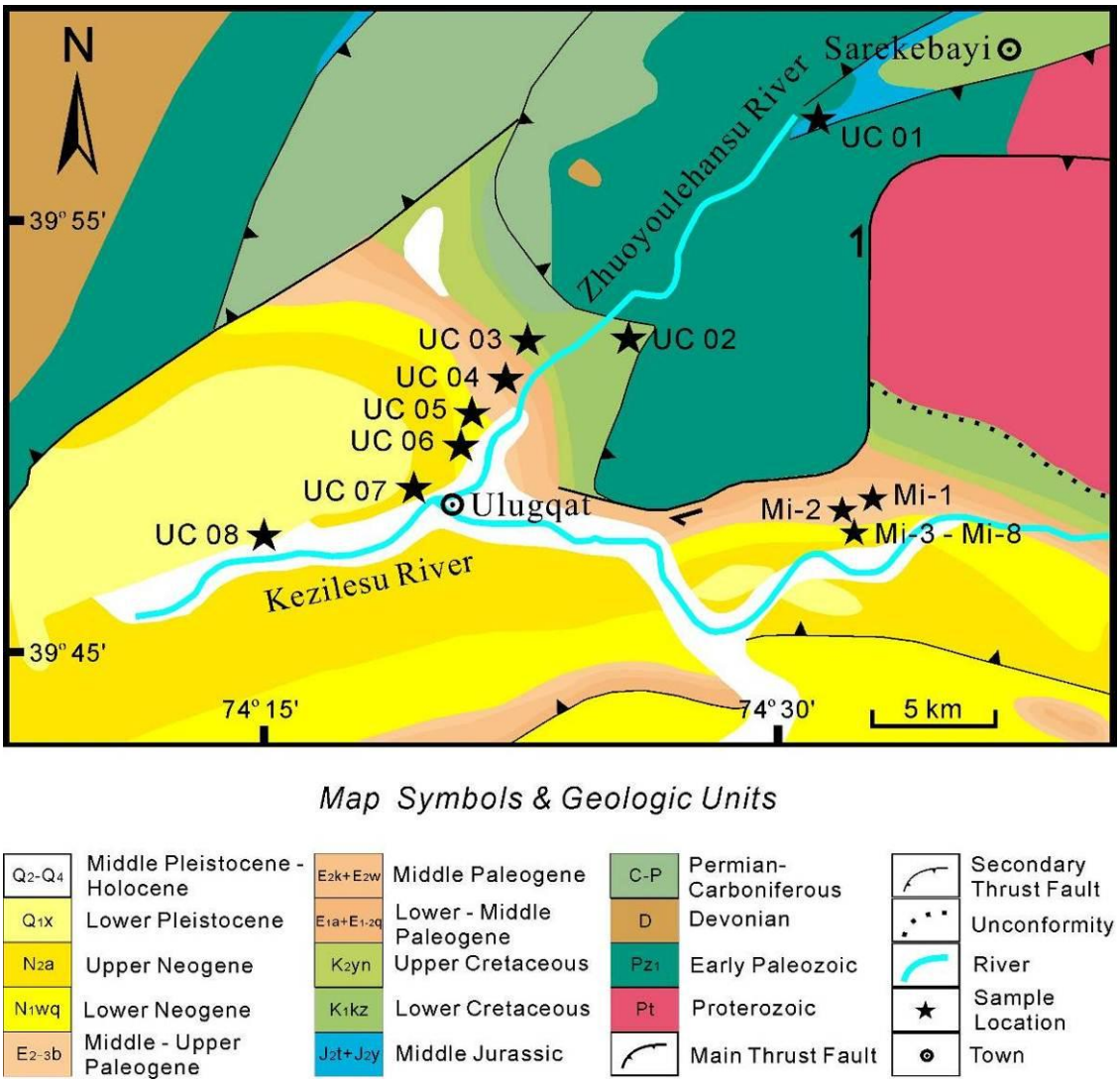

Fig. 2.3 Simplified geological map of the Ulugqat area with the position of the samples, except samples KA02 and ZKS01which are reported on Fig. 2.2 (modified after BGMRXUAR, 1978).

2.3 Sampling and analytical methods

2.3.1 Sampled strata

The exceptional preservation and exposure of the Jurassic to Quaternary sedimentary series along the sampled Zhuoyoulehansu river section (Figs. 2.2 and 2.3) allows a continuous description of the Mesozoic-Cenozoic sedimentary evolution of the westernmost part of the Tarim Basin (Fig. 2.4) summarized below.

The base of the studied profile is formed by the Middle Jurassic series, consisting in the Yangye Formation and the Taerga Formation in ascending order. Both formations are composed of fine-grained clastic deposits, mainly mudstones and sandstones. The Yangye Formation contains thin coal layers and the Taerga Formation is characterized by the occurrence of calcareous sandstones (Jia et al., 2004; Zhang et al., 2011). The two formations are considered as shore to shallow lake sedimentary series (Jia et al., 2004). The following, concordant Upper Jurassic Kuzigongsu Formation (c.a. 1930 m thick) mainly consists in conglomerates, sandstones and siltstones, and is considered as alluvial fan deposits, associated to a dry and hot climate (Jia et al., 2004; Zhang et al., 2011).

The Cretaceous series, showing a maximum thickness about 1500 m, are divided into the Kezilesu Group and the Yingjisha Group (Jia et al., 2004) (Figs. 2.3 and 2.4). The Kezilesu Group is mainly composed of conglomerates at the base and sandstones in the upper part. This succession is interpreted as a transition from alluvial to braided river sedimentary facies. The conformably overlying Yingjisha Group is mainly composed of marine platform sediments, implying a transgression phase following the deposition of the Kezilesu Group (Jia et al., 2004; Zhang et al., 2011).

The Paleogene series consists successively in the Tuyiluoke Formation, the Aertashi Formation, the Qimugen Formation, the Kalatar Formation, the Wulagen Formation and the Bashibulake Formation (Figs. 2.3 and 2.4). The Tuyiluoke and Aertashi formations are characterized by gypsum and dolomitic limestones and are interpreted as a lagoonal depositional environment. The following Qimugen Formation is mainly composed of fine-grained clastic deposits, bog-time lens and thin limestone beds reflecting neritic or littoral to lagoonal environments (e.g. Jia et al., 2004). The

Kalatar and Wulagen formations again represent a marine environment with shell limestones and fine-grained clastic deposits (Zheng et al., 1999; Gao et al., 2000; Jia et al., 2004; Bosboom et al., 2011). Finally, the Bashibulake Formation marks the onset of a regression phase with the deposition, in a neritic to littoral environment of mudstones and massive sandstones, and some of them coarse grained (Jia et al., 2004; Zhang et al., 2011; Bershaw et al., 2012).

The Neogene series consists in the Wuqia Group (Keziluoyi and Anjuan formations) and the Atushi Formation in ascending order (Figs. 2.3 and 2.4). The Wuqia Group (up to 6050 m thick) is mainly composed of mudstones and sandstones, and is generally associated to fluvial and alluvial depositional environments. The overlying 760 to 2080 m thick Atushi Formation mainly consists in conglomerates and sandstones interbedded with minor mudstones, and represents alluvial sedimentary environments (Jia et al., 2004; Zhang et al., 2011; Bershaw et al., 2012).

Finally, the Quaternary Xiyu, Wusu and Xinjiang formations (Figs. 2.3 and 2.4) are widespread throughout Central Asia and characterized by typical conglomerates, interbedded with sandstones and mudstones corresponding to alluvial fan deposits (Charreau et al., 2009).

In this study, 8 sandstone samples ranging in age from the Middle Jurassic to the Quaternary (UC01 – UC08) were collected along the Zhuoyoulehansu river section nearby the Ulugqat village in order to perform U/Pb (LA-ICP-MS) dating of detrital zircons (Figs. 2.1 and 2.2). Two additional samples from Early Cretaceous sediments (KA02, ZKS01) were collected from the Kangsu section, east of Ulugqat village, for apatite fission track analysis (Figs. 2.1 and 2.2). Finally, 8 samples from Late Paleogene to Early Neogene sediments (Mi-01 to Mi-08) were collected from the Bashibulake Mine section, immediately east of the Ulugqat river, to complement the apatite fission track analysis of the Cenozoic series (Figs. 2.1 and 2.2).

Detrital heavy minerals were separated using the standard procedures for mineral separation (e.g. Li et al., 2004). This work was conducted in the Chengxin Geology Service Co. Ltd, Langfang, Hebei Province, China. Zircons and apatites were

specifically extracted using heavy liquids and magnetic techniques and finally purified by hand picking and careful identification under a binocular microscope.

2.3.2 U/Pb on zircon

Detrital zircon U/Pb chronology has become a powerful tool for sediment provenance analysis and geodynamic studies (e.g. Fedo et al., 2003). The systematic study of the variations through time of the characteristics of detrital zircon ages populations obtained from sedimentary sequences in basins can reveal changes in basin-range relationship (e.g. Liu et al., 2013; Yang et al., 2013). A detailed study of the U/Pb detrital zircon age populations in continuous sediment series may thus help to understand the evolution of the sediment sources and thus of the surrounding topography through time (e.g. Gehrels and Dickinson, 1995; Bruguier et al., 1997; Ireland et al., 1998; Yang et al., 2013).

A quantity of zircon grains (generally more than 200) were randomly selected, enclosed in epoxy resin and polished to yield a smooth flat internal surface (slice). After being photographed under reflected and transmitted light, the samples were prepared for cathodoluminescence (CL) imaging in order to choose potential internal target sites for U/Pb dating (e.g. Yuan et al., 2007; Long et al., 2010; Yang et al., 2013).

CL imaging was carried out using a Quanta 200 FEG Scanning Electron Microscope at Peking University. CL images of typical zircon grains are presented in Fig. 2.7. Laser Ablation-Inductively Coupled Plasma-Mass Spectrometer (LA-ICP-MS) U/Pb dating was conducted on an Agilent 7500a ICP-MS connected to a 193nm Excimer laser ablation system (American New Wave UP 193 SS) at the China University of Geosciences, Beijing. The operating parameters were as follows: Ar plasma gas flow rate was 1.13 l/min, Radio Frequency (RF) power was 1350 W and elemental integral time was 10 ms for Si, Zr and 50 ms for other elements. Helium with a flow rate of 0.89 1/min was used as the carrier gas to enhance the transport efficiency of the ablated material. The spot diameter was 36 μm with an analytical laser frequency of 10 Hz. Each analysis consisted in 5 s pre-denudation and 45 s signal acquisition. The GLITTER 4.4.1 software was used to calculate the U/Pb isotope ratios and elements contents. Age calculations, plotting of relative

probability and concordia diagrams were made using ISOPLOT (version3.0) (Ludwig, 2003). Standard zircon Tomorrow (Black et al., 2003; Qi et al., 2005) was used as an external standard for correction of isotopic ratios to calculate the U/Pb ages, while zircons Qinghu and 91500 (Wiedenbeck et al., 1995) were the monitoring standards. For elemental concentration analysis, NIST 610 was the external standard, and ^{29}Si was the internal standard. Meanwhile, NIST 612 and NIST 614 were used as monitoring standards. The common-Pb correction was performed following the method described by Andersen (2002). A detailed description of the technical procedure is given in Yuan et al. (2004) and Song et al. (2010).

For usual U/Pb (LA-ICP-MS) dating of detrital zircons, about 80-120 grains for each sample can meet the requirements of statistical analysis of basic detrital ages distribution (Andersen, 2005). In this study, due to the small amount of zircon grains available in samples UC01 and UC03 collected in the Middle Jurassic (J_2y+J_2t) and Upper Cretaceous (K_2yn) series (Fig. 2.8), 43 and 48 zircon grains respectively satisfied the test conditions, while 40 and 48 effective U/Pb ages were obtained from them. However, one hundred crystals were randomly selected for analysis from each of the 6 samples collected in the Lower Cretaceous (K_1kz) to the Quaternary (Q_1x) series (Figs. 2.2, 2.3 and 2.4), so that the results should reflect the provenance characteristics. Between 100 and 99 effective U/Pb ages were obtained from these samples (Table 2.1). Those ages with discordance degree >10 % were excluded from analysis (Gehrels et al., 2003; Prokopiev et al., 2008). Isotopic ages with errors and related raw data are listed in full as appendix A.

2.3.3 Apatite fission track analysis

The apatite samples were mounted on glass slides using epoxy glue and polished. Samples were etched in 6.5 % HNO_3 (1.6 M) for 45 s at 20℃ to reveal the spontaneous fission tracks (Seward et al., 2000), before being irradiated with a neutron fluence rate of 1.0×10^{16} neutrons/cm^2 (Oregon State University Radiation Center, USA). The micas used as external detector were etched in 40% HF for 40 min

at 20 ℃ in order to reveal the induced fission tracks (Jolivet et al., 2010). The ages were calculated following the method recommended by the Fission Track Working Group of the International Union of Geological Sciences Subcommission on Geochronology (Hurford, 1990) using the zeta calibration method (Hurford and Green, 1983). CN5 glass was used as a dosimeter. Ages were calculated using an overall weighted mean zeta value of 343 ± 7 yr cm^2 (WY), obtained on both Durango (McDowell et al., 2005) and Mount Dromedary apatite standards (Green, 1985; Tagami, 1987). Fission tracks were counted in Geosciences Rennes on a Zeiss M1 microscope, using a magnification of 1250 under dry objectives and the Autoscan® software (on manual mode). Data are reported in Table 2.

Errors on ages are quoted at $\pm 2\ \sigma$. As a general standard, only crystals sections that are parallel to the *c* axis have been considered for age determination.

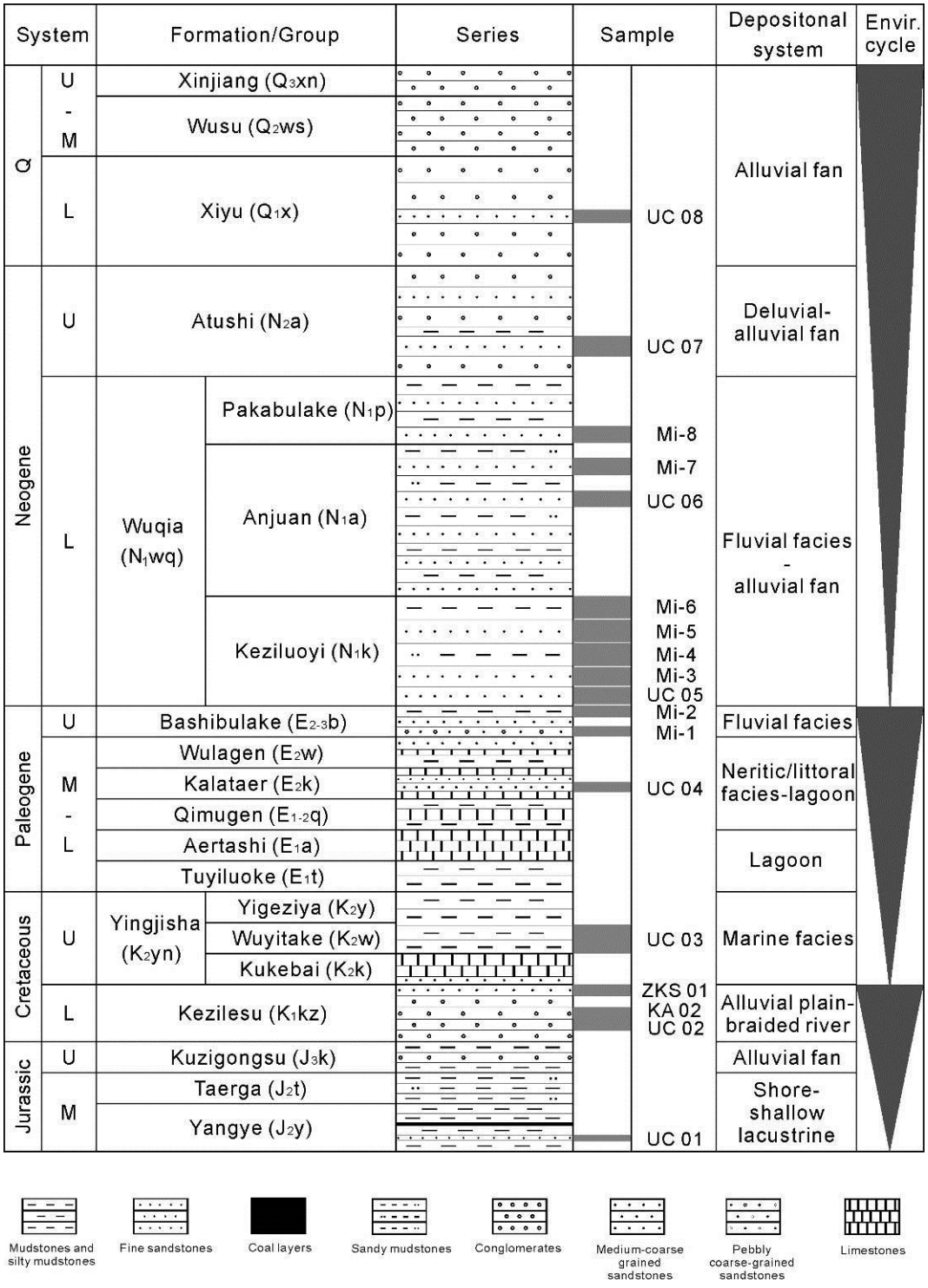

Fig. 2.4 Generalized stratigraphic column of the Middle Jurassic to Quaternary series of the studied area (modified after Zhang et al., 2011).

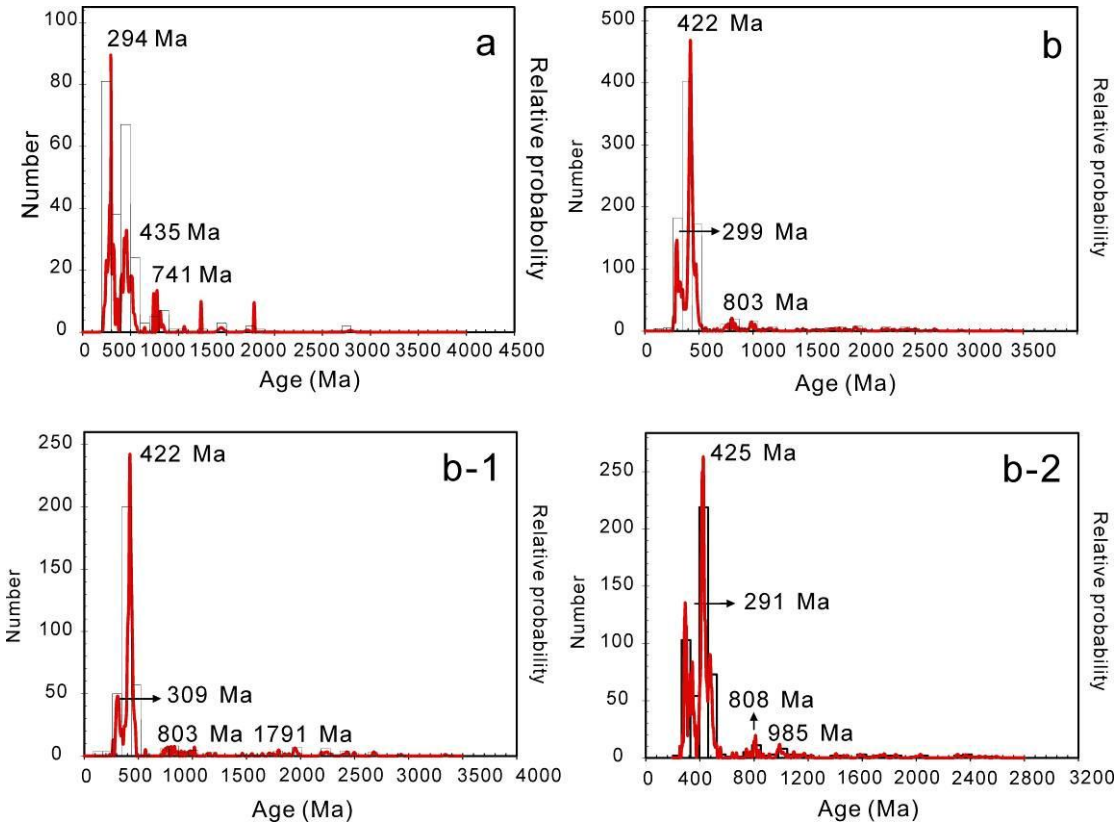

Fig. 2.5 (a) Combined relative probability density and histogram plots of the available zircon U/Pb data on basement rocks in South Tian Shan (Brookfield, 2000; Yang et al., 2001; Solomovich et al., 2002; Liu et al., 2004; Yang et al., 2006; Konopelko et al., 2007, 2009, 2012; Wang et al., 2007a; Wang et al., 2007b; Zhang et al., 2007a; Djenchuraeva et al., 2008; Sun et al., 2008; Alekseev et al., 2009; Lin et al., 2009; Yang and Zhou, 2009; Hegner et al., 2010; Li, 2010; Orozbaev et al., 2010; Su et al., 2010; Seltmann et al., 2011; Alexeive et al., 2011; Gao et al., 2011; Han et al., 2011; Kröner et al., 2012; Long et al., 2011; Gou et al., 2012; Huang et al., 2012). (b) Combined relative probability density and histogram plots of the detrital zircon U/Pb ages of sediments from the South Tian Shan piedmont. A summary plot of all available U/Pb detrital zircon ages (b-1) Summary of the U/Pb detrital zircon ages from Kuqa area (Li and Peng, 2010). (b-2) Summary of the U/Pb detrital zircon ages from Tekes area (Ren et al., 2011).

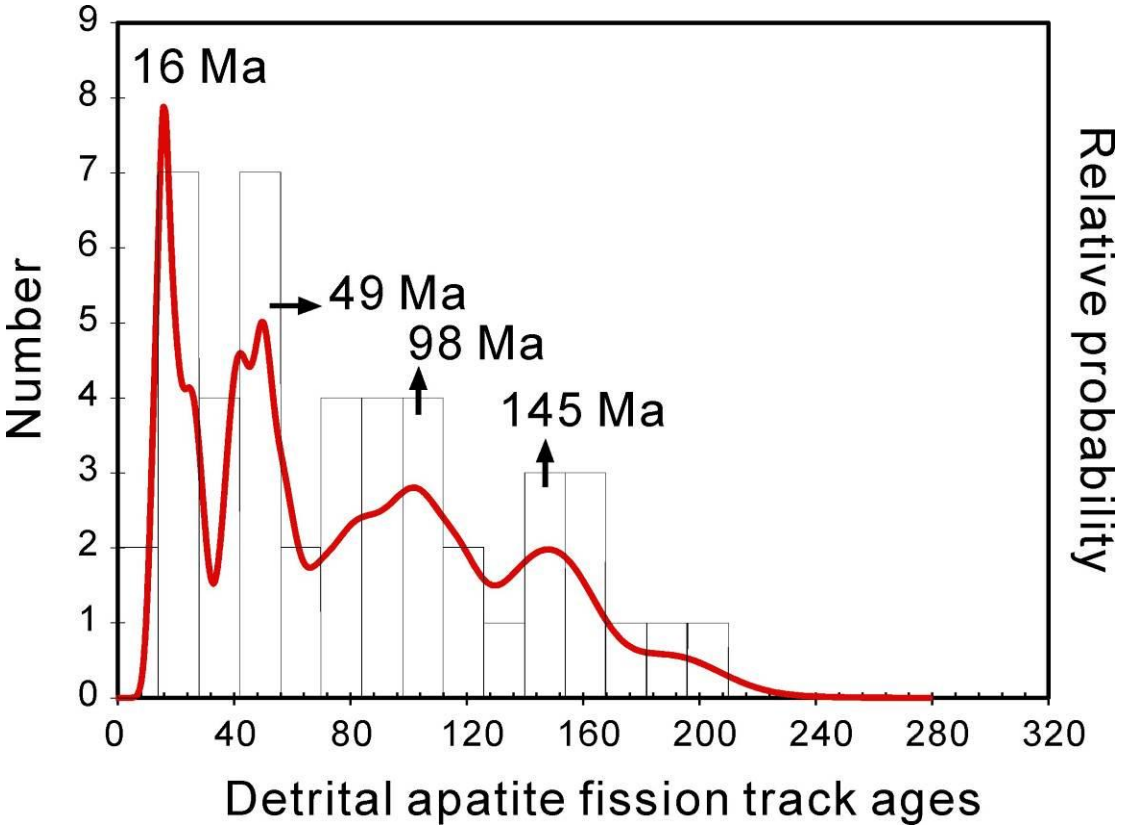

Fig. 2.6 Summary of detrital apatite fission track ages obtained from the piedmont of Southwest Tian Shan (e.g. Sobel and Dumitru, 1997; Dumitru et al., 2001; Jia et al., 2003; Sobel et al., 2006; Du et al., 2007a, 2007b; De Grave et al., 2012), 50-80 Ma (e.g. Sobel and Dumitru, 1997; Dumitru et al., 2001; Du et al., 2007a, 2007b), and 15-20 Ma (e.g. Sobel and Dumitru, 1997; Dumitru et al., 2001; Sobel et al., 2006; De Grave et al., 2012).

2.4 Results

2.4.1 U-Pb Geochronology of detrital zircons

The various age groups and the corresponding statistical data for all the samples are shown in Table 2.1.

2.4.1.1 *Mesozoic samples*

The U/Pb ages from the Middle Jurassic Yangye Formation (sample UC01) range from 271 to 2513 Ma, and can be statistically divided into four main groups: 270-300 Ma (accounting for about 5 %), 400-480 Ma (about 26 %), 720-1120 Ma (about

28.0%), and 1200-2520 Ma (about 21 %) (Figs. 2.8 and 2.9; Table 2.1). The distribution of the detrital zircon U/Pb ages of this sample is characterized by peak ages at 272, 453, 840 and 1112 Ma (Fig. 2.8). Comparing with the histogram obtained for the zircon U/Pb ages of the Tian Shan basement (Fig. 2.5a), the 270-300 Ma age group (peak age of 272 Ma) mainly reflects the Late Carboniferous – Early Permian post-collisional granites, and corresponds to the age group of 220-390 Ma (peak age at 294 Ma) in the histogram of basement U/Pb ages (e.g. Wang et al., 2007, 2009; Han et al., 2010); the 400-480 Ma age group (peak age of 453 Ma) is mainly assigned to the Ordovician to Middle Silurian magmatism (e.g. Gao et al., 1998, 2009; Lin et al., 2009), and corresponds to the age population of 400-550 Ma (sub-peak at 435 Ma) in the histogram of basement U/Pb ages; finally the age group of 720-1120 Ma (peak ages of 840 and 1112 Ma) partly reflects the Neo-Proterozoic basement in Southwest Tian Shan, corresponding to the 555-1450 Ma (sub-peak at 741 Ma) in the basement histogram. There is almost no Meso-Proterozoic – Archean signal in the histogram of basement U/Pb ages from Southwest Tian Shan. The 1200-2520 Ma age group (itself potentially formed by several sub-peaks of only a few individual ages that we willingly did not distinguish due to their poor representativity) most probably corresponds to the Proterozoic Tarim basement eroded and deposited on the northern passive margin during Early Paleozoic times (Liu et al., 2013). A number of Precambrian plutons have been dated in the Tarim block, corresponding to the break-up of the Rodinia supercontinent (peak age around 800 Ma) (e.g. Zhang et al., 2003; Zeng et al., 2006; Wu et al., 2009, 2010); the Genvilian orogeny (ca. 1300-900 Ma) (e.g. Hoffman, 1991; Li et al., 2008, 2009); the supposed Columbia supercontinent (peak age at 1870 Ma) (e.g. Daly et al., 2001; Santosh et al., 2006); and finally the initial core of the Tarim craton (peak age at 2473 Ma) (e.g. Long et al., 2010; Shu et al., 2011). The Paleozoic sediments containing those Proterozoic zircons are thus recycled during the Mesozoic evolution of the range. For this Middle Jurassic sample (UC01), the zircons ranging in the age intervals 270-300 Ma and 400-480 Ma, mainly display well-developed oscillatory zoning, interpreted to reflect a magmatic genesis (about 85 %, Fig. 2.7). However, for the detrital zircons dated in the age populations of 720-1120 Ma and 1200-2520 Ma, most grains are considered to be of metamorphic origin based on the faint internal zoning and/or the occurrence of inherited cores

(about 95 %, Fig. 2.7). Except for the very low value of 0.08, the Th/U ratios of the zircons vary from 0.11 to 2.94 and are predominantly higher than 0.40 (about 79 %) reflecting that magmatic zircons are relatively in majority (Appendix A).

In the Lower Cretaceous Kezilesu Group (sample UC02), the U/Pb detrital zircon ages range widely from 241 to 3179 Ma, and can be divided into four main groups: 250-320 Ma (about 16 %), 400-500 Ma (about 26 %), 700-1600 Ma (about 12 %) and 1800-2800 Ma (about 31 %), with peak ages of 268, 443, 854, 1853 and 2316 Ma (Figs. 2.8 and 2.9; Table 2.1). Comparing the age populations with the histogram obtained from the basement data (Fig. 2.4), the 250-320 Ma age group (peak age of 268 Ma) again reflects the Late Carboniferous – Early Permian post-collisional granites, and corresponds to the age group of 220-390 Ma (peak age at 294 Ma) in the histogram of basement data; the 400-500 Ma age group characterized by a peak age of 443 Ma, is mainly assigned to the Ordovician to Middle Silurian magmatism, and would correspond to the age population of 400-550 Ma (peak age of 435 Ma) in the basement histogram; Similarly, the age populations of 700-1600 Ma (peak age of 854 Ma) and 1800-2800 Ma (peak ages of 1853 and 2316 Ma), partly representing the Neo-Proterozoic basement, and partly the Meso--Proterozoic - Archean basement, would respectively correspond to the 555-1450 Ma (peak age of 741 Ma) in the histogram of basement U-Pb ages from Southwest Tian Shan, and recycling of the Early Paleozoic passive margin fragments of the Tarim craton. The zircon crystals ranging in the age groups of 250-320 Ma and 400-500 Ma are dominantly characterized by relatively distinct oscillatory zoning (about 83 %, Fig. 2.7) indicating the predominantly magmatic origin of the zircons. However, a small proportion (about 17 %) of metamorphic grains are also observed. On the other hand, the zircons dated in the age populations of 700-1600 Ma and 1800-2800 Ma mainly display faint internal zoning, and/or inherited cores, reflecting their metamorphic origin (about 89 %, Fig. 2.7). Only a few can be regarded as magmatic zircons. Except for four grains with very low values of 0.01, 0.05 and 0.09 (two grains), the Th/U ratios of the zircons vary from 0.13 to 2.94 and are predominantly higher than 0.40 (about 80 %) indicating that magmatic zircons are also in majority (Appendix A).

In the Upper Cretaceous Yingjisha Group (sample UC03) the U/Pb ages range from 288 to 2570 Ma, and can be statistically divided into three main groups: 280-320 Ma (accounting for about 10 %), 400-540 Ma (50 %), and 600-2570 Ma (about 27 %) (Figs. 2.8 and 2.9; Table 2.1). The age spectrum of this sample is characterized by peak ages of 307, 437 and 2540 Ma (Fig. 2.8). Comparison with the basement data suggests that the 280-320 Ma characterized by a peak age of 307 Ma might again reflect the post-collisional granites in Tian Shan, and corresponds to the age group of 220-390 Ma (peak age at 294 Ma) in the histogram of basement data; the 400-540 Ma age population (peak age of 437 Ma), mainly suggesting the Ordovician to Middle Silurian magmatism, should corresponds to the age population of 400-550 Ma (peak age of 435 Ma) in the U/Pb basement ages histogram. Finally, the age group of 600-2570 Ma characterized by a peak age of 254 Ma is partly assigned to the Neo-Proterozoic basement, and partly to the Meso--Proterozoic - Archean basement, respectively reflecting the 555-1450 Ma (peak age of 741 Ma) age group and recycling of the Tarim basement. The zircons ranging in the age intervals 280-320 Ma and 400-540 Ma, mainly display well-developed oscillatory zoning, interpreted to reflect a magmatic genesis (about 87 %, Fig. 2.7). However, for the detrital zircons dated in the age population of 600-2570 Ma, most grains are considered to be of metamorphic origin based on the faint internal zoning and/or the occurrence of inherited cores (about 88 %, Fig. 2.7). The Th/U ratios of the zircons from this sample vary from 0.13 to 1.56 and are predominantly higher than 0.40 (about 88 %) suggesting that magmatic zircons are again in majority (Appendix A).

2.4.1.2 *Cenozoic samples*

The U/Pb detrital ages from the Eocene Kalatar Formation (sample UC04) range widely between 222 and 2602 Ma, and can be divided into four main groups: 250-320 Ma (23 %), 400-520 Ma (29 %), 720-1240 Ma (13 %) and 1670-2610 Ma (17 %) (Figs. 2.8 and 2.9; Table 2.1). The U/Pb detrital zircon ages distribution of this sample is characterized by peak ages of 269, 460, 819, 919 and 1836 Ma (Fig. 2.8). Comparing with the histogram obtained for the zircon U/Pb ages of the Tian Shan basement (Fig. 2.5a), the 250-320 Ma age group (peak age of 269 Ma) mainly reflects the Late Carboniferous – Early Permian post-collisional granites, and corresponds to

the age group of 220-390 Ma (peak age of 294 Ma) in the basement histogram; the 400-520 age group (peak age of 460 Ma) would be assigned to the Ordovician to Middle Silurian magmatism, and corresponds to the 400-550 Ma (peak age of 435 Ma) in the basement histogram. The age groups of 720-1240 Ma (peak ages of 819 and 919 Ma) and 1670-2610 Ma (peak age of 1836 Ma), reflect both the Neo-Proterozoic basement and the Meso-Proterozoic – Archean basement, respectively corresponding to the 555-1450 Ma (peak age of 741 Ma) in the basement histogram and recycling of the Early Paleozoic passive margin fragments of the Tarim craton. The zircon crystals ranging in the age groups of 250-320 Ma and 400-520 Ma are dominantly characterized by relatively distinct oscillatory zoning (about 89 %, Fig. 2.7). This zoning indicates the predominantly magmatic origin of the zircons. However, a small proportion (about 11 %) of metamorphic grains is also observed. Zircons dated in the age populations of 720-1240 Ma and 1670-2610 Ma mainly display faint internal zoning, and/or inherited cores, reflecting their metamorphic origin (about 88 %, Fig. 2.7). Only a few can be regarded as magmatic zircons. Except for two grains with very low values of 0.03 and 0.04, the Th/U ratios of the zircons vary from 0.12 to 3.03 and are predominantly higher than 0.40 (80 %) indicating that magmatic zircons are in majority (Appendix A).

Within the Lower Neogene Keziluoyi Formation (sample UC05), the U/Pb detrital zircon ages range from 222 to 2602 Ma, and can be statistically divided into four main groups: 250-320 Ma (16 %), 400-490 Ma (23 %), 550-1200 Ma (23 %) and 1500-2610 Ma (27 %), with peak ages of 261, 452, 621, 995 and 2020 Ma (Figs. 2.8 and 2.9; Table 2.1). The 250-320 Ma age group (peak age of 261 Ma) again reflects the post-collisional granites, and corresponds to the age group of 220-390 Ma (peak age of 294 Ma) in the histogram of basement data from Southwest Tian Shan. Similarly, the age group of 400-490 Ma (peak age of 452 Ma) mainly represents the Ordovician to Middle Silurian magmatism, reflecting the age population of 400-550 Ma (sub-peak of 435 Ma). Finally, the age groups of 550-1200 Ma (peak ages of 621 and 995 Ma) and 1500-2610 Ma (peak age of 2020 Ma), are partly assigned to the Neo-Proterozoic basement, and partly to the Meso--Proterozoic - Archean basement, respectively reflecting the 555-1450 Ma (sub-peak age of 741 Ma) age group and recycling of the Tarim basement. The zircons ranging in the age intervals 250-320 Ma

and 400-490 Ma, mainly display well-developed oscillatory zoning, interpreted to reflect a magmatic genesis (about 92 %, Fig. 2.7). However, for the detrital zircons belonging to the age populations of 550-1200 Ma and 1500-2610 Ma, most grains are considered to be of metamorphic origin based on the faint internal zoning and/or the occurrence of inherited cores (about 78 %, Fig. 2.7). Except for four grains with very low values of 0.01, 0.05, 0.07 and 0.09, the Th/U ratios of the zircons from this sample vary from 0.12 to 1.75 and are predominantly higher than 0.40 (about 70 %) suggesting that magmatic zircons are again in majority (Appendix A).

The U/Pb detrital zircon ages from the Anjuan Formation (sample UC06) in the Early Neogene Wuqia Group, range from 231 to 2621 Ma, and can be generally divided into three main groups: 240-320 Ma (accounting for 14 %), 400-520 Ma (29 %), and 1700-2630 Ma (41 %) (Figs. 2.8 and 2.9; Table 2.1). The age spectrum of this sample is characterized by peak ages of 254, 307, 422, 1814 and 2295 Ma (Fig. 2.8). Comparing the age populations with the histogram obtained from the basement data (Fig. 2.5a), the 240-320 Ma age group (peak ages of 254 and 307 Ma) mainly reflects the Late Carboniferous – Early Permian post-collisional granites, and corresponds to the age group of 220-390 Ma (peak age of 294 Ma) in the basement histogram; the 400-520 age group (peak age of 422 Ma) is assigned to the Ordovician to Middle Silurian magmatism, and corresponds to the 400-550 Ma (sub-peak age of 435 Ma) in the basement histogram. Finally, the age group of 1700-2630 Ma (peak ages of 1814 and 2295 Ma) reflects both the Neo-Proterozoic basement and the Meso-Proterozoic – Archean basement, respectively corresponding to the 555-1450 Ma (sub-peak age of 741 Ma) in the basement histogram and recycling of the Early Paleozoic passive margin fragments of the Tarim craton. The zircon crystals ranging in the age groups of 240-320 Ma and 400-520 Ma are dominantly characterized by relatively distinct oscillatory zoning (about 96 %, Fig. 2.7). This zoning indicates the predominantly magmatic origin of the zircons. However, metamorphic grains are also observed in small proportion (about 10 %). On the other hand, the zircons belonging to the age population of 1700-2630 Ma mainly display faint internal zoning, and/or inherited cores, reflecting their metamorphic origin (about 91 %, Fig. 2.7). Only a few can be regarded as magmatic zircons. Except for five grains with very low values of 0.02 (two grains), 0.08 (two grains) and 0.09, the Th/U ratios of the zircons vary from

0.2 to 1.54 and are predominantly higher than 0.40 (85 %) indicating that magmatic zircons are in majority (Appendix A).

The detrital U/Pb zircon age composition of the Late Neogene Atushi Formation (sample UC07) is characterized by peak ages of 299, 431, 949 and 2004 Ma (Fig. 2.8). The individual ages range widely from 230 to 2771 Ma and can be statistically divided into four main groups: 250-320 Ma (accounting for about 20 %), 400-520 Ma (about 28 %), 760-1100 Ma (about 12 %) and 1500-2780 Ma (about 31 %) (Figs. 2.8 and 2.9; Table 2.1). The 250-320 Ma age group (peak age of 299 Ma) again reflects the post-collisional granites and corresponds to the age group of 220-390 Ma (peak age of 294 Ma) in the histogram of basement data. Similarly, the age group of 400-520 Ma characterized by a peak age of 431 Ma reflects the Ordovician to Middle Silurian magmatism and corresponds to the 400-550 Ma age population with a sub-peak of 435 Ma in the basement histogram. Finally the 760-1100 Ma (peak age of 949 Ma) and 1500-2780 Ma (peak age of 2004 Ma) are assigned to the Neo-Proterozoic and Meso--Proterozoic - Archean basement, respectively reflecting the 555-1450 Ma age group (sub-peak age of 741 Ma) and recycling of the Tarim basement. The zircons ranging in the age intervals 250-320 Ma and 400-520 Ma, mainly display well-developed oscillatory zoning, reflecting their magmatic origin (about 93 %, Fig. 2.7). However, for the detrital zircons included in the age populations of 760-1100 Ma and 1500-2780 Ma, most grains are considered to be of metamorphic origin based on the faint internal zoning and/or the occurrence of inherited cores (about 84 %, Fig. 2.7). The Th/U ratios of the zircons from this sample vary from 0.11 to 2.70 and are predominantly higher than 0.40 (about 78 %) suggesting that magmatic zircons are in majority (Appendix A).

In the Quaternary Xiyu Formation (sample UC08) the detrital zircon U/Pb ages range widely from 232 to 2685 Ma, and can be divided into four main groups: 260-320 Ma (3 %), 400-480 Ma (8 %), 550-1120 Ma (69 %) and 1640-2690 Ma (16 %), with the peak ages of 269, 452, 613, 766, 1034 Ma and 2028 Ma (Figs. 2.8 and 2.9; Table 2.1). Comparing the age populations with the histogram obtained from the basement data (Fig. 2.5a), the 260-320 Ma age group (peak age of 269 Ma) reflects the Late Carboniferous – Early Permian post-collisional granites, and corresponds to

the age group of 220-390 Ma (peak age of 294 Ma) in the histogram; the 400-480 Ma age group (peak age of 452 Ma) is assigned to the Ordovician to Middle Silurian magmatism, and corresponds to the 400-550 Ma (sub-peak age of 435 Ma) in the basement histogram. The age populations of 550-1120 Ma (peak ages of 613, 766 and 1034 Ma) and 1640-2690 Ma (peak age of 2028 Ma) reflect both the Neo-Proterozoic and the Meso-Proterozoic – Archean basement, respectively corresponding to the 555-1450 Ma (sub-peak age of 741 Ma) in the basement histogram and recycling of the Early Paleozoic passive margin fragments of the Tarim craton. The zircon crystals ranging in the age groups of 260-320 Ma and 400-480 Ma are magmatic, characterized by relatively distinct oscillatory zoning (about 95 %, Fig. 2.7). However, a small proportion (about 5 %) of metamorphic grains is also observed. On the other hand, the zircons dated in the age populations of 550-1120 Ma and 1640-2690 Ma mainly display faint internal zoning, and/or inherited cores, reflecting their metamorphic origin (about 72 %, Fig. 2.7). Only a small proportion can be regarded as magmatic zircons. Except for four grains with very low values of 0.01, 0.07 (two grains) and 0.09, the Th/U ratios of the zircons vary from 0.11 to 2.78 and are mostly higher than 0.40 (71 %) indicating that magmatic zircons are in majority (Appendix A).

In summary, the measured detrital zircons U/Pb ages from the 8 sediment samples ranging in deposition age from Middle Jurassic to Quaternary, vary widely from 222 to 3179 Ma and can be divided into four main groups: 240-320 Ma (peak age of 268 Ma), 400-540 Ma (peak age of 443 Ma) 550-1600 Ma (peak age of 834 Ma) and 1640-2800 Ma (peak age of 1822 Ma) (Fig. 2.10). Based on their morphological characteristics, internal texture and Th/U ratios, the genetic origin of the various types of zircons has been determined showing that magmatic zircons are slightly dominant (51 %), associated to metamorphic crystals (49 %) (Fig. 2.7 and Appendix A). Recycling of the Early Paleozoic passive margin fragments of the Tarim craton is significant within the Mesozoic series, decreasing gradually from the Middle Jurassic to Late Cretaceous. From the Paleogene, recycling increased again until Late Cenozoic times. During the sedimentation of the Quaternary Xiyu Formation, the remarkable amount and diversity of Precambrian zircons recalls the strong recycling

of sediments from the entire Mesozoic and Tertiary sedimentary sequences in the Southwest Tian Shan piedmont (see discussion; Figs. 2.8 and 2.9).

Table 2.1 Summary of the various age groups from the U-Pb geochronology of detrital zircons and the corresponding statistical data for the 8 samples.

Sample code	Main detrital zircon age groups (Ma)	Number of grains in that group	% of total zircon pop.	Number of effective data points
Mesozoic samples				
UC01	270-300	2	5	39
	400-480	10	26	
	720-1120	11	28	
	1200-2520	8	21	
UC02	250-320	16	16	99
	400-500	26	26	
	700-1600	12	12	
	1800-2800	31	31	
UC03	280-320	5	10	48
	400-540	24	50	
	600-2570	13	27	
Cenozoic samples				
UC04	250-320	23	23	100
	400-520	29	29	
	720-1240	13	13	
	1670-2610	17	17	
UC05	250-320	16	16	100
	400-490	23	23	
	550-1200	23	23	
	1500-2610	27	27	
UC06	240-320	14	14	100
	400-520	29	29	
	1700-2630	41	41	
UC07	250-320	20	20	99
	400-520	28	28	
	760-1100	12	12	
	1500-2780	31	31	
UC08	260-320	3	3	100
	400-480	8	8	
	550-1120	69	69	
	1640-2690	16	16	

2.4.2 Fission-track geochronology

The apatite fission track analytical and statistical data for all the samples are shown in Table 2.2.

2.4.2.1 *Mesozoic samples*

Four Mesozoic sediment samples were analyzed using the apatite fission track method (Figs. 2.2 and 2.3). Central ages range from 95.0 ± 4.1 (ZKS01) to 16.6 ± 2.8 Ma (UC02) (Tabel 2.2 and Fig. 2.11).

Only 8 apatite crystals could be dated in sample UC01, from the Middle Jurassic Yangye Formation. However, the central fission track age of 18.5 ± 5.2 Ma obtained for this sample is consistent with the Late Oligocene to Miocene basement exhumation shown by fission track ages previously reported in South Tian Shan (e.g. Dumitru et al., 2001; Sobel et al., 2006; Wang et al., 2009; De Grave et al., 2012). We thus consider that this sample has been totally reset and that the central AFT age represents the age of exhumation during the Tertiary orogenic phase (Fig. 2.11).

Sample UC02, from the Lower Cretaceous Kezilesu Group, shows a central fission track age of 16.6 ± 2.8 Ma obtained from 15 apatite crystals (Fig. 2.11). Although still poorly constrained, this age corresponds to the AFT age obtained in sample UC01 and is again consistent with the Late Oligocene to Miocene basement exhumation.

Sample KA02 was also collected from the Lower Cretaceous Kezilesu Group but further to the east (Fig. 2.2). 97 apatite crystals were analyzed and provided a central fission track age of 76.5 ± 3.7 Ma, very different from the age of 16.6 ± 2.8 Ma obtained in sample UC02. Individual grain ages range from 160 Ma to 35 Ma, indicating that this sample has been partially reset. Individual ages can be separated in two groups: 160 – 70 Ma and 65 – 35 Ma (Fig. 2.11). The first group would broadly correspond to the source ages and record the Middle Jurassic to Late Cretaceous exhumation of the range (e.g. Dumitru et al., 2001; Jia et al., 2003; Glorie et al., 2010; Jolivet et al., 2010). The second group represents crystals that have been more affected by partial resetting (probably due to their different chemical composition) and displays an intermediate age between the Mesozoic sources ages of the first group

and the Tertiary exhumation age of c.a. 18 to 16 Ma as recorded in samples UC01 and UC02.

Sample ZKS01, again from the Lower Cretaceous Kezilesu Group, displays a central fission track age of 95.0 ± 4.1 Ma and is thus again partially reset. 100 apatite crystals have been dated with individual ages ranging between 50 Ma and 212 Ma. The individual fission track ages can be clearly separated into two groups (the *P* (χ^2) value of 0.1 % confirms the occurrence of several age populations) (Tabel 2.2 and Fig. 2.11). A first population of grains with ages ranging between 140 and 120 Ma would correspond, like in the previous samples, to the Middle Jurassic - Cretaceous exhumation phase. The second group, with ages ranging between 90 and 60 Ma displays partially reset ages again intermediate between the previous source ages and the Tertiary exhumation age of c.a. 18 to 16 Ma.

2.4.2.2 *Cenozoic samples*

Twelve Cenozoic samples were analyzed using the apatite fission track method. The central ages obtained from these samples range between 87.4 ± 42.3 (UC04) and 37.2 ± 2.4 Ma (Mi-6) (Table 2.2 and Fig. 2.11).

Sample UC04, from the Eocene Kalatar Formation, has a central age of 87.4 ± 42.3 Ma. However, due to the small amount of apatite crystals available in this sample, only 2 grains were analyzed and the central age is only indicative. Nonetheless, it suggests that this sample has not been, or only slightly been reset (Tabel 2.2 and Fig. 2.11).

Sample Mi-1 from the base of the Upper Paleogene Bashibulake Formation, has a central age of 48.3 ± 2.9 Ma (Table 2.2). The 55 individual ages obtained range between 27 ± 11 Ma and 89 ± 33 Ma. The *P* (χ^2) value of 100 % suggests one single age group. However, the proportion of ages younger than 60 Ma largely increased to 76.4 % and those over 100 Ma disappeared (Fig. 2.11).

Sample Mi-2 from the top of the Upper Paleogene Bashibulake Formation displays a central age of 40.6 ± 5.3 Ma with individual grain ages spread between 28 Ma and

73 Ma (Table 2.2 and Fig. 2.11). However, only 11 grains could be analysed in this sample that should thus only be considered as indicative.

Sample UC05, from the early Neogene Keziluoyi Formation, displays a central age of 69.3 ± 3.5 Ma. The individual ages of the 88 crystals analysed are spread between 112 Ma and 26 Ma, however, has suggested by the *P* (χ^2) value of 100 % that no more than one group can be statistically distinguished (Table 2.2 and Fig. 2.11). The proportion of Tertiary ages younger than 60 Ma (accounting for about 35 %) significantly increased compared to the previous Mesozoic samples. This sample is nonetheless not reset prior to the 18 – 16 Ma exhumation event, with the youngest individual age at 26 Ma. It also implies that none of the younger samples will be reset. However, the occurrence of individual ages similar to the stratigraphic age (within error margin) indicates rapid exhumation within the source area.

Sample Mi-3 from the base of the Lower Neogene Keziluoyi Formation shows a central age of 39.9 ± 2.6 Ma with individual ages (40 crystals analysed) ranging between 26 Ma and 75 Ma. The *P* (χ^2) value of 91 % still suggests one single statistic ages group (Table 2.2). However, the age distribution histogram (Fig. 2.11) displays 2 individual sets of ages, one between c.a. 25 Ma and 50 Ma and the other between c.a. 55 Ma and 80 Ma (Fig. 2.11). This suggests two different apatite sources of which one is being actively exhumed (the younger individual ages are close to the stratigraphic age).

In sample Mi-4 from the Lower Neogene Keziluoyi Formation, only 9 apatite crystals could be analysed. The central age of 47.1 ± 7.8 Ma is only indicative (Table 2.2). The individual ages are spread between 27 Ma and 94 Ma with a *P* (χ^2) value of 66 % suggesting one single statistical ages group. However, as in sample Mi-3 the age distribution histogram displays 2 sets of ages between c.a. 25 Ma and 50 Ma and between c.a. 70 ma and 100 Ma, respectively (Fig. 2.11). Given the small number of data this should be considered with caution.

Sample Mi-5 from the Lower Neogene Keziluoyi Formation has a central age of 42.6 ± 3.2 Ma and a *P* (χ^2) value of 91 % indicating one single statistical ages group (Table 2.2). The individual grain ages range from 26 Ma to 112 Ma but as in sample

Mi-1 and Mi-3, the ages younger than 50 Ma are in majority (72.1 %) indicating a mixture between a Mesozoic source and a Cenozoic source. The occurrence of ages identical to the stratigraphic age of the sample indicates, like in previous samples, an active denudation within the range.

Sample Mi-6 from the Lower Neogene Keziluoyi Formation displays the youngest central age of 37.2 ± 2.4 Ma with a *P* (χ^2) value of 99 % still indicating a single statistical ages group (Table 2.2). The 53 individual ages obtained range between 26 Ma and 102 Ma. However, a large majority of these ages are comprised between c.a. 20 and 50 Ma (81.5 %) reinforcing for the general younging trend in the individual ages observed in the previous samples (Fig. 2.11). The youngest ages are again similar to the stratigraphic age, which indicates continuous exhumation of the source area while older sources are still involved.

Sample Mi-7 from the Lower Neogene Anjuan Formation shows a central age of 45.6 ± 3 Ma (Table 2.2). The 60 individual ages range between 18 Ma and 88 Ma (Fig. 2.11). However, the *P* (χ^2) value of 3 % suggests several statistically different age groups and the ages distribution histogram (Fig. 2.11) can be split in two groups: from c.a. 20 Ma to 40 Ma and from c.a. 40 Ma to 90 Ma. Compared to the previous samples, the proportion of "old" ages (> 40 to 50 Ma) increased (56.7 %) suggesting a variation in the sources and especially in the diversity of sources.

Sample Mi-8 from the Lower Neogene Anjuan Formation has a central age of 53.5 ± 5.3 Ma (Table 2.2). The 39 individual ages range between 21 Ma and 134 Ma and as in sample Mi-7, the *P* (χ^2) value of 0 % suggests several statistical age groups. The individual age distribution histogram (Fig. 2.11) does not clearly display several age groups but a peak between 20 and 30 Ma associated to a pattern with largely spread ages. This, like in sample Mi-7, suggests several sources, of which one corresponds to an area that is still actively exhumed.

Sample UC07, from the Upper Neogene Atushi Formation, shows a central age of 72.1 ± 4.3 Ma. Once again, the 56 individual grains fission track ages range between 133 Ma and 33 Ma and seem to belong to a same group (*P* (χ^2) value of 100 %) (Table 2.2 and Fig. 2.11). While the wide distribution of the individual ages is very similar to

that of samples Mi-8 and Mi-7, the youngest ages are older than the proposed stratigraphic age implying that active denudation within the source area strongly decreased or that the source area changed.

Finally, sample UC08, from the Quaternary Xiyu Formation, has a central age of 72.4 ± 4.2 Ma. 43 crystals were analyzed and the individual ages range between 128 Ma and 31 Ma without significant grouping (P (χ^2) value of 100 %). The amount of fission track ages younger than 60 Ma decreased to some extent (accounting for about 28 %), reinforcing the hypothesis of either a strong decrease of the exhumation in the source area or a change within the drainage system leading to a change in sediment feeding area (Table 2.2 and Fig. 2.11).

Table 2.2 Apatite fission track results. Nb is the number of crystals analyzed. ρ_d is the density of induced fission track density (per cm^2) that would be obtained in each individual sample if its U concentration was equal to the U concentration of the CN5 glass dosimeter. Number in brackets is the total number of tracks counted. ρ_s and ρ_i represent sample spontaneous and induced track densities per cm^2. [U] is the calculated uranium density (in ppm). P (χ^2) is the probability in % of χ^2 for ν degrees of freedom (where ν = number of crystals – 1). FT age is the apatite fission-track central age in Ma. Error is $\pm 2\sigma$.

Sample	Rock type	Latitude/longitude	Altitude (m)	Nb	$\rho_d \times 10^4$ cm^{-2}	$\rho_s \times 10^4$ cm^{-2}	$\rho_i \times 10^4$ cm^{-2}	[U]	$P(\chi^2)$ (%)	FT age (Ma) ($\pm 2\sigma$)
UC01	Sandstone	N 39°54′56″/E 74°24′46″	2578	8	133.5 (13,136)	17.95 (14)	221.79 (173)	19	79.78	18.5 ± 5.2
UC02	Sandstone	N 39°54′45″/E 74°24′24″	2572	15	132.4 (13,136)	22.16 (37)	302.99 (506)	27	99.85	16.6 ± 2.8
UC04	Sandstone	N 39°51′59″/E 74°21′32″	2486	2	128.2 (13,136)	10.91 (6)	27.27 (15)	4	62.69	87.4 ± 42.3
UC05	Sandstone	N 39°51′35″/E 74°20′38″	2508	88	131.4 (13,136)	71.57 (632)	231.48 (2044)	22	100.0	69.3 ± 3.5
UC07	Sandstone	N 39°48′32″/E 74°19′00″	2525	56	130.3 (13,136)	58.82 (457)	180.95 (1406)	17	98.68	72.1 ± 4.3
UC08	Sandstone	N 39°46′21″/E 74°10′22″	2603	43	129.3 (13,136)	80.69 (489)	245.87 (1490)	23	71.81	72.4 ± 4.2
KA02	Sandstone	N 39°48′14″/E 74°50′41″	2820	97	139.2 (13,136)	97.31 (724)	302.15 (2248)	28	99.71	76.5 ± 3.7
ZKS01	Sandstone	N 39°46′47″/E 74°57′24″	2538	100	161.7 (13,136)	104.11 (1749)	308.04 (5175)	22	0.10	95.0 ± 4.1
Mi-1	Sandstone	N 39°51′02″/E 74°32′49″	2825	55	130.1 (12,771)	47.54 (405)	218.90 (1865)	20	100.0	48.3 ± 2.9
Mi-2	Sandstone	N 39°50′46″/E 74°32′25″	2846	11	99.5 (10,204)	58.46 (76)	245.38 (319)	29	82.24	40.6 ± 5.3
Mi-3	Sandstone	N 39°50′44″/E 74°33′46″	2806	40	106.2 (10,405)	68.80 (322)	313.46 (1467)	34	91.39	39.9 ± 2.6
Mi-4	Sandstone	N 39°50′35″/E 74°33′38″	2804	9	110.7 (10,405)	50.00 (46)	201.09 (185)	20	65.93	47.1 ± 7.8
Mi-5	Sandstone	N 39°50′23″/E 74°32′44″	2803	42	109.5 (10,405)	43.68 (242)	191.88 (1063)	21	90.80	42.6 ± 3.2
Mi-6	Sandstone	N 39°50′08″/E 74°32′50″	2772	53	104.5 (10,405)	49.13 (337)	236.30 (1621)	27	99.26	37.2 ± 2.4
Mi-7	Sandstone	N 39°49′58″/E 74°33′18″	2765	60	102.8 (10,405)	53.99 (508)	213.18 (2006)	25	2.82	45.6 ± 3.0
Mi-8	Sandstone	N 39°49′37″/E 74°33′08″	2735	39	132.0 (12,771)	57.63 (287)	266.87 (1329)	24	0.01	53.5 ± 5.3

UC 01

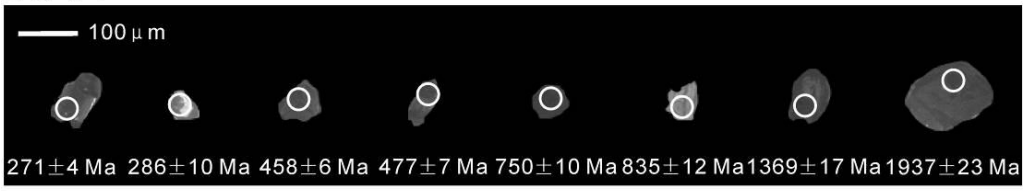

UC 02

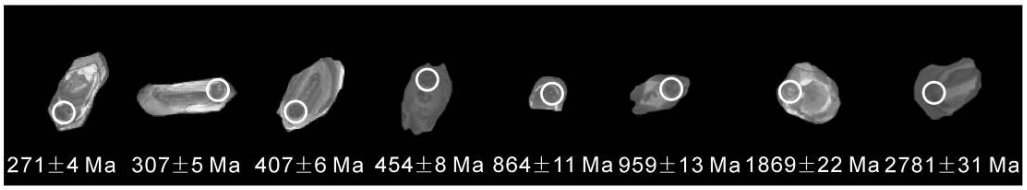

UC 03

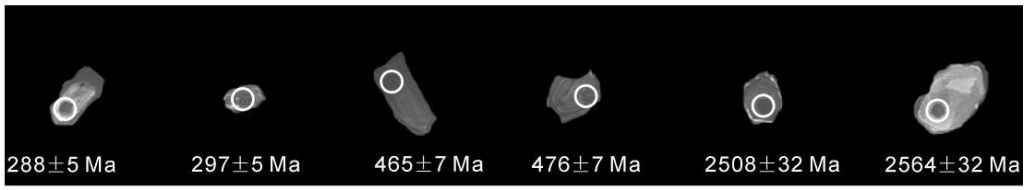

UC 04

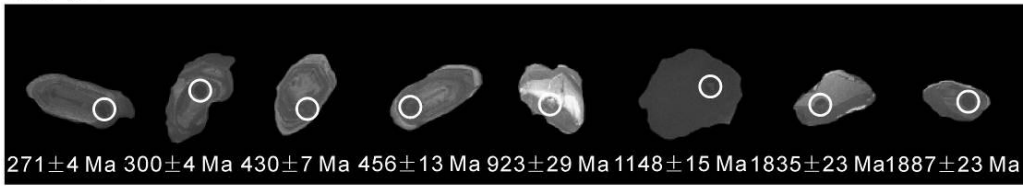

UC 05

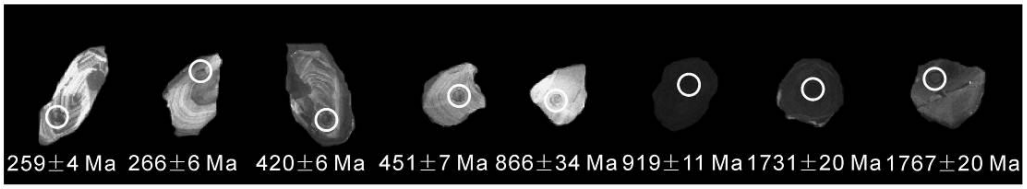

UC 06

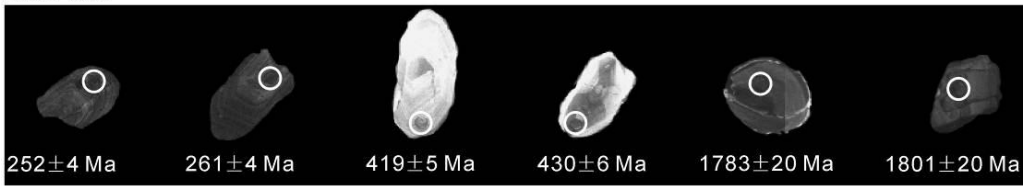

UC 07

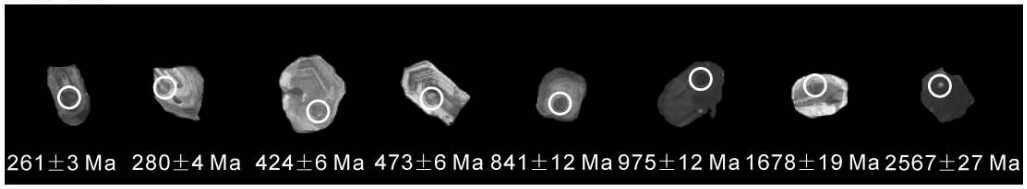

UC 08

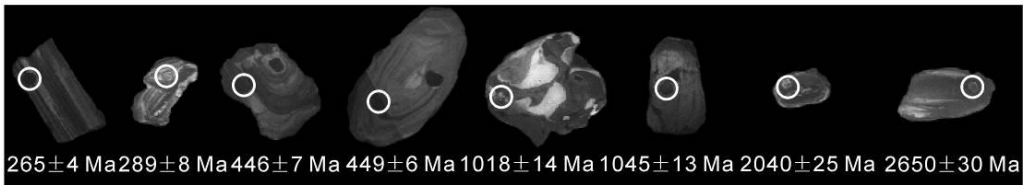

Fig. 2.7 Representative CL images of zircons from the 8 sandstone samples. White circles show location of U/Pb analysis. Numbers are U/Pb ages in Ma**.**

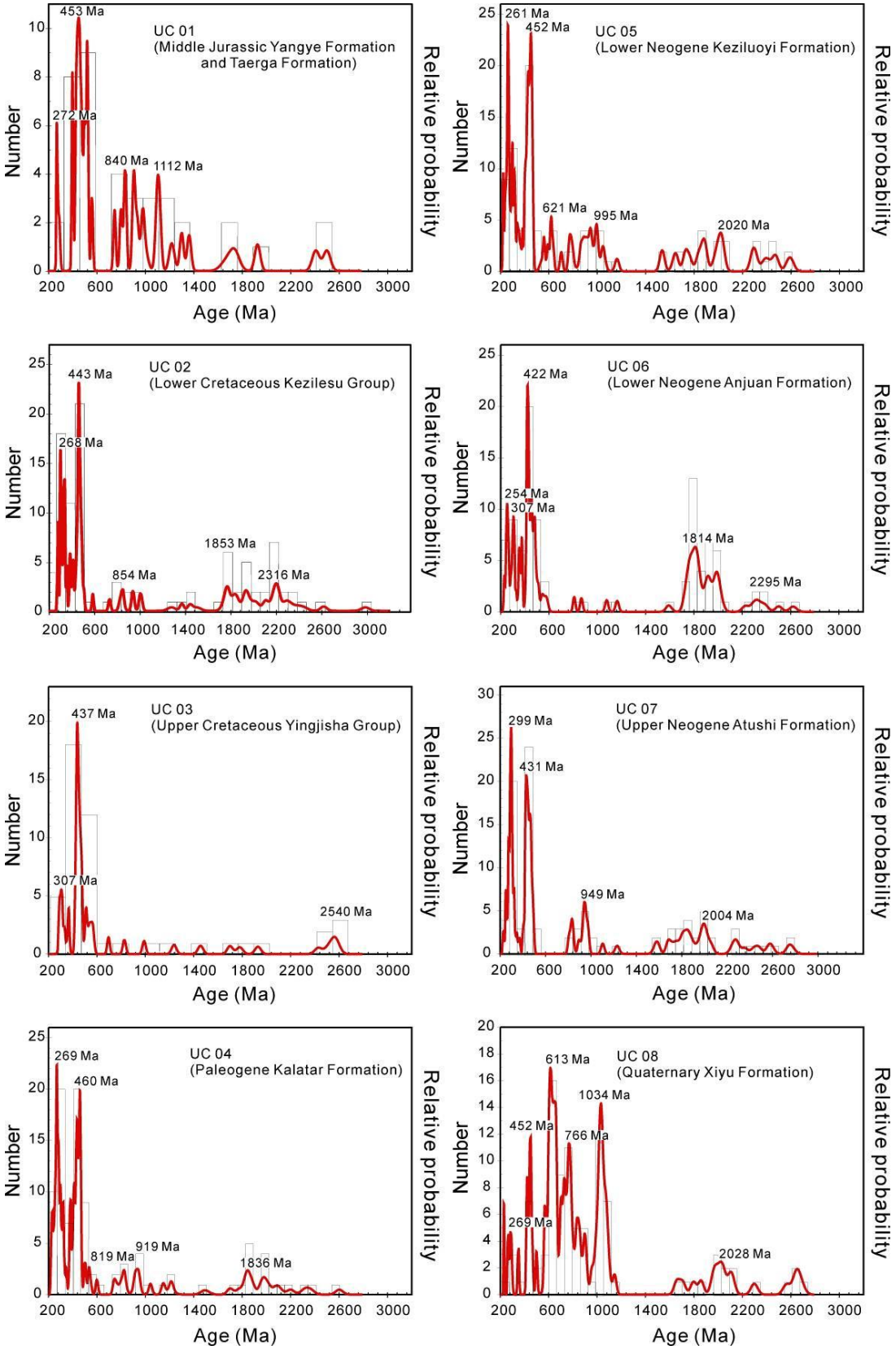

Fig. 2.8 Relative-age-probablity plots and number histograms of U/Pb ages of detrital zircons from Middle Jurassic to Quaternary sandstone samples collected in the Zhuoyoulehansu section.

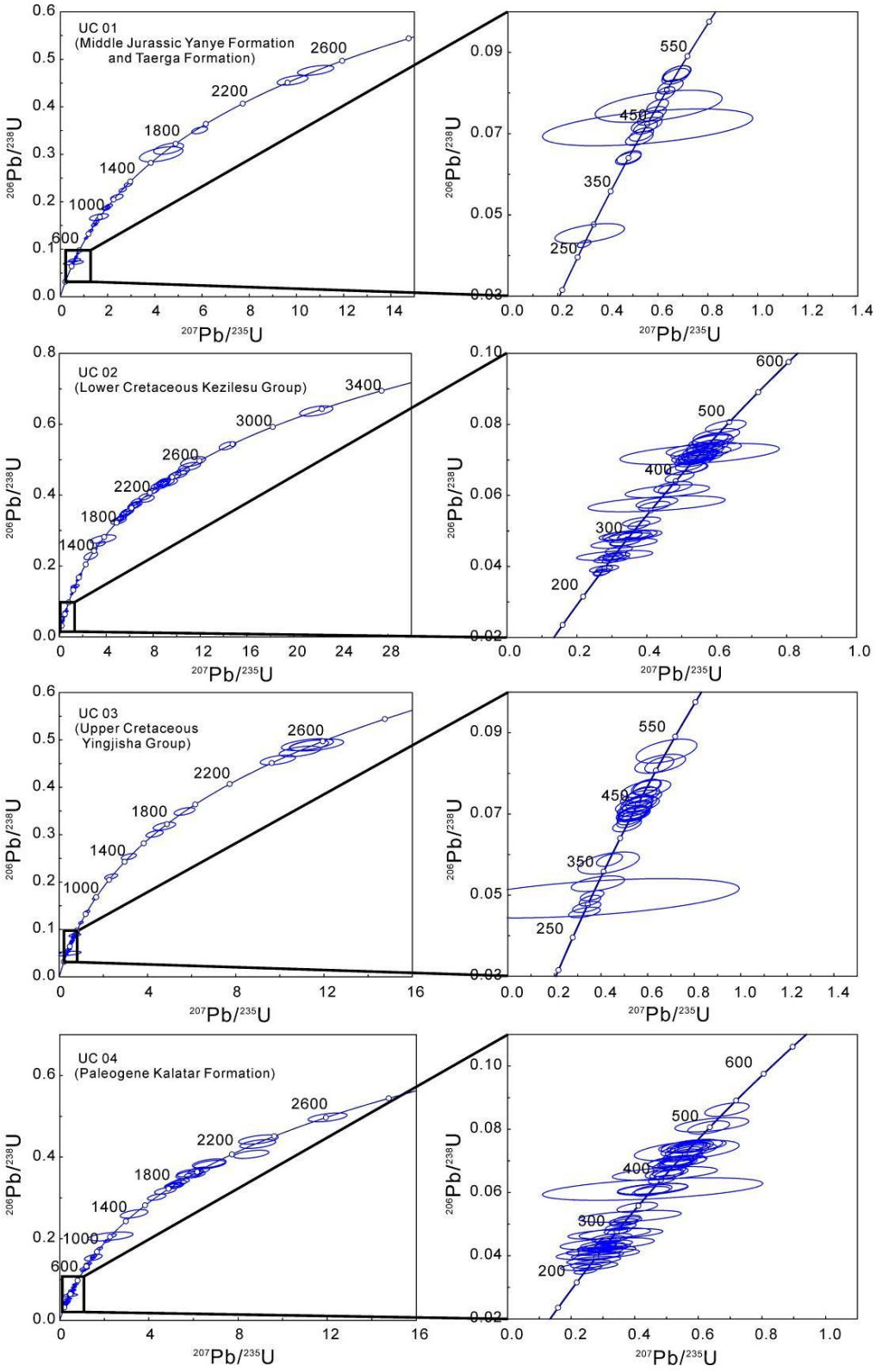

Fig. 2.9 U/Pb concordia diagrams for zircon grains of the 8 sandstone samples.

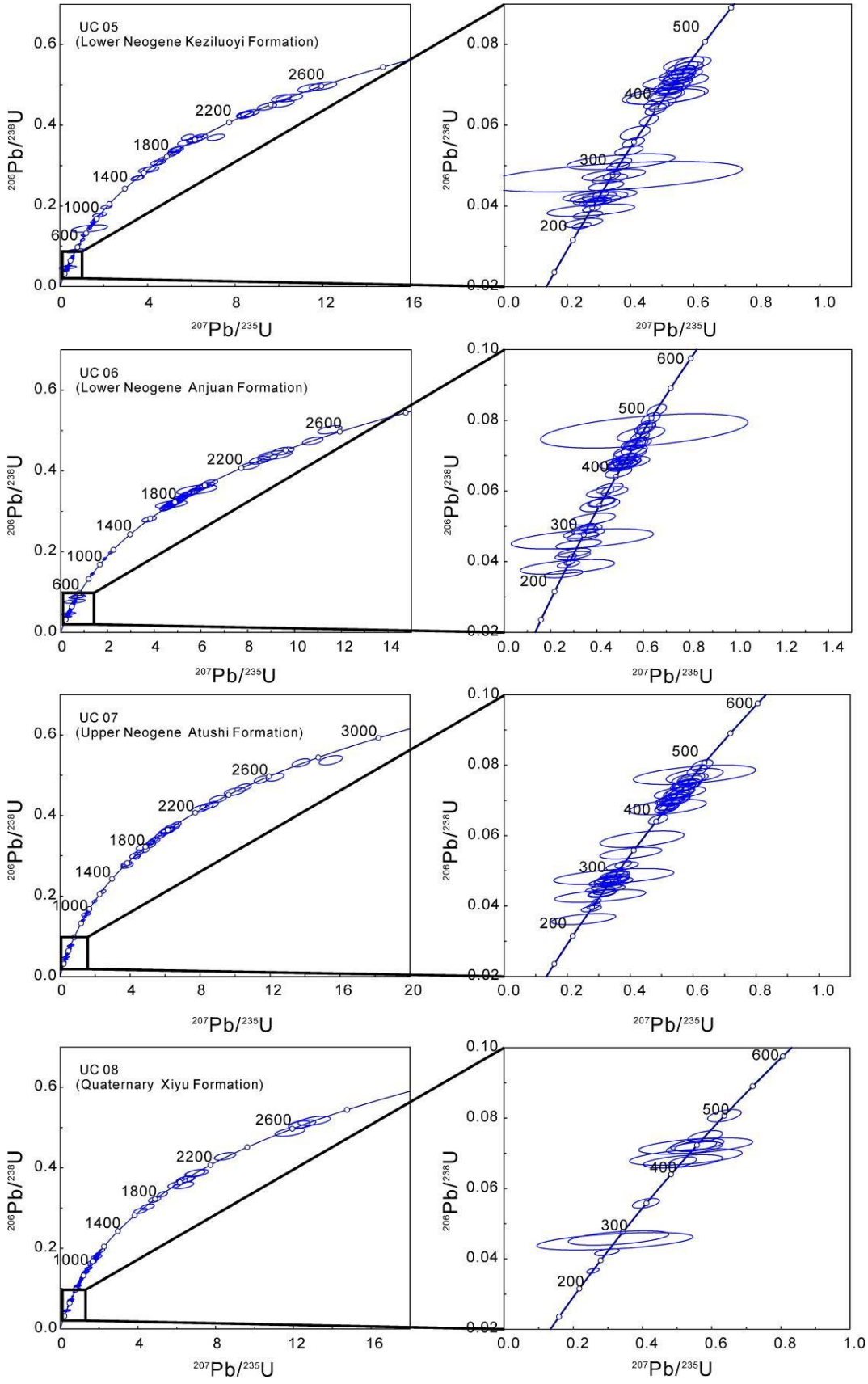

Fig. 2.9 (continued).

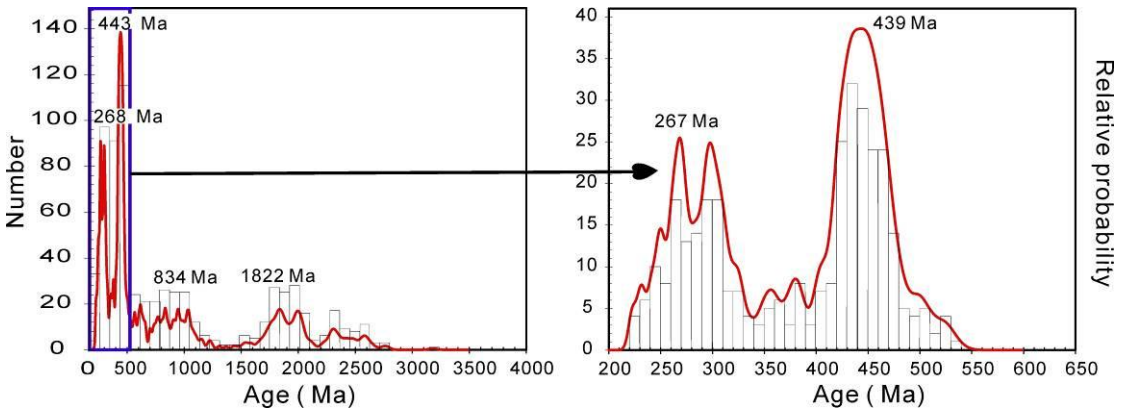

Fig. 2.10 Combined relative probability density and histogram plots of the 8 samples. The diagram to the left corresponds to the blue box in the first diagram.

2.5 Discussion

The discussion below integrates the U/Pb data on detrital zircons and the AFT data on detrital apatites, as well as the bibliography, to describe the evolution of the sediment sources along the Zhuoyoulehansu river section through time. This evolution will be interpreted in terms of topographic evolution of the Southwest Tian Shan Range since the provenance area of the sediments in the NW Tarim Basin has most probably always been situated in the Tian Shan area. As discussed in the geological setting, the Pamir range might have provided sediment only in the latest phases of deformation. This is further supported by exclusively north-to-south paleocurrent directions available in Cenozoic sedimentary records throughout the Southwest Tian Shan (e.g. Chen, J., 2002; Scharer et al., 2004; Heermance et al., 2007).

2.5.1 Middle Jurassic to Late Cretaceous evolution

The Middle Jurassic sample UC01 (Figs. 2.8 and 2.9) displays a very wide variety of detrital zircon ages spanning the entire range of ages identified within all the samples. This indicates that either the source area was vast, encompassing most of the tectonic blocks of Tian Shan or that recycling of previous sediment series containing those zircons occurred. Numerous studies have already indicated that the Middle Jurassic time was a tectonically quiet period during which only a small amount of

erosion and thus exhumation occurred (e.g. Hendrix, 2000; Fang et al., 2005; Jolivet et al., 2010, 2011; Yang et al., 2013). A wide coal-rich sedimentation system was prevailing over the whole area (Fig. 2.4) (e.g. Li et al., 2004; Fang et al., 2005; Li and Peng, 2010) implying a relatively flat topography with only restricted amounts of clastic sediment being produced. These observations would then be in favour of a wide drainage system and thus of a wide source area for the Middle Jurassic samples in Southwest Tian Shan. However, in the Kuqa sub-basin, both groups of zircon ages are poorly represented (Li and Peng, 2010), suggesting that lateral variations in the source area throughout the piedmont existed.

From Middle Jurassic (sample UC01) to Upper Cretaceous (sample UC03), the proportion of Neo-Proterozoic zircons (with a peak age of 834 Ma on the general histogram of Fig. 2.10) decreased to near zero. The proportion of Meso-Proterozoic to Archean zircons (with a peak age of 1822 on Fig. 2.10) seems to increase slightly during the Lower Cretaceous (sample UC02) but is also negligible in the Upper Cretaceous (sample UC03). This is again consistent with a general flattening of the topography as recorded by basement fission track data throughout the range (e.g. Jolivet et al., 2001, 2007, 2009, 2010; Vassallo et al., 2007). The very diverse sources observed in the Middle Jurassic sample tend to be more and more restricted possibly because of burying of the available source rocks below the Jurassic and Cretaceous deposits (both the outcropping basement and the potentially recycled Late Paleozoic – Early Mesozoic sediments were buried). Finally, it is not possible to exclude that the reduction in the range of detrital ages was linked to the erosion of a single, more local source area. However, this would poorly explain the decrease in Neo-Proterozoic ages, typical of the STS basement. Small-scale inversion described along the northern margin of the Tarim basin during the Lower Cretaceous, possibly in relation with the docking of the Lhasa block to the south (e.g. Hendrix et al., 1992; Li and Peng, 2010), might account for the renewed recycling of the north Tarim Paleozoic series as indicated by the increase of Meso-Proterozoic to Archean zircons in sample UC02 (Fig. 2.10). Similar U/Pb ages on detrital zircon are reported in the Kuqa sub-basin (Li and Peng, 2010) indicating that this might have been a regional feature rather than related to a local source. By Upper Cretaceous, the diversity of ages reached a minimum in the whole sedimentation history. These are restricted to the Late

Carboniferous – Early Permian post-collisional granites of NTS and CTS, and to the Late Ordovician granites of STS. Based on basement apatite fission track data, the Upper Cretaceous represents the climax of general flattening of the range (De Grave et al., 2007; Glorie et al., 2010; Jolivet et al., 2010) and only a few, localised exhumation events occurred in the north Tarim (Zhang et al., 2009). In the south Junggar basin, Yang et al. (2013) reported that although some tectonic movements probably occurred, they had very limited impact in terms of topography building. This flattening of the topography is further attested by the detrital AFT data obtained on the two non-to-poorly reset Lower Cretaceous samples (KA02 and ZKS01). In both samples the older ages are Jurassic, which indicates that following the Late Triassic – Early Jurassic final erosion of the Late Paleozoic range, exhumation had become so low that the corresponding AFT ages have been preserved until at least the Upper Cretaceous.

2.5.2 Tertiary evolution

During the late Paleogene to Early Miocene (samples UC04 and UC05), the amount of Proterozoic and Archean zircons increased again marking the onset of a new erosion phase. A similar pattern is observed in the Kuqa sub-basin (Li and Peng, 2010) indicating that this renewed diversity in ages is a regional feature. Based on geomorphological analyses, authors such as Burchfield et al. (1999) or Fu et al. (2003) suggested that the deformation in the southern Tian Shan piedmont propagated towards the Tarim Basin during the Early Pleistocene. However, many authors agree that the Tertiary deformation within the southern Tian Shan piedmont initiated around the Oligocene-Miocene boundary (e.g. Sobel and Dumitru, 1997; Yin et al., 1998; Sobel et al., 2006; Heermance et al., 2008) thus slightly after the deposition of sample UC04 and contemporaneously with the deposition of sample UC05. However, we interpret the renewed age diversity observed in sample UC04 as the erosion and recycling of at least the Lower Cretaceous and possibly Jurassic series that display the exact same detrital zircon ages distribution as in UC04. This recycling would be consistent with the wide spread in individual apatite fission track ages observed in the Early Miocene sample UC05, although very old ages (> 150 Ma) found in the Lower Cretaceous samples KA02 and ZKS01 are not represented. This interpretation implies

that deformation and thus uplift and erosion occurred along the southern piedmont of the Tian Shan as early as Eocene. Low temperature thermochronology data on basement showed that localized strong tectonic movements affected the Permian inherited large strike-slip faults inside the Tian Shan Range during the Late Cretaceous – Early Paleogene (Jolivet et al., 2010). It is thus reasonable to suspect that small-scale deformation also occurred in the southern piedmont of the Tian Shan Range during the Paleogene even if they were small enough not to be detected by low temperature thermochronology or sedimentology analyses. The erosion associated to this deformation only became strong enough to be registered by obvious variations within the Tarim Basin in the Oligo-Miocene.

The Miocene sample UC06 displays a strong increase in the proportion of Meso-Proterozoic to Archean zircons associated to a near absence of Neo-Proterozoic ages. However, the younger Pliocene UC07 sample shows a zircon ages distribution very similar to the Eocene distribution with the occurrence of both groups of Proterozoic ages. This seems to indicate a transient modification of the source area and/or composition during the Miocene. Many authors suggested that in Southwest Tian Shan the Tertiary deformation evolved as pulses from about 25 Ma onward (e.g. Sobel et al., 2006; Heermance et al., 2008). One of those pulses is dated around 16 Ma (middle Miocene) and induced the formation of a new trend of thrust faults, southward of the main Tian Shan frontal basement fault (locally represented by the Maidan fault). This strong exhumation event is attested by the AFT age of 18.5 ± 5.2 and 16.6 ± 2.8 Ma obtained from the totally reset Jurassic and Lower Cretaceous samples UC01 and UC02 (Fig. 2.4). The geological map of the study area (Figs. 2.2 and 2.3) shows a wide outcrop of Proterozoic basement rocks east of the Zhuoyoulehansu river section. Exhumation of that basement during the Miocene might explain the sudden increase in Meso-Proterozoic to Archean ages in sample UC06. This interpretation is consistent with the general evolution trend observed in the individual detrital apatite fission track ages distributions of the Early Neogene samples (UC05 or Mi-6). Within those samples, the proportion of young ages increases through time, with the youngest ones being consistently similar to the stratigraphic age of the samples. This indicates a strong exhumation in the source area while some “old” sources are preserved but slowly decrease due to increasing

exhumation. A sharp change in the individual apatite fission track ages distribution is observed in sample Mi-7 and following. The amount of “old” ages increased again indicating a variation in the source area. The apatite fission track ages distribution pattern of sample Mi-7 is very similar to the one of sample UC05 in the same way that the zircon ages distribution of sample UC07 is similar to that of sample UC05. Following that description, samples UC06 to Mi-6 would represent a middle Miocene climax of an Early Neogene exhumation period.

The fact that the Lower Cretaceous sample UC02 situated along the Zhuoyoulehansu river section has been totally reset prior to the Miocene exhumation while the similar Lower Cretaceous samples KA02 and ZKS01 situated further east where poorly to non-reset indicate strong lateral variations in the amount of burying. In that respect, the eastern area seems to have been less buried by post-Lower Cretaceous series. The exhumation of this area of the Southwest Tian Shan is controlled by thrust faults that form a complex horsetail structure on the southern termination of the strike-slip Talas Fergana Fault, facing the Pamir salient to the south (Figs. 2.1 and 2.2). The deformation in that area is thus closely linked to the Tertiary tectonic activity of the Talas Fergana Fault. This major fault accommodated several tens of kilometres of movement during the Late Cenozoic. Based on geomorphic and paleomagnetic data, Burtman et al. (1996) suggested that the Tertiary deformation on the Talas-Fergana Fault initiated after 10 Ma. If the increase in Meso-Proterozoic to Archean zircon ages observed in sample UC06 is due to the exhumation of the Proterozoic basement outcropping east of the study area along the southern horsetail-like termination of the Talas Fergana Fault, then the right-lateral strike-slip movement on the fault itself might be as old as middle Miocene. However, further detailed study will be necessary to fully assess the time of exhumation of that basement and its exact relation with the Talas Fergana Fault.

Has previously said, the Pliocene sample UC07 displays a detrital zircon age spectrum similar to the Paleogene one, although the Ordovician granites of STS are mostly lacking. Nonetheless these are present in the Quaternary sample (UC08) together with all the other groups of ages. The detrital AFT ages are also widely distributed in both samples, encompassing the Mesozoic and the Tertiary exhumation

phases. Both sets of ages (AFT and zircon U/Pb) clearly represent a combination between sediment recycling from the underlying Mesozoic and Early Cenozoic series and basement erosion within the growing range. A similar pattern is observed in the Kuqa sub-basin (Li and Peng, 2010) as well as on the northern piedmont of the Tian Shan Range (Yang et al., 2013).

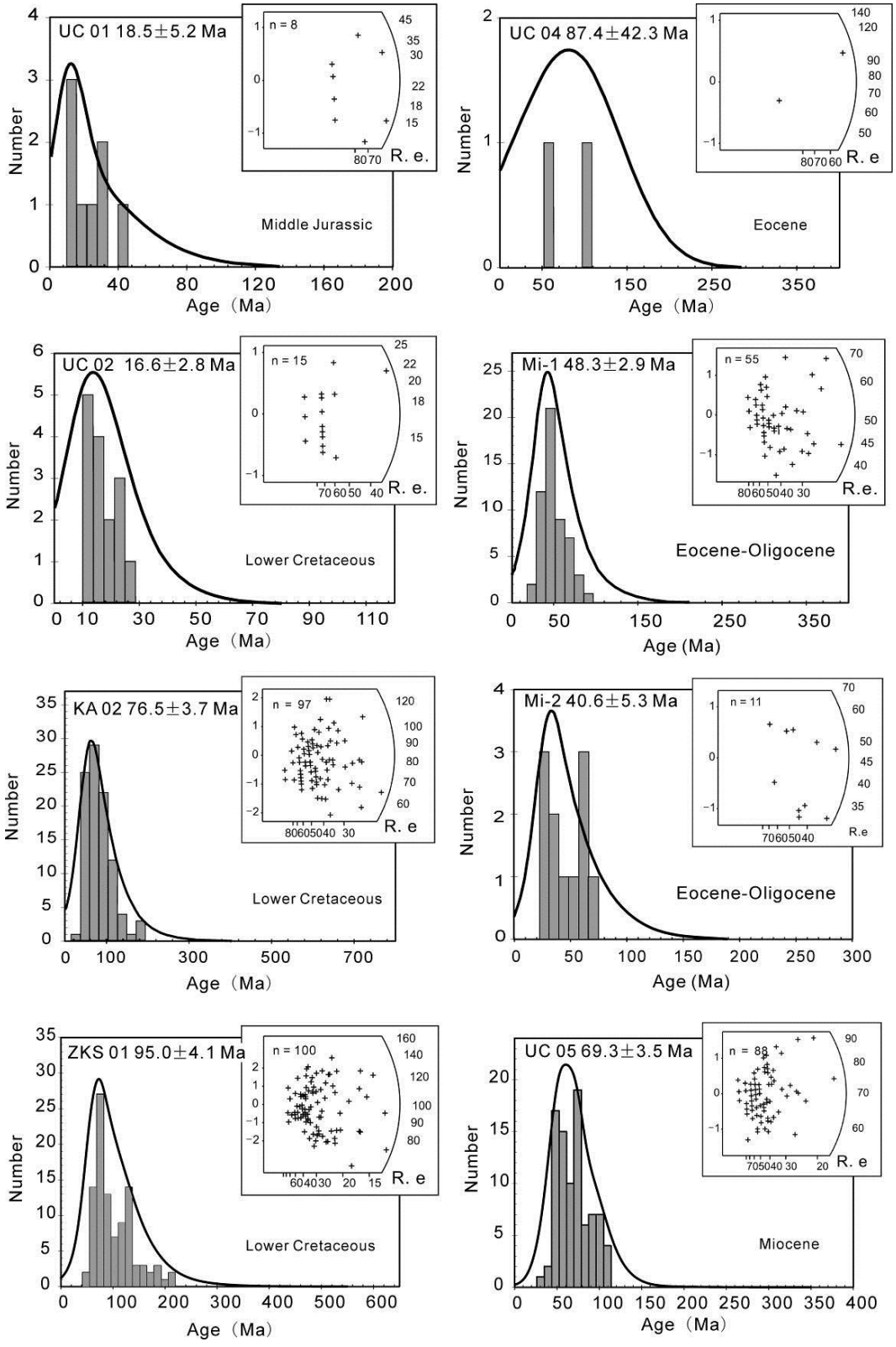

Fig. 2.11 Single grain apatite fission track age distributions of the samples presented in age spectra and radial plots. Age spectra (black lines) were created according to Hurford et al. (1984).

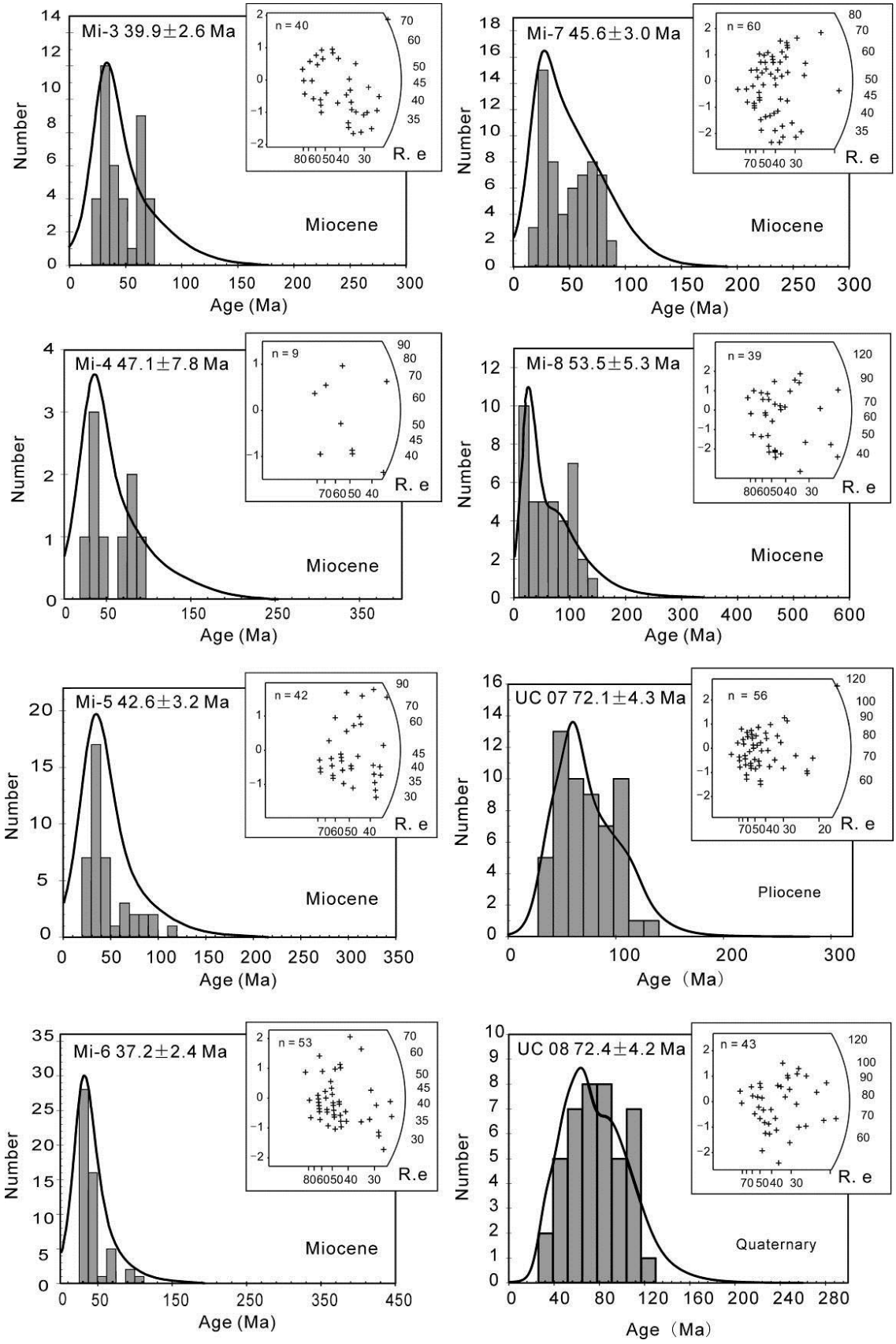

Fig. 2.11 (continued).

2.6 Conclusions

The data obtained in this study, associated to already published sedimentological and thermochronological results allow a better understanding of the topographic evolution of the SW Chinese Tian Shan piedmont. The large range of U/Pb ages on detrital zircons observed in the Middle Jurassic sediments encompasses most of the available sources in the range implying a wide drainage pattern developing on a rather flat topography. This is consistent with the already largely described Mesozoic planation of the Paleo-Tian Shan Range. Furthermore, the strong decrease in detrital zircon ages variety during the Early Cretaceous, reaching its maximum in Upper Cretaceous is consistent with progressive burying of the basement exposures by sediments. Only a slight increase of Meso-Proterozoic to Archean zircons in the Lower Cretaceous sediments, observed on several places along the southern piedmont, might indicate small-scale uplift related to the docking of the Lhasa block along the southern margin of Eurasia. Renewed erosion during the Eocene might correspond to the onset of Tertiary deformation along the Southern piedmont of the range which would be older than the previously admitted Oligocene – Miocene. Finally, the AFT data indicate exhumation of the totally reset Middle Jurassic and Lower Cretaceous sediments between 18 and 16 Ma. This is consistent with already published data that show a middle Miocene pulse of tectonic activity corresponding to the activation of a series of thrust faults, south of the main South Tian Shan thrust. We relate those movements as well as the exhumation of the Proterozoic basement NE of our study area to the activation of the Talas Fergana strike-slip fault. Further investigation on that fault will be necessary but our data seem to indicate that the Talas Fergana Fault, which is largely controlling the deformation in both the Western Tian Shan Range and the Fergana Basin, was already active in middle Miocene and not in upper – Miocene to Pliocene as suggested before.

The use of detrital zircon U/Pb dating in sediments allows tracking variations in source areas, themselves controlled by topographic variations. While low temperature thermochronology requires several kilometres of exhumation (and thus uplift), detrital geochronology can potentially detect minor topographic changes resulting in modifications of the drainage pattern. While this method has a higher resolution than low temperature thermochronology, it might also be sensible to the effects of climate

variations on sediment supply. This in turn can hide or be mistaken as a tectonic event and further researches will be necessary to address that question.

CHAPTER 3
Magnetostratigraphy from the Ulugqat area, Northwest China: implications for the Cenozoic tectonic evolution of the Southwest Tian Shan

Wei Yang[a,b], Guillaume Dupont-Nivet[a,b,c], Marc Jolivet[b], Zhaojie Guo[a], Laurie Bougeois[b], Roderic Boshoom[c], Bei Zhu[a], Ziya Zhang[a], Gloria Heilbronn[b]

[a] *Key Laboratory of Orogenic Belts and Crustal Evolution, Ministry of Education, School of Earth and Space Sciences, Peking University, Beijing, China 100871*

[b] *Géosciences Rennes, Université Rennes 1, UMR 6118,CNRS/INSU, Rennes, France*

[c] *Faculty of Geosciences, Utrecht University, The Netherlands*

* *Corresponding author.*

Abstract

The Tian Shan range is an inherited intracratonic structure reactivated since the Oligo-Miocene boundary in response to the India-Asia collision. Despite a growing body of thermochonologic and magnetostratigraphic datasets showing that the range grew through several tectonic pulses during the Miocene, the driving tectonic mechanisms of these pulses remain unclear. Particularly enigmatic is the time lag between the Eocene India-Asia collision and the onset of Tian Shan exhumation over 25 millions of years later. During the peculiar period along the southwestern part of the Tian Shan, recently dated late Eocene marine deposits gave way to the deposition of continental foreland basin sediments of unknown age. Here we provide magnetostratigraphic dating of these continental sediments supported by previously published detrital apatite fission track and U/Pb zircon ages. Primary Characteristic Remanent Magnetizations carried by a combination of magnetite and hematite were obtained throughout the 1700-m-thick section. The most likely correlation to the geomagnetic polarity time scale of the obtained pattern of polarity zones indicates the section comprises an age span from ~ 20.8 to 13.3 Ma with a major increase of accumulation rates ca. 19-18 Ma. This implies the entire Oligocene period is missing from the

record between the last marine and the first continental sediments, as also suggested by previous magnetostratigraphic results throughout the southern Tian Shan piedmont. This differs from the southwestern Tarim basin where Eocene marine deposits are continuously overlain by late Eocene to Oligocene continental sediments. This supports a simple evolution model of the Tarim basin with Eocene-Oligocene foreland basin activation in the south related to the Kulun Shan northward thrusting, followed by early Miocene activation of the northern foreland basin related to the south Tian Shan overthrusting. Our data also supports southward propagation of the Tian Shan piedmont ca. 20-18 Ma that may relate to the activation of a major strike slip system along the Tarim basin enabling to transfer deformation from the India-Asia collision zone to the Tian Shan and possibly the Talas Fergana fault.

Keywords: Magnetostratigraphy; Southwest Tian Shan; Tarim Basin; Sediment accumulation rates; hiatus

3.1 Introduction

The Tian Shan is a 2500-km-long, up to 7400-m-high range extending through western China, Kazakhstan, and Kyrgyzstan. This range belongs to the larger Central Asian Orogenic Belt (CAOB) extending from the Urals to the Pacific across the East European, Siberian North China, and Tarim cratons (e.g. Şengör et al., 1993; Windley et al., 2007; Jolivet et al., 2010). The Cenozoic tectonic uplift of the Tian Shan is predominantly attributed to a response to the tectonic rejuvenation and intracontinental deformation due to the India-Asia collision (e.g. Molnar and Tapponnier, 1975; Tapponnier and Molnar, 1979; Patriat and Achache, 1984; Avouac et al., 1993; Yin et al., 1998; Sun et al., 2009; Huang et al., 2010). Thick Cenozoic accumulations of sediments derived mostly from the uplifting mountain range form the terrigenous depositional sequences that are well preserved and exposed in foreland basins of the Tian Shan (Hendrix, 2000; Fang et al., 2005, 2006; Wu et al., 2006; Charreau et al., 2009; Yang et al., 2013). The Tian Shan has provided an ideal setting

for the understanding of Cenozoic intracontinental deformations in central Asia and the associated effects on regional environment and global climate. However, vigorous debates and gaps in understanding still largely exist concerning the Cenozoic history and driving mechanism of the Tian Shan orogeny arising mainly from the lack of accurate constraints on the exact time of deformation and uplift and associated deposition. In particular, the early history of the range is poorly constrained. While the onset of exhumation is fairly well constrained to have occurred at around the Oligo-Miocene boundary, it remains unclear why deformation really picks up only in the Middle to Late Miocene. More fundamentally, it remains unresolved why deformation from the India-Asia collision starting in the Eocene (ca. 50 Ma) propagated to the Tian Shan only in the Miocene over 25 Myrs later.

In detail, apatite fission track analyses from basements and sediments in the Tian Shan, as well as its piedmonts predominately suggest an initiation of rapid uplift at ~25 – 20 Ma (e.g. Hendrix et al., 1994; Sobel and Dumitru, 1997; Dumitru wt al., 2001; Sobel et al., 2006). However, Bullen et al. (2001, 2003) demonstrated that the rapid uplift of the Kyrgyz Tian Shan commenced at ~ 11 Ma, and younger exhumation ages ranging between 6-8 Ma are also reported from the Chinese Southwest Tian Shan (e.g. Wang, et al., 2010). Recent magnetostratigraphic studies have also been conducted on the Cenozoic sediments from both the northern and southern piedmonts of the Tian Shan. Several main pulses in sedimentation rate were detected, reflecting the multi-phased uplift and deformation of the Tian Shan respectively commenced at ~ 26-23 Ma, ~ 17-16 Ma, ~13-11 Ma, ~7 Ma and ~ 4 Ma (e.g. Bullen et al., 2001; Sun et al., 2004, 2009; Charreau et al., 2005; Huang et al., 2006, 2010; Jin et al., 2008; Lu et al., 2010; Li et al., 2011). However, these studies have been concentrated on the Miocene and later Tian Shan evolution focusing on correctly constraining the Cenozoic episodic uplift of the Tian Shan. What happened in the mysterious Oligocene period between the Eocene India-Asia collision and the Miocene Tian Shan exhumation remains to be explored.

In that period, recent studies have focused on the record of the westward retreat of the vast epicontinental sea that covered the Tarim Basin at the eastern end of a shallow sea that formerly extended across the Eurasian continent (e.g. Ramstein et al., 1997;

Garzione et al., 2005; Graham et al., 2005; Zhang et al., 2007; Kent-Corson et al., 2009; Bosboom et al., 2011). Accurate age estimates on the youngest marine sediments are now available indicating that the sea finally retreated from the northern Tarim basin in the late Eocene (Bosboom et al., accepted, in press a). However, it remains unclear what happened between the deposition of these last marine deposits and the overlying continental deposits because the latter are virtually unconstrained in age. They have been usually attributed an Oligocene to Miocene age based mainly on the fact that they lie on marine sediments of Eocene and erroneously attributed Oligocene ages.

In this paper, we report a detailed magnetostratigraphic study of such continental sediments at the Mine section in Ulugqat area, located in the piedmont of the Southwest Tian Shan (Fig. 3.1). This section has been chosen because it lies directly on dated marine deposits (Bosboom et al., accepted) thus providing a basal age constraints and because it encompasses a complete and well developed sequence of the early continental deposits with a total thickness of ~ 1700 m. This section also bears previously published detrital Apatite Fission Track (AFT) ages and detrital U/Pb zircons ages that provide additional age and provenance information (Yang et al., 2013).

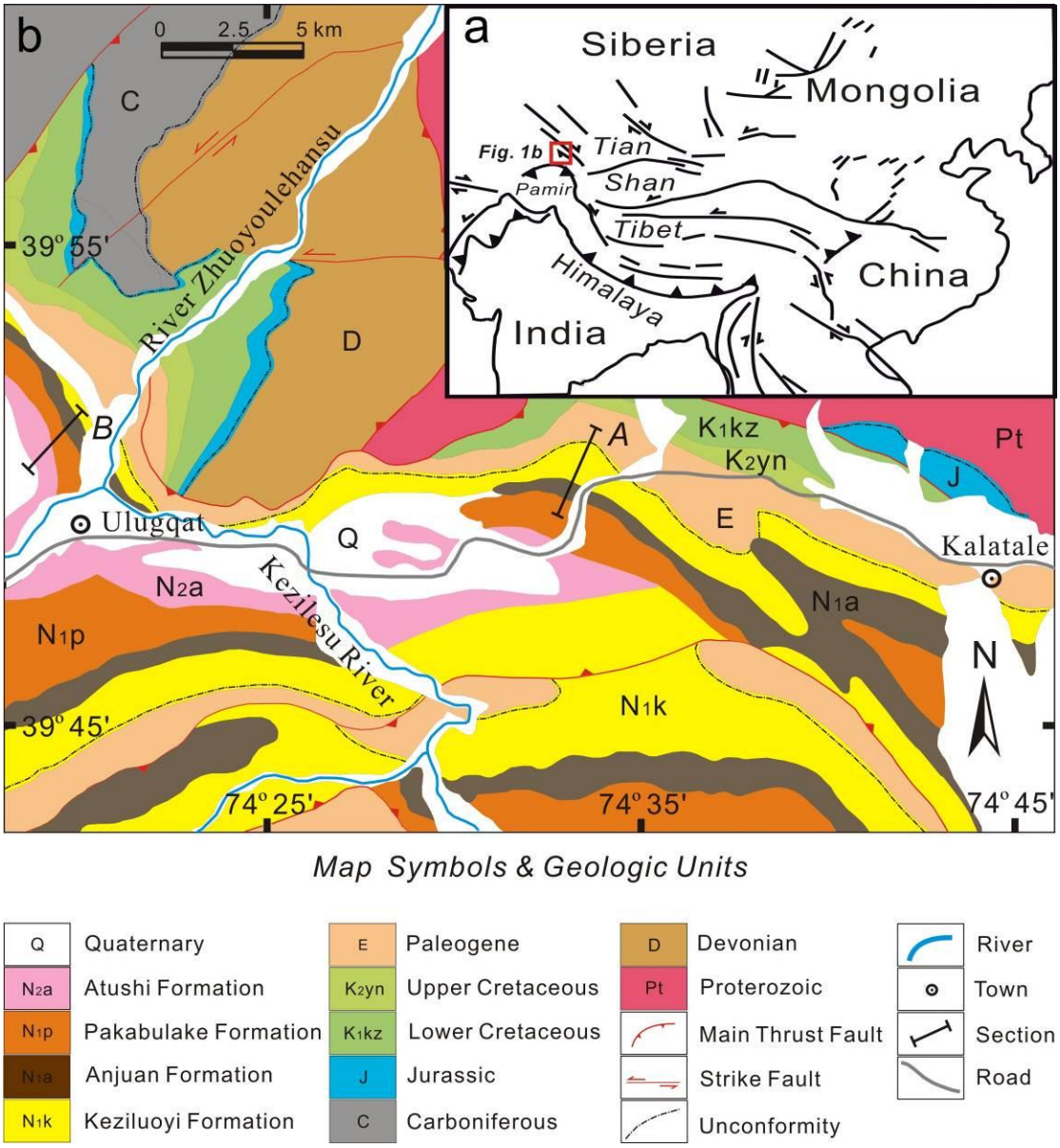

Fig. 3.1 (a) Location of the studied area shown on large-scale map of Asia. (b) Simplified geological map of the Ulugqat area with location of the Mine (A) and Ulugqat (B) sections.

Table 3.1 Simplified litho-biostratigraphic correlation of the Kuqa subbasin, Ferghana-Alai and Afghan-Tadjik Basins to the chronological framework recognized in the southwest Tarim Basin. The wavy line represents a gap between the Late Eocene and Oligocene in the western Tarim Basin. The Bashibulake Formation in western Tarim corresponds to the lower Suweiyi Formaiton in northern Tarim (Jia et al., 2004; Bosboom et al., in revision), the Sanglak Formation in Afghan-Tadjik Basin (Dzhalilov et al., 1982), as well as the Rishtan, Isfara, Hanabad, Sumsar, and Shurysay Formations in Ferghana-Alai Basin (Pomazkov, 1972; Bosboom et al., in revision); the Keziluoyi Formation corresponds to the upper Suweiyi and lower Jidike Formations in northern Tarim (Jia et al., 2004), the Massaget Formation in Ferghana-Alai Basin (Pomazkov, 1972), as well as Hissarak, Shurysay, and Baldzhua complex/Kamoli Formations in Afghan-Tadjik Basin (Dzhalilov et al., 1982; Bosboom et al., in revision); the Anjuan Formation corresponds to the upper Jidike Formation in northern Tarim (Jia et al., 2004), the Baktry Formation in Ferghana-Alai Basin (Coutand et al., 2002; Bosboom et al., in revision), as well as the Childara and lower Hingou Formaitons in Afghan-Tadjik Basin (Dzhalilov et al., 1982); finally the Pakabulake Formation corresponds to the Kangcun Formation in Northern Tarim (Jia et al., 2004), the Sokh Formation in Ferghana-Alai Basin (Coutand et al., 2002), as well as the upper Hingou and Tavildara Formations in Afghan-Tadjik Basin (Dzhalilov et al., 1982; Bosboom et al., in revision).

<table>
<tr><th colspan="2">Age (Ma)</th><th>Afghan-Tadjik Basin</th><th>Ferghana-Alai Basin</th><th>Kuqa subbasin (Northern Tarim)</th><th>Western Tarim Basin</th></tr>
<tr><td rowspan="8">Neogene</td><td rowspan="4">Miocene</td><td>Tavildara Formation</td><td rowspan="2">Sokh Formation</td><td>Kangcun Formation</td><td>Pakabulake Formation</td></tr>
<tr><td>Hingou Formation</td><td rowspan="2">Baktry Formation</td><td rowspan="2">Jidike Formation</td><td>Anjuan Formation</td></tr>
<tr><td>Childara Formation</td><td rowspan="3">Keziluoyi Formation</td></tr>
<tr><td>Baldzhua complex/
Kamoli Formation</td><td rowspan="3">Massaget Formation</td><td rowspan="6">Suweiyi Formation</td></tr>
<tr><td rowspan="3">Paleogene</td><td rowspan="2">Oligocene*</td><td>Shurysay Formation</td></tr>
<tr><td>Hissarak Formation</td></tr>
<tr><td>Late
Eocene</td><td>Sanglak Formation</td><td>Shurysay Formation</td><td rowspan="5">Bashibulake Formation</td></tr>
<tr><td colspan="3"></td><td>Sumsar Formation</td></tr>
<tr><td colspan="3"></td><td>Hanabad Formation</td></tr>
<tr><td colspan="3"></td><td>Isfara Formation</td></tr>
<tr><td colspan="3"></td><td>Rishtan Formation</td></tr>
</table>

* Notes: We show here that the age of the Keziluoyi Formaiton is actually Miocene.

3.2 Geological setting

The studied area is located at the junction of the Southwest Tian Shan to the north and the western Kunlun/northern Pamir to the south, whose tectonic evolution is summarized as follows.

To the north of the studied area, the east-west trending Tian Shan extends through western China, Kazakhstan and Kyrgyzstan and represents an important part of the Central Asian Orogenic Belt (CAOB). The present topography of the Tian Shan formed during Late Cenozoic times as a result of the distant effects of the ongoing India-Eurasia collision (e.g. Molnar and Tapponnier, 1975; Tapponnier and Molnar, 1977; Burchfiel and Royden, 1991; Avouac et al., 1993; Yin et al., 1998; Burchfiel et al., 1999; Dumitru et al., 2001; Buslov et al., 2004, 2007; Jolivet et al., 2010). The Southwest Chinese Tian Shan (SWTS), as an important segment of the South Tian Shan orogen, is characterized by ~ 9 km of Cenozoic sediments accumulated in the foreland (e.g. Chen et al., 2002; Heermance et al., 2007). Cenozoic deformation, shorterning and uplift in the SWTS and its piedmonts commenced at ~ 25-20 Ma, characterized by the significant exhumation around the Oligocene-Miocene boundary (~ 24 Ma) (e.g. Hendrix et al., 1994; Yin et al., 1998; Sobel et al., 1995, 2006; Sobel and Dumitru, 1997; Yin et al., 1998; Ji et al., 2008). Subsequently, the SWTS underwent a renewed exhumation at 19 $\pm$ 3 Ma (Sobel et al., 2006; Heermance et al., 2007) and a stepwise deformation dominated by several abrupt increases in accumulation rates respectively at ~ 16, 13 Ma (e.g. Heermance et al., 2007), and 4 Ma (Heermance et al., 2007; Li et al., 2011). To the south of the studied area, the western Kunlun is the eastern limb of the Pamir salient orogenic belt, extending from the northern margin of the Tibetan Plateau to the south to the southern margin of the Tarim Basin to the north (Pan, 1990, 1996; Yin and Bian, 1995; Deng, 1996; Matte et al., 1996; Ding et al., 1996; Searle, 1996; Mattern and Schneider, 2000; Wang, 2004; sun and Jiang, 2013; Bosboom et al., submitted). The present-day convergence rate was estimated at 13 $\pm$ 4 mm a^{-1} by Global Positional System data (e.g. Zubovich et al., 2010) and it is generally assumed that the far-field effects of the India-Eurasia collision induced multi-stages uplift and erosion during the Cenozoic within the western Kunlun and Pamir (Burtman and Molnar, 1993; Sobel and Dumitru, 1997;

Jolivet et al., 2001; Cui et al., 2006; Wang et al., 2006; Liu et al., 2010; Sobel et al., 2011, 2013). Sobel and Dumitru (1997) and Yin et al. (2002) suggested that strong exhumation and cooling occurred during the Late Oligocene to Middle Miocene, based on sedimentary facies, provenance changes, and thermochronological data from the southwestern Tarim Basin. Recent thermochronological results account for a more complex exhumation and deformation pattern, divided into three distinct stages: the Late Oligocene to Early Miocene (Li et al., 2007; Cao et al., 2009; Liu et al., 2010), the Middle to Late Miocene (Wang et al., 1999; Wang et al., 2001; Wang et al., 2002; Cao et al., 2009; Liu et al., 2010) and the Late Miocene to present day (e.g. Li et al., 2005; Li et al., 2007; Cao et al., 2009; Liu et al., 2010). Sedimentation and drainage patterns changed with the uplift of the western Kunlun causing thick accumulations of sediments in the foreland (e.g. Zheng et al., 2006). Additionally, the initial collision between the Pamir and SWTS is recently dated as the Oligocene-Miocene time but still poorly constrained (e.g. Sobel et al., 2011; Cao et al., 2013a).

3.3 Regional stratigraphy and setting

A series of representative forelands, characterized by well-preserved infillings of Cenozoic sediments, were emplaced surrounding the Pamir, western Kunlun and SWTS, such as the Kuqa subbasin (e.g. Li et al., 2004), the Ferghana-Alai Basin (e.g. Burtman, 2000; De Grave et al., 2012), and the Afghan-Tadjik Basin (e.g. Thomas et al., 1994) from east to west. These basins are clearly related to the significant Miocene deformation widely developed diacronously across these basins separately as characterized by dramatic increased accumulation rates recorded at various times (Sobel and Dumitru, 1997; Yin et al., 2002; Sobel et al., 2006; Heermance et al., 2007; Amidon and Hynek, 2010; Li et al., 2011; Liao et al., 2012). Preceding these tectonic events, loosely dated late Paleogene to early Neogene sediments are regionally consistent suggesting they were part of a larger basin that has been later segmented. Although age constraints are still lacking, these strata have been correlated regionally across basins from Central Asia based mainly on lithofacies and marine micro- and macro-fossil assemblages (Table 3.1; Coutand et al., 2002; Jia et al., 2004; Bosboom et al., 2011, 2014, accepted). Due to this lack of age constraints it remains unclear

whether these strata can be associated with the onset of the ensuing Miocene tectonism or to other processes such as eustatism, tectonism or simply basin infilling. The associated subsidence in these basins is still unclear. This is particularly the case for the continental deposits of unknown age of the Wuqia group that directly overlies the marine strata of the Kashi group dated using biostratigraphy.

In the studied area, Cenozoic strata exposed at the western Tarim consist of the Kashi Group, which comprises in chronological order the Aertashi, Qimugen, Kalatar, Wulagen and Bashibulake Formations (e.g. Mao and Norris, 1988; Jia et al., 2004; Bosboom et al., 2011). The overlying continental Wuqia Group consists of the Kezilouyi, Anjuan and Pakabulake Formations, and the Pliocene-Quaternary Xiyu Formation is characterized by the typical Xiyu conglomerates. A summary of the observed and published descriptions of lithologies and depositional systems is presented below along with the existing age determinations (Jia et al., 2004).

The Bashibulake Formation can be divided into five segments of mainly marine environment (Jia et al., 2004; Bosboom et al., accepted and Table 3.1). it is characterized by littoral and neritic deposits. It has been dated with biostratigraphy of mainly dinoflagelates, nannoplancton, foraminifers, ostracods and bivalves (Mao and Norris, 1988; Lan and Wei, 1995; Yang et al., 1995; Lan, 1997; Jia et al., 2004; Bosboom et al., accepted and Table 3.1).

The bottom of the Keziluoyi Formation discomformably or unconformably overlies the Bashibulake Formation (BGMRXUAR, 1985; Jia et al., 2004). The Keziluoyi Formation consists largely of fluvio-lacustrine facies (e.g. Tang et al., 1989; Jia et al., 2004). The Keziluoyi Formation contains foraminifers, ostracods, Chareae and sporopollen (Table 3.1). Although the presence of ostracods *Pontocyprismican* can suggest a marine sedimentary environment, ostracods *C.speciosu*s and *Hemicyprideis* indicate a fresh water sedimentary environment, supported by the appearance of Charophyta algae.

The Anjuan Formation conformably overlies the Keziluoyi Formation. The contact between these two formations is vaguely based on the increased siltstone and sandstone occurrences within brown-red mudstones to grey-green mudstones. The

Anjuan Formation comprises dominantly fluvial to shallow lacustrine deposits (e.g. Tang et al., 1989; Jia et al., 2004). The Anjuan Formation contains foraminifers, ostracods, chareae and sporopollen (Table 3.1). The presence of ostracods *Darwinula stevensoni*, *Limnocythere aligra*, *Cyclocypris cf*., *cavernosa*, *Limnocythere argulata*, *Ilyocypris evidens* suggests a fresh water sedimentary environment, while ostracods *Cypinotus daductus* and *Leptocythere parva* respectively indicate fresh water to brackish environment. Additionally, the foraminifers association composed of *Ammonia honyaensis*, *A. hatatatensis*, *A.beccarii*, *A.japonica* and *A.tepida* suggests a brackish water sedimentary environment, proved by the appearance of association composed of ostracods *Candona sp*., *Cyprinotus deformis*, *Ilyocypris errabundis*, *Hemicyprinotus valvaetumidus* and *Eucypris sp*., as well as foraminifers *Pararotalia armata*, *Cibicides borislavensis*, *Eponides sp*., *Nonion bogdanowiczi* and *Elphidium sp*.

The Pakabulake Formation conformably overlies the Anjuan Formation. The contact is vaguely defined as the appearance of gray-green thick-bedded and massive sandstones within the stratigraphy dominanted by red-brown to dark gray mudstones interbedded by sandy mudstones. The Pakabulake Formation is inferred to be fluvio – shore shallow lacustrine deposits (e.g. Tang et al., 1989; Jia et al., 2004). It contains foraminifers, ostracods, chareae and sporopollen (Table 3.1).

The marine Bashibulake Formation corresponding to the fifth and last sea retreat from the westernmost Tarim has been accurately assigned a Late Eocene depositional age ranging between ~ 38.5 and 35.5 Ma by recent biostratigraphic analysis (Mao and Norris, 1988; Lan and Wei, 1995; Yang et al., 1995; Lan, 1997; Jia et al., 2004; Bosboom et al., submitted and Table 3.1). However, the overlying continental strata are virtually unconstrained in age. The directly overlying Keziluoyi Formation was broadly assigned a Late Oligocene-Early Miocene age based mainly that it lies on top of the Bashibulake Formation previously and incorrectly assigned an Oligocene age (e.g. Lan and Wei, 1995; Lan, 1997; Zheng et al., 1999; Gao et al., 2000; Yin et al., 2002). The Kezilouyi Formation was further defined as belonging to the Xiejian stage of the continental Miocene series in China (early to middle Aquitanian age from ~ 23.0 to 21.0 Ma according to GTS2012;) based on a review of continental

biostratigraphic evidences recovered from those strata (see Jia et al., 2004). Following the stages of the continental Miocene series in China, the overlying Anjuan Formation was assigned to the Shanwangia stage (late Aquitanian-Burdigalian from ~ 21.0 to 16.0 Ma GTS2012), and the and Pakabulake Formation to the Tonggurian and Baodean stages (Langhian-Messinian from ~ 16.0 to 5.3 Ma GTS2012) based mainly on lithostratigraphic correlation and scarce and poorly constrained biostratigraphy (Zheng et al., 1999; Gao et al., 2000; Jia et al., 2004).

3.4 Age constraints from apatite fission track analyses

Additional age constraints are provided by detrital apatite fission track (AFT) analyses on seven samples from the studied area and previously published in Yang et al. (2013). Six sandstone samples directly from the studied magnetostratigraphic sequence in the Mine Section (four from the Keziluoyi Formation, one from the Anjuan and one from the Pakabulake Formation, respectively). One more sandstone sample (UC05) collected from the Keziluoyi Formation in the adjacent Ulugqat section was also analyzed (Fig. 3.2; Yang et al., 2013). The 331 individual ages obtained from these samples range between 18.22 ± 7.83 Ma and 134.43 ± 98.22 Ma (Table 2.2). Yang et al. (2013) indicate that the obtained AFT age populations in the Wuqia group have not been partially reset and can therefore be used to infer maximum depositional ages.

For the four Keziluoyi Formation samples (Mi-3, Mi-4, Mi-5 and Mi-6), the 232 individual grain ages obtained range from 25.56 ± 12.24 Ma to 111.75 ± 39.59 Ma. Mi-3 (35 meter-level) has two youngest ages respectively at 26.34 and 26.93 Ma, Mi-4 (175 meter-level) has one youngest age at 27.08 Ma, and Mi-5 (370 meter-level) has three youngest ages respectively at 27.57, 27.77 and 27.77 Ma. Mi-6 (570 meter-level) provides the youngest and the largest cluster with four youngest ages (25.56 ± 12.24, 25.56 ± 12.24, 25.56 ± 13.68 and 25.56 ± 19.33 Ma, respectively) suggesting the maximum depositional age around 25 Ma.

For the Anjuan Formation sample collected around level 1075 (Mi-7), the 60 individual grain ages respectively spread from 18.22 ± 7.83 Ma to 87.59 ± 32.41 Ma, and the youngest two ages (18.22 ± 7.83 and 18.54 ± 9.75 Ma) can be interpreted as the maximum depositional age of this level. Finally for the Pakabulake Formation sample collected around level 1720 m (Mi-8), the 39 individual ages range between 20.93 ± 9.79 Ma and 134.43 ± 98.22 Ma suggesting a depositional age within error relative to the underlying Anjuan Formation samples. The apparent older age may be interpreted as reworking of the underlying sediments or a change within the drainage system (Yang et al., 2013).

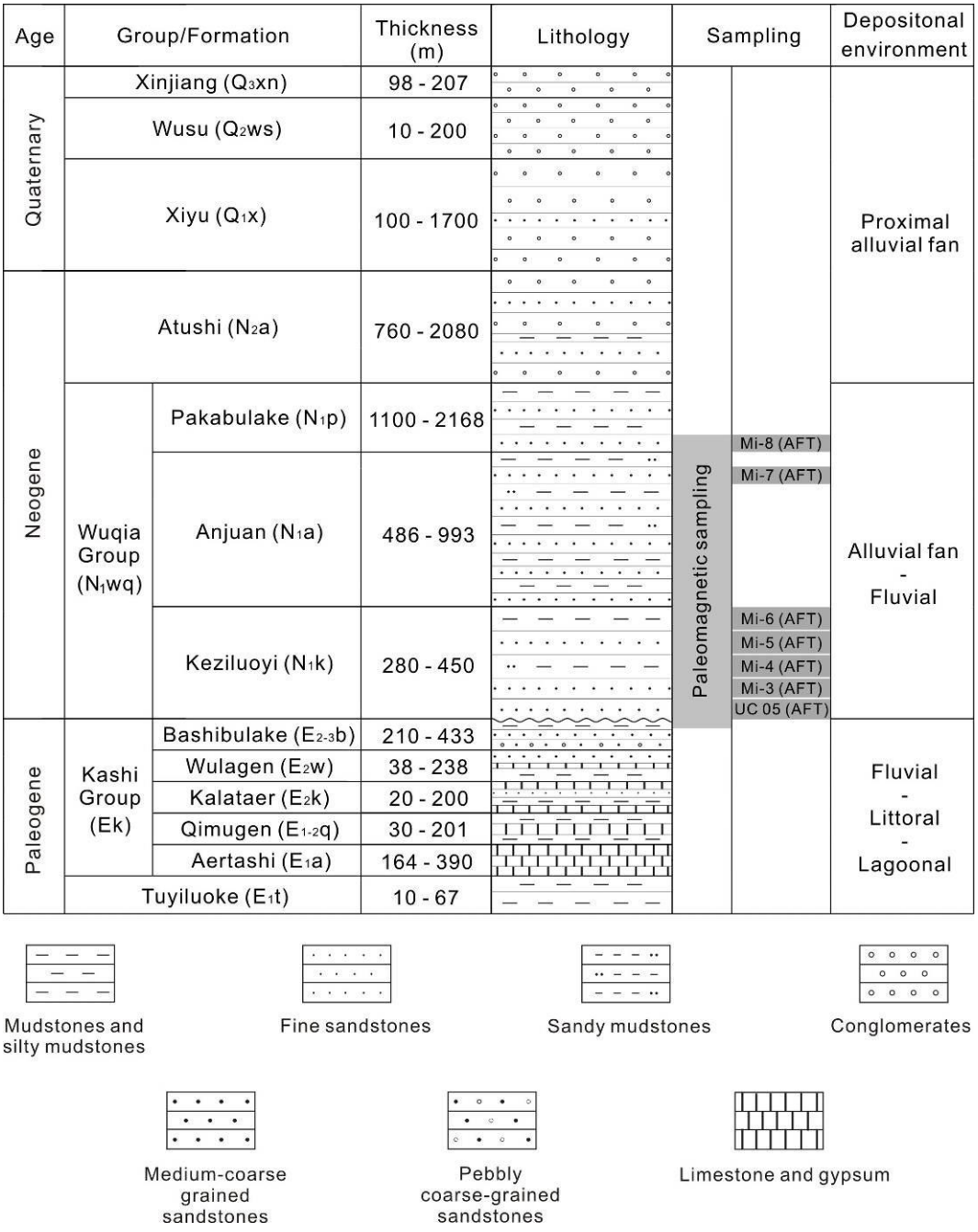

Fig. 3.2 Generalized stratigraphic column of the Cenozoic series of the studied Ulugqat area (modified after Yang et al., 2013).

3.5 Sampling and methods

3.5.1 Lithostratigraphy of sampled sections

Here we focus on the Mine section (39 °51'N, 74 °32'E) situated at the western margin of the Tarim Basin (Fig. 3.1). The Mine section (named after a nearby recently active mine) is close or identical to the Bashibulake section which has been part of earlier biostratigraphic studies by Lan & Wei (1995), Lan (1997), Mao & Norris (1988) and Tang et al. (1989). The last marine sediments belong to the Bashibulake Formation, corresponding to the final transgression which - according to previous studies of facies and fossil fauna, was restricted to the area west of Kashgar and did not extend in the southwest depression of the Tarim Basin (Bosboom et al., in press a; Lan, 1997; Lan and Wei, 1995). The lower marine part has been previously described and dated with biostratigraphy to range until the Priabonian (38.5-35.5 Ma, Bosboom et al., accepted). Following on this previous work, the continental strata overlying these marine deposits are here described and dated using magnetostratigraphy. The strata are exposed continuously in a tributary valley with variable dipping attitudes through gentle folding but no significant faults. The stratigraphic thicknesses of the recognized lithostratigraphic units were measured to decimetric precision above the zero meter level defined by the last shell bed of the marine Bashibulake formation.

Here we describe the lithostratigraphy and perform preliminary lithofacies analyses by comparison to the regional lithostratigraphic descriptions presented above (Dequan et al., 1996; Jia et al., 2004; Mao and Norris, 1988; Tang et al., 1989; Yang et al., 2012)

A complete description of the Bashibulake Formation at the Mine secton is available in Bosboom et al. (accepted). The Bashibulake Formation can be divided into five segments, and mainly composed of red-brown mudstones, sandy mudstones, orange and gray-green sandstones, pebbled sandstones, polymere quartz fine sandstones interbedded with gypsum, green-gray sandy limestone rich in bivalves. The first segment is mainly characterized by red-brown mudstones and siltstones, only containing foraminifers (Jia et al., 2004; Bosboom et al., accepted and Table 3.1). The lower part of the second segment mainly consists of red-brown silty mudstones

containing foraminifers, bivalve, ostracods, dinoflagellate and sporopollen, while the upper part is predominantly characterized by grey-green silty mudstones containing scolites, foraminifers, ostracods, dinoflagellate, coccolith and sporopollen. The third segment of the Bashibulake Formation is mainly composed of grey-green mudstones and lumachelle containing gasteropod, foraminifers, bivalve, ostracods, dinoflagellate, coccolith and sporopollen. The fourth segment mainly consists of dark purple mudstones interbedded with grey-gray shell marl containing foraminifers, gastropods, bivalve, ostracods, chlorophyceae, coccolith, dinoflagellate and sporopollen. The fifth segment is again composed of red-brown mudstones and silty mudstones containing pebbles, foraminifers and ostracods (Mao and Norris, 1988; Lan and Wei, 1995; Yang et al., 1995; Lan, 1997; Jia et al., 2004; Bosboom et al., accepted and Table 3.1). The Bashibulake Formation is thus characterized by littoral and neritic deposits.

An unconformity presents between the Keziluoyi Formation and the underlying Bashibulake Formation, characterized by a fine gravel conglomerate layer with a thickness of ~ 0.5 m (~ 15 m level). This gravel is directly overlain tan sandstone beds with well-developed meter-scale trough-cross-bedding The lower unit of the Keziluoyi Formation mainly consists of red-brown mudstones interbedded with grey-green silty mudstones, argillaceous sandstones and siltstones. The upper unit is dominated by red-brown and purple-red mudstones, irregularly interbedded with grey-green thin-bedded massive sandstones and thin-bedded siltstones and occasional laminated gypsum. The lithological associations between dark mudstones and grey-green sandstones above are indicative of a fluvio-lacustrine environment (Fig. 3.3). The Keziluoyi Formation covers a total thickness of ~ 570 m.

The Anjuan Formation conformably overlyies the Keziluoyi Formation with a relatively gradual transition such that the boundary is poorly constrained (~ 585 m level) (Fig. 3.3). The basal unit in the Anjuan Formation consists dominantly of brown and more regular occurences of grey-green fine-medium sandstones with trough-cross-bedding. Interbeddings of medium-thick bedded medium-grained sandstones and brown mudstones characterizes the next unit of the Anjuan Formation. Upward brown mudstones and thin-bedded fine-grained sandstones present as intercalated beds in the third unit, while brown and grey-green thick-bedded

sandstones are dominant in the top unit interbedded with dark brown mudstones and carbonaceous black mudstones. The lithological associations dominated by medium-thick bedded sandstones above are interpreted as shallow lacustrine deposits, and a general coarsening upwards sequence can be recognized in the Anjuan Formation with beds getting thicker (10-meter thick). Well-developed lenticular river beds present, indicating meandering system with overbank deposits. The Anjuan Formation spans ~ 723 m in thickness.

For the Pakabulake Formation conformably overlies the Anjuan Formation. It is defined by the first occurrence (~ 1308 m level) of grey conglomerates and conglomeratic sandstones within red-brown mudstones to sandstones constitute the basal unit, and a thin-bedded gravel layer presents at the bottom. The second unit consists dominantly of brown poorly sorted pebbly sandstones interbedded with red-brown siltstones characterized by braided channels (Fig. 3.3). The studied sequence from the Pakabulake Formation covers ~ 419 m in thickness.

3.5.2 Magnetostratigraphy

Paleomagnetic sampling at the Mine sections was performed using a portable electric drill powered by a portable gasoline generator. 541 samples were collected at an average 4-meter resolution (intervals ranging from 0.2 to 22.8 m) through the continuous Mine section ranging from the uppermost Bashibulake, through the Kezilouyi, Anjuan and Pakabulake formation. A broad fold within the section enabled to sample for a paleomagnetic fold test in order to check the reliability of the Characteristic Remanent Magnetization. Samples were orientated with a standard magnetic compass. After fieldwork, samples were cut into core specimens of approximately 2 cm in length for further paleomagnetic analyses.

3.5.2.1 Rock magnetism and thermal demagnetization

Within the shielded room of the paleomagnetic Laboratory of the of the Faculty of Geosciences at the Université de Rennes 1, specimens were thermally demagnetized

in a shielded oven (MMTD80) by using up to 21 temperature steps varying between room temperature (~25 ℃) and 690 ℃ with intervals of 50 ℃ up to 550 ℃, of 25 ℃ from 550 to 650 ℃, of 10 ℃ from 650 to 670 ℃, and of 5 ℃ from 670 to 690 ℃. Natural Remanent Magnetizations (NRM) of samples were measured on a 2G Enterprises DC SQUID cryogenic magnetometer. To monitor mineral changes upon heating, bulk magnetic susceptibility was measured for each sample between each step on a Bartington MS2 magnetic susceptibility meter. Demagnetization behaviors varied with lithologies and can be distinguished into three main groups as follows.

The first group (Group A) includes most samples of the marine red sediments of the Bashibulake Formation. These samples are characterized by low initial NRM intensities on the order of 10^{-4} A/m that are demagnetized mainly below 450-500 ℃ with demagnetization paths generally towards the origin (Fig. 3.4). After 450-500 ℃ NRM intensities and bulk susceptibilities strongly increase and the demagnetization path become erratic. These properties are similar to the one obtained from the marine red marine deposits of the Wulagen formation collected at the Aertashi and Mine sections of the southwestern Tarim basin (Bosboom et al., in press a) where they were interpreted as resulting from the combination of magnetite blurred by the mineral transformation of iron sulfides.

The second group (Group B) was observed in most of the samples. It includes mostly finer grained sandstones from the continental red beds of the overlying Wuqia group (Kezilouyi, Anjuan and Pakabulake Formations). These display higher initial intensities on the order of 10^{-3} A/m. A Low Temperature Component (LTC) in the normal present day field direction representing usually only a small portion of the NRM is demagnetized from room temperature to below 250 to 400 ℃. Most of the NRM is constituted by an Intermediate Temperature Component demagnetized from 250 - 400 ℃ up to 600-650 ℃ and a High temperature Component from 600-650 ℃ to 660-690 ℃. In this group the ITC and the HTC were defined as the Characteristic Remanent Magnetizations (ChRM) as they generally have the same directions and decay linearly towards the origin. They are interpreted to represent a combination of magnetite and hematite.

The third group (Group C) includes mostly coarser grained sandstones from the continental red beds of the overlying Wuqia group (Kezilouyi, Anjuan and Pakabulake Formations). They display low initial intensities on the order of 10^{-4} A/m. Demagnetization behaviors are similar to the ones of Group B except that demagnetization path are erratically decaying towards the origin. The LTC, ITC are often overlapping and difficult to separate and the HTC is often not distinguishable. An increase in the susceptibility at around 350 ℃ followed by a later decrease suggest the additional presence of maghemite in these coarser lithologies more prone to alteration.

3.5.2.2 ChRM direction analyses

The ChRM directions were determined by principal component analysis thermal demagnetization diagrams (Kirschvink, 1980) on a minimum of four main successive steps without anchoring the line-fit to the origin, except for some highly erratic demagnetization path of Groups A and C. Maximum angular deviations (MAD) on the line-fits were usually below 15°, but MAD of up to 30° were accepted if the polarity could be clearly discerned. In total, 478 ChRM directions in all were obtained from the 541 collected samples. These ChRM directions are separated into 'Quality1' if the direction and polarity were clearly determined (mostly from Group B); 'Quality 2' if the polarity is clearly determined but not the direction such as when using anchored line fits (mostly Group A and C); 'Quality 3' if neither direction nor polarity are clearly determined although a direction can be calculated (mostly Group A and C).

Most ChRM directions from the Bahibulake Formation (Group A) clearly depart from the rest of the directions from the overlying formations. They are in a normal polarity orientation before tilt-correction strongly suggesting post-folding remagnetization. This is similar to paleomagnetic results obtained from the marine red sediments of the Wulagen formation obtained in the west central Tarim Basin. Together these results suggest that marine sediments from the Tarim Basin have similar magnetic properties yielding remagnetizations. Caution should be used when interpreting paleomagnetic result from these rocks to infer magnetostratigraphic ages or tectonic rotation (see Bosboom et al., 2014). These directions were discarded by applying the following procedure.

In order to systematically filter out unreliable directions, Virtual Geomagnetic Pole (VGP) directions were calculated from the ChRM directions and VGP directions that were more than 45 ° from the mean VGP were iteratively discarded (see Dupont-Nivet and Krijgsman, 2011). This was done separately for normal and reversed polarity directions. After bedding tilt correction, the remaining directions separate in two antipodal clusters of normal and reversed polarities.

To assess the primary nature of the selected ChRM directions the reversals and fold tests were applied to this dataset (Tauxe, 1998). The fold test is clearly positive with clustering of directions at maximum unfolding indicating a pre-folding acquisition of the ChRM (Fig. 3.5). The reversals test, however, is not positive at the 95% confidence level although the directions are close to antipodal. This probably results from the incomplete separation of components of samples from Group C and even possibly the presence of an unidentified overlapping normal component in some sample of group B with an apparent linear trajectory towards the origin. The absence of a positive reversals test, however, does not affect the reliability of the magnetostratigraphy based on the correct determination of polarities rather than directions (see Dupont-Nivet and Krijgsman, 2011).

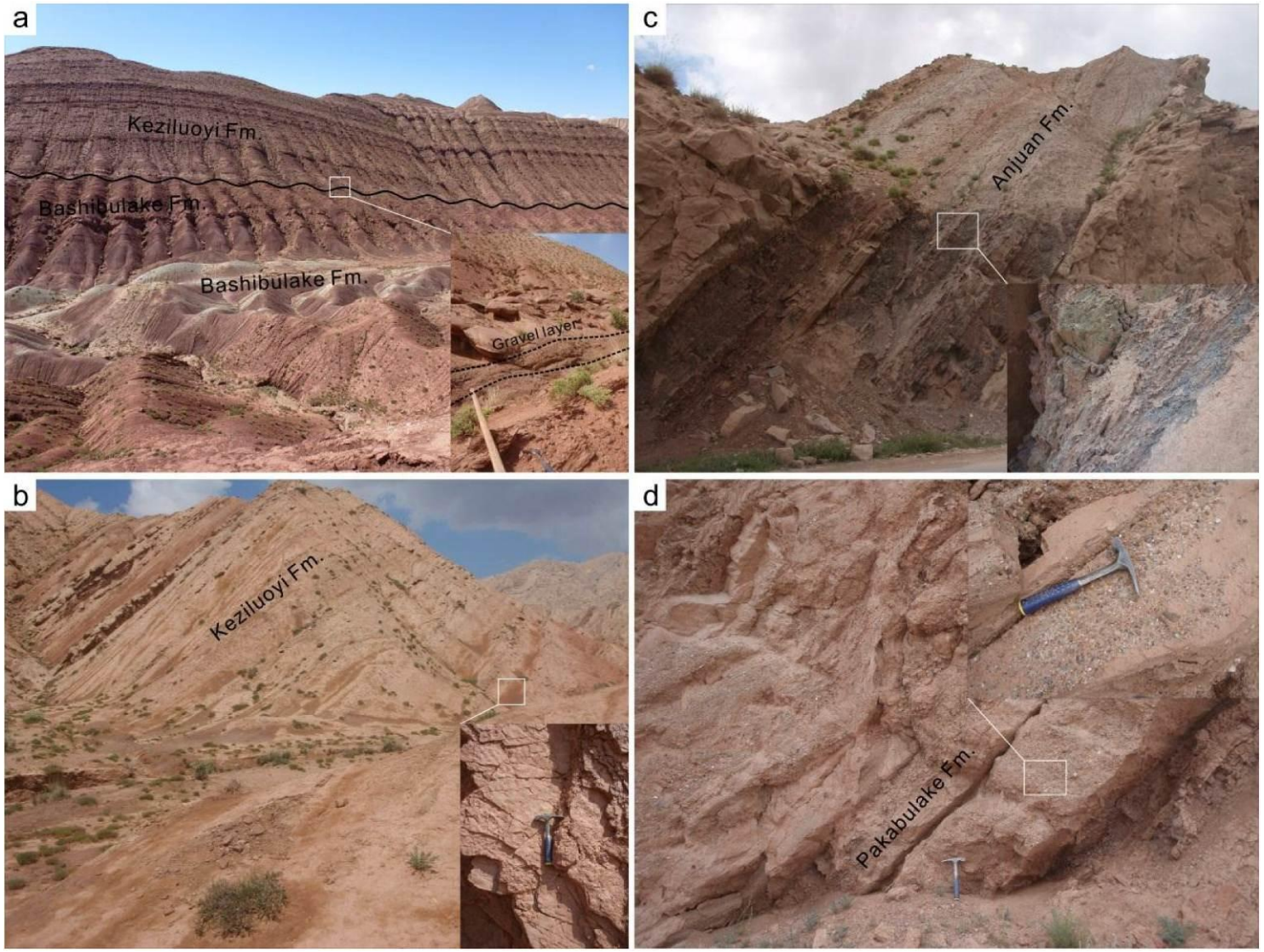
a
Keziluoyi Fm.
Bashibulake Fm.
Bashibulake Fm.
Gravel layer
c
Anjuan Fm.
b
Keziluoyi Fm.
d
Pakabulake Fm.

Fig. 3.3 Field photographs of formations and sedimentological features at the Mine section. (a) Angular unconformity between the Bashibulake and Keziluoyi Formation, channel sandstone beds of the Bashibulake Formation indicative of a fluvial depositional environment, and the gravel layer at the bottom of the Keziluoyi Formation. (b) Red mudstones interbedded with thick-bedded sandstones of the upper of Keziluoyi Formation indicative of the fluvio-lacustrine facies. Sinuous-crested ripples are locally developed. (c) Brown-red mudstones interbedded with gray-green mudstones, siltstones and sandstones of the Anjuan Formation indicative of a fluvio-lacustrine environment. (d) Conglomeratic sandstones, occasional red-brown mudstones and sandy mudstones of the basal unit of the Pakabulake Formation indicative of fluvial to alluvial fan deposits, with a thin-bedded gravel layer presents at the bottom.

(a)

Thermal Demagnetization

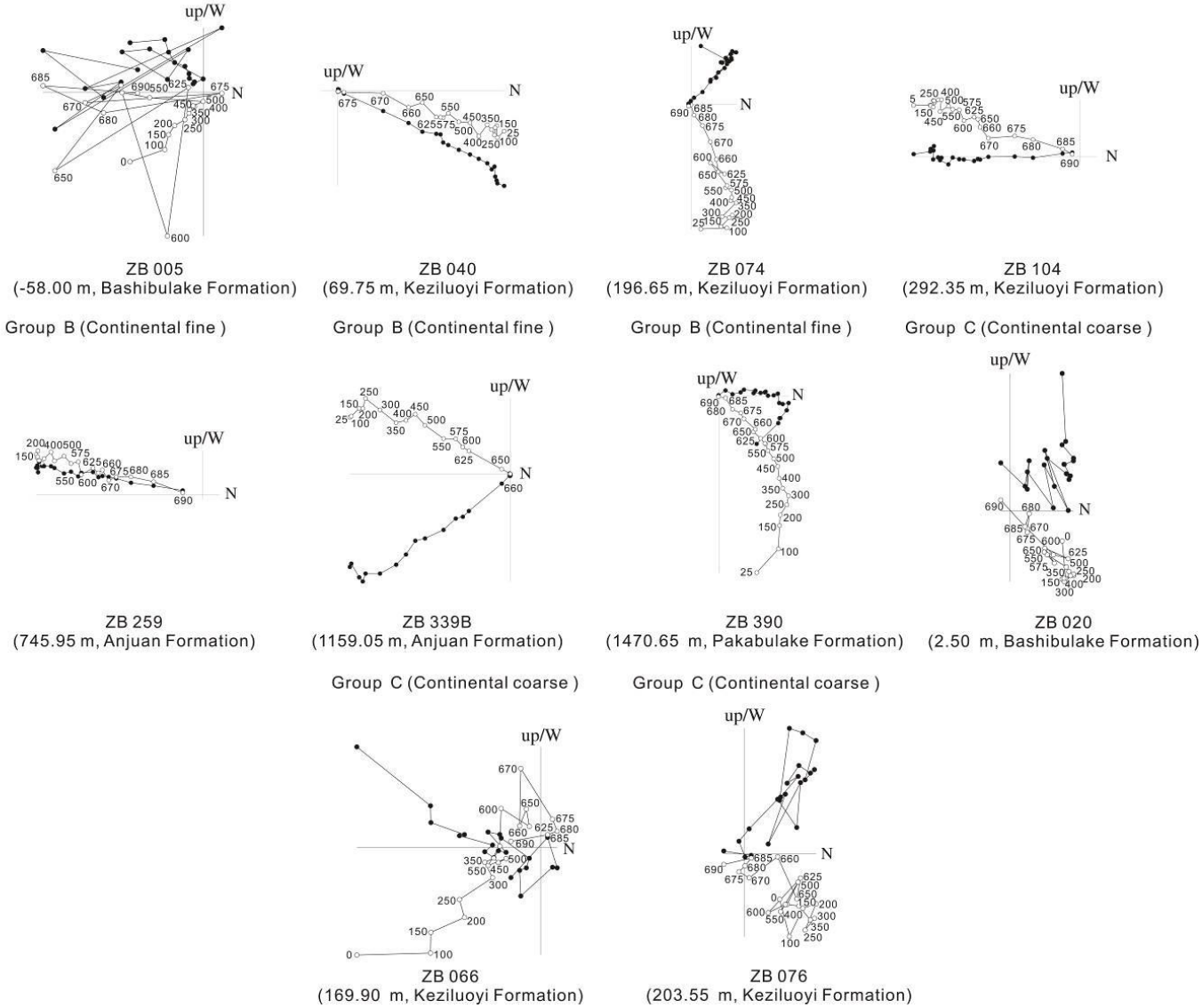

Fig. 3.4 (a) Plots showing typical thermal demagnetization behaviors of representative specimens of Groups A, B and C with Quality 1, 2 and 3 (see text). Numbers next to symbols indicate temperature of demagnetization steps in ℃. (b) Associated behavior of bulk susceptibility (SI) and (c) NRM intensity (10^{-5} A.m^{-2}).

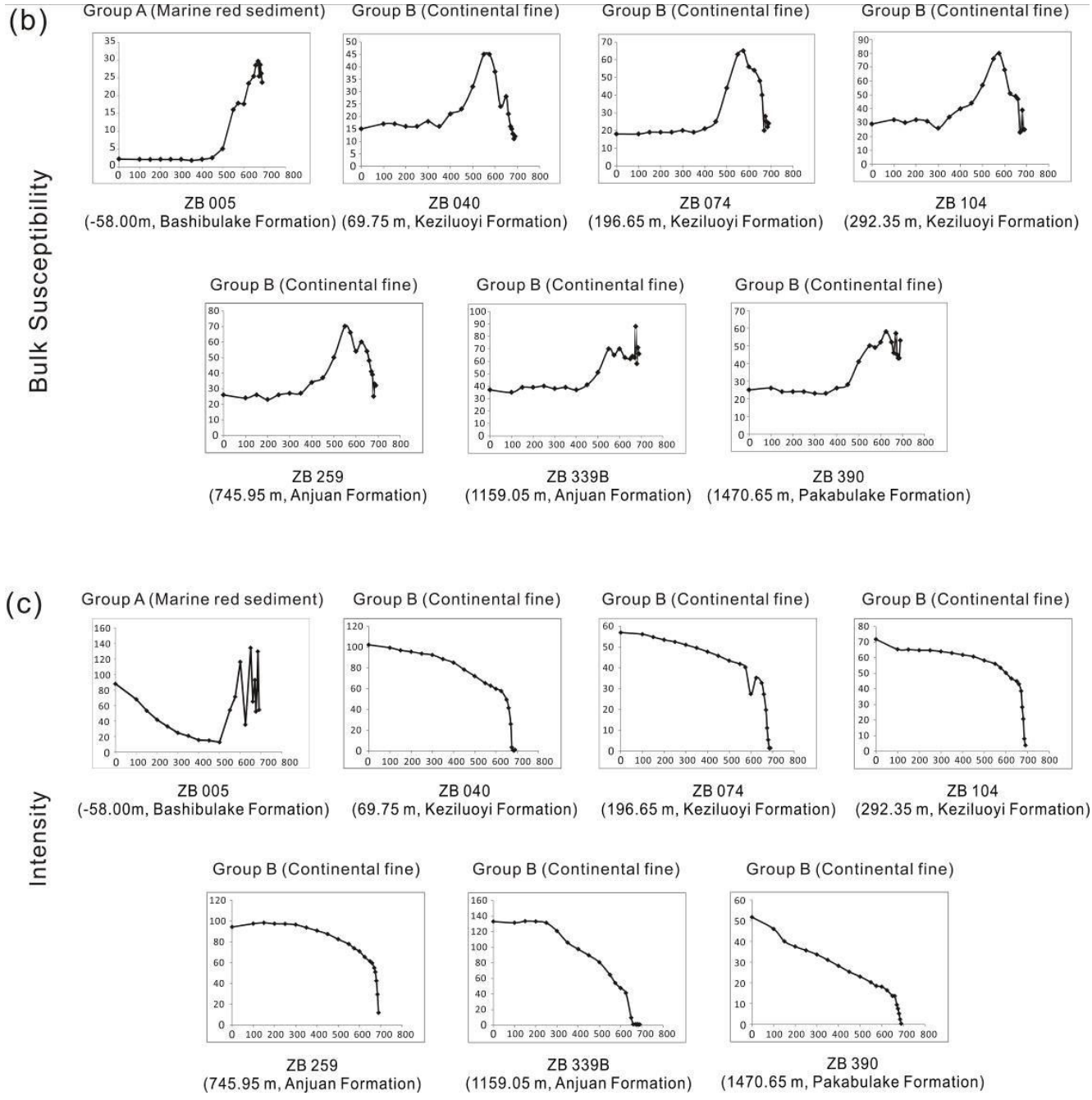

Fig. 3.4 Continued.

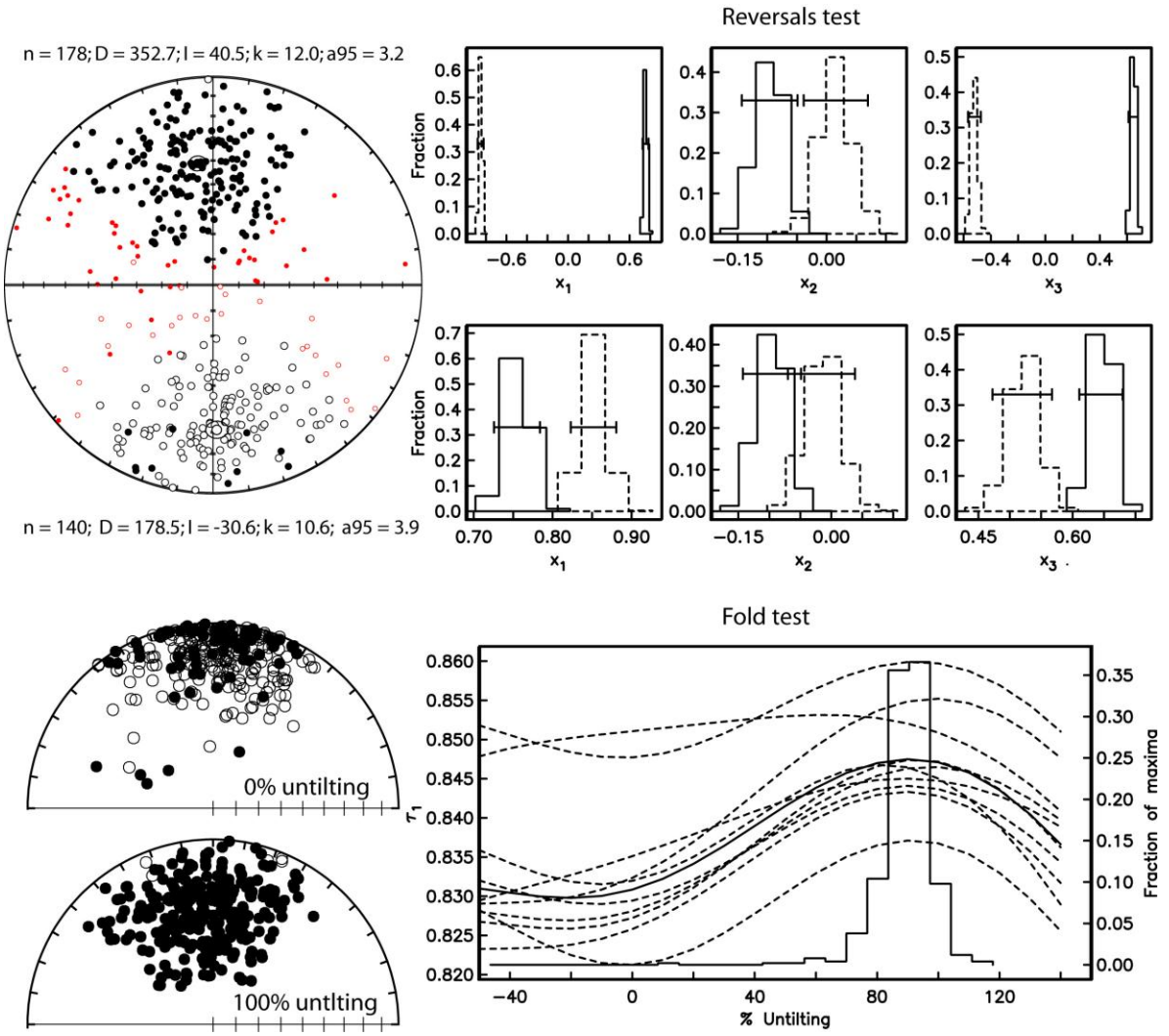
Reversals test
n = 178; D = 352.7; I = 40.5; k = 12.0; a95 = 3.2
n = 140; D = 178.5; I = -30.6; k = 10.6; a95 = 3.9
Fraction
x1
x2
x3
0% untilting
100% untlting
Fold test
τ1
% Untilting
Fraction of maxima

Fig. 3.5 ChRM directions, reversals test and fold test. Full symbols are projections on the horizontal plane and open symbols on the vertical plane.

3.6 Magnetostratigraphic correlation

Polarity zones were defined by at least two consecutive levels yielding accepted VGP latitudes with the same polarity (Fig. 3.6). This resulted in the definition of a total of 14 normal and 13 reversed polarity intervals recorded in this section, marked as N1-N14 and R1-R13 from top to bottom, respectively (Fig. 3.6).

Correlation to the Geomagnetic Polarity Time Scale (GPTS 2012) of Gradstein et al. (2012) was initially guided by age constraints arising from biostratigraphic constraints of the underlying marine deposits of the Bashibulake Formation dated late Bartonian - early Priabonian (38.5 – 35.5 Ma). However, these sediments are separated from the overlying Kezilouyi formation at the base of our section by a slightly angular uncomformity of unknown duration. Additional constraints are provided by the youngest population of detrital AFT ages presented above. For the Kezilouyi Formation the younger clusters of AFT ages range from ca. 27 Ma at the base (35 meter-level) to ca. 25 Ma at the top (570 meter-level). Additional constraints are provided for the upper part in Anjuan Formation at level 1075 by the youngest detrital AFT ages around 18 Ma (18.22 ± 7.83 and 18.54 ± 9.75 Ma). These clusters of detrital AFT ages actually represent exhumation ages that are therefore significantly older than the depositional age depending on the lag time (Bernet et al., 2004). These considerations provide a relatively broad timeframe on which we explored for possible magnetostratigraphic correlations based on the pattern of observed polarity zones.

As a starting point, we consider the longest and conspicuous reversed polarity zone R5 that includes the AFT ages ca. 18 Ma. Long reversed chrons around that time that may be correlated with R5 are C5r (ca. 11.5 Ma), C5Br (ca. 15.5 Ma), C5Cr (ca. 17 Ma), C6Ar together with C6AAr (ca. 21 Ma, assuming short normal chrons within have been missed) or C6Cr (ca. 23.5 Ma). Several of these options can be immediately rejected given the rest of the recorded polarity pattern observed above

and below R5. Above R5, two short normal zones precede three very large normal zones separated by short reversed zones. This enables to exclude correlating N5 with C5r because this pattern does not correspond to the very long C5n above C5r. It also excludes correlating N5 with C5.Cr because the long reversed C5Br would not be found in the observed pattern above N5. Correlating N5 with C6Cr is not excluded by the observed pattern above N5 but very unlikely given the pattern below N5 with three short normal zones separated by short reversed zones and underlain by another long reversed zone R8. This pattern below N5 cannot be reconciled by the dominantly normal chron pattern below C6Cr such that this correlation is rejected. We now consider the two remaining possible correlations, N5 with C5Br (correlation 1) as or N5 with C6Ar and C6Aar (correlation 2) illustrated on Figs. 3.6 and 3.7. Both yield realistic rates ranging from about 5 to 50 cm/kyr without major fluctuations although more fluctuations are observed for correlation 2. In both correlations, average rates are increasing upsection in agreement with the coarsening upwards lithologies. An abrupt increase in rates is observed within R4 (C9n ca. 28-27 Ma) and within N3 (C5Er ca. 19-17 Ma) respectively for correlations 1 and 2. For correlation 1, the increase corresponds to the apparition and increase of siltstone and sandstone beds while there is no lithologic change associated to the rate increase for correlation 2 within a dominantly mudstone interval.

Correlation 2 is found less likely because it requires several normal chrons to have been missed throughout the correlation. In particular, within R5, R7 and R8 while these intervals are well defined by high-resolution sampling yielding reliable ChRMs. It is also less favored because it would imply a 21 Ma depositional age at the 1075 meter-level that yielded detrital AFT ages ca. 18 Ma. On the other hand, correlation 1 is found more likely as it provides a realistic correlation for each of the observed polarity zones without missing any chrons. The pattern fit is optimal with the exception of R7 that is slightly too thick. This correlation is also favored by the record of detrital AFT ages. Correlation 1 yields a depositional age ca. 15.5 Ma for the 1075 meter-level that is realistically younger than the AFT ca. 18 Ma age cluster obtained at this level.

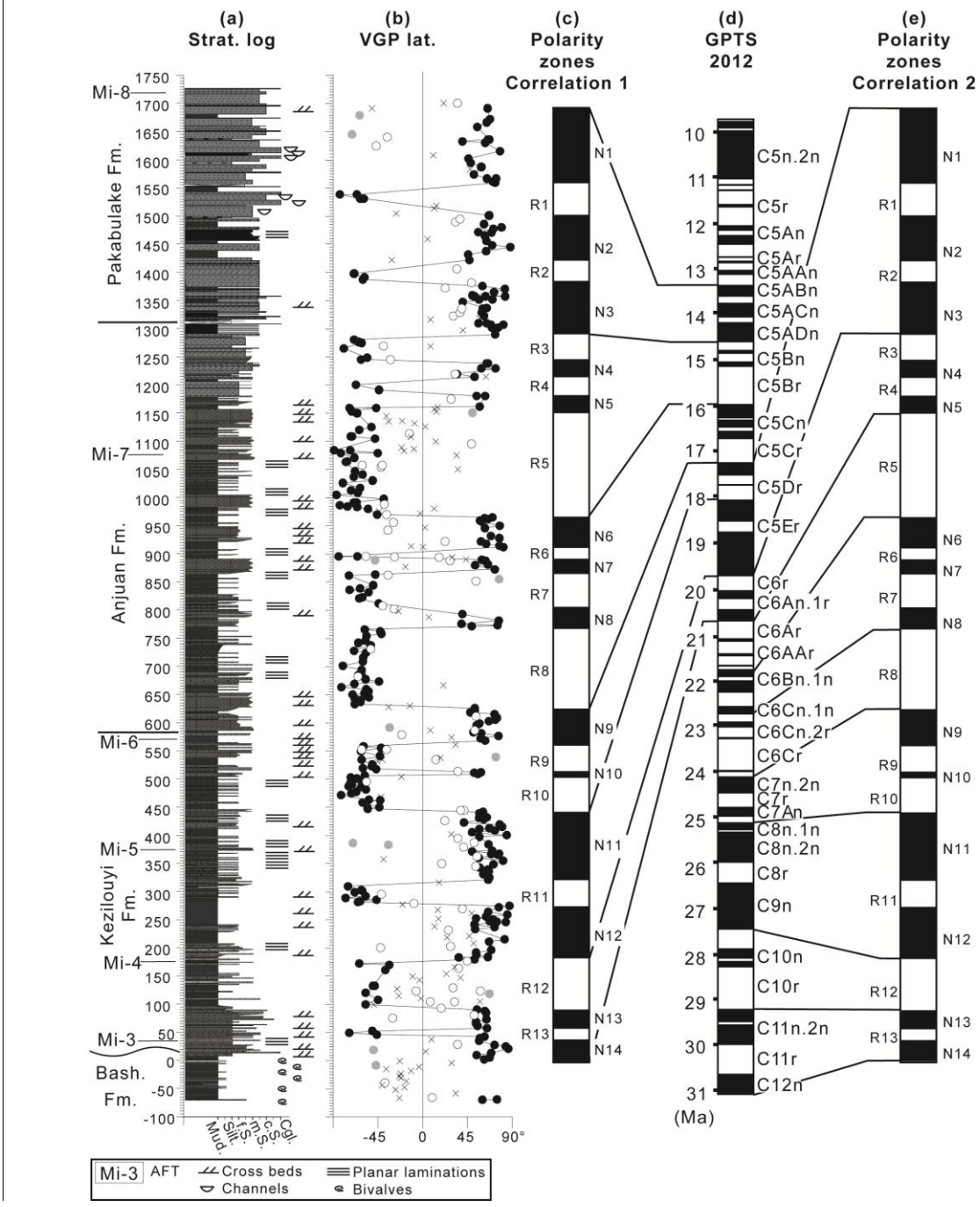

Fig. 3.6 Magnetostratigraphy of the Mine section. (a) Stratigraphic description of the measured section in meters (m). (b) VGP latitude represented by circles for Quality 1 and 2 directions (see text). Crosses are unreliable 'Quality 3' (see text) directions that have been discarded. Open circles are outlying directions that have been discarded by

applying an iterative 45 ℃ut off. Grey dots are isolated polarity directions that have been discarded. Black circles are the remaining reliable directions used to construct the magnetic polarity zones. (c) Corresponding magnetic polarity zones with preferred correlation 1 and (e) alternative correlation 2 (see text). (d) GPTS 2012: geomagnetic polarity time scale (Gradstein et al., 2012).

In summary, based on the most likely correlation to the GPTS (Gradstein et al., 2012), the Kezilouyi Formation was deposited at the Mine section between 20.6 Ma and 17.5 Ma with a marked increase in accumulation rates ca. 19-18 Ma. The Anjuan Formation was deposited from 17.5 to 14.6 Ma, and the overlying Pakabulake Formation initiated with the first conglomerate at around 14.6 Ma. We discuss below the potential tectonic significances of these results.

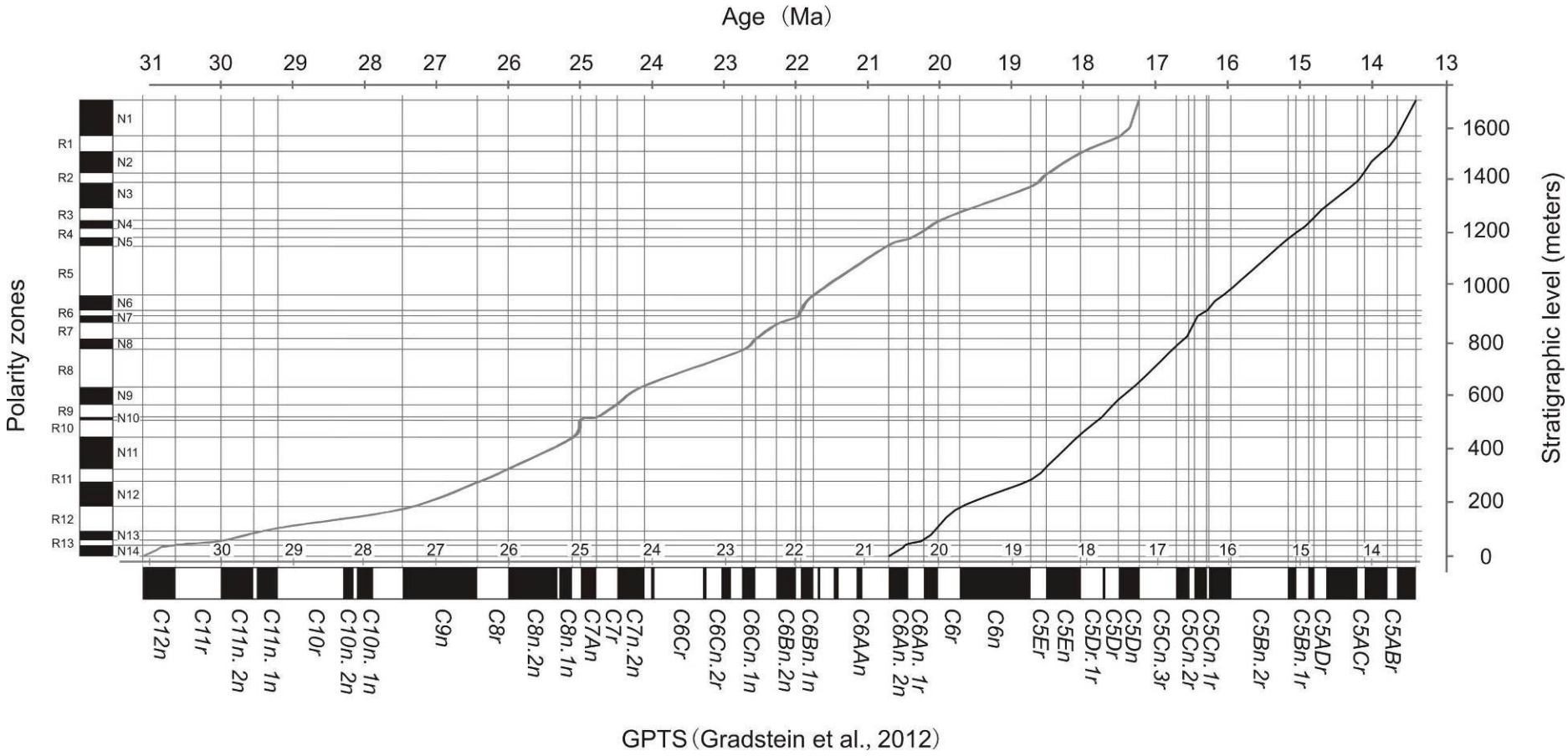

Fig. 3.7 Correlation of the polarity zones recognized in the Mine section to the GPTS 2012 (Gradstein et al., 2012) with corresponding accumulation rates. The preferred (alternative) correlation is represented by the thick black (grey) line.

3.7 Discussion

Our results reveal a major Oligocene hiatus in the southwestern Tian Shan foreland basin. At the studied section, the onset of continental deposits at 20.8 Ma overlies directly the last marine deposits of the marine Bashibulake Formation recently dated using biostratigraphy to late Eocene age between the late Bartonian and early Priabonian (38.5-35.5 Ma; Bosboom et al., 2011; accepted). This very long discontinuity may reflect a major erosional event and/or the prolonged absence of sediment accumulation.

The latter is supported by several observations. At the Mine section this major hiatus recognized between the Bashibulake and overlying Keziluoyi Formations occurs at the 15 meter level is expressed by a fine gravel layer of ~ 0.5 m thickness. The angle of the uncomformity is less that a few degrees and discernable only on extensive outcrops over several 100s of meters length (Fig. 3.3). The contact between these Formations is reported as a parallel discomformity in other sections of the Wuqia area (e.g. Ulugqat; Jin et al., 2003). Also suggesting the hiatus does not stem from a major erosional event, is that the Bahsibulake Formation represents the youngest marine deposits regionally reported below the Kezilouyi Formation (see Bosboom et al., accepted and references therein). At the Mine section, the complete stratigraphy of the five members of the Bashibulake Formation is found below the hiatus. We thus infer that little erosion affected the Bashibulake Formation at the Mine section. This Oligocene hiatus is, according to existing magnetostratigraphic records of continental deposits, widespread in southwestern Tian Shan (Kashi foreland; Heermance et al., 2006) and probably along the rest of southern Tian Shan in the Kuche foreland with generally post-Oligocene onset of continental deposition (Charreau et al, 2006, 2008). Note that continental deposits as old as 28 Ma have been reported but based on magnetostratigraphic records that become poorly correlated in the oldest part (Huang et al., 2006). In southwestern Tarim (Yecheng sub-basin, Fig. 3.1), however, this large hiatus is not present in the recently dated marine to continental transition (Bosboom et al., in press a). There, the marine deposits end with the Wulagen Formation (the Bashibulake Formation is not present) and are conformably overlain by the ca. 41 Ma continental deposits of the Kezilouyi Formation continuously deposited through the

Oligocene except for a gap including the Eocene Oligocene transition as constrained with magnetostratigraphy. Thick continuous deposition through the Oligocene in southwest Tarim and the coeval lack of accumulation in Northern Tarim along the southern Tian Shan is consistent with Tarim isopach maps (Yang and Liu., 2002; Wei et al., 2013). Our results thus support a simple model for the evolution of the basin with subsidence starting in the southwest in response to Eocene to Oligocene Kunlun Shan northward thrusting (e.g. Jolivet et al., 2001) while the south Tian Shan foreland remained mostly inactive until the earliest Miocene onset of subsidence and accumulation associated with Tian Shan exhumation (e.g. Hendrix et al., 1994; Dumitru et al., 2001; Sobel et al., 2006; Wang et al., 2009; De Grave et al., 2012).

After the major hiatus at the Mine section, overlying continental sediments of the basal Kezilouyi Formation start being deposited at 20.8 Ma. These sediments yield a young cluster of AFT detrital ages ca. 27-25 Ma and a notable increased diversity of U/Pb ages indicating recycling of material from the Paleozoic and Mesozoic southwest Tian Shan piedmont (Yang et al., 2013). This suggests deposition of the Keilouyi Formation can be associated with the early Miocene south Tian Shan exhumation (Dumitru et al., 2001; Sobel et al., 2006; Wang et al., 2009; De Grave et al., 2012). Our results fit well within the regional model of southward propagation of deformation of the Kashi foreland basin constrained by magnetostratigraphy and thermochronology (Heermance et al., 2007, 2008; Sobel et al., 2006). These indicate an onset of exhumation at the Oligocene–Miocene boundary (~ 24 Ma) along thrust sheets (the Maidan and Muziduke thrusts, which bound the southern side of the Kokshaal range) that are located on the other side of the Talas Fergana fault to the east. This suggests that the timing of the onset of south Tian Shan exhumation was similar on either side of the Talas Fergana fault.

Further up in the Mine section, we report a significant increase in sediment accumulation at ~ 18.5 Ma, coeval with a lithologic transition from dominantly red-brown mudstones to more fluvial dark mudstones and grey-green sandstones (Table 3.2). This age compares well with results from the detrital apatite fission track dating from the nearby Ulugqat section (Yang et al., 2013). There, two sandstone samples (UC01 from Middle Jurassic strata and UC02 from Early Cretaceous strata) yield

central fission track ages of 18.5 ± 5.2 and 16.6 ± 2.8 Ma, respectively. These two samples are interpreted to be totally reset with the central AFT ages representing the age of subsequent exhumation. This suggests that thrust sheets north of the Mine section propagated southwards at this time inducing the increased accumulation rates and the cluster of ca. 18 Ma detrital AFT ages in associated sediments of the Mine section. Regionally, this age corresponds well with the 18.9 ± 3.3 Ma southward propagation of deformation into the Kashi foreland basin (the Kashi basin-bounding thrust, Sobel et al., 2006) with associated southward propagating increased accumulation rates and conglomeratic deposition into the Kashi basin from 15.5 Ma onwards (Heermance et al., 2007).

Finally, our results are concordance in time and space with recently proposed models for tectonic evolution of the Pamir salient (Bosboom et al., in press a; Cowgill et al., 2010; Sobel et al., 2013). Accordingly, during the Early Eocene-Late Oligocene the deformation was far to the south of the south Tian Shan as the the Pamir indented into Tarim with exhumation along the Kunlun Shan. Exhumation started in the Tian Shan near the Oligo-Miocene boundary but propagated southwards ca. 20-18 Ma. At this time, the Kashgar-Yecheng Transfer System (KYTS), the main 300 km dextral slip shear zone separating Tarim from the Eastern Pamir initiated (Cowgill et al., 2010; Sobel and Dumitru, 1997; Sobel et al., 2006, 2011; Cao et al., 2013). This suggests this fault system transferred slip northward across the Tarim into the Southwestern Tian Shan, enhancing thrusting and exhumation and possibly reactivating the Talas Fergana Fault at this time.

Table 3.2 Sedimentation accumulation rates.

Level (m)	Polatity zones	Preferred correlation				Possible correlation			
		Chron	Age (Ma)	Rate (cm/Kyr)	Av. rate (cm/Kyr)	Chron	Age (Ma)	Rate (cm/Kyr)	Av. rate (cm/Kyr)
6.00	Top R1	Top C6Ar	20.709	13.80	14.77	Top C12r	31.034	8.41	4.75
43.25	R2	Base C6An.1r	20.439	6.37		Base C11r	30.591	2.32	
57.65		Top C6An.1r	20.213	27.25		Top C11r	29.970	5.99	
104.8	R3	Base C6r	20.040	22.59		Base C10r	29.183	4.12	
176.65		Top C6r	19.722	10.11	10.09	Top C9r	27.439	9.67	
275.15	R4	Base C5Er	18.748	22.41		Base C8r	26.420	11.59	12.63
325.35		Top C5Er	18.524	24.91	24.37	Top C8r	25.987	13.13	
441.95	R5	Base C5Dr.1r	18.056	21.17		Base C7Ar	25.099	58.17	
508.85		Top C5Dr.1r	17.740	38.70		Top C7Ar	24.984	3.99	3.99
517.75	R6	Base C5Dr	17.717	27.45		Base C7r	24.761	17.60	
568.25		Top C5Dr	17.533	21.98		Top C7r	24.474	17.95	13.39
633.75	R7	Base C5Cn.3r	17.235	25.72		Base C7n.1r	24.109	9.76	
765.95		Top C5Cn.3r	16.721	23.65		Top C6Cn.1r	22.754	22.16	
808.05	R8	Base C5Cn.2r	16.543	78.17		Base C6Br	22.564	18.75	
863.55		Top C5Cn.2r	16.472	15.80	26.62	Top C6Br	22.268	9.67	
890.25	R9	Base C5Cn.1r	16.303	62.00		Base C6Bn.1r	21.992	38.75	18.22
911.95		Top C5Cn.1r	16.268	19.80		Top C6Bn.1r	21.936	34.44	
970.15	R10	Base C5Bn.2r	15.974	23.21		Base C6AAr.3r	21.767	17.85	
1159.05		Top C5Bn.2r	15.160	17.19		Top C6Ar	20.709	8.15	
1181.05	R11	Base C5Bn.1r	15.032	20.62		Base C6An.1r	20.439	14.78	
1214.45		Top C5Bn.1r	14.870	32.00		Top C6An.1r	20.213	17.57	
1244.85	R12	Base C5ADr	14.775	21.69		Base C6r	20.040	11.32	10.11
1280.85		Top C5ADr	14.609	21.21		Top C6r	19.722	9.71	
1375.45	R13	Base C5ACr	14.163	50.11		Base C5Er	18.748	20.80	
1422.05		Top C5ACr	14.070	23.87		Top C5Er	18.524	16.88	20.87
1501.05	R14	Base C5ABr	13.739	44.58		Base C5Dr.1r	18.056	11.17	
1559.45		Top C5ABr	13.608	53.71		Top C5Dr	17.533	44.16	
1691.05	Top N14	Base C5AAr	13.363	—		Base C5Cn.3r	17.235	—	

* Notes: Level – stratigraphic level from the studied section; Age – age of correlated chron based on GPTS 2012 (Gradstein et al., 2012); Rate – calculated sediment accumulation rate; Av. rate – average rate for longer intervals.

3.8 Conclusions

A longstanding enigma - since it has been established with thermochronology that the Tian Shan has been reactivated in the earliest Miocene (Hendrix et al., 1994) – is to understand why this occurred so late after the Eocene India-Asia collision. To answer that question we have provided here magnetostratigraphic ages on the sedimentary successions of the Kezilouyi Fomation that has been previously attributed to start in the Oligocene and therefore may have recorded the earliest south Tian Shan evolution. We show here using magnetostratigraphy that deposition of these sediments started only in the early Miocene and therefore reveal the existence of a major hiatus between them and the underlying marine successions recently dated as late Eocene (38.5-35.5 Ma; Bosboom et al., accepted). Compared with the coeval thick foreland deposition in southwestern Tarim, this hiatus shows that the Oligocene was relatively quiet along the southern Tian Shan piedmont where significant subsidence started only in the early Miocene together with the exhumation of the range. In addition, our results support that increased exhumation and propagation of the Tian Shan range ca. 20-18 Ma may be related to the activation of a major strike slip system along the eastern Pamir range allowing transfer of slip from the India-Asia collision to the Tian Shan. Although our results confirm that India-Asia deformation had not propagated to the Tian Shan before the early Miocene, it remains unclear why it did not do so previously. We can only speculate that either the terranes between the India-Asia collision and the Tian Shan acted as a buffer protecting from northward propagation of deformation from 50 to 25 Ma and then that the strike slip system activation between Tarim and the Pamir range significantly increased that transfer of deformation ca. 20-18 Ma. Alternatively, it is possible that the collision itself changed drastically at around 25 Ma to be able to propagate deformation much further into Asia. This may result, as previously proposed, from a change from soft to hard

collision related to various stages of slab break off (e.g. Chemenda et al., 2000) and/or to a two stage collision with the actual continental collision occurring only at the Oligo-Miocene boundary (van Hinsbergen et al., 2012).

General Conclusions

Here I review the main results of each chapter and synthesize them with respect to the two critical scientific issues I developed in the general introduction.

Main results and implications

Northern Tian Shan detrital U/Pb zircon provenance record

The tectonic evolution of the Tian Shan, as for most ranges in continental Asia is dominated by north-south compression since the Cenozoic India-Asia collision. However, precollision governing tectonic processes remain enigmatic. An excellent record is provided by thick Palaeozoic – Cenozoic lacustrine to fluvial depositional sequences that are well preserved in the southern margin of the Junggar Basin and exposed along a foreland basin associated to the Late Cenozoic rejuvenation of the Tian Shan ranges. U/Pb (LA-ICP-MS) dating of detrital zircons from 14 sandstone samples from a continuous series ranging in age from latest Palaeozoic to Quaternary is used to investigate changes in sediment provenance through time and to correlate them with major tectonic phases in the range. Samples were systematically collected along two nearby sections in the foreland basin. The results show that the detrital zircons are mostly magmatic in origin, with some minor input from metamorphic zircons. The U-Pb detrital zircon ages range widely from 127 to 2856 Ma and can be divided into four main groups: 127-197 (sub-peak at 159 Ma), 250-379 (sub-peak at 318 Ma), 381-538 (sub-peak at 406 Ma) and 543-2856 Ma (sub-peak at 912 Ma). These groups indicate that the zircons were largely derived from the Tian Shan area to the south since a Late Carboniferous basin initiation. The provenance and basin-range pattern evolution of the southern margin of Junggar Basin can be generally divided into four stages: (1) Late Carboniferous-Early Triassic basin evolution in a half-graben or post-orogenic extensional context; (2) From Middle Triassic to Upper Jurassic times, the southern Junggar became a passively subsiding basin until (3) being inverted during Lower Cretaceous-Palaeogene; (4) During the Neogene, a piedmont developed along the northern margin of the North Tian Shan block and Junggar Basin became a true foreland basin.

Southern Tian Shan detrital U/Pb zircon provenance and Apatite Fission Track ages

Recent studies have shown that both the general tectonic framework of Tian Shan and some of its actual topographic features were inherited from the still poorly constrained Late Paleozoic–Mesozoic evolution of the range. Better understanding of the tectonic and topographic evolution of the South Western Tian Shan (SWTS) during the Mesozoic-Early Cenozoic times is required to discuss the critical scientific issues we proposed. We present here U/Pb (LA-ICP-MS) dating of detrital zircons and apatite fission track analysis on detrital apatites from the exceptionally well-exposed Jurassic to Cenozoic sediment series of the still poorly constrained southwestern Tian Shan piedmont to investigate changes in sediment provenance through time. The U/Pb detrital zircon ages range widely from 222 to 3179 Ma and can be statistically separated in four main groups: 240–320 Ma, 400–540 Ma, 550–1600 Ma and 1640–2800 Ma. These zircons were derived from the Tian Shan area to the north and from recycling of the Paleozoic North Tarim margin. The detrital apatite fission track ages encompass sources with preserved Mesozoic ages as well as much younger sources exhumed during middle Miocene times. Combined together those data show a general planation of the range from Middle Jurassic to Late Cretaceous associated to a wide drainage system. The progressive decrease in the variety of sources through the Mesozoic is consistent with burying of the basement exposures by sediments. Detrital zircon U/Pb data indicate an initial Tertiary uplift of the southern Tian Shan piedmont around Eocene times and a possible activation of the Talas Fergana Fault between 18 and 16 Ma.

Southern Tian Shan magnetostratigraphy

The differing hypotheses, even vigorous debates derived from different sections put forward the necessity to look for more effective evidences to correctly constrain the Cenozoic episodic uplift of the SWTS. Here, we present a detailed magnetostratigraphic study from the Ulugqat area in piedmont of the Southwest Tian Shan, in order to improve understanding of the uplift and deformation history of the Southwest Tian Shan during the Cenozoic. The 1700-m-thick section comprises an age span from ~ 20.8 to 13.3 Ma according to the most likely correlation to the

geomagnetic polarity time scale. An unconformity between the onset of continental depostins of the Keziluoyi Formation and the last marine deposits of the Bashibulake Formation is detected around 20.8 Ma. This major depositional hiatus spreading from the 38.5-35.5 to 20.8 Ma corresponds to the absence of Oligocene foreland deposits in the northwestern Tarim. This contrast with the southwestern Tarim basin where Eocene marine records are overlain continuously by continental foreland deposits. This suggest foreland deformation initiated earlier in the southern Tarim basin in response to Eocene-Oligocene activation of the Kunlun Shan to the south. Along the southern Tian Shan, however, significant tectonic activity only initiated in the early Miocene as supported by thermochronologic studies. There sediment accumulation rates increase conspicuously at ~ 18.5 Ma, concurrent with the previous detrital apatite fission-track analysis from the Ulugqat area, yielding totally reset central ages respectively at 18.5 ± 5.2 and 16.6 ± 2.8 Ma. This age corresponds to the southward propagation of deformation of the Tian Shan piedmont into the Tarim basin. This change of tectonic regime is also coeval with the tectonic activation of a major strike-slip system separating the Tarim basin from the Pamir salient to the west. This together suggests that this system enabled from 20-18 Ma onwards to transfer compressional deformation from the India-Asia collision to the Tian Shan and possibly the Talas Ferghana Fault.

Mesozoic tectonic setting and basin-range of the Tian Shan region

As already discussed above, erosion of the Paleo-Tian Shan initiated in the Middle Triassic results in the general peneplanation of the Mesozoic Tian Shan dominated by a wide drainage system and long-lasting tectonic quiescence. The northern piedmont of the Tian Shan was characterized by a post-extensional thermally subsiding basin without much tectonic activity, and the southern piedmont also experienced a general flattening of topography. During the Early Jurassic, Early Cretaceous and Late Cretaceous, there are three minor tectonic inversions and adjustments of basin-range pattern in the Tian Shan, potentially and respectively corresponding to the accretions of Cimmerian, Lhasa, and Kohistan-Dras in the southern margin of the Eurasian plate. These are synthetically evidenced by detrital zircon U-Pb geochronology, detrital

apatite fission-track analysis and magnetostratigraphy from the northern and southern piedmonts of the Tian Shan.

Spatio-temporal differences in the Cenozoic Tian Shan uplift

Detrital zircon U-Pb and apatite fission-track data indicate an initial late Cretaceous – Early Tertiary basin reorganization and coeval renewed erosion along the southern Tian Shan piedmont. This is consistent with scarce cooling ages extracted from previous studies on the CTS, STS and Kyrgyz Tian Shan, as well as the poorly dated late Cretaceous to Paleogene conglomerates and related provenance adjustment in Kuqa subbasin. We thus interpreted this late Cretacesou to Paleogene activity in STS as the initial response of the distant effects of India-Eurasia collision as previously argued. However, more work evidently needs to be performed on that aspect to carefully date this activity and determine its nature. In addition to the thermochronologic work presented here, magnetostratigraphic and sedimentologic analyses should be performed on the numerous existing stratigraphic sections of this age presently exposed in the SWTS.

During the Late Cenozoic, the major reactivation of the Tian Shan initiated around the Late Oligocene-Early Miocene times. This is evidenced mainly from the detrital zircon U-Pb geochronology in the northern piedmont of the Tian Shan, the apatite fission-track data suggesting a possible activation of the Talas Fergana Fault between 18 and 16 Ma, the major Oligocene depositional hiatus and conspicuous increase in accumulation rates at ~ 18.5 Ma revealed by the magnetostratigraphic results in the southern piedmont of the Tian Shan.

Therefore, here we inferred that Cenozoic uplift of the Tian Shan propagated northwards and evolved from local to regional effects during the late Cretaceous to Miocene times. This is also consistent with the northward propagation of far-field effects of the Indo-Asia collision.

Perspectives

This work is favored for better understanding the Mesozoic-Cenozoic tectonic evolution and basin-range relations of the northern and southern piedmonts of the Tian Shan, by using the detrital zircon U-Pb dating, apatite fission-track analysis and magnetostratigraphy. However, there is still plenty of space to discuss the related important scientific issues. Further research ought to be carried out in the northern piedmont of the Tian Shan in terms of low temperature thermochronology, especially for the Cenozoic series that are still constrained poorly in that aspect although they are already fairly well dated using magnetostratigraphy. This would enable to gain more insights on the exhumation history of NTS during the Early Cenozoic period.

We targeted the Kezilouyi Formation in the Ulugqat area to fill a significant gap in the geochronological database for the evolution of the STS in a key area where no regional tectono-sedimentary framework was constructed with proper age resolution. However, this should can be considered a first shot at solving this problem. It would be significant to present the correlation of this with different sections along the southern Tian Shan piedmont within the similar lithostratigraphic units by using similar geochronological approaches. In particular, this would provide opportunities to further test the potential difference in tectonic deformation between the ETS and WST, across the Talas Ferghana Fault, and the possible lateral propagation of the crustal shortening of the Tian Shan region.

References

Alekseev, D.V., Degtyarev, K.E., Kotov, A.B., Sal'nikova, E.B., Tret' yakov, A.A., Yakovleva, S.Z., Anisimova, L.V., Shatagin, K.N. (2009), Late Paleozoic subductional and collisional igneous complex in the Naryn Segment of the Middle Tien Shan (Kyrgyzstan). Doklady Earth Sciences 427, 760-763.

Allen, M.B., Sengor, A.M.C. and Natalin, B.A. (1995), Junggar, Turpan, and Alakol basins as Late Permian to Early Triassic extensional structures in a sinistral shear zone in the Altaid orogenic collage, central Asia. *Geologcical Society of London*, 152, 327-338.

Allen, M.B., Vincent, S.J. and Wheeler, P.J. (1999), Late Cenozoic tectonics of the Kepingtoge thrust zone: interaction between the TianShan and the Tarim Basin, Northwest China. *Tectonics*, 18, 639-654.

Allen, M.B., Vincent, S.J., Wheeler, P.J. (1999), Late Cenozoic tectonics of the Kepingtoge thrust zone: interaction between the TianShan and the Tarim Basin, Northwest China. *Tectonics*, 18, 639-654.

Allen, M.B., Windley, B.F. and Zhang, C. (1992), Paleozoic collisional tectonics and magmatism of Chinese Tian Shan, central Asia. *Tectonophysics*, 220, 89-115.

Allen, M.B., Windley, B.F. and Zhang, C. (1994), Cenozoic tectonics in the Urumqi-Korla region of the Chinese Tien Shan. *Geological Rundsch*, 83, 406-416.

Allen, M.B., Windley, B.F., Zhang, C. (1992), Paleozoic collisional tectonics and magmatism of Chinese Tian Shan, central Asia. *Tectonophysics*, 220, 89-115.

Andersen, T. (2002), Correction of common lead in U-Pb analyses that do not report ^{204}Pb. *Chemical Geological*, 192, 59-79.

Andersen, T. (2005), Detrital zircons as tracers of sedimentary provenance: limiting conditions from statistics and numerical simulation. *Chemical Geologial*, 216 (3-4), 249-270.

Andersen, T. (2002), Correction of common lead in U-Pb analyses that do not report ^{204}Pb. *Chemical Geology*, 192, 59-79.

Andersen, T. (2005), Detrital zircons as tracers of sedimentary provenance: limiting conditions from statistics and numerical simulation. *Chemical Geology*, 216 (3-4), 249-270.

Avouac, J.P., Tapponnier, P., Bai, M.H., You, H. and Wang, G. (1993), Active thrustingland folding along the northern Tian Shan and late Cenozoic rotation of the Tarim relative to Dzungaria and Kazakhstan. *Journal of Geophysical Research*, 98, 6755-6804.

Avouac, J.P., Tapponnier, P., Bai, M.H., You, H., Wang, G. (1993), Active thrustingland folding along the northern Tian Shan and late Cenozoic rotation of the Tarim relative to Dzungaria and Kazakhstan. *Journal of Geophysical Research*, 98, 6755-6804.

Bernet, M., Spiegel, C. (2004), Introduction : Detrital thermochronology. In: Bernet, M., Spiegel, C. (eds.), Detrital Thermochronology-Provenance analysis. Exhumation and Landscape Evolution of Mountain Belts. *Geological Society of America Special Publication*, 378, 1-6.

Bershaw, J., Garzione, C.N., Schoenbohm, L., Gehrels, G., Li, T. (2012), Cenozoic evolution of the Pamir plateau based on stratigraphy, zircon provenance, and stable isotopes of foreland basin sediments at Oytag (Wuyitake) in the Tarim Basin (west China). *Journal of Asian Earth Sciences*, 44 (30), 136-148.

BGMRXUAR (Bureau of Geology and Mineral Resources of Xinjiang Uygur Autonomous Region). (1993), Regional Geology of Xinjiang Uygyr Autonomous Region. *Geological Publishing House*, Beijing, 841 (in Chinese).

BGMRXUAR (Bureau of Geology and Mineral Resources of Xinjiang Uygur Autonomous Region). (2008), The research on the nationwide multifold stratigraphic division and correlation-the lithostratigraphy of Xinjiang Uygur Autonomous Region. *China University of Geosciences Press*, Wuhan, 1-112 (in Chinese).

BGMRXUAR (Bureau of Geology and Mineral Resources of Xinjiang Uygur Autonomous Region). (1978), The report of regional geological survey at scale 1:200000 in Shichang area, P.R.C.. *China Industry Press*, 1-56 (in Chinese).

BGMRXUAR (Bureau of Geology and Mineral Resources of Xinjiang Uygur Autonomous Region). (1993), Regional Geology of Xinjiang Uygur Autonomous Region. *Geological Publishing House*, Beijing. 841pp (in Chinese).

BGMRXUAR (Bureau of Geology and Mineral Resources of Xinjiang Uygur Autonomous Region). (1978), The report of regional geological survey at scale 1:200000 in Shichang area, P.R.C. *China Industry Press*, Beijing. pp. 1-56 (in Chinese).

Biske, J.S. and Seltmann, R. (2010), Paleozoic Tian Shan as a transitional region between the Rheic and Urals-Turkestan oceans. *Gondwana Research*, 17, 602-613.

Biske, J.S., Seltmann, R. (2010), Paleozoic Tian Shan as a transitional region between the Rheic and Urals-Turkestan oceans. *Gondwana Research*, 17, 602-613.

Black, L.P., Kamo, S.L., Allen, C.M., Aleinikoff, J.N., Davis, D.W., Korsch, R.J. and Foudoulis, C. (2003), TEMORA 1: a new zircon standard for Phanerozoic U-Pb geochronology. *Chemical Geology*, 200 (1-2), 155-170.

Black, L.P., Kamo, S.L., Allen, C.M., Aleinikoff, J.N., Davis, D.W., Korsch, R.J., Foudoulis, C. (2003), TEMORA 1: a new zircon standard for Phanerozoic U-Pb geochronology. *Chemical Geology*, 200 (1-2), 155-170.

Bosboom, R.E., Dupont-Nivet, G., Grothe, A., Brinkhuis, H., Villa, G., Mandic, O., Stoica, M., Huang, W., Yang, W., Guo, Z.J., Krijgsman, W. (2014), Linking Tarim Basin sea retreat (west China) and Asian aridification in the late Eocene. *Basin research*, doi: org/10.1111/bre.12054.

Bosboom, R.E., Dupont-Nivet, G., Grothe, A., Brinkhuis, H., Villa, G., Mandic, O., Stoica, M., Kouwenhoven, T., Huang, W. and Guo, Z. (accepted),

Palaeogeography of the late Eocene stepwise sea retreat from the Tarim Basin (west China). *Palaeogeography, Palaeoclimatology, Palaeoecology*.

Bosboom, R.E., Dupont-Nivet Guillaume, Houben, A.J.P., Brinkhuis, H., Villa, G., Mandic, O., Stoica, M., Zachariasse, W.J., Guo, Z.J., Li, C.X., Krijgsman, W. (2011), Late Eocene sea retreat from the Tarim Basin (west China) and concomitant Asian paleoenvironmental change. *Palaeogeography, Palaeoclimatology, Palaeoecology*, 299, 317-331.

Bosboom, R.E., Dupont-Nivet Guillaume, Huang, W., Yang, W., Guo, Z.J. (2014), Oligocene clockwise rotations along the eastern Pamir: tectonic and paleogeographic implications. *Tectonics*, 2013TC003388.

Brookfield, M.E. (2000), Geological development and Phanerozoic crustal accretion in the western segment of the southern Tien Shan (Kyrgyzstan, Uzbekistan and Tajikistan). *Tectonophysics*, 328, 1-14.

Bruguier, O., Lancelot, J.R., Malavieille, J. (1997), U-Pb dating on single detrital zircon grains from the Triassic Songpan-Ganze flysch (Central China): provenance and tectonic correlations. *Earth and Planetary Science Letters*, 152, 217-231.

Burbank, D.W. and Anderson, R.S. (2001), Tectonic Geomorphology, *Blackwell Science*, USA, 26-33.

BurchfieL, B.C. and Royden, L.H. (1991), Tectonics of Asia 50 years after the death of Emile Argand. *Eclogae Geologicae Helvetiae*, 84, 599-629.

Burchfiel, B.C., Brown, E.T., Deng, Q.D., Feng, X.Y., LI, J., Monlar, P., Shi, J.B., Wu, Z.M. and You, H.C. (1999), Crustal shortening on the margins of the Tien Shan, Xinjiang, China. *International Geology Review*, 41, 665-700.

Burchfiel, B.C., Brown, E.T., Deng, Q.D., Feng, X.Y., Li, J., Monlar, P., Shi, J.B., Wu, Z.M., You, H.C. (1999), Crustal shortening on the margins of the Tien Shan, Xinjiang, China. *International Geology Review*, 41, 665-700.

Burchfiel, B.C., Royden, L.H. (1991), Tectonics of Asia 50 years after the death of Emile Argand. *Eclogae Geologicae Helvetiae*, 84, 599-629.

Burtman, V.S. (2008), Nappes of the southern Tien Shan. *Russian Journal of Earth Sciences*, 10 (1), 1-35. doi:10.2205/2007ES000223, 2008.

Burtman, V.S., Molnar, P. (1993), Geological and geophysical evidence for deep subduction of continental crust beneath the Pamir. *Geological Society of America*, Special Paper, 281.

Burtman, V.S., Skobelev, S.F., Molnar, P. (1996), Late Cenozoic slip on the Talas-Ferghana Fault, the Tien Shan, central Asia. *Geological Society of American Bulletin*, 108, 1004-1021.

Buslov, M.M., De Grave, J. and Bataleva, E.A.V. (2004), Cenozoic tectonics and geodynamic evolution of the Tien Shan mountain belt. *Himalayan Journal of Scienes*, 2, 106-107.

Buslov, M.M., De Grave, J., Bataleva, E.A.V. and Batalev, V.Y. (2007), Cenozoic tectonic and geodynamic evolution of the Kyrgyz Tien Shan Mountains: A review of geological, thermochronological and geophysical data. *Journal of Asian Earth Sciences*, **29**, 205-214.

Buslov, M.M., De Grave, J., Bataleva, E.A.V. (2004), Cenozoic tectonics and geodynamic evolution of the Tien Shan mountain belt. *Himalayan Journal of Sciences*, 2, 106-107.

Buslov, M.M., De Grave, J., Bataleva, E.A.V., Batalev, V.Y. (2007), Cenozoic tectonic and geodynamic evolution of the Kyrgyz Tien Shan Mountains: A review of geological, thermochronological and geophysical data. *Journal of Asian Earth Sciences*, 29, 205-214.

Cai, Z.X., Chen, F.J. and Jia, Z.Y. (2000), Types and tectonic evolution of Junggar Basin. *Frontiers of Earth Science*, **7** (4), 431-440.

Cao, K., Wang, G.C., Liu, C., Meng, Y.N. (2009), Thermochronological evidence of the Cenozoic differential uplift process of the West Kunlun and its adjacent area.

Earth Science – Journal of China University of Geosciences, 34 (6), 895-906 (in Chinese with English abstract).

Carroll, A.R., Brassell, S.C. and Graham, S.A. (1992), Upper Permian lacustrine oil shales, southern Junggar basin, NW China. *American Association of Petroleum Geologists*, 76, 1874-1902.

Carroll, A.R., Brassell, S.C., Graham, S.A. (1992), Upper Permian lacustrine oil shales, southern Junggar basin, NW China. *American Association of Petroleum Geologists Bulletin*, 76, 1874-1902.

Carroll, A.R., Graham, S.A., Hendrix, M.S., Ying, D. and Zhou, D. (1995), Late Paleozoic tectonic amalgamation of northwestern China: Sedimentary record of the northern Tarim, northwestern Turpan, and southern Junggar Basins. *Geological Society of America Bulletin*, 107, 571-594.

Carroll, A.R., Graham, S.A., Hendrix, M.S., Ying, D., Zhou, D. (1995), Late Paleozoic tectonic amalgamation of northwestern China: Sedimentary record of the northern Tarim, northwestern Turpan, and southern Junggar Basins. *Geological Society of America Bulletin*, 107, 571-594.

Carroll, A.R., Liang, Y., Graham, S.A., Xiao, X., Hendrix, M.S., Chu, J.C. and Mcknight, C.L. (1990), Junggar Basin, northwest China: Trapped late Paleozoic ocean. *Tectonophysics*, 181, 1-14.

Carroll, A.R., Liang, Y., Graham, S.A., Xiao, X., Hendrix, M.S., Chu, J.C., Mcknight, C.L. (1990), Junggar Basin, northwest China: Trapped late Paleozoic ocean. *Tectonophysics*, 181, 1-14.

Charreau, J., Avouac, J.P., Chen Y., Dominguez, S. and Gilder, S. (2008), Miocene to present kinematics of fault-bend folding across the Huerguosi anticline, northern Tianshan (China), derived from structural, seismic, and magnetostratigraphic data. *Geology*, 36 (11), 871-874.

Charreau, J., Chen, Y., Gilder, S., Barrier, L., Dominguez, S., Augier, R., Sen, S., Avouac, J.P., Gallaud, A., Graveleau, F. and WANG, Q. (2009a), Neogene uplift

of the Tian Shan Mountains observed in the magnetic record of the Jingou River section (northwest China). *Tectonics*, 28 (2), doi: 10.1029/2007TC002137.

Charreau, J., Gumiaux, C., Avouac, J.P., Augier, R., Chen, Y., Barrier, L., Gilder, S., Dominguez, S., Charles, N. and Wang, Q.C. (2009b), The Neogene Xiyu Formation, a diachronous prograding gravel wedge at front of the Tianshan: Climatic and tectonic implications. *Earth Planetary Science Letters*, 287 (3-4), 298-310.

Charreau, J., Gumiaux, C., Avouac, J-P., Augier, R., Chen, Y., Barrier, L., Gilder, S., Dominguez, S., Charles, N., Wang, Q.C. (2009), The Neogene Xiyu Formation, a diachronous prograding gravel wedge at front of the Tianshan: Climatic and tectonic implications. *Earth and Planetary Science Letters*, 287 (3-4), 298-310.

Charvet, J., Laurent-Charvet, S. and Shu, L.S. (2004) Paleozoic geodynamic evolution of Tianshan orogenic belt (NW China): Welding of Tarim and Junggar continental blocks. In: *Symposium G05-09 Tethys Reconstruction*, Abstract, 155.

Charvet, J., Laurent-Charvet, S., Shu, L.S. (2004), Paleozoic geodynamic evolution of Tianshan orogenic belt (NW China): Welding of Tarim and Junggar continental blocks. In: *Symposium G05-09 Tethys Reconstruction*, Abstract 155.

Charvet, J., Shu, L.S. and Laurent-Charvet, S. (2007), Paleozoic structural and geodynamic evolution of eastern Tianshan (NW China): welding of the Tarim and Junggar plates. *Episodes*, 30, 162-186.

Charvet, J., Shu, L.S., Laurent-Charvet, S. (2007), Paleozoic structural and geodynamic evolution of eastern Tianshan (NW China): welding of the Tarim and Junggar plates. *Episodes*, 30, 162-186.

Charvet, J., Shu, L.S., Laurent-Charvet, S., Wang, B., Michel, F., Dominique, C., Chen, Y. and Koen, D.J. (2011), Palaeozoic tectonic evolution of the Tianshan belt, NW China. *Science China Earth Sciences*, 54 (2), 166-184.

Charvet, J., Shu, L.S., Laurent-Charvet, S., Wang, B., Michel, F., Dominique, C., Chen, Y., Koeno, D.J. (2011), Paleozoic tectonic evolution of the Tianshan belt, NW China. *Science China Earth Sciences*, 54 (2), 166-184.

Chemenda, A.I., Burg, J-P., Mattauer, M. (2000), Evolution model of the Himalaya-Tibet system: geopoem based on new modeling, geological and geophysical data. *Earth and Planetary Science Letters*, 174, 397-409.

Chen, C., Lu, H., Jia, D., Cai, D. and Wu, S. (1999), Closing history of the southern Tianshan oceanic basin, western China: an oblique collisional orogeny. *Tectonophysics*, 302, 23-40.

Chen, C.M., Lu, H.F., Jia, D., Cai, D.S., Wu, S. (1999), Closing history of the southern Tianshan oceanic basin, Western China: an oblique collisional orogeny. *Tectonophysics*, 302, 23-40.

Chen, D.C., Zhao, S.M. and Deng, J. (2010a), U-Pb dating of the Carboniferous sandstone detrital zircon from the north of the Bogda Mountains, Eastern Xinjiang, and its geological significances. *Acta Geologica Sinica*, 84 (12), 1770-1780.

Chen, F.J., Wang, X.W. and Wang, X.W. (2005), Prototype tectonic evolution of Junggar Basin, Northwestern China. *Frontiers of Earth Science*, 12 (3), 77-89 (in Chinese with English abstract).

Chen, J., Burbank, D.W., Scharer, K.M., Sobel, E., Yin, J.H., Rubin, C., Zhao, R.B. (2002), Magnetochronology of the Upper Cenozoic strata in the Southwestern Chinese Tian Shan: rates of Pleistocene folding and thrusting. *Earth and Planetary Science Letters*, 195, 113-130.

Chen, J.F., Han, B.F., Ji, J.Q., Zhang, L., Xu, Z., He, G.Q. and Wang, T. (2010b), Zircon U-Pb ages and tectonic implications of Paleozoic plutons in northern West Junggar, North Xinjiang, China. *Lithos*, 115, 137-152.

Chen, K., Gumiaux, C., Augier, R., Chen, Y., Wang, Q.C., Lin, W. and Wang, S.L. (2011), The Mesozoic palaeorelief of the northern Tian Shan (China). *Terra Nova*, 23, 195-205.

Chen, S.P., Zhang, Y.W., Tang, L.J. and Bai, G.P. (2001), Tectonic evolution of the Junggar Basin in the Late Carboniferous-Permian. *Acta Geologica Sinica*, 75 (4), 398-408.

Chen, X., Lu, H.F., Shu, L.S., Wang, H.M. and Zhang, G.Q. (2002), Study on tectonic evolution of Junggar Basin. *Geological Journal China University*, 8 (3), 257-266 (in Chinese with English abstract).

Chen, Y.B., Hu, A.Q., Zhang, G.X., Zhang, .Q.F. (2000), Zircon U-Pb age of granitic gneiss on Duku highway in western Tianshan of China and its geological implications. *Chinese Science Bulletin*, 45, 649-653.

Coleman, R.G. (1989), Continental growth of northwest China. *Tectonics*, 8 (3), 621-635.

Coleman, R.G. (1989), Continental growth of northwest China. *Tectonics*, 8 (3), 621-635.

Corfu, F., Hanchar, J.M., Hoskin, P.W. and Kinny, P. (2003), Atlas of zircon textures. *Reviews in Mineralogy Geochemistry*, 53, 468-500.

Coutand, I., Strecker, M.R., Arrowsmith, J.R., Hilley, G., Thiede, R.C., Korjenkov, A., Omuraliev, M. (2002), Late Cenozoic tectonic development of the intramontane Alai Valley, (Pamie-Tien Shan region, central Asia): An example of intracontinental deformation due to the Indo-Eurasia collision. *Tectonics*, 21 (6), 1053. doi:10.1029/2002TC001358, 2002.

Cowgill, E. (2010), Cenozoic right-slip faulting along the eastern margin of the Pamir salient, northwestern China. *Geological Society of American Bulletin*, 122 (1-2), 145-161.

Cui, J.W., Guo, X.P., Ding, X.Z., Li, P.W., Zhang, X.W. (2006), Mesozoic-Cenozoic defoemtion structures and their dynamics in the basin-range junction belt of the

west Kunlun-Tarim basin. *Frontiers of Earth Science*, 13 (4), 103-118 (in Chinese with English abstract).

Daly, J.S., Balagansky, V.V., Timmerman, M.J., Whitehouse, M.J., de Jong, K., Guise, P.G., Bogdanova, S., Gorbatchey, R., Bridgwater, D. (2001), Ion microprobe U-Pb zircon geochronology and isotopic evidence for a transcrustal suture zone in the Lapland-Kola Orogen, Northern Fennnoscandian Shield. *Precambrian Research*, 105, 289-314. doi: 10.1016/S0301-9268(00)00116-9.

De Grave, J., Buslov, M.M. and Van Den Haute, P. (2004), Intracontinental deformation in central Asia: distant effects of India-Eurasia convergence revealed by apatite fission-track thermochronology. *Himalayan Journal of Sciences*, 2, 121-122.

De Grave, J., Buslov, M.M. and Van Den Haute, P. (2007), Distant effects of India-Eurasia convergence and Mesozoic intracontinental deformation in central Asia: constraints from apatite fission-track thermochronology. *Journal of Asian Earth Sciences*, 29, 188-204.

De Grave, J., Buslov, M.M., Van Den Haute, P. (2007), Distant effects of India-Eurasia convergence and Mesozoic intracontinental deformation in central Asia: constraints from apatite fission-track thermochronology. *Journal of Asian Earth Sciences*, 29, 188-204.

De Grave, J., Glorie, S., Ryabinin, A., Zhimulev, F., Buslov, M.M., Lzmer, A., Elburg, M., Vanhaecke, F., Van den haute, P. (2012), Late Paleozoic and Meso-Cenozoic tectonic evolution of the southern Kyrgyz Tien Shan: Constraints from multi-method thermochronology in the Trans-Alai, Turkestan-Alai segment and the southeastern Ferghana Basin. *Journal of Asian Earth Sciences*, 44, 149-168.

De Jong, K., Wang, B., Faure, M., Shu, L.S., Cluzel, D., Charvet, J., Ruffet, G. and Chen, Y. (2009), New $^{40}Ar/^{39}Ar$ age constraints on the late Tian Shan (Xinjiang, north-western China), with emphasis on Permian fluid ingress. *International Journal of Earth Sciences*, 98 (6), 1239-1258.

Deng, Q.D., Feng, X.Y., Zhang, P.Z., Xu, X.W., Yang, X.P., Peng, S.Z. and Li, J. (2000), Active tectonics of the Chinese Tianshan Mountains. *Seismological Press*, Beijing, 1-399 (in Chinese).

Deng, W.M. (1996), The Ophiolites of the Geotraversers from Yecheng to Shiquanhe. In: Pan, Y.S (Ed.), Geological Evolution of the Karakorum and Kunlun Mountains. *Seismological Press*, Beijing, 51-93.

Deng, X.L., Shu, L.S., Zhu, W.B., Ma, D.S., Wang, B. (2008), Precambrian tectonism, magmatism and geochronology of igneous rocks in the Xindi fault zone, Xinjiang. *Acta Petrologica Sinica*, 24 (11), 2800-2808.

Di Crescenzo, G. and Santo, A. (2005), Debris slides-rapid earth flows in the carbonate massifs of the Campania region (Southern Italy): morphological and morphometric data for evaluating triggering susceptibility. *Geomorphology*, 66, 255-276.

Ding, D.G., Wang, D.X., Liu, W.X., Sun, S.Q. (1996), The west Kunlun orogenic belts and basins. *Geological Publishing House*, Beijing, pp. 125-143 (in Chinese with English abstract).

Djenchuraeva, R.D., Borisov, F.I., Pak, N.T., Malyukova, N.N. (2008), Metallogeny and geodynamics of the Aktiuz-Boordu Mining District, Northern Tien Shan, Kyrgyzstan. *Journal of Asian Earth Sciences*, 32, 280-299.

Du, Z.L., Wang, Q.C. (2007a), Mesozoic and Cenozoic uplifting history of the Tianshan Region: Insight from apatite fission track. *Acta Geologica Sinica*, 81 (8), 1081-1101 (in Chinese with English abstract).

Du, Z.L., Wang, Q.C., Zhou, X.H. (2007b), Mesozoic and Cenozoic uplifting history of the Kuqa-South Tianshan Basin-Mountain System from the evidence of apatite fission track analysis. *Acta Petrologica et Mineralogica*, 26 (5), 399-408 (in Chinese with English abstract).

Dumitru, T.A., Zhou, D., Chang, E.Z. and Graham, S.A. (2001), Uplift, exhumation, and deformation in the Chinese Tian Shan. In: *Paleozoic and Mesozoic Tectonic*

evolution of Central Asia: From Continental Assembly to Intracontinental Deformation (Ed. by M.S. Hendrix and G.A. Davis, *Geological Society of America Memoirs*, 194, 71-99).

Dumitru, T.A., Zhou, D., Chang, E.Z., Graham, S.A. (2001), Uplift, exhumation, and deformation in the Chinese Tian Shan. In: Hendrix, M.S. and Davis, G.A. (Eds.), Paleozoic and Mesozoic Tectonic evolution of Central Asia: From Continental Assembly to Intracontinental Deformation. *Geological Society of American Memoir*, 194, 71-99.

Dupont-Nivet, G., Krijgsman, W. (2012), Magnetostratigraphic methods and applications. In: Busby, C., Azor, A. (Eds.), *Recent Advances in Tectonics of Sedimentary Basins*. Wiley-Blackwell, 80-94.

Fang, S.H., Guo, Z.J., Jia, C.Z., Zhang, Z.C., Wang, X.L. and Wang, M.N. (2006b), Meso-Cenozoic heavy minerals' assemblages in the southern Junggar Basin and its implications for basin-orogen pattern. *Chinese Journal of Geology*, 41 (4), 648-662 (in Chinese with English abstract).

Fang, S.H., Guo, Z.J., Jia, C.Z., Zhang, Z.C., Wang, X.L., Wang, M.N. (2006), Meso-Cenozoic heavy minerals' assemblages in the southern Junggar Basin and its implications for basin-orogen pattern. *Chinese Journal of Geology*, 41 (4), 648-662 (in Chinese with English abstract).

Fang, S.H., Guo, Z.J., Song, Y., Wu, C.D., Zhang, Z.C., Wang, M.N. and Fan, R.D. (2005), Sedimentary facies evolution and basin pattern of the Jurassic in southern margin area of Junggar Basin. *Journal of Palaeogeography*, **7** (3), 347-356 (in Chinese with English abstract).

Fang, S.H., Guo, Z.J., Song, Y., Wu, C.D., Zhang, Z.C., Wang, M.N., Fan, R.D. (2005), Sedimentary facies evolution and basin pattern of the Jurassic in southern margin area of Junggar Basin. *Journal of Palaeogeography*, 7 (3), 347 – 356 (in Chinese with English abstract).

Fang, S.H., Guo, Z.J., Wu, C.D., Zhang, Z.C., Wang, M.N. and Yuan, Q.D. (2006a), Jurassic clastic composition in the southern Junggar Basin, Northwest China:

implications for basin-range pattern and tectonic attributes. *Acta Geologica Sinica*, 80 (2), 196-209 (in Chinese with English abstract).

Fang, S.H., Guo, Z.J., Zhang, Z.C. and Wu, C.D. (2004), Discussion on Mesozoic-Cenozoic evolution of Tian Shan and its adjacent basins. *Acta Scientiarum Naturalium Universitatis Pekinensis*, 40 (6), 886-897 (in Chinese with English abstract).

Fang, S.H., Jia, C.Z., Song, Y., Guo, Z.J., Yuan, S.W. and Wang, X.L. (2007), Mesozoic-Cenozoic tectonic events and structural constraints in the southern Junggar Basin: evidence from detrital compositions. *Chinese Journal of Geology*, 42 (4), 753-765 (in Chinese with English abstract).

Fedo, C.M., Sircombe, K.N. and Rainbird, R.H. (2003), Detrital zircon analysis of the sedimentary record. *Reviews in Mineralogy and Geochemistry*, 53 (1), 277-303.

Fedo, C.M., Sircombe, K.N., Rainbird, R.H., 2003. Detrital zircon analysis of the sedimentary record. *Reviews in Mineralogy and Geochemistry*, 53 (1), 277-303.

Feng, Z.S., Zhang, Z.C., Li, J.F. and Guo, Z.J. (2010), Geochemistry and geological significance of the Cretaceous OIB-type mafic dykes in Sanweishan, Dunhuang, Gansu Province. *Acta Petrologica Sinica*, 26 (2), 607-616 (in Chinese with English abstract).

Fu B.H., Lin, A.M., Kano, K.I., Maruyama, T., Guo, J.M. (2003), Quaternary folding of the eastern Tian Shan, northwest China. *Tectonophysics*, 369, 79-101.

Fu, B.H., Ninomiya, Y., Guo, J.M. (2010), Slip partitioning in the northeast Pamir-Tian Shan convergence zone. *Tectonophysics*, 483, 344-364.

Gao, J., Klemd, R., Qian, Q., Zhang, X., Li, J.L., Jiang, T. and Yang, Y.Q. (2011), The collision between the Yili and Tarim blocks of the Southwestern Altaids: Geochemical and age constraints of a leucogranite dike crosscutting the HP-LT metamorphic belt in the Chinese Tianshan Orogen. *Tectonophysics*, 499, 118-131.

Gao, J., Klemd, R., Qian, Q., Zhang, X., Li, J.L., Jiang, T., Yang, Y.Q. (2011), The collision between the Yili and Tarim blocks of the Southwestern Altaids: geochemical and age constraints of a leucogranite dike crosscutting the HP-LT metamorphic belt in the Chinese Tianshan Orogen. *Tectonophysics*, 499, 118-131.

Gao, J., Li, M.S., Xiao, X.C., Tang, Y.Q. and He, G.Q. (1998), Paleozoic tectonic evolution of the Tianshan orogen, northwestern China. *Tectonophysics*, 287, 213-231.

Gao, J., Li, M.S., Xiao, X.C., Tang, Y.Q., He, G.Q. (1998)， Paleozoic tectonic evolution of the Tianshan orogen, northwestern China. *Tectonophysics*, 287, 213-231.

Gao, J., Long, L.L., Klemd, R., Qian, Q., Liu, D.Y., Xiong, X.M., Su, W., Liu, W., Wang, Y.T. and Yang, F.Q. (2009)， Tectonic evolution of the southern Tian Shan orogen and adjacent regions, NW China: geochemical and age constraints of granitoid rocks. *International Journal of Earth Sciences*, 98 (6), 1221-1238.

Gao, J., Long, L.L., Klemd, R., Qian, Q., Liu, D.Y., Xiong, X.M., Su, W., Liu, W., Wang, Y.T., Yang, F.Q. (2009), Tectonic evolution of the South Tian Shan orogeny and adjacent regions, NW China: geochemical and age constrains of granitoid rocks. *International Journal of Earth Sciences*, 98, 1221-1238.

Gao, Z.J., Chen, K.Q., Wei, J.Y. (2000), The Lithostratigraphic Dictionary of China. *The Press of Geological University*, Beijing, pp. 627 (in Chinese).

Garzione, C., Ikari, M.J., Basu, A.R. (2005), Source of Oligocene to Pliocene sedimentary rocks in the Linxia basin in northeastern Tibet from Nd isotopes: implications for tectonic forcing of climate. *Geological Society of American Bulletin*, 117 (9), 1156-1166.

Ge, Y.F., Zhu, W.B., Wu, H.L., He, J.W., Zheng, B.H. (2013a), Timing and mechanisms of multiple episodes of migmatization in the Korla Complex, northern Tarim Craton, NW China: Constraints from zircon U-Pb-Lu-Hf isotopes and implications for crustal growth. *Precambrian Research*, 231, 136-156.

Ge, Y.F., Zhu, W.B., Wu, H.L., He, J.W., Zheng, B.H. (2013b), Zircon U-Pb ages and Lu-Hf isotopes of Paleoproterozoic metasedimentary rocks in the Korla Complex, NW China: Implications for metamorphic zircon formation and geological evolution of the Tarim Craton. *Precambrian Research*, 231, 1-18.

Ge, Y.F., Zhu, W.B., Zheng, B.H., Wu, H.L., He, J.W., Zhu, X.Q. (2012), Early Pan-African magmatism in the Tarim Craton: Insights from zircon U-Pb-Lu-Hf isotope and geochemistry of granitoids in the Korla Area, NW China. *Precambrian Research*, 212-213, 117-138.

Gehrels, G.E., Dickinson, W.R. (1995), Detrital xircon provenance of Cambrian to Triassic miogeoclinal and eugeoclinal strata in Nevada. *American Journal of Science*, 295, 18-48.

Gehrels, G.E., Yin, A. and Wang, X.F. (2003), Detrital-zircon geochronology of the northeastern Tibetan plateau. *Geological Society America Bulletin*, 115 (7), 881-896.

Gehrels, G.E., Yin, A., Wang, X.F. (2003), Detrital-zircon geochronology of the northeastern Tibetan plateau. *Geological Society America Bulletin*, 115 (7), 881-896.

Glorie, S., De Grave, J., Buslov, M.M., Elburg, M.A., Stockli, D.F., Gerdes, A. and Haute, P.V. (2010), Multi-method chronometric constraints on the evolution of the northern Kyrgyz Tien Shan batholiths (Central Asian Orogenic Belt): From emplacement to exhumation. *Journal of Asian Earth Sciences*, 38, 131-146.

Glorie, S., De Grave, J., Buslov, M.M., Elburg, M.A., Stockli, D.F., Gerdes, A., Haute, P.V. (2010), Multi-method chronometric constraints on the evolution of the northern Kyrgyz Tien Shan batholiths (Central Asian Orogenic Belt): From emplacement to exhumation. *Journal of Asian Earth Sciences*, 38, 131-146.

Gou, L.L., Zhang, L.F., Tao, R.B., Du, J.X. (2012), Ageochemical study of syn-subduction and post-collisional granitoids at Muzhaerte River in the Southwest Tianshan UHP belt, NW China. *Lithos*, 136-139, 201-224.

Graham, S.A., Hendrix M.S., Wang, L.B. and Carroll, A.R. (1993), Collision successor basin of western China: impact of tectonic inheritance on sand composition. *Geological Society America Bulletin*, 10**5**, 323-344.

Graham, S.A., Page Chamberlain, C., Yue, Y.J., Ritts, B., Hanson, A.D., Horton, T.W., Waldbauer, J.R., Poage, M.A., Feng, X. (2005), Stable isotope records of Cenozoic climate and topography, Tibetan plateau and Tarim basin. *American Journal of Science*, 305 (2), 101-118.

Green, P. F. (1985), A comparison of zeta calibration baselines in zircon, sphene and apatite, *Chemical Geology*, 58, 1 – 22, doi:10.1016/0009-2541(85)90175-5.

Green, P. F. (1985), A comparison of zeta calibration baselines in zircon, sphene and apatite, *Chemical Geology*, 58, 1 – 22, doi:10.1016/0009-2541(85)90175-5.

Greene, T.J., Carroll, A.R., Wartes, M., Graham, S.A. and Wooden, J.L. (2005), Integrated provenance analysis of a complex orogenic terrane: Mesozoic uplift of the Bogda Shan and inception of the Turpan-Hami Basin, NW China. *Journal of Sedimentary Research*, 75 (2), 251-267.

Greene, T.J., Carroll, A.R., Wartes, M., Graham, S.A., Wooden, J.L. (2005), Integrated provenance analysis of a complex orogenic terrane: Mesozoic uplift of the Bogda Shan and inception of the Turpan-Hami Basin, NW China. *Journal of Sedimentary Research*, 75 (2), 251-267.

Gu, J.Y. (1996), Characteristics of sequence stratigraphy and sedimentary evolution of Tarim Basin, Northwest China. *Petroleum Industry Press*, Beijing, 8-9, 206-225 (in Chinese).

Guo, L.Z., Zhu, W.B., Ma, R.S., Sun, Y. and Wang, F. (2003), Discussion on the structural coupling. *Geotectonica Et Metallogenia*, 27 (3), 197-205 (in Chinese with English abstract).

Guo, Z.J., Han, B.F., Zhang, Y.Y. and Chen, S. (2010), Mesozoic and Cenozoic crust-mantle interaction in the Central Asian Orogenic Belt: A comparative study of

mantle-derived magmatic rocks in northern Xinjiang. *Acta Petrologica Sinica*, 26 (2), 431-439 (in Chinese with English abstract).

Guo, Z.J., Wu, C.D., Zhang, Z.C., Wang, M.N. and Fang, S.H. (2005), Mesozoic-Cenozoic relationships between Tianshan Mountain and peripheral basins: evidence from sedimentary and exhumation of Jurassic in Houxia area, Urumchi. *Geological Journal China Universities*, 11 (4), 558-567 (in Chinese with English abstract).

Guo, Z.J., Yin, A., Robinson, A., Jia, C.Z. (2005), Geochronology and geochemistry of deep-drill-core samples from the basement of the central Tarim basin. *Journal of Asian Earth Sciences*, 25, 45–56.

Guo, Z.J., Zhang, Z.C. (2003), Strata sequence and rock assemblages of the early Precambrian basemen in the Tarim Craton: new evidences of zircon U–Pb ages. *Acta Petrologica Sinica*, 19 (3), 537–542.

Guo, Z.J., Zhang, Z.C., Wu, C.D., Fang, S.H. and Zhang, R. (2006), The Mesozoic and Cenozoic exhumation history of Tianshan and comparative studies to the Junggar and Altai Mountains. *Acta Geologica Sinica*, 80 (1), 1-15 (in Chinese with English abstract).

Guo, Z.J., Zhang, Z.C., Wu, C.D., Fang, S.H., Zhang, R. (2006), The Mesozoic and Cenozoic exhumation history of Tianshan and comparative studies to the Junggar and Altai Mountains. *Acta Geologica Sinica*, 80 (1), 1-15.

Han, B.F., Guo, Z.J., Zhang, Z.C., Zheng, L., Chen, J.F. and Song, B. (2010), Age, geochemistry, and tectonic implications of a late Paleozoic stitching pluton in the North Tian Shan suture zone, western China. *Geological Society of America Bulletin*, 122, 627-640.

Han, B.F., Guo, Z.J., Zhang, Z.C., Zheng, L., Chen, J.F., Song, B. (2010), Age, geochemistry, and tectonic implications of a late Paleozoic stitching pluton in the North Tian Shan suture zone, western China. *Geological Society of America Bulletin*, 122, 627-640.

Han, B.F., He, G.Q. and Wang, S.G. (1999), Postcollisional mantle-derived magmatism, underplating and implications for basement of the Junggar Basin. *Science in China (Series D)*, 42 (2), 113-119.

Han, B.F., He, G.Q., Wang, S.G. (1999), Postcollisional mantle-derived magmatism, underplating and implications for basement of the Junggar Basin. *Science in China (Series D)*, 42 (2), 113-119.

Han, B.F., He, G.Q., Wang, X.C., Guo, Z.J. (2011), Late Carboniferous collision between the Tarim and Kazakhstan-Yili terranes in the western segment of the South Tian Shan Orogen, Central Asia, and implications for the Northern Xinjiang, western China. *Earth-Science Reviews*, 109 (3-4), 74-93.

Han, B.F., He, G.Q., Wu, T.R. and Li, H.M. (2004), Zircon U-Pb dating and geochemical features of early Paleozoic granites from Tianshan, Xinjiang: implications for tectonic evolution. *Xinjiang Geology*, 22 (1), 3-11 (in Chinese with English abstract).

Han, B.F., Wang, S.G., Jahn, B.M., Hong, D.W., Kagami, H. and Sun, Y.L. (1997), Depleted-mantle source for the Ulungur River A-type granites from North Xinjiang, China: geochemistry and Nd-Sr isotope evidence, and implications for Phanerozoic crustal growth. *Chemical Geology*, 138, 135-159.

Han, B.F., Wang, S.G., Jahn, B.M., Hong, D.W., Kagami, H., Sun, Y.L. (1997), Depleted-mantle source for the Ulungur River A-type granites from North Xinjiang, China: geochemistry and Nd-Sr isotope evidence, and implications for Phanerozoic crustal growth. *Chemical Geology*, 138, 135-159.

Hanchar, J.M. and Rundnick, R.L. (1995), Revealing hidden structures: The application of cathodoluminescence and back-scattered electron imaging to dating zircons from lower crustal xenoliths. *Lithos*, 36, 289-303.

He, D.F., Chen, X.F., Zhang, Y.J., Kuang J., Shi, X. and Zhang, L.P. (2004), Enrichment characteristics of oil and gas in Jungagr basin. *Acta Petrologica Sinica*, 25 (3), 1-10 (in Chinese with English abstract).

He, Z.Y., Zhang, Z.M., Zhong, K.Q., Wang, W., Santosh, M. (2012), Neoproterozoic granulites from the northeastern margin of the Tarim Craton: Petrology, zircon U-Pb ages and implications for the Rodinia assembly. *Precambrian Research* 212-213, 21-33.

Heermance, R. V., Chen, J., Burbank, D. W., Miao, J. (2008), Temporal constraints and pulsed Late Cenozoic deformation during the structural disruption of the active Kashi foreland, northwest China. *Tectonics*, 27, doi:10.1029/2007TC002226.

Heermance, R. V., Chen, J., Burbank, D. W., Wang, C.S. (2007), Chronology and tectonic controls of Late Tertiary deposition in the southwestern Tian Shan foreland, NW China. *Basin Research*, 19, 599-632. doi: 10.1111/j.1365-2117.2007.00339.x.

Hegner, E., Klemd, R., Kröner, A., Corsini, M., Alexeiev, D.V., Iaccheri, L.M., Zack, T., Dulski, P., Xia, X., Windley, B.F. (2010), Mineral ages and P-T conditions of Late Paelozoic high-pressure eclogite and provenance of m dange sediments from Atbashi in the South Tianshan Orogen of Kyrgyzstan. *American Journal of Science*, 310, 916-950.

Hendrix, M.S. (2000), Evolution of Mesozoic sandstone compositions, southern Junggar, northern Tarim, and western Turpan basins, Northwest China: a detrital record of the ancestral Tian Shan. *Journal of Sedimentary Research*, 70 (3), 520-532.

Hendrix, M.S. (2000), Evolution of Mesozoic sandstone compositions, southern Junggar, northern Tarim, and western Turpan basins, Northwest China: a detrital record of the ancestral Tian Shan. *Journal of Sedimentary Research*, 70 (3), 520 – 532.

Hendrix, M.S., Graham, S.A., CARROLL, A.R., SOBER, E.R., Mcknight, C.L., Shulein, B.J. and Wang, Z.X. (1992), Sedimentary record and climatic implications of recurrent deformation of the Tien Shan: evidence from Mesozoic

strata of the North Tarim, South Junggar and Turpan basins. *Geological Society of America Bulletin*, 104, 53-79.

Hendrix, M.S., Graham, S.A., Carroll, A.R., Sober, E.R., Mcknight, C.L., Shulein, B.J., and Wang, Z.X. (1992), Sedimentary record and climatic implications of recurrent deformation of the Tien Shan: evidence from Mesozoic strata of the North Tarim, South Junggar and Turpan basins. *Geological Society of America Bulletin*, 104, 53-79.

Hoffman, P.F. (1991), Did the breakout of Laurentia turn Gondwanaland inside out? *Science*, 252, 1409-1412.

Hoskin, P.W.O. and Black, L.P. (2000), Metamorphic zircon formation by solid-state recrystallization of protolith igneous zircons. *Journal of Metamorphic Geology*, 18, 423-439.

Hu, A.Q., Jahn, B.M., Zhang, G.X., Chen, Y.B., Zhang, Q.F. (2000), Crustal evolution and Phanerozoic crustal growth in northern Xinjiang: Nd isotopic evidence. Part Ⅰ. Isotopic characterization of basement rocks. *Tectonophysics*, 328, 15-51.

Hu, A.Q., Wang, Z.G., Tu, G.Z. (1997), Geological evolution and diagenic and metallogenetic regularity in Northern Xinjiang. *Science Press*, Beijing, pp. 9-105 (in Chinese).

Hu, A.Q., Wei, G.J., Jiang, B.M., Zhang, J.B., Deng, W.F. and Chen, L.L. (2010), Formation of the 0.9 Ga Neoproterozoic granitoids in the Tianshan Orogen, NW China: constraints from the SHRIMP zircon age determination and its tectonic significance. *Geochemica*, 39 (3), 197-212 (in Chinese with English abstract).

Hu, A.Q., Zhang, J.B., Zhang, Z.G., Zhao, D.J., Liu, J.Y., Yang, S.Z., Peng, J.H., Zhou, W. (1986), U-Pb age and evolution of Precambrian metamorphic rocks of Middle Tianshan uplift zone eastern Tianshan, China. *Geochemica*, 1, 23-35 (in Chinese with English abstract).

Huang, B., Piper, J.D.A., Peng, S., Liu, T., Li, Z., Wang, Q., Zhu, R, (2006). Magnetostratigraphic study of the Kuche depression, Tarim Basin, and Cenozoic uplift of the Tian Shan Range, Western China. *Earth and Planetary Science Letters*, 251, 346-364.

Huang, H., Zhang, Z.C., Kusky, T., Zhang, D.Y., Hou, T., Liu, J.L., Zhao, Z.D. (2012), Geochronology and geochemistry of the Chuanwulu complex in the South Tianshan, western Xinjiang, NW China: Implications for petrogenesis and Phanerozoic continental growth. *Lithos*, 140-141, 66-85.

Huang, J.Q., Ren, J.S., Jiang, C.F., Zhang, Z.K. and Qin, D.Y. (1980), *Geotectonic evolution of China*. *China Science Press*, Beijing, 1-124 (in Chinese).

Huang, J.Q., Ren, J.S., Jiang, C.F., Zhang, Z.K., Qin, D.Y. (1980), Geotectonic evolution of China. *China Science Press*, Beijing, pp. 1-124 (in Chinese).

Hurford, A. J. (1990), Standardization of fission track dating calibration: Recommendation by the Fission Track Working Group of the I.U.G.S. Subcommission on Geochronology. *Chemical Geology*, 80, 171 – 178.

Hurford, A. J. (1990), Standardization of fission track dating calibration: Recommendation by the Fission Track Working Group of the I.U.G.S. Subcommission on Geochronology. *Chemical Geology*, 80, 171 – 178.

Hurford, A. J., Green P. F. (1983), The zeta age calibration of fission-track dating. *Chemical Geology*, 41, 285 – 317. doi:10.1016/S0009-2541(83)80026-6.

Hurford, A. J., Green P. F. (1983), The zeta age calibration of fission-track dating. *Chemical Geology*, 41, 285 – 317. doi:10.1016/S0009-2541(83)80026-6.

Hurford, A.J., Fitch, F.J., Clarke, A. (1984), Resolution of the age structure of the detrital zircon populations of two Lower Cretaceous sandstones from the Weald of England by fission track dating. *Geological Magazine*, 121, 269–277.

Ireland, T., Flöttmann, T., Fanning, C., Gibson, G., Preiss, W. (1998), Development of the early Paleozoic Pacific margin of Gondwana from detrital-zircon ages across the Delamerian orogeny. *Geology*, 26 (3), 243.

Jahn, B.M. (2004), Phanerozoic continental growth in Central Asia. *Journal of Asian Earth Sciences*, 23, 599-603.

Jahn, B.M., Wu, F.Y. and Chen, B. (2000a), Granitoids of the Central Asian Orogenic Belt and continental growth in the Phanerozoic. *Geological Society of America*, 91, 181-193.

Jahn, B.M., Wu, F.Y. and Chen, B. (2000b), Massive granitoid generation in Central Asia: Nd isotope evidence and implication for continental growth in the Phanerozoic. *Episodes*, 23, 82-92.

Ji, J.Q., Han, B.F., Zhu, M.F., Chu, Z.Y. and Liu, Y.L. (2006), Cretaceous-Paleogene alkaline magmatism in Tuyon basin, southwest Tianshan mountains: geochronology, petrology and geochemistry. *Acta Petrologica Sinica*, 22 (5), 1324-1340 (in Chinese with English abstract).

Jin, X., Wang, J., Chen, B., Ren, L. (2003), Cenozoic depositional sequences in the piedmont of the West Kunlun and their paleogeographic and tectonic implications. *Journal of Asian Earth Sciences*, 21, 755-765.

Jia, C.Z., Chen, H.L., Yang, S.F., Lu, H.F., Zhou, Y.Z. (2003), Late Cretaceous uplifting process and its geological response in Kuqa depression. *Acta Petrolei Sinica*, 24 (3), 1-5 (in Chinese with English abstract).

Jia, C.Z., Wei, G.Q., Li, B.L., Xiao, A.C. and Ran, Q.G. (2003), Tectonic evolution of two epochs foreland basin and its control for natural gas accumulation in Middle-Western China. *Acta Petrological Sinica*, 24 (2), 13-27 (in Chinese with English abstract).

Jia, C.Z., Zhang, S.B., Wu, S.Z. (2004), Stratigraphy of the Tarim Basin and Adjacent Areas. *Science Press*, Beijing. 1063pp (in Chinese).

Jiang, T., Gao, J., Klemd, R., Qian, Q., Zhang, X., Xiong, X.M., Wang, X.S., Tan, Z., Chen, B.X. (2014), Paleozoic ophiolitic mélanges from the South Tianshan Orogen, NW China: Geological, geochemical and geochronological implications for the geodynamic setting. *Tectonophysics*, 612-613, 106-127.

Jolivet, M., Arzhanikov, S., Arzhanikova, A., Chauvet, A., Vassallo, R., Braucher, R. (2011), Geomorphic Mesozoic and Cenozoic evolution in the Oka-Jombolok region (East-Sayan ranges, Siberia). *Journal of Asian Earth Sciences*, 24, doi: 10. 1016/j.jseaes. 2011. 09. 017.

Jolivet, M., Arzhannikov, S., Arzhannikov, A., Chauvet, A., Vassallo, R. and Braucher, R. (2011), Geomorphic Mesozoic and Cenozoic evolution in the Oka-Jombolok region (East-Sayan ranges, Siberia). *Journal of Asian Earth Sciences*, doi: 10. 1016/j.jseaes. 2011. 09. 017.

Jolivet, M., Brunel, M., Seward, D., Xu, Z., Yang, J., Roger, F., Tapponnier, P., Malavieille, J., Arnaud, N. and Wu, C. (2001), Mesozoic and Cenozoic tectonics of the northern edge of the Tibetan plateau: fission-track constraints. *Tectonophysics*, 343 (1-2), 111-134.

Jolivet, M., Brunel, M., Seward, D., Xu, Z., Yang, J., Roger, F., Tapponnier, P., Malavieille, J., Arnaud, N., Wu, C. (2001), Mesozoic and Cenozoic tectonics of the northern edge of the Tibetan plateau: fission-track constraints. *Tectonophysics*, 343 (1-2), 111-134.

Jolivet, M., De Boisgrollier, T., Petit, C., Fournier, M., Sankov, V.A., Ringenbach, J.-C., Byzov, L., Miroshnichenko, A.I., Kovalenko, S.N. and Anisimova, S.V. (2009), How old is the Baikal Rift Zone ? Insight from apatite fission track thermochronology. *Tectonics*, doi: 10. 1029/2008TC002404.

Jolivet, M., De Boisgrollier, T., Petit, C., Fournier, M., Sankov, V.A., Ringenbach, J.-C., Byzov, L., Miroshnichenko, A.I., Kovalenko, S.N., Anisimova, S.V. (2009), How old is the Baikal Rift Zone ? Insight from apatite fission track thermochronology. *Tectonics*, 28, TC3008 doi:10.1029/2008TC002404.

Jolivet, M., Dominguez, S., Charreau, J., Chen, Y., Li, Y.A. and Wang, Q.C. (2010), Mesozoic and Cenozoic tectonic history of the Central Chinese Tian shan: Reactivated tectonic structures and active deformation. *Tectonics*, doi: 10. 1029/2010TC002712.

Jolivet, M., Dominguez, S., Charreau, J., Chen, Y., Li, Y.A., Wang, Q.C. (2010), Mesozoic and Cenozoic tectonic history of the Central Chinese Tian Shan: Reactivated tectonic structures and active deformation. *Tectonics*, 29, TC6019 doi:10.1029/2010TC002712.

Jolivet, M., Dominguez, S., Charreau, J., Chen, Y., Li, Y.A., Wang, Q.C. (2010), Mesozoic and Cenozoic tectonic history of the Central Chinese Tian Shan: Reactivated tectonic structures and active deformation. *Tectonics*, 29, TC6019 doi:10.1029/2010TC002712.

Jolivet, M., Ritz, J.F., Vassallo, R., Larroque, C., Braucher, R., Todbileg, M., Chauvet, A., Sue, C., Arnaud, N., Vicente, R.D., Arzhanikova, A. and Arzhanikov, S. (2007), Mongolian summits: An uplifted, flat, old but still preserved erosion surface. *Geology*, 35 (10), 871-874.

Jolivet, M., Ritz, J.F., Vassallo, R., Larroque, C., Braucher, R., Todbileg, M., Chauvet, A., Sue, C., Arnaud, N., Vicente, R.D., Arzhanikova, A., Arzhanikov, S. (2007), Mongolian summits: An uplifted, flat, old but still preserved erosion surface. *Geology*, 35 (10), 871-874.

Kent-Corson, M.L., Ritts, B.D., Zhuang, G.S., Bovet, P.M., Graham, S.A., Page Chamberlain, C. (2009), Stable isotopic constraints on the tectonic, topographic, and climatic evolution of the northern margin of the Tibetan Plateau. *Earth and Planetary Science Letters*, 282 (1-4), 158-166.

Kiselev, V.V. (1999), The U-Pb (by zircons) geochronology of magmatic suits of the Northern Tien Shan. In: Bakirov, A.B. and Dikikl, A.N. (Eds.), *Problems of geology and geography in Kyrgystan (Proceedings of the National Academy of Sciences of Kyrgyz Republic)*. Ilim, Bishkek, 21-33 (in Russian).

Klubertanz, G., Laloui, L. and Vulliet, L. (2009), Identification of mechanisms for landslide type initiation of debris flows. *Enginnering Geology*, 109, 114-123.

Konopelko, D., Biske, G., Seltmann, R., Eklund, O. and Belyatsky, B. (2007), Hercynian post-collisional A type granites of the Kokshaal range, southern Tien Shan, Kyrgyzstan. *Lithos*, 97, 140-160.

Konopelko, D., Biske, G., Seltmann, R., Eklund, O., Belyatsky, B. (2007), Hercynian post-collisional A-type granites of the Kokshaal Range, Southern Tien Shan, Kyrgyzstan. *Lithos*, 97, 140-160.

Konopelko, D., Biske, G., Seltmann, R., Kiseleva, M., Matukov, D., Sergeev, S. (2008), Deciphering Caledonian events: timing and geochemistry of the Caledonian magmatic arc in the Kyrgyz Tien Shan. *Journal of Asian Earth Sciences*, 32, 131–141.

Konopelko, D., Kullerud, K., Apayarov, F., Sakiev, K., Baruleva, O., Ravna, E., Lepekhina, E. (2012), SHRIMP zircon chronology of HP-UHP rocks of the Makbal metamorphic comple in the Northern Tien Shan, Kyrgyzstan. *Gondwana Research*, 22 (1), 300-309.

Konopelko, D., Seltmann, R., Biske, G., Lepekhina, E., Sergeev, S. (2009), Possible source dichotomy of contemporaneous post-collision barren I-type versus tin-bearing A-type granites, lying on opposite sides of the South Tien Shan suture. *Ore Geology Reviews*, 35, 206-216.

Kovalenko, V.I., Yarmolyuk., V.V. and Kovach, V.P. (1996), Sources of Phanerozoic granitoids in Central Asia: Sm-Nd isotope data. *Geochemistry International*, 34, 628-640.

KrÖner, A., Alexeiev, D.V., Hegner, E., Rojas-Agramonte, Y., Corsini, M., Chao, Y., Wong, J., Windley, B.F., Liu, D., Tretyakov, A.A. (2012), Zircon and muscovite ages, geochemistry, and Nd-Hf isotopes for the Aktyuz metamorphic terrane: Evidence for an Early Ordovician collisional belt in the northern Tianshan of Kyrgyzstan. *Gondwana Research*, 21 (4), 901-927.

Laurent-Charvet, S., Charvet, J., Monié, P. and Shu, L.S. (2003), Late Paleozoic strike-slip shear zones in eastern central Asia (NW China): new structural and geochronological data. *Tectonics*, 22 (2), 1009.

Laurent-Charvet, S., Charvet, J., Shu, L.S., Ma, R.S. and Lu, H.F. (2002), Palaeozoic late collisional strikeslip deformations in Tian Shan and Altay, Eastern Xinjiang, NW China. *Terra Nova*, 14, 249-256.

Li, C.X., Dupont-Nivet, G. and Guo, Z.J. (2011), Magnetostratigraphy of the Northern Tian Shan foreland, Taxi He section, China. *Basin Research*, 23 (1), 101-117.

Li, C.X., Guo, Z.J. and Dupont-Nivet, G. (2010), Late Cenozoic tectonic deformation across the northern foreland of the Chinese Tian Shan. *Journal of Asian Earth Sciences*, doi: 10. 1016/j.jseaes. 2010. 08. 009.

Li, D.P., Zhao, Y., Hu, J.M., Li, X.L., Zhou, X.K., Wang, X.L., Du, S.X., Xiao, A.F. (2007), Zircon TIMS U-Pb dating of the Qitaidaban granite in the West Kunlun Mountains and its thermal evolution history. *Geology in China*, 34 (6), 1013-1021 (in Chinese with English abstract).

Li, J.B. (2010), Late Paelzoic sedimentary Basin and tectonic evolution in Southwestern Tianshan Mountains, Xinjiang. A dissertation submitted to Chengdu University of Technology, China for Doctoral Degree. *Chengdu University of Technology, China*, (in Chinese with English abstract).

Li, T.M. (1993), The tectonic evolution and hydrocarbon accumulation in the Junggar Basin. *Report for the Geological Survey of Xinjiang*, 129 (in Chinese).

Li, X.C., Wang, Y., Ding, X.Z. (2005), The age of Late Cenozoic molasse in the front of the western Kunlun Xinjiang and its significance. *Journal of Geomechanics*, 11 (2), 181-186 (in Chinese with English abstract).

Li, X.H., Li, W.X., Li, Z.X., Lo, C.H., Wang, J., Ye, M.F., Yang, Y.H. (2009), Amalgamation between the Yangtze and Cathaysia blocks in South China: constraints from SHRIMP U-Pb zircon ages, geochemistry and Nd-Hf isotopes of the Shuangxiwu volcanic rocks. *Precambrian Research*, 174, 117-128.

Li, Y., Yang, J.S., ZhangHANG, J., Li, T.F., Chen, S.Y., Ren, Y.F. and Xu, X.Z. (2011), Tectonic significance of the Carboniferous volcanic rocks in eastern Tianshan. *Acta Petrologica Sinica*, 27 (1), 193-209 (in Chinese with English abstract).

Li, Y.J., Yang, G.X., Guo, W.J., Bi, M.B., Luan, X.D., Li, Z.C., Li, H. and Tong, L.M. (2007), The disintergration and geological significance of the Kuoerku granite

batholith in Awulale, western Tian Shan. *Xinjiang Geology*, 25 (3), 233-236 (in Chinese with English abstract).

Li, Z, Peng, S.T. (2010), Detrital zircon geochronology and its provenance implications: responses to Jurassic through Neogene basin-range interactions along northern margin of the Tarim Basin, Northwest China. *Basin Research*, 22, 126-138.

Li, Z., Song, W.J., Peng, S.T., Wang, D.X. and Zhang, Z.P. (2004), Mesozoic-Cenozoic tectonic relationships between the Kuqa Subbasin and Tian Shan, northwest China: constraints from depositional records. *Sedimentary Geology*, 172, 223-249.

Li, Z., Song, W.J., Peng, S.T., Wang, D.X., Zhang, Z.P. (2004), Mesozoic-Cenozoic tectonic relationships between the Kuqa Subbasin and Tian Shan, northwest China: constraints from depositional records. *Sedimentary Geology*, 172, 223-249.

Li, Z.Q. and Chen, G.S. (1998), Discussion on the extensional dynamic setting in the south border of Junngar basin, Xinjiang, China. *Geological Journal of China Universities*, 4 (1), 73-78 (in Chinese with English abstract).

Li, Z.X., Bogdanova, S.V., Collins, A.S., Davidson, A., De Waele, B., Ernst, R.E., Fitzsimons, I.C.W., Fuck, R.A., Gladkochub, D.P., Jacobs, J., Karlstrom, K.E., Lu, S., Natapoy, L.M., Pease, V., Pisarevsky, S.A., Thrane, K., Vernikovsky, V. (2008), Assembly, configuration, and break-up history of Rodinia: a synthesis. *Precambrian Research*, 160, 179-210.

Lin, W., Faure, M., Shi, Y., Wang, Q., Li, Z. (2009), Paleozoic tectonics of the southwestern Chinese Tianshan: new insights from a structural study of the high-pressure/low –temperature metamorphic belt. *International Journal of Earth Sciences*, 98, 1259-1274.

Liu, C.X., Xu, B.L., Zhou, T.R., Lu, F.X., Tong, Y., Cai, J.H. (2004), Petrochemistry and tectonic signifance of Hercynian alkaline rocks along the Northern margin of

the Tarim platform and its adjacent area. *Xinjiang Geology*, 22 (1), 43-49 (in Chinese with English abstract).

Liu, D.D., Jolivet, M., Yang, W., Zhang, Z.Y., Cheng, F., Zhu, B., Guo, Z.J. (2013), Latest Paleozoic-Early Mesozoic basin-range interactions in South Tian Shan (northwest China) and their tectonic significance: Constraints from detrital zircon U/Pb ages. *Tectonophysics*, 599, 197-213.

Liu, H., Wang, G.C., Cao, K., Meng, Y.N., Wang, A., Zhang, K.X. (2010), The detrital zircon fission-track ages constraint to tectonic process in west Kunlun and adjacent regions. *Frontiers of Earth Science*, 17 (3), 64-78 (in Chinese with English abstract).

Liu, H.F., Liang, H.S., Cai, L.G., Xia, Y.P. and Liu, L.Q. (1994), Evolution and structural style of Tianshan and adjacent basins, Northwestern China. *Earth Science-Journal of China University of Geosciences*, 19 (6), 727-741 (in Chinese with English abstract).

Liu, H.F., Wang, Z.C., Xiong, B.X., Li, Y.L., Liu, L.Q. and Zhang, J.Z. (2000), Coupling analysis of Mesozoic-Cenozoic foreland basin and mountain system in central and western China. *Frontiers of Earth Science*, **7** (3), 55-72 (in Chinese with English abstract).

Long, L.L., Gao, J., Klemd, R., Beier, C., Qian, Q., Zhang, X., Wang, J.B. and Jiang, T. (2011), Geochemical and geochronological studies of granitoid rocks from the Western Tianshan Orogen: implications for continental growth in the southwestern Central Asian Orogenic Belt. *Lithos*, 126, 321-340.

Long, L.L., Gao, J., Klemd, R., Beier, C., Qian, Q., Zhang, X., Wang, J.B., Jiang, T., (2011), Geochemical and geochronological studies of granitoid rocks from the Western Tianshan Orogen: Implications for continental growth in the southwestern Central Asian Orogenic Belt. *Lithos*, 126, 321-340.

Long, L.L., Gao, J., Xiong, X.M. and Qian, Q. (2007), Geochemistry and geochronology of granitoids in Bikai region, southern Central-Tianshan

mountains, Xinjiang. *Acta Petrologica Sinica*, 23 (4), 719-732 (in Chinese with English abstract).

Long, X.P., Sun, M., Yuan, C., Kröner, A., Hu, A.Q. (2012), Zircon REE patterns and geochemical characteristics of Paleoproterozoic anatectic granite in the northern Tarim Craton, NW China: Implications for the reconstruction of the Columbia supercontinent. *Precambrian Research*, 222-223, 474-487.

Long, X.P., Yuan, C., Sun, M., Kröner, A., Zhao, G.C., Wilde, S.A., Hu, A.Q. (2011a), Reworking of the Tarim Craton by underplating of mantle plume-derived magmas: evidence from Neoproterozoic adakitic rocks and I-type granites in the Kuluketage area, NW China. *Precambrian Research*, 187, 1-14.

Long, X.P., Yuan, C., Sun, M., Xiao, W.J., Zhao, G.C., Wang, Y.J., Cai, K.D., Xia, X.P. and Xie, L.W. (2010), Detrital zircon ages and Hf isotopes of the early Paleozoic flysch sequence in the Chinese Altai, NW China: New constrains on depositional age, provenance and tectonic evolution. *Tectonophysics*, 480, 213-231.

Long, X.P., Yuan, C., Sun, M., Xiao, W.J., Zhao, G.C., Wang, Y.J., Cai, K.D., Xia, X.P., Xie, L.W. (2010), Detrital zircon ages and Hf isotopes of the early Paleozoic flysch sequence in the Chinese Altai, NW China: New constrains on depositional age, provenance and tectonic evolution. *Tectonophysics*, 480, 213-231.

Long, X.P., Yuan, C., Sun, M., Xiao, W.J., Zhao, G.C., Zhou, K.F., Wang, Y.J., Hu, A.Q. (2011b), The discovery of the oldest rocks in the Kuluketage area and its geological implications. *Science in China Series D-Earth Sciences*, 54, 342-348.

Long, X.P., Yuan, C., Sun, M., Zhao, G.C., Wu, F.Y., Wang, Y.J., Cai, K.D., Hu, A.Q. (2010), Archean crustal evolution of the Tarim Craton, NW China: Zircon U-Pb and Hf isotopic constraints and implications. *Precambrian Research*, 180, 272-284.

Lu, H.F., Howell, D.G. and Jia, D. (1994), Rejuvenation of the Kuqa foreland basin, northern flank of the Tarim basin, Northwest China. *International Geology Review*, 36, 1151-1158.

Lu, H.F., Howell, D.G., Jia, D. (1994), Rejuvenation of the Kuqa foreland basin, northern flank of the Tarim basin, Northwest China. *International Geology Review*, 36, 1151-1158.

Lu, H.H., Douglas, W.B., Li, Y.L. and Liu, Y.M. (2010), Late Cenozoic structural and stratigraphic evolution of the northern Chinese Tian Shan foreland. *Basin Research*, 22, 249-269.

Lu, H.H., Douglas, W.B., Li, Y.L., Liu, Y.M. (2010), Late Cenozoic structural and stratigraphic evolution of the northern Chinese Tian Shan foreland. *Basin Research*, 22, 249-269.

Lu, S.N., Li, H.K., Zhang, C.L., Niu, G.H. (2008), Geological and geochronological evidence for the Precambrian evolution of the Tarim Craton and surrounding continental fragments. *Precambrian Research*, 160, 94-107.

Ludwig, K.R. (2003), User's Manual for Isoplot 3.0: a Geochronological Toolkit for Microsoft Excel Berkeley Geochronology Center. *Special Publication*, 4, 1-71.

Ludwig, K.R. (2003), User's Manual for Isoplot 3.0: a Geochronological Toolkit for Microsoft Excel Berkeley Geochronology Center. *Special Publication*, 4, 1-71.

Ma, X.X., Shu, L.S., Jahn, B.M., Zhu, W.B., Faure, M. (2012a), Precambrian tectonic evolution of Central Tianshan, NW China: constraints from U-Pb dating and in-situ Hf isotopic analysis of detrital zircons. *Precambrian Research*, 222-223, 450-473.

Ma, X.X., Shu, L.S., Santosh, M., Li, J.Y. (2012b), Detrital zircon U-Pb geochronology and Hf isotope data from Central Tianshan suggesting a link with the Tarim Block: implications on Proterozoic supercontinent history. *Precambrian Research*, 206-207, 1-16.

Ma, X.X., Shu, L.S., Santosh, M., Li, J.Y. (2013), Paleoproterozoic collisional orogeny in Central Tianshan: Assembling the Tarim Block within the Columbia supercontinent. *Precambrian Research*, 228, 1-19.

Matte, P., Tapponnier, P., Arnaud, N., Bourjot, L., Avouac, J.P., Vidal, P., Liu, Q., Pan, Y.S., Wang, Yi. (1996), Tectonics of Western Tibet, between the Tarim and the Indus. *Earth and Planetary Science Letters*, 142, 311-330.

Mattern, F., Schneider, W. (2000), Suturing of the Proto- and Paleo-Tethys oceans in the western Kunlun (Xinjiang, China). *Journal of Asian Earth Sciences*, 18, 637-650.

McDowell, F.W., McIntosh, W.C., Farley, K.A. (2005), A precise ^{40}Ar-^{39}Ar reference age for the Durango apatite (U-Th)/He and fission-track dating standard, *Chemical Geology*, 214, 249-263, doi:10.1016/j.chemgeo.2004.10.002.

McDowell, F.W., McIntosh, W.C., Farley, K.A. (2005), A precise ^{40}Ar-^{39}Ar reference age for the Durango apatite (U-Th)/He and fission-track dating standard, *Chemical Geology*, 214, 249-263, doi:10.1016/j.chemgeo.2004.10.002.

McFadden, P.L., McElhinny, M.W. 1990. Classification of the Reversal Test in Palaeomagnetism. *Geophysical Journal International*, 103, 725-729.

McFadden, P.L., McElhinny, M.W. 1988. The combined analysis of remagnetization circles and direct observations in palaeomagnetism. *Earth and Planetary Science Letters*, 87, 161-172.

Molnar, P. and Tapponnier, P. (1975), Cenozoic tectonics of Asia: effects on a continental collision. *Science*, 189, 419-426.

Molnar, P., Tapponnier, P. (1975), Cenozoic tectonics of Asia: effects on a continental collision. *Science*, 189, 419-426.

Molnar, P., Tapponnier, P. (1978), Active tectonics of Tibet. *Journal of Geophysical Research*, 83, 148-227. doi: 10.1029/0JGREA000083000B11005361000001.

Orozbaev, R.T., Takasu, A., Bakirov, A.B., Tagiri, M., Sakiev, S. (2010), Metamorphic history of eclogites and country rock gneisses in the Aktyuz area, Northern Tien-Shan, Kyrgyzstan: a record from initiation of subduction through to oceanic closure by continent-continent collision. *Journal of Metamorphic Geology*, 28, 317-339.

Pan, Y.S. (1990), The tectonic characteristics and evolution of West Kunlun region. *Scientia Geologica Sinica*, 3, 224-232 (in Chinese with English abstract).

Pan, Y.S. (1996), Geological Evolution of the Karakorum and Kunlun Mountains. *Seismological Press*, Beijing.

Patriat, P., Achache, J. (1984), India- Asia collision chronology has implications for crustal shortening and driving mechanism of plates. *Nature*, 311, 615-621.

Prokopiev, A.V., Toro, J., Miller, E.L. and Gehrels, G.E. (2008), The paleo-Lena River-200 m.y. of transcontinental zircon transport in Siberia. *Geology*, 36 (9), 699-702.

Prokopiev, A.V., Toro, J., Miller, E.L., Gehrels, G.E. (2008), The paleo-Lena River-200 m.y. of transcontinental zircon transport in Siberia. *Geology*, 36 (9), 699-702.

Qi, C.S., Li, X.H., Liang, X.R., Liu, Y. and Tu, X.L. (2005), High-precision measurement of Hf isotopic reference values for the U-Pb geochronology standard zircons by Multi-collector Inductively Coupled Plasma-Mass Spectrometry. *Journal of Chinese Mass Spectrometry Society*, 26 (3), 149-154 (in Chinese with English abstract).

Qi, C.S., Li, X.H., Liang, X.R., Liu, Y., Tu, X.L. (2005), High-precision measurement of Hf isotopic reference values for the U-Pb geochronology standard zircons by Multi-collector Inductively Coupled Plasma-Mass Spectrometry. *Journal of Chinese Mass Spectrometry Society*, 26 (3), 149-154 (in Chinese with English abstract).

Qiu, N.S., Chang, J., Li, J.W., Li, W.Z., Yun, L., Li, H.L. (2012), New evidence on the Neogene uplift of South Tianshan: constraints from the (U-Th)/He and AFT

ages of borehole samples of the Tarim Basin and implications for hydrocarbon generation. *International Journal of Earth Sciences*, 101 (6), 1625-1643.

Qiu, N.S., Zha, M., Wang, X.L. and Yang, H.B. (2005), Tectono-thermal evolution of the Junggar Basin, NW China: constraints from R_o and apatite fission track modeling. *Petroleum Geoscience*, 11, 361-372.

Qiu, N.S., Zhang, Z.H. and Xu, E.S. (2008), Geothermal regime and Jurassic source rock maturity of the Junggar Basin, northwest China. *Journal of Asian Earth Science*, 31, 4-6.

Ramstein, G., Fluteau, F., Besse, J., Joussaume, S. (1997), Effect of orogeny, plate motion and land-sea distribution on Eurasian climate change over the past 30 million years. *Nature*, 386, 788-795.

Ren, R., Han, B.F., Ji, J.Q., Zhang, L., Xu, Z., Su, L. (2011), U-Pb age of detrital zircons from the Tekes River, Xinjiang, China, and implications for tectonomagmatic evolution of the South Tian Shan Orogen. *Gondwana Research*, 19, 460-470.

Robinson, A.C., Yin, A., Manning, C.E., Harrison, T.M., Zhang, S.H., and Wang, X.F. (2007), Cenozoic evolution of the eastern Pamir: Implications for strain accommodation mechanisms at the western end of the Himalayan-Tibetan orogen: *Geological Society of America Bulletin*, 119, 882–896. doi: 10.1130/B25981.1.

Robinson, A.C., Yin, A., Manning, C.E., Harrison, T.M., Zhang, S.H., Wang, X.F. (2004), Tectonic evolution of the northeastern Pamir: Constraints from the northern portion of the Cenozoic Kongur Shan extensional system. *Geological Society of American Bulletin*, 116, 953-974.

Roger, F., Jolivet, M. and Malavieille, J. (2010), The tectonic evolution of the Songpan Garze (North Tibet). *Journal of Asian Earth Science*, 39, 254-269.

Roger, F., Jolivet, M., Cattin, R. and Malavieille, J. (2011), Mesozoic-Cenozoic tectonothermal evolution of the eastern part of the Tibetan plateau (Songpan-

Garze, Longmen Shan area): insights from thermochronological data and simple thermal modeling. *Geological Society London, Special Publication*, 353, 9-25.

Roger, F., Jolivet, M., Cattin, R., Malavieille, J. (2011), Mesozoic-Cenozoic tectonothermal evolution of the eastern part of the Tibetan plateau (Songpan-Garze, Longmen Shan area): insights from thermochronological data and simple thermal modeling. *Geological Society London, Special Publications*, 353, 9-25.

Roger, F., Jolivet, M., Malavieille, J. (2010), The tectonic evolution of the Songpan Garze (North Tibet). *Journal of Asian Earth Sciences*, 39, 254-269.

Santosh, M., Sajeev, K., Li, J.H. (2006), Extreme crustal metamorphism during Columbia supercontinent assembly: evidence from North China Craton. *Gondwana Research*, 10, 256-266.

Scharer, K.M., Burbank, D.W., Chen, J., Weldon, R.J., Rubin, C., Zhao, R., Shen, J. (2004), Detachment folding in the Southwestern Tian Shan-Tarim foreland, China: shorting estimates and rates. *Journal of Structural Geology*, 26, 2119-2137.

Searle, M.P. (1996), Cooling history, erosion, exhumation, and kinematics of the Himalaya-Karakoram-Tibet orogenic belt. In: Yin, A. and Harrison, T.M. (Eds.), The Tectonic Evolution of Asia. C*ambridge University Press*, New York, 110-137.

Seltmann, R., Konopelko, D., Biske, G., Divaev, F., Sergeev, S. (2011), Hercynian post-collisional magmatism in the context of Paleozoic magmatic evolution of the Tien Shan orogenic belt. *Journal of Asian Earth Sciences*, 42, 821-838.

Sengör, A.M.C. and Natalin, B.A. (1996), Palaeotectonics of Asia: fragments of a synthesis. In: *The tectonic evolution of Asia* (Ed. By Yin, A. and Harrison, M.), pp. 486-640. Rubey Colloquium, Cambridge University Press, Cambridge.

Şengör, A.M.C., Natal'in, B.A., Burtman, V.S. (1993), Evolution of the Altaid tectonic collage and Paleozoic crustalgrowth in Eurasia. *Nature*, 364, 299-307. doi: 10.1038/364299a0.

Seward, D., Spikings, R., Viola, G., Kounov, A., Ruiz, G.M.H., and Naeser, N. (2000), Etch times and operator variation for spontaneous track lengths measurements in apatites: An intra-laboratory check. *OnTrack*, 10, 16 – 21.

Seward, D., Spikings, R., Viola, G., Kounov, A., Ruiz, G.M.H., and Naeser, N. (2000), Etch times and operator variation for spontaneous track lengths measurements in apatites: An intra-laboratory check. OnTrack 10, 16 – 21.

Shu, L.S., Charvet, J., Lu, H.F. and Laurent-Charvet, S. (2002), Paleozoic accretion-collision events and kinematics of ductile deformation in the central-southern Tianshan Belt, China. *Acta Geologica Sinica*, 76 (3), 308-323.

Shu, L.S., Charvet, J., Lu, H.F., Laurent-Charvet, S. (2002), Paleozoic accretion-collision events and kinematics of ductile deformation in the central-southern Tianshan Belt, China. *Acta Geologica Sinica*, 76 (3), 308-323.

Shu, L.S., Deng, X.L., Zhu, W.B., Ma, D.S., Xiao, W.J. (2011), Precambrian tectonic evolution of the Tarim Block, NW China: New geochronological insights from the Quruqtagh domain. *Journal of Asian Earth Sciences*, 42 (5), 774-790.

Shu, L.S., Guo, Z.J., Zhu, W.B., Lu, H.F. and Wang, B. (2004), Post-collision tectonism and basin-range evolution in the Tianshan belt. *Geological Journal of China Universities*, 10 (3), 393-404 (in Chinese with English abstract).

Shu, L.S., Guo, Z.J., Zhu, W.B., Lu, H.F., Wang, B. (2004), Post-collision tectonism and basin-range evolution in the Tianshan belt. *Geological Journal of China Universities*, 10 (3), 393-404 (in Chinese with English abstract).

Shu, L.S., Shi, Y.S., Lu, H.F., Charvet, J. and Laurent-Charvet, S. (1999), Paleozoic terrane tectonics in Northern Tian Shan, northwestern China. In: *Terrane Paths 99 Circum-Pacific Terrane Conference, Okanagan Valley. B.C., Canada* (Ed. By Evenchick, C.A., Woods-worth, G.J. and JONGENS, R.), pp. 63-65. Circum Pacific Terrane Conference Abstract and Program, Canada.

Shu, L.S., Wang, .B., Zhu, W.B. (2007), Age and tectonic significance of radiolarian fossils from the Heiyingshan ophiolitic mélange, southern Tianshan Belt, NW China. *Acta Geologica Sinica*, 81, 1-8.

Sobel, E.R. and Arnaud, N. (2000), Cretaceous Paleogene basaltic rocks of the Tuoyun basin, NW China and the Kyrgyz Tian Shan: The race of a small plume. *Lithos*, 50, 191-215.

Sobel, E.R., Chen, J., Heermance, R.V. (2006), Late Oligocene - Early Miocene initiation of shorting in the Southwestern Chinese Tian Shan: Implications for Neogene shorting rate variations. *Earth and Planetary Science Letters*, 247, 70-81.

Sobel, E.R., Dumitru, T.A. (1997), Exhumation of the margins of the western Tarim basin during the Himalayan orogeny. *Journal of Geophysical Research*, 102, 5043-5064.

Sobel, E.R., Schoenbohm, L.M., Chen, J., Thiede, R., Stockli, D.F., Sudo, M., Strecker, M.R. (2011), Late Miocene-Pliocene deceleration of dextral slip between Pamir and Tarim: Implications for Pamir orogenesis. *Earth and Planetary Science Letters*, 304, 369-378.

Solomovich, L.I., Trifonov, B.A. (2002), Postcollisional granites in the South Tien Shan Variscan Collisional Belt, Kyrgyzstan. *Journal of Asian Earth Sciences*, 21, 7-21.

Song, S.G., Niu, Y.L., Wei, C.J., Ji, J.Q., Su, L. (2010), Metamorphism, anatexis, zircon ages and tectonic evolution of the Gongshan block in the northern Indochina continent - An eastern extension of the Lhasa Block. *Lithos*, 120 (3-4), 327-346.

Su, C.Q., Jiang, C.Y., Xia, M.Z., Zhang, L., Ji, H.G., Guo, F.F. and Liu, X.J. (2008), Zircon SHRIMP U-Pb dating from granite of the metamorphic core complex system in Jueluotage tectonic belt and its geological significance. *Acta Petrologica Sinica*, 24 (12), 2789-2799 (in Chinese with English abstract).

Su, W., Gao, J., Klemd, R., Li, J.L., Zhang, X., Li, X.H., Chen, N.S., Zhang, L. (2010), U-Pb zircon geochronology of Tianshan eclogites in NW China: implication for the collision between the Yili and Tarim blocks of the southwestern Altaids. *European Journal of Mineralogy*, 22, 473-478.

Sun, L.H., Wang, Y.J., Fan, W.M., Zi, J.W. (2008), Post-collisional potassic magmatism in the Southern Awulale Mountain, western Tianshan Orogen: Petrogenetic and tectonic implications. *Gondwana Research*, 14, 383-394.

Sun, X., Wang, P. (2005), How old is the Asian monsoon system ? Palaeobotanical records from China. *Palaeogeography, Palaeoclimatology, Palaeoecology*, 222, 181-222.

Tagami, T. (1987), Determination of zeta calibration constant for fission track dating. *Nuclear Tracks and Radiation Measurements*, 13, 127-130. doi: 10.1016/1359-0189(87)90023-9.

Tagami, T. (1987), Determination of zeta calibration constant for fission track dating. *Nuclear Tracks and Radiation Measurements*, 13, 127-130. doi: 10.1016/1359-0189(87)90023-9.

Tang, J.G., Chen, H.H., Wang, Q., Zhao, Z.H., Wyman, D.A., Jiang, Z.Q. and Jia, X.H. (2008), Geochronological age and tectonic background of the Dabate A-type granite pluton in the west Tianshan. *Acta Petrologica Sinica*, 24 (5), 947-958 (in Chinese with English abstract).

Tapponnier, P. and Molnar, P. (1977), Active faulting and tectonics in China. *Journal of Geophysical Research*, 82, 2905-2929.

Tapponnier, P. and Molnar, P. (1979), Active faulting and Cenozoic tectonics of the Tien Shan, Mongolia, and Baykal Regions. *Journal of Geophysical Research*, 84, 3425-3459.

Tapponnier, P., Molnar, P. (1977), Active faulting and tectonics in China. *Journal of Geophysical Research*, 82, 2905-2929.

Tapponnier, P., Molnar, P. (1979), Active faulting and Cenozoic tectonics of the Tien Shan, Mongolia, and Baykal Regions. *Journal of Geophysical Research*, 84, 3425-3459.

Tauxe, L., Gallet, Y. (1991), A jackknife for magnetostratigraphy. *Geophysical Research Letters*, 18, 1783-1786.

Tauxe, L. (1998), Paleomagnetic principles and practice. Dordrecht/Boston/London, Kluwer Academic Publisher, *Modern Approaches in Geophysics*, pp. 299.

Thomas, J.C., Chauvin, A., Gapias, D., Bazhenov, M.L., Perroud, H., Cobbold, P.R., Burtman, V.S. (1994), Paleomagnetic evidence for Cenozoic block rotations in the Tadjik depression. Central Asia. *Journal of Geophysical Research*, 99, 15141-15160.

Tian, W., Campbell, I.H., Allen, C.M., Guan, P., Pan, W.Q., Chen, M.M., Yu, H.J., Zhu, W.P. (2010), The Tarim picrite-basalt-rhyolite suite, a Permian flood basalt from northwest China with contrasting rhyolites produced by fractional crystallization and anatexis. *Contributions to Mineralogy and Petrology*, 160, 407–425.

Tong, Y., Wang, T., Hong, D.W., Han, B.F., Zhang, J.J., Shi, X.J. and Wang, C. (2010), Spatial and temporal distribution of the Carboniferous-Permian granitoids in northern Xinjiang and its adjacent areas, and its tectonic significance. *Acta Petrologica et Mineralogica*, 29 (6), 619-641 (in Chinese with English abstract).

Van Hinsbergen, D.J.J., Lippert, P.C., Dupont-Nivet, G., McQuarrie, N., Doubrovine, P.V., Spakman, W., Torsvik, T.H, (2012), Greater India Basin Hypothesis and a Two-Stage Cenozoic Collision between India and Asia. *Proceedings of the National Academy of Sciences*, 109, 7659-7664.

Vassallo, R., Jolivet, M., Ritz, J.F., Braucher, R., Larroque, C., Sue, C., Todbileg, M. and Javkhlanbold, D. (2007), Uplift age and rates of the Gurvan Bogd system

(Gobi-Altay) by apatite fission track analysis. *Earth and Planetary Science Letters*, 259, 333-346.

Vassallo, R., Jolivet, M., Ritz, J.F., Braucher, R., Larroque, C., Sue, C., Todbileg, M., Javkhlanbold, D. (2007), Uplift age and rates of the Gurvan Bogd system (Gobi-Altay) by apatite fission track analysis. *Earth and Planetary Science Letters*, 259, 333-346.

Wang, B., Faure, M., Cluzel, D., Shu, L.S., Charvet, J., Meffre, S. (2006), Late Paleozoic tectonic evolution of the northern West Tianshan, NW China. *Geodinamica Acta*, 19 (3-4), 237-247.

Wang, B., Shu, L.S., Cluzel, D., Faure M. and Charvet, J. (2007), Geochronological and geochemical studies on the Borohoro plutons, north of Yili, NW Tian Shan and their tectonic implication. *Acta Petrologica Sinica*, 23 (8), 1885-1990 (in Chinese with English abstract).

Wang, B., Shu, L.S., Cluzel, D., Faure, M., Charvet, J. (2007a), Geochronological and geochemical studies on the Borohoro plutons, north of Yili, NW Tianshan and their tectonic implication. *Acta Petrologica Sinica*, 23 (8), 1885-1900.

Wang, C., Liu, L., Luo, J.H., Che, Z.C., Teng, Z.H., Cao, X.D., Zhang, J.Y. (2007b), Late Paleozoic post-collisional magmatism in the Southwestern Tianshan orogenic belt, take the Baleigong pluton in the Kokshal region as an example. *Acta Petrologica Sinica*, 23 (8), 1830-1840.

Wang, F., Zhou, X.H., Zhang, L.C., Ying, J.F., Zhang, Y.T., Wu, F.Y. and Zhu, R.X. (2006), Late Mesozoic volcanism in the Great Xing' an range (NE China): timing and implications for the dynamic setting of NE Asia. *Earth and Planetary Science Letters*, 251, 179-198.

Wang, H.L., Deng, H.W. and Sun, D.J. (2000a), Characteristics of sequence stratigraphy and prediction of favorable gas zones for the south edge of the Junggar Basin. *Petroleum Geology and Experimant*, 22 (4), 336-341 (in Chinese with English abstract).

Wang, J., Jin, X.C., Ren, L.D., Chen, B.W. (1999), Apatite fission track study of Cenozoic deposits of the Keliyang section, West Kunlun. *Acta Geoscientia Sinica*, 20, 159-164 (in Chinese with English abstract).

Wang, L.N., Ji, J.Q., Sun, D.X., Xu, Q.Q., Tu, J.Y., Zhang, Z.C., Han, B.F. (2010), The uplift history of south-western Tianshan – Implications from AFT analysis of detrital samples. *Chinese Journal of Geophysics*, 53 (4), 931-945 (in Chinese with English abstract).

Wang, Q.C., Li, S.J. and Du, Z.L. (2009), Differential uplift of the Chinese Tian Shan since the Cretaceous: constraints from sedimentary petrography and apatite fission-track dating. *International Journal of Earth Sciences*, 98, 1341-1363.

Wang, Q.C., Li, S.J., Du, Z.L. (2009), Differential uplift of the Chinese Tian Shan since the Cretaceous: constraints from the sedimentary petrography and apatite fission-track dating. *International Journal of Earth Sciences*, 98, 1341-1363.

Wang, X.F., Zhang, Z.C., Guo, Z.J. and Zhang, C. (2004), Geochemical characteristics and tectonic significance of the Early Cretaceous volcanic rocks in the southern margin of Jiuxi basin. *Geological Journal of China Universities*, 10 (4), 569-577 (in Chinese with English abstract).

Wang, Y., Li, G.D., Xiao, X.C., Chi, Z.Q., Min, L.R., Wang, J., Wang, Y.B. (2006), Late Cenozoic tectonic movement in the front of the West Kunlun Mountains and uplift of the northwestern margin of the Qinghai-Tibetan Plateau. *Geology in China*, 33 (1), 41-47 (in Chinese with English abstract).

Wang, Y., Wang, Y.B., Liu, X., Xiao, X.C. (2002), Apatite fission-track ages of Late Cenozoic sediments from Kokyar section in western Kunlun foreland basin and their significance. *Xinjiang Geology*, 20, 43-46 (in Chinese with English abstract).

Wang, Y.B., Wang, Y., Liu, X., Fu, D.R., Wang, J., Wang, S.C. (2001), Apatite fission-track records of Mesozoic and Cenozoic episodic reactivation of the Tianshan and West Kunlun Mountains. *Regional Geology of China*, 20 (1), 94-99 (in Chinese with English abstract).

Wang, Y.B., Wang, Y., Liu, X., Fu, D.R., Xiao, X.C. and Qi, L.S. (2000b), Geochemical characteristics and genesis of Late Cretaceous to Paleogene basalts in Tuyon basin, south Tianshan Mountain. *Acta Petrologica et Mineralogica*, 19 (2), 131-139 (in Chinese with English abstract).

Wang, Z.H. (2004), Tectonic evolution of the western Kunlun orogenic belt, western China. *Journal of Asian Earth Sciences*, 24, 153-161.

Wang, Z.X., Wu, J.Y. and Lu, X.C. (1990), Multicycle tectonic evolution and metallogenesis in Tian Shan. *China Science Press*, Beijing, 1-217 (in Chinese).

Wang, Z.X., Wu, J.Y., Lu X.C. (1990), Multicycle tectonic evolution and metallogenesis in Tian Shan. *China Science Press,* Beijing, pp. 1-217 (in Chinese).

Wartes, M.A., Carroll, A.R. and Greene, T.J. (2002), Permian sedimentary record of the Turpan-Hami basin and adjacent regions, northwest China: constraints on post amalgamation tectonic evolution. *Geological Society of America Bulletin*, 114 (2), 131-152.

Watson, M.P., Hayward, A.B., Parkinson, D.N. and Zhang, Z.H. (1987), Plate tectonic history, basin development and petroleum source rock deposition onshore China. *Marine and Petroleum Geology*, 4, 205-225.

Watson, M.P., Hayward, A.B., Parkinson, D.N., Zhang, Z.H. (1987), Plate tectonic history, basin development and petroleum source rock deposition onshore China. *Marine and Petroleum Geology*, 4, 205-225.

Wiedenbeck, M., Alle, P., Corfu, F., Griffin, W.L., Meier, M., Oberli, F., Vonquadt, A., Roddick, J.C. and Speigel, W. (1995), Three National Zircon Standards for U-Th-Pb, Lu-Hf, Trace-element and REE Analyses. *Geostandards Newsletter*, 19, 1-23.

Wiedenbeck, M., Alle, P., Corfu, F., Griffin, W.L., Meier, M., Oberli, F., Vonquadt, A., Roddick, J.C., Speigel, W. (1995), Three National Zircon Standards for U-

Th-Pb, Lu-Hf, Trace-element and REE Analyses. *Geostandard Newsletter*, 19, 1-23.

Windley, B.F., Alexeiev, D., Xiao, W., Kroner, A. and Badarch, G. (2007), Tectonic models for accretion of the Central Asian Orogenic Belt. *Journal of Geological Society, London*, 164, 31-47.

Windley, B.F., Alexeiev, D., Xiao, W., Kroner, A. and Badarch, G. (2007), Tectonic models for accretion of the Central Asian Orogenic Belt. *Journal of Geological Society, London*, 164, 31-47.

Windley, B.F., Allen, M.B., Zhang, C., Zhao, Z.Y. and Wang, G.R. (1990), Paleozoic accretion and Cenozoic redeformation of the Chinese Tian Shan Range. *Geology of Central Asia*, 128-131.

Windley, B.F., Allen, M.B., Zhang, C., Zhao, Z.Y., Wang, G.R. (1990), Paleozoic accretion and Cenozoic redeformation of the Chinese Tian Shan. *Geology*, 18 (2), 128-131.

Wu, C.D., Guo, Z.J., Fang, S.H. and Zhang Z.C. (2006), The Mesozoic filling sequences and controlling factors in the southern Junggar Basin. In: *Mesozoic-Cenozoic intercontinental orogeny and mineralization of the sandstone-type uranium deposit in the Central Asian Orogenic Belt, Northwest China* (Ed. By Guo, Z.J., Chen, Z.L., Shu, L.S. and Li, S.X.), pp. 80-94. Geological Publishing House, Beijing (in Chinese with English abstract).

Wu, G.H., Sun, J.H., Guo, Q.Y., Tang, T., Chen, Z.Y., Feng, X.J. (2010), The distribution of detrital zircon U-Pb ages and its significance to Precambrian basement in Tarim Basin. *Acta Geoscientica Sinica*, 31, 65-72 (in Chinese with English abstract).

Wu, G.H., Zhang, B.H., Guo, C.L., Wang, C.L., Gao, H. (2009), Detrital zircon U-Pb dating for the Silurian in Northern Tarim Basin and its significance. *Geotectonica et Metalbgenia*, 33, 418-426.

Xiao, W.J., Zhang, L.C., Qin, K.Z., Sun, S. and Li, J.L. (2004), Paleozoic accretionary and collisional tectonics of the eastern Tianshan (China): implications for the continental growth of Central Asia. *American Journal of Science*, 304, 370-395.

Xiao, X.C., Tang, Y.Q. and Feng, Y.M. (1992), Tectonic evolution of northern Xinjiang and its adjacent regions. *Geological Publishing House*, Beijing, 1-169 (in Chinese with English abstract).

Xiao, X.C., Tang, Y.Q., Feng, Y.M. (1992), Tectonic evolution of northern Xinjiang and its adjacent regions. *Geological Publishing House*, Beijing, pp. 1-169 (in Chinese with English abstract).

Xiao, X.C., Tang, Y.Q., Zhao, M., Wang, J. (1994), Tectonic evolution of North Xinjiang, N.W. China: an introduction to the tectonics of the southern part of the paleo-Asia ocean. *Proceedings of the 29th International Geological Congress*, Part B, pp. 25-37.

Xie, J.Y. (1994), The volcanic debris flow and the pyroclastic flow deposits. *Volcanology and Mineral Resources*, 15 (3), 53-54 (in Chinese).

Xu, X., Chen, C., Ding, T.F., Liu, X.Y. and Li, H.Q. (2008), Discovery of Lisa basalt northwestern edge of Junggar Basin and its geological significance. *Xinjiang Geology*, 26 (1), 9-16 (in Chinese with English abstract).

Xu, X.S., Liu, B.J. and Xu, Q. (1997a), The Permian-Triassic sequence stratigraphy and basin-range conversion and coupling of the western Yangzi craton. *Geological Publishing House*, Beijing, 31-53 (in Chinese).

Xu, X.S., Liu, B.J., Xu, Q., Pan, G.T., Yan, Y.J., Wu, Y.L., Chen, Z.L., Pu, X.C., Yin, F.G., Qiu, D.Z. and Wang, L.Z. (1997b), Analysis of large-scale basins in west China and their geodynamic characteristics. *Geological Publishing House*, Beijing, 16-37 (in Chinese).

Xu, X.Y., Ma, Z.P., Xia, L.Q., Wang, Y.B., Li, X.M., Xia, Z.C. and Wang, L.S. (2005), SHRIMP dating of plagiogranite from Bayingou ophiolite in the northern

Tianshan mountains. *Geological Review*, 51 (5), 523-527 (in Chinese with English abstract).

Xu, X.Y., Xia, L.Q., Ma, Z.P., Wang, Y.B., Xia, Z.C., Li, X.M. and Wang, L.S. (2006), SHRIMP zircon U-Pb geochronology of the plagiogranite from Bayingou ophiolite in North Tianshan mountains and the petrogenesis of the ophiolite. *Acta Petrologica Sinica*, 22 (1), 83-94 (in Chinese with English abstract).

Yang , F.Q., Wang, L, Ye, J.H., Fu, X.J., Li, H.M. (2001), Zircon U-Pb ages of granites in the Huoshi Bulak area, Xinjiang. *Regional Geology of China*, 20 (3), 2001 (in Chinese with English abstract).

Yang, J.S., Meng, F.C., Zhang, J.X. and Li, H.B. (2001), The shoshonitic volcanic rocks at Hongliuxia: Pulses of the Altyn Tagh fault in Cretaceous? *Science China (Series D)*, 44, 99-102.

Yang, S.F., Li, Z.L., Chen, H.L., Santosh, M., Dong, C.W., Yu, X. (2007), Permian bimodal dyke of Tarim Basin, NW China: geochemical characteristics and tectonic implications. *Gondwana Research*, 12, 113-120.

Yang, S.H., Zhou, M.F. (2009), Geochemistry of the ~430 Ma Jingbulake mafic-ultramafic intrusion in Western Xinjiang, NW China: Implications for subductuion related magmatism in the South Tianshan orogenic belt. *Lithos*, 113, 259-273.

Yang, T.N., Li, J.Y., Sun, G.H. and Wang, Y.B. (2006), Earlier Devonian active continental arc in Central Tianshan: evidence of geochemical analyses and zircon SHRIMP dating on mylonitized granitic rock. *Acta Petrologica Sinica*, 22 (1), 41-48 (in Chinese with English abstract).

Yang, T.N., Li, J.Y., Sun, G.H., Wang, Y.B. (2006), Earlier Devonian active continental arc in Central Tianshan: evidence of geochemical analyses and zircon SHRIMP dating on mylonitized granitic rock. *Acta Petrologica Sinica*, 22, 41-48.

Yang, W., Jolivet, M., Dupont-Nivet, G., Guo, Z.J., Zhang, Z.C., Wu, C.D. (2013), Source to sink relations between the Tian Shan Range and Junggar Basin (northwest China) from Late Paleozoic to Quaternary: evidence from detrital U-Pb zircon geochronology. *Basin Research*, 24, doi:10.1111/j.1365–2117.2012.00558.x.

Yang, Y., Liu, M. (2002), Cenozoic deformation of the Tarim plate and the implications for mountain building in the Tibetan Plateau and the Tian Shan. *Tectonics*, 21, 1059. doi:10.1029/2001TC001300.

Yin, A., Harrison, T.M. (2000), Geologic evolution of the Himalayan-Tibetan orogen: *Annual Review of Earth and Planetary Sciences*, 28, 211-280. doi: 10.1146/annurev.earth.28.1.211.

Yin, A., Nie, S., Craig, P., Harrison, T.M. (1998), Late Cenozoic tectonic evolution of the southern Chinese Tian Shan. *Tectonics*, 17 (1), 1-27.

Yin, A., Nie, S., Craig, P., Harrison, T.M., Ryerson, F.J., Qian, X.L. and Yang, G. (1998), Late Cenozoic tectonic evolution of the southern Chinese Tian Shan. *Tectonics*, 17, 1-27.

Yin, A., Rumelhart, P.E., Butler, R., Cowgill, E., Harrison, T.M., Foster, D.A., Ingersoll, R.V., Zhang, Q., Zhou, X.Q., Wang, X.F., Hanson, A., and Raza, A. (2002), Tectonic history of the Altyn Tagh fault system in northern Tibet inferred from Cenozoic sedimentation. *Geological Society of America Bulletin*, 114 (10), 1257-1295.

Yin, J., Bian, Q. (1995), Geologic Map of the Karakorum-Western Kunlun and Adjacent Regions (1:2M). *Science Press*, Beijing.

Yuan, C., Sun, M., Long, X.P., Xia, X.P., Xiao, W.J., Li, X.H., Lin, S.F. and Cai, K.D. (2007), Constraining the deposition time and tectonic background of the Habahe Group of the Altai. *Acta Petrologica Sinica*, 23 (7), 1635-1644 (in Chinese with English abstract).

Yuan, C., Sun, M., Long, X.P., Xia, X.P., Xiao, W.J., Li, X.H., Lin, S.F., Cai, K.D. (2007), Constraining the deposition time and tectonic background of the Habahe Group of the Altai. *Acta Petrologica Sinica*, 23 (7), 1635-1644.

Yuan, H.L., Gao, S. and Liu, X.M. (2004), Accurate U-Pb age and trace element determinations of zircon by laser ablation-inductively coupled plasma mass spectrometry. *Geostandards and Geoanalytical Research*, 28 (3), 353-370.

Yuan, H.L., Gao, S., Liu, X.M. (2004), Accurate U-Pb age and trace element determinations of zircon by laser ablation-inductively coupled plasma mass spectrometry. *Geostandards and Geoanalytical Research*, 28 (3), 353-370.

Zeng, J.Y., Yang, H.Y., Wan, Y.S., Liu, D.Y., Wen, D.R., Lin, Z.Q., Dong, G.A. (2006), The discovery of magmatism record of middle Neoproterozoic metamorphic complex in the North Qilian Mountains: The evidence from the zircon SHRIMP U-Pb ages. *Chinese Science Bulletin*, 51 (5), 575-581 (in Chinese with English abstract).

Zhang, C.L., Yu, H.F., Shen, J.L., Dong, Y.G., Ye, H.M., Guo, K.Y. (2004), Zircon SHRIMP age determination of the Giant-crystal gabbro and basalt in K (u) da, West Kunlun: Dismembering of the K (u) da Ophiolite. *Geological Review*, 50 (6), 639-643 (in Chinese with English abstract).

Zhang, C.L., Zhao, Y., Guo, K.Y., Dong, Y.G., Wang, A.G. (2003), Grenville orogeny in north of the Qinghai-Tibet plateau: first evidence from isotopic dating. *Chinese Journal of Geology*, 38 (4), 535-538 (in Chinese with English abstract).

Zhang, C.L., Zou, H.B., Wang, H.Y., Li, H.K., Ye, H.M. (2012), Multiple phases of the Neoproterozoic igneous activity in Quruqtagh of the northeastern Tarim Block, NW China: Interaction between plate subduction and mantle plume? *Precambrian Research*, 222-223, 488-502.

Zhang, D.Y., Zhou, T.F., Yuan, F., Fan, Y., Liu, S., Du, H.X. (2010a), LA-ICPMS U–Pb ages, Hf isotope characteristics of zircons from basalts in the Kupukuziman Formation, Keping area, Tarim Basin. *Acta Petrologica Sinica*, 26, 963–974 (in Chinese with English abstract).

Zhang, G.C., Chen, X.F., Liu, L.J., Yu, L.P. and Wang, Z. (1999), The architecture of Junggar Basin and the distribution of oil and gas fields. *Acta Petrologia Sinica*, 1, 1-10 (in Chinese).

Zhang, J.X., Yu, S.Y., Gong, J.H., Li, H.K., Hou, K.J. (2013), The latest Neoarchean – Paleoproterozoic evolution of the Dunhuang block, the eastern Tarim craton of northwestern China: evidence from zircon U-Pb datings and Hf isotopic analyses. *Precambrian Research*, 226, 21-42.

Zhang, L.F., Ai, Y.L., Li, X.P., Rubatto, D., Song, B., Williams, S., Song, S.G., Ellis, D., Liou, J.G. (2007a), Triassic collision of western Tianshan orogenic belt, China: evidence from SHRIMP U-Pb dating of zircon from HP/UHP eclogitic rocks. *Lithos*, 96, 266-280.

Zhang, W., Qi, J.F., Lei, G.L., Wei, W., Zeng, X.Z. (2011), Analysis of structure model and formation mechanism of Fusha structure zone in south-western depression of Tarim Basin. *Journal of Southwest Petroleum University (Science and Technology Edition)*, 33 (1), 42-48 (in Chinese with English abstract).

Zhang, Y.T., Liu, J.Q., Guo, Z.F. (2010b), Permian basaltic rocks in the Tarim basin, NW China: implications for plume–lithosphere interaction. *Gondwana Research*, doi:10.1016/j.gr.2010.03.006.

Zhang, Z., Wang, H., Guo, Z., Jiang, D. (2007c), What triggers the transition of palaeoenvironmental patterns in China, the Tibetan Plateau uplift or the Paratethys Sea retreat ? *Palaeogeography, Palaeoclimatology, Palaeoecology*, 245 (3-4), 317-331.

Zhang, Z.C., Guo, Z.J. and Han, Z.Z. (1998), Geochemistry and geological significance of the Mid-Jurassic volcanic rocks in Dunhuang basin. *Acta Scientiarum Naturalium Universitatis Pekinensis*, 34 (1), 72-79 (in Chinese with English abstract).

Zhang, Z.C., Guo, Z.J., Wu, C.D., Fang, S.H. (2007b), Thermal history of the Jurassic strata in the Northern Tianshan and its geological significance, revealed by

apatite fission-track and vitrinite-reflectance analysis. *Acta Petrologica Sinica*, 23 (7), 1683-1695 (in Chinese with English abstract).

Zhang, Z.Y., Zhu, W.B., Shum L.S., Wan, J.L., Yang, W., Su, J.B., Zheng, B.H. (2009), Apatite fission track thermochronology of the Precambrian Aksu blueschist, NW China: Implications for thermo-tectonic evolution of the north Tarim basement. *Gondwana Research*, 16 (2), 182-188.

Zhao, G.C., Cawood, P.A. (2012), Precambrian geology of China. *Precambrian Research*, 222-223, 13-54.

Zhao, G.C., Guo, J.H. (2012), Precambrian geology of China: Preface. *Precambrian Research*, 222-223, 1-12.

Zheng, H.B., Huang, X.T., Butcher, K. (2006), Lithostratigraphy, petrography and facies analysis of the Late Cenozoic sediments in the foreland basin of the West Kunlun. *Palaeogeography, Palaeoclimatology, Palaeoecology*, 241, 61-78.

Zheng, J.J., He, X.X., Liu, S.W. (1999), Dictionary of Chinese stratigraphy-Tertiary. *Geology Press*, Beijing, pp. 163 (in Chinese).

Zheng, Y.F., Xiao, W.J., Zhao, G.C. (2013), Introduction to tectonics of China. *Gondwana Research*, 23, 1189-1206.

Zhou, D., Graham, S.A., Chang, E.Z., Wang, B. and Hacker, B. (2001), Paleozoic tectonic amalgamation of the Chinese Tian Shan: evidence from a transect along the Dushanzi-Kuqa Highway. In: *Paleozoic and Mesozoic Tectonic Evolution of Central and Eastern Asia: From Continental Assembly to Intracontinental Deformation* (Ed. by M.S. Hendrix and G.A. Davis, *Geological Society of America Memoirs*, 194, 23-46).

Zhou, Z.Y., Chen, P.J. (1990), Biostratigraphy and Geological Evolution of Tarim Basin. *Science Press*, Beijing. 439pp (in Chinese).

Zhu, Y.F., Song, B. (2006), Petrology and SHRIMP chronology mylonitized Tianger granite, Xinjiang, also about the dating on hydrothermal zircon rim in granite. *Acta Petrologica Sinica*, 22 (1), 135-144 (in Chinese with English abstract).

Zhu, Z.X. (2007), The Geological components and tectonic evolution of south Tianshan, Xinjiang. PhD thesis. *Chinese Academy of Geological Sciences*, Beijing.

APPENDIX 1

Analysis number	*Th/U*	Isotopic ratios and erros						Ages and errors(Ma)						Disc.%
		$^{207}Pb/^{206}Pb$	1σ	$^{207}Pb/^{235}U$	1σ	$^{206}Pb/^{238}U$	1σ	$^{207}Pb/^{206}Pb$	1σ	$^{207}Pb/^{235}U$	1σ	$^{206}Pb/^{238}U$	1σ	
XJ09-092														
XJ09-092-1	0.76	0.05413	0.00275	0.38576	0.01948	0.05169	0.00077	376	87	331	14	325	5	1.85
XJ09-092-2	0.65	0.05163	0.0014	0.36525	0.00996	0.05131	0.00066	269	39	316	7	323	4	-2.17
XJ09-092-3	0.47	0.05291	0.00294	0.37106	0.02047	0.05087	0.00076	325	98	320	15	320	5	0
XJ09-092-4	0.68	0.05387	0.00203	0.37568	0.01412	0.05058	0.0007	366	60	324	10	318	4	1.89
XJ09-092-5	0.6	0.05712	0.00386	0.40167	0.02682	0.051	0.00089	496	117	343	19	321	5	6.85
XJ09-092-6	0.99	0.05245	0.0028	0.37508	0.01935	0.05186	0.00071	305	125	323	14	326	4	-0.92
XJ09-092-7	0.56	0.05531	0.00181	0.37938	0.01238	0.04975	0.00067	425	49	327	9	313	4	4.47
XJ09-092-8	0.91	0.05356	0.00206	0.40613	0.01559	0.055	0.00076	353	62	346	11	345	5	0.29
XJ09-092-9	0.66	0.05609	0.0015	0.37732	0.01016	0.04879	0.00063	456	37	325	7	307	4	5.86
XJ09-092-10	0.52	0.05306	0.00247	0.37701	0.01743	0.05154	0.00076	331	78	325	13	324	5	0.31
XJ09-092-11	0.48	0.05707	0.00341	0.41518	0.02452	0.05276	0.00088	494	101	353	18	331	5	6.65
XJ09-092-12	0.68	0.0511	0.00254	0.35977	0.01778	0.05106	0.00075	245	87	312	13	321	5	-2.8
XJ09-092-13	0.79	0.05154	0.00202	0.35033	0.01369	0.04929	0.00069	265	64	305	10	310	4	-1.61
XJ09-092-14	0.5	0.05514	0.00164	0.39043	0.01167	0.05136	0.00068	418	43	335	9	323	4	3.72

XJ09-092-15	0.88	0.05316	0.00141	0.36472	0.00975	0.04976	0.00064	336	37	316	7	313	4	0.96
XJ09-092-16	0.78	0.05353	0.00298	0.43622	0.0235	0.0591	0.00084	352	129	368	17	370	5	-0.54
XJ09-092-17	0.61	0.05551	0.00123	0.561	0.01274	0.0733	0.00092	433	29	452	8	456	6	-0.88
XJ09-092-18	0.7	0.05576	0.00327	0.39197	0.02278	0.05099	0.00082	443	101	336	17	321	5	4.67
XJ09-092-19	0.43	0.05346	0.00233	0.36516	0.01515	0.04954	0.00067	348	101	316	11	312	4	1.28
XJ09-092-20	1.93	0.04978	0.00355	0.33809	0.02389	0.04926	0.0008	185	130	296	18	310	5	-4.52
XJ09-092-21	1.41	0.05444	0.00207	0.38663	0.01464	0.05151	0.00071	389	60	332	11	324	4	2.47
XJ09-092-22	0.75	0.05213	0.00229	0.37007	0.01613	0.05149	0.00074	291	73	320	12	324	5	-1.23
XJ09-092-23	0.48	0.05293	0.00145	0.36812	0.01017	0.05044	0.00065	326	39	318	8	317	4	0.32
XJ09-092-24	1.25	0.05462	0.00236	0.37016	0.01589	0.04915	0.00071	397	70	320	12	309	4	3.56
~~**XJ09-092-25**~~	~~1.36~~	~~0.06019~~	~~0.00694~~	~~0.42202~~	~~0.04784~~	~~0.05086~~	~~0.00131~~	~~610~~	~~204~~	~~357~~	~~34~~	~~320~~	~~8~~	~~11.56~~
XJ09-092-26	1.23	0.05292	0.00266	0.36912	0.01839	0.05059	0.00075	325	86	319	14	318	5	0.31
XJ09-092-27	1.17	0.05573	0.00195	0.39796	0.01386	0.05179	0.00071	442	53	340	10	326	4	4.29
XJ09-092-28	0.54	0.05367	0.00117	0.36781	0.0082	0.0497	0.00062	357	28	318	6	313	4	1.6
XJ09-092-29	0.46	0.05415	0.00205	0.36797	0.0139	0.04928	0.00068	377	60	318	10	310	4	2.58
XJ09-092-30	0.93	0.05423	0.00133	0.38929	0.00966	0.05206	0.00066	381	33	334	7	327	4	2.14
XJ09-092-31	0.83	0.05313	0.00327	0.38583	0.02306	0.05266	0.00077	335	143	331	17	331	5	0
XJ09-092-32	1.18	0.05574	0.00158	0.3944	0.01124	0.05132	0.00067	442	40	338	8	323	4	4.64

XJ09-092-33	1.14	0.05187	0.00278	0.38896	0.02071	0.05439	0.00082	280	94	334	15	341	5	-2.05
XJ09-092-34	0.63	0.05398	0.00132	0.37458	0.00931	0.05033	0.00064	370	33	323	7	317	4	1.89
XJ09-092-35	1.09	0.05356	0.00504	0.37285	0.03439	0.05048	0.00092	353	215	322	25	317	6	1.58
XJ09-092-36	1.45	0.05385	0.00254	0.36713	0.0172	0.04945	0.00073	365	79	318	13	311	4	2.25
XJ09-092-37	0.43	0.05581	0.00402	0.40502	0.0289	0.05264	0.00089	445	129	345	21	331	5	4.23
XJ09-092-38	0.67	0.0549	0.00155	0.40428	0.01151	0.05341	0.0007	408	40	345	8	335	4	2.99
XJ09-092-39	1.32	0.05355	0.00161	0.37826	0.01141	0.05123	0.00068	352	44	326	8	322	4	1.24
XJ09-092-40	0.8	0.05308	0.00176	0.37852	0.01254	0.05172	0.0007	332	50	326	9	325	4	0.31
XJ09-092-41	0.44	0.05077	0.00311	0.36081	0.02193	0.05154	0.0008	230	111	313	16	324	5	-3.4
XJ09-092-43	0.91	0.05363	0.00161	0.36943	0.01111	0.04996	0.00066	356	44	319	8	314	4	1.59
XJ09-092-44	0.54	0.05198	0.00216	0.3892	0.01608	0.05431	0.00077	285	68	334	12	341	5	-2.05
XJ09-092-45	0.67	0.05163	0.00228	0.3767	0.01649	0.05292	0.00076	269	74	325	12	332	5	-2.11
XJ09-092-46	1.15	0.05101	0.004	0.37454	0.0291	0.05325	0.00092	241	145	323	21	334	6	-3.29
XJ09-092-47	0.9	0.05126	0.00215	0.37946	0.01581	0.05369	0.00075	253	70	327	12	337	5	-2.97
XJ09-092-48	0.91	0.05318	0.00187	0.36575	0.01285	0.04988	0.00068	336	55	316	10	314	4	0.64
XJ09-092-49	0.85	0.05418	0.00299	0.36421	0.01991	0.04875	0.00075	379	95	315	15	307	5	2.61
XJ09-092-50	0.85	0.05279	0.00185	0.36978	0.01296	0.0508	0.00069	320	55	319	10	319	4	0
XJ09-092-51	0.88	0.0562	0.00282	0.39973	0.01991	0.05158	0.00078	460	84	341	14	324	5	5.25

XJ09-092-52	0.84	0.0517	0.00238	0.3863	0.01766	0.05419	0.00078	272	78	332	13	340	5	-2.35
XJ09-092-53	0.95	0.04785	0.002	0.34852	0.01457	0.05283	0.00072	92	70	304	11	332	4	-8.43
XJ09-092-54	0.89	0.05549	0.00191	0.38327	0.01318	0.05009	0.00069	432	52	329	10	315	4	4.44
XJ09-092-55	0.5	0.05398	0.00197	0.38323	0.01393	0.05149	0.00071	370	57	329	10	324	4	1.54
XJ09-092-56	1.06	0.05125	0.00346	0.36149	0.02417	0.05116	0.00083	252	124	313	18	322	5	-2.8
XJ09-092-57	0.49	0.05844	0.00336	0.40349	0.02297	0.05008	0.0008	546	97	344	17	315	5	9.21
XJ09-092-58	1.74	0.05373	0.00158	0.38839	0.01149	0.05243	0.00069	360	43	333	8	329	4	1.22
XJ09-092-59	0.59	0.05494	0.00367	0.39936	0.02644	0.05272	0.00087	410	119	341	19	331	5	3.02
XJ09-092-60	1.67	0.05206	0.00325	0.34299	0.02122	0.04778	0.00076	288	113	299	16	301	5	-0.66
XJ09-092-61	2.24	0.05371	0.00189	0.35946	0.01263	0.04854	0.00067	359	54	312	9	306	4	1.96
XJ09-092-62	0.86	0.05184	0.00184	0.36253	0.0128	0.05072	0.0007	278	55	314	10	319	4	-1.57
XJ09-092-63	0.56	0.05923	0.00563	0.43392	0.04053	0.05313	0.00121	576	165	366	29	334	7	9.58
XJ09-092-64	0.85	0.05437	0.00195	0.38036	0.01357	0.05074	0.0007	386	55	327	10	319	4	2.51
XJ09-092-65	0.88	0.0521	0.00246	0.36997	0.01732	0.0515	0.00076	290	80	320	13	324	5	-1.23
XJ09-092-66	0.81	0.05483	0.004	0.38206	0.02757	0.05054	0.00089	405	131	329	20	318	5	3.46
XJ09-092-67	0.88	0.05297	0.0022	0.39447	0.01631	0.05401	0.00078	328	67	338	12	339	5	-0.29
XJ09-092-68	1.02	0.05409	0.0027	0.40108	0.01982	0.05378	0.00082	375	84	342	14	338	5	1.18
XJ09-092-69	0.66	0.05613	0.00599	0.42762	0.04517	0.05525	0.00112	458	201	361	32	347	7	4.03

XJ09-092-70	1.27	0.05137	0.00428	0.3678	0.03038	0.05193	0.0009	257	156	318	23	326	6	-2.45
~~**XJ09-092-71**~~	~~0.7~~	~~0.04605~~	~~0.00684~~	~~0.31332~~	~~0.04627~~	~~0.04935~~	~~0.00079~~	~~—~~	~~271~~	~~277~~	~~36~~	~~311~~	~~5~~	~~-10.93~~
XJ09-092-72	1.2	0.05106	0.00185	0.34869	0.01256	0.04953	0.00068	244	58	304	9	312	4	-2.56
XJ09-092-73	0.42	0.09125	0.00222	3.29528	0.08117	0.26192	0.00338	1452	28	1480	19	1500	17	-3.2
XJ09-092-74	1.02	0.05418	0.00221	0.55214	0.02234	0.07391	0.00105	379	65	446	15	460	6	-3.04
XJ09-092-75	0.63	0.05371	0.00216	0.39911	0.01598	0.05389	0.00077	359	64	341	12	338	5	0.89
XJ09-092-76	0.74	0.05166	0.00147	0.31604	0.00903	0.04437	0.00058	270	42	279	7	280	4	-0.36
XJ09-092-77	0.58	0.05412	0.00278	0.3714	0.01889	0.04977	0.00077	376	87	321	14	313	5	2.56
XJ09-092-78	0.48	0.04836	0.00591	0.31985	0.03882	0.04797	0.00097	117	231	282	30	302	6	-6.62
XJ09-092-79	0.92	0.05219	0.00222	0.3644	0.01541	0.05064	0.00073	294	70	315	11	318	4	-0.94
XJ09-092-80	1.07	0.05409	0.00175	0.38585	0.01246	0.05173	0.0007	375	48	331	9	325	4	1.85
XJ09-092-81	0.49	0.05116	0.00193	0.36941	0.01388	0.05237	0.00073	248	61	319	10	329	4	-3.04
XJ09-092-82	1.07	0.05404	0.00291	0.37697	0.0201	0.05059	0.00079	373	92	325	15	318	5	2.2
XJ09-092-83	0.89	0.05583	0.00181	0.38782	0.01253	0.05038	0.00068	446	48	333	9	317	4	5.05
XJ09-092-84	0.87	0.05738	0.00434	0.40846	0.03057	0.05163	0.00092	506	134	348	22	325	6	7.08
XJ09-092-85	0.4	0.05519	0.00371	0.39146	0.02608	0.05145	0.00086	420	119	335	19	323	5	3.72
XJ09-092-86	1.56	0.05207	0.00161	0.39188	0.01216	0.05459	0.00073	288	46	336	9	343	4	-2.04
XJ09-092-87	1.53	0.05427	0.00629	0.3534	0.04041	0.04723	0.0009	382	265	307	30	297	6	3.37

XJ09-092-88	0.94	0.05571	0.00238	0.39118	0.01658	0.05093	0.00075	441	68	335	12	320	5	4.69
XJ09-092-89	0.69	0.05661	0.00299	0.4188	0.02193	0.05365	0.00084	476	88	355	16	337	5	5.34
XJ09-092-90	0.47	0.05604	0.00282	0.3923	0.01957	0.05077	0.00078	454	83	336	14	319	5	5.33
XJ09-092-91	0.77	0.05468	0.00224	0.38772	0.01576	0.05143	0.00074	399	65	333	12	323	5	3.1
XJ09-092-92	0.95	0.05366	0.00208	0.39722	0.0153	0.05369	0.00076	357	61	340	11	337	5	0.89
XJ09-092-93	0.78	0.05105	0.00404	0.35916	0.0282	0.05103	0.00089	243	146	312	21	321	5	-2.8
XJ09-092-94	1.98	0.05301	0.00213	0.37985	0.01519	0.05197	0.00074	329	65	327	11	327	5	0
XJ09-092-95	0.57	0.05144	0.00185	0.354	0.01268	0.04991	0.00069	261	57	308	10	314	4	-1.91
XJ09-092-96	0.49	0.05397	0.00241	0.4437	0.01969	0.05963	0.00088	370	73	373	14	373	5	0
XJ09-092-97	0.79	0.05241	0.00311	0.37623	0.02213	0.05206	0.00084	303	105	324	16	327	5	-0.92
XJ09-092-98	0.53	0.05322	0.00186	0.37123	0.01294	0.05059	0.0007	338	54	321	10	318	4	0.94
XJ09-092-99	0.63	0.05377	0.00258	0.40249	0.01912	0.05429	0.00082	361	80	343	14	341	5	0.59
XJ09-092-100	1.22	0.05324	0.00203	0.36293	0.01378	0.04944	0.0007	339	60	314	10	311	4	0.96
XJ10-009														
XJ10-009-1	1.07	0.14424	0.00397	8.43513	0.23732	0.42391	0.00615	2279	29	2279	26	2278	28	0.04
XJ10-009-2	0.83	0.05116	0.00172	0.27926	0.00947	0.03957	0.00059	248	51	250	8	250	4	0
XJ10-009-3	0.99	0.16927	0.00472	11.34535	0.32266	0.48585	0.00711	2550	28	2552	27	2553	31	-0.12
XJ10-009-4	0.25	0.05477	0.00178	0.53229	0.01742	0.07045	0.00105	403	47	433	12	439	6	-1.37

XJ10-009-5	0.72	0.05169	0.0032	0.31319	0.01924	0.04392	0.00075	272	110	277	15	277	5	0
XJ10-009-6	0.46	0.06069	0.00209	0.85691	0.02973	0.10235	0.00155	628	49	628	16	628	9	0
XJ10-009-7	0.16	0.06941	0.00234	1.46004	0.0494	0.15248	0.00231	911	45	914	20	915	13	-0.11
XJ10-009-8	0.6	0.06671	0.0024	1.15168	0.0415	0.12514	0.00193	829	49	778	20	760	11	2.37
XJ10-009-9	0.57	0.06298	0.00242	1.00623	0.0387	0.11581	0.0018	708	55	707	20	706	10	0.14
XJ10-009-10	1.04	0.05323	0.00314	0.39843	0.02348	0.05426	0.00085	339	105	341	17	341	5	0
XJ10-009-11	0.65	0.0529	0.00258	0.37297	0.01803	0.05111	0.00085	325	79	322	13	321	5	0.31
XJ10-009-12	0.93	0.05395	0.00252	0.42989	0.02002	0.05776	0.00092	369	76	363	14	362	6	0.28
XJ10-009-13	0.6	0.06509	0.00238	0.91245	0.03328	0.10161	0.00156	777	51	658	18	624	9	5.45
XJ10-009-14	0.83	0.05291	0.00303	0.37535	0.02137	0.05142	0.00085	325	99	324	16	323	5	0.31
XJ10-009-15	0.85	0.11837	0.00406	5.45941	0.1872	0.33436	0.00508	1932	40	1894	29	1859	25	3.93
XJ10-009-16	0.8	0.07134	0.00284	1.62739	0.06424	0.16537	0.00265	967	54	981	25	987	15	-0.61
XJ10-009-17	1.32	0.06538	0.0041	1.17953	0.07293	0.13078	0.00247	787	98	791	34	792	14	-0.13
XJ10-009-18	0.96	0.09164	0.00328	3.22425	0.11519	0.25506	0.00391	1460	45	1463	28	1465	20	-0.34
XJ10-009-19	0.63	0.05512	0.00411	0.32413	0.02352	0.04265	0.00072	417	171	285	18	269	4	5.95
XJ10-009-20	0.53	0.15048	0.00552	9.14062	0.33334	0.44037	0.0068	2351	41	2352	33	2352	30	-0.04
XJ10-009-21	0.28	0.05876	0.00274	0.66503	0.03058	0.08205	0.00138	558	71	518	19	508	8	1.97
XJ10-009-22	0.78	0.05303	0.00285	0.3837	0.02039	0.05245	0.0009	330	89	330	15	330	6	0

XJ10-009-23	0.52	0.15925	0.00627	10.09691	0.39339	0.45968	0.00724	2448	45	2444	36	2438	32	0.41
XJ10-009-24	0.77	0.0524	0.0027	0.35576	0.01811	0.04922	0.00081	303	86	309	14	310	5	-0.32
~~**XJ10-009-25**~~	~~0.67~~	~~0.16164~~	~~0.00711~~	~~5.44814~~	~~0.23506~~	~~0.24438~~	~~0.00423~~	~~2473~~	~~49~~	~~1892~~	~~37~~	~~1409~~	~~22~~	~~75.51~~
XJ10-009-26	0.79	0.05614	0.00281	0.56971	0.02802	0.07358	0.00126	458	79	458	18	458	8	0
XJ10-009-27	0.49	0.05567	0.00317	0.53602	0.03002	0.06982	0.00123	439	93	436	20	435	7	0.23
XJ10-009-28	1.12	0.12713	0.00587	6.04023	0.27383	0.3445	0.00587	2059	56	1982	39	1908	28	7.91
XJ10-009-29	0.46	0.07192	0.00352	1.62306	0.0778	0.16365	0.00281	984	69	979	30	977	16	0.2
XJ10-009-30	0.31	0.07223	0.00342	1.65764	0.07688	0.16641	0.00281	992	67	992	29	992	16	0
XJ10-009-31	0.79	0.05556	0.00504	0.53393	0.04793	0.06969	0.00134	435	167	434	32	434	8	0
XJ09-094														
XJ09-094-1	1.42	0.05242	0.00147	0.37004	0.01041	0.05119	0.00067	304	40	320	8	322	4	-0.62
XJ09-094-2	1.02	0.05059	0.00169	0.36138	0.01205	0.0518	0.00069	222	52	313	9	326	4	-3.99
XJ09-094-3	1.31	0.05032	0.00135	0.34382	0.00927	0.04955	0.00064	210	39	300	7	312	4	-3.85
XJ09-094-4	1.04	0.05317	0.00135	0.38316	0.00986	0.05226	0.00067	336	35	329	7	328	4	0.3
XJ09-094-5	0.48	0.05274	0.00109	0.38349	0.00815	0.05273	0.00066	318	26	330	6	331	4	-0.3
XJ09-094-6	0.6	0.05366	0.00167	0.39579	0.01229	0.05348	0.00071	357	46	339	9	336	4	0.89
XJ09-094-7	0.79	0.05193	0.00113	0.34483	0.00764	0.04815	0.0006	282	29	301	6	303	4	-0.66
XJ09-094-8	1.69	0.05378	0.00195	0.38764	0.01397	0.05226	0.00072	362	56	333	10	328	4	1.52

XJ09-094-9	0.83	0.05501	0.00183	0.40915	0.01356	0.05394	0.00073	413	50	348	10	339	4	2.65
XJ09-094-10	1.21	0.05276	0.00149	0.3855	0.01091	0.05298	0.00069	318	41	331	8	333	4	-0.6
XJ09-094-11	0.71	0.05427	0.00131	0.43034	0.01054	0.0575	0.00073	382	33	363	7	360	4	0.83
XJ09-094-12	0.71	0.054	0.00135	0.40653	0.01026	0.05459	0.0007	371	34	346	7	343	4	0.87
~~**XJ09-094-13**~~	~~1.11~~	~~0.04566~~	~~0.00207~~	~~0.34965~~	~~0.01577~~	~~0.05553~~	~~0.00077~~	~~-20~~	~~68~~	~~304~~	~~12~~	~~348~~	~~5~~	~~-12.64~~
XJ09-094-14	0.85	0.05214	0.00101	0.37857	0.00753	0.05265	0.00065	292	24	326	6	331	4	-1.51
XJ09-094-15	0.89	0.05223	0.00145	0.4416	0.01234	0.06131	0.0008	295	40	371	9	384	5	-3.39
XJ09-094-16	0.92	0.05234	0.00227	0.39189	0.01692	0.05429	0.00077	300	72	336	12	341	5	-1.47
XJ09-094-17	0.68	0.05486	0.00218	0.40756	0.01612	0.05388	0.00076	407	63	347	12	338	5	2.66
XJ09-094-18	1.04	0.05417	0.00214	0.37575	0.01477	0.0503	0.0007	378	63	324	11	316	4	2.53
XJ09-094-19	0.71	0.0526	0.00189	0.39092	0.01398	0.0539	0.00073	312	57	335	10	338	4	-0.89
XJ09-094-20	0.66	0.0559	0.0026	0.39481	0.01821	0.05122	0.00076	448	76	338	13	322	5	4.97
XJ09-094-21	0.66	0.05594	0.00124	0.51005	0.01146	0.06612	0.00083	450	28	418	8	413	5	1.21
XJ09-094-22	0.47	0.05244	0.00271	0.37329	0.01912	0.05162	0.00078	305	89	322	14	324	5	-0.62
XJ09-094-23	0.6	0.05166	0.00102	0.35953	0.00731	0.05046	0.00062	270	25	312	5	317	4	-1.58
XJ09-094-24	0.91	0.05122	0.0022	0.37779	0.01612	0.05349	0.00075	251	72	325	12	336	5	-3.27
XJ09-094-25	1.39	0.05118	0.00146	0.42514	0.01219	0.06023	0.00079	249	42	360	9	377	5	-4.51
XJ09-094-26	0.82	0.05239	0.00133	0.38251	0.00979	0.05295	0.00068	302	35	329	7	333	4	-1.2

XJ09-094-27	0.6	0.05185	0.0021	0.36998	0.0149	0.05174	0.00072	279	67	320	11	325	4	-1.54
XJ09-094-28	0.81	0.0509	0.0024	0.38003	0.01777	0.05415	0.00079	236	81	327	13	340	5	-3.82
XJ09-094-29	0.41	0.05371	0.00288	0.3772	0.02008	0.05093	0.00076	359	93	325	15	320	5	1.56
XJ09-094-30	0.87	0.05485	0.00191	0.39404	0.01363	0.05209	0.00071	406	53	337	10	327	4	3.06
XJ09-094-31	0.89	0.05193	0.00177	0.38266	0.01303	0.05343	0.00072	282	53	329	10	336	4	-2.08
XJ09-094-32	0.95	0.0521	0.00134	0.35955	0.00928	0.05004	0.00064	290	36	312	7	315	4	-0.95
XJ09-094-33	1.56	0.05631	0.00138	0.38131	0.00942	0.04911	0.00063	465	32	328	7	309	4	6.15
XJ09-094-34	1.04	0.05082	0.00163	0.35741	0.01147	0.051	0.00068	233	49	310	9	321	4	-3.43
XJ09-094-35	0.57	0.05393	0.00326	0.37283	0.02234	0.05013	0.00079	368	107	322	17	315	5	2.22
XJ09-094-36	0.84	0.0504	0.00155	0.35334	0.01087	0.05084	0.00067	213	47	307	8	320	4	-4.06
XJ09-094-37	1.2	0.05211	0.00128	0.36533	0.00904	0.05084	0.00065	290	34	316	7	320	4	-1.25
XJ09-094-38	0.82	0.05123	0.00231	0.3734	0.01672	0.05285	0.00075	251	77	322	12	332	5	-3.01
XJ09-094-39	0.72	0.05613	0.00251	0.40939	0.01814	0.05289	0.00077	458	72	348	13	332	5	4.82
XJ09-094-40	0.6	0.05061	0.00142	0.40868	0.0115	0.05856	0.00076	223	41	348	8	367	5	-5.18
XJ09-094-41	1.04	0.05079	0.00258	0.36043	0.01819	0.05146	0.00075	231	90	313	14	323	5	-3.1
XJ09-094-42	0.92	0.05068	0.00218	0.3614	0.01548	0.05171	0.00073	226	73	313	12	325	4	-3.69
XJ09-094-43	0.98	0.05235	0.00155	0.37299	0.01107	0.05167	0.00068	301	44	322	8	325	4	-0.92
XJ09-094-44	0.5	0.05553	0.00245	0.49355	0.02164	0.06446	0.00092	434	72	407	15	403	6	0.99

XJ09-094-45	0.71	0.05097	0.00304	0.37369	0.02212	0.05317	0.00083	239	108	322	16	334	5	-3.59
XJ09-094-46	0.64	0.05052	0.0024	0.36089	0.01704	0.0518	0.00075	219	82	313	13	326	5	-3.99
XJ09-094-47	0.82	0.04934	0.00315	0.34097	0.02163	0.05012	0.00078	164	115	298	16	315	5	-5.4
XJ09-094-48	0.57	0.05154	0.00284	0.42123	0.02305	0.05926	0.00089	265	98	357	16	371	5	-3.77
XJ09-094-49	0.6	0.05272	0.00261	0.38748	0.01903	0.05329	0.00078	317	85	333	14	335	5	-0.6
XJ09-094-50	0.23	0.05413	0.00176	0.38183	0.01236	0.05115	0.00069	376	48	328	9	322	4	1.86
XJ09-094-51	1.3	0.05042	0.0017	0.3477	0.01168	0.05	0.00067	214	53	303	9	315	4	-3.81
XJ09-094-52	0.87	0.05211	0.00208	0.3811	0.01511	0.05304	0.00074	290	65	328	11	333	5	-1.5
~~**XJ09-094-53**~~	~~0.79~~	~~0.04154~~	~~0.00244~~	~~0.30296~~	~~0.01769~~	~~0.05288~~	~~0.00077~~	~~202~~	~~105~~	~~269~~	~~14~~	~~332~~	~~5~~	~~-18.98~~
XJ09-094-54	1.05	0.05262	0.00161	0.36234	0.01106	0.04993	0.00066	312	45	314	8	314	4	0
XJ09-094-55	0.52	0.05506	0.00135	0.55538	0.01368	0.07314	0.00093	415	33	449	9	455	6	-1.32
XJ09-094-56	1.41	0.05307	0.00133	0.36778	0.00928	0.05025	0.00064	332	34	318	7	316	4	0.63
XJ09-094-57	0.94	0.05087	0.00223	0.36277	0.01579	0.05172	0.00073	235	74	314	12	325	4	-3.38
XJ09-094-58	0.78	0.05162	0.00186	0.36984	0.01327	0.05196	0.00071	269	57	320	10	327	4	-2.14
XJ09-094-59	0.89	0.05335	0.0014	0.37801	0.00998	0.05138	0.00066	344	37	326	7	323	4	0.93
XJ09-094-60	0.46	0.05198	0.00156	0.47344	0.0142	0.06604	0.00087	285	45	394	10	412	5	-4.37
XJ09-094-61	0.7	0.05087	0.00255	0.37479	0.01859	0.05342	0.00079	235	87	323	14	335	5	-3.58
XJ09-094-62	0.86	0.0573	0.00231	0.39912	0.0159	0.05051	0.00072	503	62	341	12	318	4	7.23

XJ09-094-63	1.07	0.05313	0.00174	0.38174	0.01243	0.0521	0.0007	334	49	328	9	327	4	0.31
XJ09-094-64	0.78	0.05298	0.00282	0.39307	0.02016	0.05381	0.00075	328	124	337	15	338	5	-0.3
XJ09-094-65	0.76	0.05541	0.00157	0.39665	0.01121	0.05191	0.00068	429	40	339	8	326	4	3.99
XJ09-094-66	0.83	0.05436	0.00171	0.39709	0.01243	0.05297	0.00071	386	46	340	9	333	4	2.1
XJ09-094-67	1.36	0.05132	0.00169	0.36911	0.01211	0.05215	0.0007	255	51	319	9	328	4	-2.74
XJ09-094-68	0.71	0.05568	0.00213	0.40682	0.01543	0.05298	0.00075	440	59	347	11	333	5	4.2
XJ09-094-69	0.71	0.0502	0.00154	0.36037	0.01101	0.05205	0.00069	204	46	312	8	327	4	-4.59
XJ09-094-70	1.37	0.05206	0.00144	0.35928	0.00994	0.05004	0.00065	288	40	312	7	315	4	-0.95
XJ09-094-71	0.51	0.05307	0.00138	0.37186	0.0097	0.05081	0.00066	332	36	321	7	319	4	0.63
XJ09-094-72	0.96	0.0521	0.00248	0.35931	0.01693	0.05001	0.00073	290	81	312	13	315	4	-0.95
XJ09-094-73	0.89	0.05321	0.00149	0.3679	0.01026	0.05014	0.00066	338	39	318	8	315	4	0.95
XJ09-094-74	0.59	0.05436	0.0023	0.45433	0.01901	0.06061	0.00087	386	68	380	13	379	5	0.26
XJ09-094-75	1.18	0.05868	0.00154	0.4184	0.01098	0.0517	0.00067	555	35	355	8	325	4	9.23
XJ09-094-76	1.13	0.05319	0.00144	0.36658	0.00992	0.04998	0.00065	337	38	317	7	314	4	0.96
XJ09-094-77	1.06	0.05412	0.00235	0.4054	0.01737	0.05431	0.0008	376	70	346	13	341	5	1.47
XJ09-094-78	1.06	0.05267	0.00185	0.36875	0.01289	0.05076	0.0007	315	54	319	10	319	4	0
XJ09-094-79	0.85	0.05194	0.00161	0.35997	0.01111	0.05025	0.00067	283	46	312	8	316	4	-1.27
XJ09-094-80	0.51	0.05397	0.00144	0.40889	0.01093	0.05493	0.00071	370	37	348	8	345	4	0.87

XJ09-094-81	0.75	0.05008	0.00156	0.35681	0.01106	0.05167	0.00069	199	47	310	8	325	4	-4.62
XJ09-094-82	1.05	0.052	0.00184	0.3687	0.01294	0.05142	0.00071	285	55	319	10	323	4	-1.24
XJ09-094-83	0.86	0.05512	0.00137	0.40649	0.01013	0.05348	0.00069	417	33	346	7	336	4	2.98
XJ09-094-84	0.87	0.05311	0.00171	0.38241	0.01222	0.05221	0.0007	333	48	329	9	328	4	0.3
XJ09-094-85	1.07	0.04954	0.00239	0.36826	0.01757	0.0539	0.0008	173	83	318	13	338	5	-5.92
XJ09-094-86	1.03	0.05303	0.00137	0.37916	0.00976	0.05184	0.00067	330	35	326	7	326	4	0
XJ09-094-87	0.77	0.05599	0.00235	0.41149	0.01707	0.0533	0.00077	452	66	350	12	335	5	4.48
XJ09-094-88	0.77	0.05463	0.00138	0.50176	0.01272	0.06661	0.00086	397	34	413	9	416	5	-0.72
XJ09-094-89	0.64	0.05055	0.00307	0.36971	0.02215	0.05303	0.00088	220	107	319	16	333	5	-4.2
XJ09-094-90	0.75	0.05283	0.00176	0.383	0.01265	0.05257	0.00071	322	50	329	9	330	4	-0.3
XJ09-094-91	0.92	0.05412	0.00189	0.36592	0.01267	0.04903	0.00067	376	53	317	9	309	4	2.59
XJ09-094-92	0.57	0.0514	0.00288	0.37687	0.02089	0.05317	0.00082	259	99	325	15	334	5	-2.69
XJ09-094-93	1.62	0.05158	0.00153	0.35835	0.01053	0.05038	0.00067	267	43	311	8	317	4	-1.89
XJ09-094-94	1.15	0.05098	0.00227	0.3499	0.01542	0.04977	0.00071	240	75	305	12	313	4	-2.56
XJ09-094-95	0.79	0.05586	0.00192	0.54876	0.01869	0.07123	0.00098	447	51	444	12	444	6	0
XJ09-094-96	1.25	0.05261	0.00221	0.39159	0.01627	0.05397	0.00079	312	68	336	12	339	5	-0.88
XJ09-094-97	1.38	0.05294	0.00177	0.371	0.01226	0.05082	0.00069	326	50	320	9	320	4	0
XJ09-094-98	1.11	0.05254	0.00211	0.36467	0.01447	0.05033	0.00073	309	64	316	11	317	4	-0.32

XJ09-094-99	0.83	0.05274	0.00212	0.3759	0.01493	0.05168	0.00074	318	64	324	11	325	5	-0.31
XJ09-094-100	1.2	0.05309	0.00169	0.38105	0.01202	0.05205	0.0007	333	47	328	9	327	4	0.31
XJ10-011														
XJ10-011-1	1	0.05319	0.00191	0.39038	0.01423	0.05323	0.00077	337	56	335	10	334	5	0.3
XJ10-011-2	0.69	0.05644	0.00183	0.58615	0.01934	0.07532	0.0011	470	47	468	12	468	7	0
XJ10-011-3	0.83	0.05293	0.00252	0.38181	0.01828	0.05232	0.00079	326	81	328	13	329	5	-0.3
XJ10-011-4	0.37	0.05681	0.00133	0.6071	0.01483	0.0775	0.00108	484	30	482	9	481	6	0.21
XJ10-011-5	0.61	0.05342	0.00165	0.40445	0.01274	0.0549	0.00078	347	46	345	9	345	5	0
XJ10-011-6	0.56	0.05544	0.00113	0.52777	0.01146	0.06904	0.00096	430	25	430	8	430	6	0
XJ10-011-7	0.68	0.05433	0.00149	0.45817	0.01293	0.06116	0.00086	385	38	383	9	383	5	0
XJ10-011-8	1.04	0.05351	0.00146	0.41742	0.01168	0.05657	0.00081	350	38	354	8	355	5	-0.28
XJ10-011-9	0.35	0.07483	0.00117	1.81728	0.03175	0.17611	0.00238	1064	16	1052	11	1046	13	1.72
XJ10-011-10	0.5	0.05589	0.00161	0.55387	0.01636	0.07186	0.00101	448	41	448	11	447	6	0.22
XJ10-011-11	0.55	0.0533	0.00237	0.38061	0.01699	0.05178	0.00079	342	73	327	12	325	5	0.62
XJ10-011-12	0.87	0.05278	0.00123	0.37123	0.00908	0.05101	0.0007	319	31	321	7	321	4	0
XJ10-011-13	0.64	0.05677	0.00303	0.53578	0.02734	0.06845	0.00105	482	121	436	18	427	6	2.11
XJ10-011-14	0.66	0.05425	0.0014	0.41509	0.01108	0.05549	0.00078	381	35	353	8	348	5	1.44
XJ10-011-15	0.56	0.05559	0.00148	0.53784	0.01487	0.07016	0.00098	436	37	437	10	437	6	0

XJ10-011-16	0.65	0.08803	0.00134	2.90574	0.04986	0.23938	0.00323	1383	15	1383	13	1383	17	0
XJ10-011-17	0.78	0.05343	0.00119	0.38394	0.00902	0.05211	0.00071	347	29	330	7	327	4	0.92
XJ10-011-18	1.2	0.05222	0.00101	0.36173	0.00754	0.05023	0.00069	295	24	314	6	316	4	-0.63
XJ10-011-19	1.09	0.05298	0.00105	0.38041	0.00805	0.05207	0.00071	328	25	327	6	327	~~4~~	0
XJ10-011-20	0.69	0.05471	0.00143	0.48098	0.01303	0.06375	0.00089	400	36	399	9	398	5	0.25
XJ10-011-21	0.16	0.06968	0.00109	1.47257	0.02585	0.15325	0.00206	919	17	919	11	919	12	0
XJ10-011-22	0.87	0.05644	0.00193	0.57587	0.01997	0.07399	0.00107	470	51	462	13	460	6	0.43
XJ10-011-23	0.81	0.05356	0.00152	0.4121	0.01202	0.05579	0.00079	353	41	350	9	350	5	0
XJ10-011-24	0.5	0.0549	0.00116	0.49522	0.01107	0.06541	0.0009	408	27	408	8	408	5	0
XJ10-011-25	0.78	0.07359	0.0038	1.70271	0.08345	0.1678	0.0027	1030	107	1010	31	1000	15	3
XJ10-011-26	0.7	0.05477	0.00156	0.48813	0.01425	0.06463	0.00092	403	40	404	10	404	6	0
XJ10-011-27	1	0.05291	0.0022	0.37806	0.01574	0.05181	0.00079	325	67	326	12	326	5	0
~~**XJ10-011-28**~~	~~1.11~~	~~0.06562~~	~~0.00241~~	~~0.43123~~	~~0.01599~~	~~0.04766~~	~~0.00071~~	~~794~~	~~53~~	~~364~~	~~11~~	~~300~~	~~4~~	~~21.33~~
XJ10-011-29	0.82	0.05573	0.00131	0.54041	0.01332	0.07031	0.00097	442	31	439	9	438	6	0.23
XJ10-011-30	0.42	0.0559	0.00189	0.32607	0.01115	0.0423	0.00063	448	50	287	9	267	~~4~~	7.49
XJ10-011-31	0.64	0.05371	0.00256	0.42331	0.02028	0.05715	0.00085	359	81	358	14	358	5	0
XJ10-011-32	0.3	0.05433	0.00137	0.46101	0.01204	0.06153	0.00087	385	34	385	8	385	5	0
XJ10-011-33	0.65	0.19145	0.00299	14.06934	0.24592	0.5329	0.00727	2755	13	2754	17	2754	31	0.04

XJ10-011-34	0.78	0.05488	0.0015	0.4934	0.01389	0.0652	0.00093	407	38	407	9	407	6	0
XJ10-011-35	0.93	0.05354	0.00172	0.41244	0.01345	0.05586	0.0008	352	48	351	10	350	5	0.29
XJ10-011-36	0.72	0.05403	0.00122	0.44329	0.01048	0.05949	0.00082	372	29	373	7	373	5	0
XJ10-011-37	0.31	0.05601	0.00155	0.56566	0.01612	0.07324	0.00103	453	39	455	10	456	6	-0.22
XJ10-011-38	0.65	0.20319	0.00323	15.59344	0.27624	0.5565	0.0076	2852	13	2852	17	2852	31	0
XJ10-011-39	0.82	0.05301	0.00171	0.38407	0.01259	0.05254	0.00076	329	48	330	9	330	5	0
XJ10-011-40	0.62	0.05416	0.00272	0.41675	0.01993	0.05581	0.00084	378	116	354	14	350	5	1.14
XJ10-011-41	0.91	0.05497	0.0014	0.49782	0.01308	0.06567	0.00093	411	34	410	9	410	6	0
XJ10-011-42	0.74	0.09845	0.00162	3.81015	0.06928	0.28063	0.0038	1595	16	1595	15	1595	19	0
XJ10-011-43	1.21	0.05233	0.0018	0.34469	0.01202	0.04777	0.00069	300	53	301	9	301	4	0
XJ10-011-44	0.75	0.0531	0.00138	0.38725	0.01043	0.05289	0.00074	333	36	332	8	332	5	0
XJ10-011-45	0.94	0.05844	0.00355	0.40143	0.02353	0.04982	0.00079	546	136	343	17	313	5	9.58
XJ10-011-46	0.55	0.05397	0.00139	0.44199	0.01181	0.05938	0.00084	370	35	372	8	372	5	0
XJ10-011-47	0.46	0.07441	0.0015	1.80585	0.03886	0.17599	0.00243	1053	22	1048	14	1045	13	0.77
XJ10-011-48	0.84	0.0536	0.00178	0.41896	0.01414	0.05668	0.00082	354	50	355	10	355	5	0
XJ10-011-49	0.53	0.05605	0.00107	0.56478	0.01154	0.07306	0.001	454	23	455	7	455	6	0
XJ10-011-50	0.73	0.05415	0.00125	0.44951	0.01087	0.06019	0.00084	377	30	377	8	377	5	0
XJ10-011-51	0.84	0.06133	0.0022	0.5506	0.01981	0.0651	0.001	651	51	445	13	407	6	9.34

XJ10-011-52	0.43	0.05581	0.00106	0.55089	0.01127	0.07157	0.00097	445	23	446	7	446	6	0
XJ10-011-53	0.58	0.05623	0.00129	0.57104	0.01371	0.07364	0.00102	461	30	459	9	458	6	0.22
XJ10-011-54	0.3	0.06928	0.00141	1.4404	0.0312	0.15076	0.00208	907	23	906	13	905	12	0.11
XJ10-011-55	1.05	0.05435	0.00405	0.45417	0.03338	0.0606	0.00123	386	129	380	23	379	7	0.26
XJ10-011-56	0.43	0.17859	0.00298	12.44679	0.22891	0.50537	0.00684	2640	15	2639	17	2637	29	0.11
XJ10-011-57	0.91	0.1014	0.00181	4.07651	0.07894	0.2915	0.00398	1650	18	1650	16	1649	20	0.06
XJ10-011-58	0.53	0.05321	0.00222	0.39574	0.01664	0.05393	0.0008	338	68	339	12	339	5	0
XJ10-011-59	0.58	0.05579	0.00155	0.55396	0.0158	0.072	0.00103	444	38	448	10	448	6	0
XJ10-011-60	0.95	0.05332	0.0015	0.37178	0.01072	0.05056	0.00073	342	39	321	8	318	4	0.94
XJ10-011-61	0.7	0.05454	0.00127	0.47614	0.01158	0.0633	0.00088	393	30	395	8	396	5	-0.25
XJ10-011-62	0.56	0.0545	0.0014	0.43811	0.0116	0.05829	0.00082	392	35	369	8	365	5	1.1
XJ10-011-63	0.91	0.0556	0.00127	0.53322	0.01277	0.06954	0.00096	436	30	434	8	433	6	0.23
XJ10-011-64	0.65	0.05262	0.00284	0.35902	0.01938	0.04947	0.00076	312	95	311	14	311	5	0
XJ10-011-65	0.67	0.05233	0.00279	0.33588	0.01786	0.04655	0.00076	300	91	294	14	293	5	0.34
XJ10-011-66	0.99	0.05508	0.00189	0.50636	0.01756	0.06666	0.00098	415	51	416	12	416	6	0
XJ10-011-67	0.57	0.05312	0.00122	0.38974	0.00937	0.0532	0.00074	334	30	334	7	334	5	0
XJ10-011-68	1.57	0.0523	0.00346	0.33839	0.02211	0.04691	0.00089	299	115	296	17	296	5	0
XJ10-011-69	0.58	0.05393	0.00137	0.43817	0.0115	0.05892	0.00083	368	34	369	8	369	5	0

XJ10-011-70	0.46	0.04872	0.00117	0.13748	0.00344	0.02046	0.00028	134	34	131	3	131	2	0
XJ10-011-71	0.77	0.08727	0.00164	2.78074	0.05604	0.23104	0.00316	1366	19	1350	15	1340	17	1.94
XJ10-011-72	0.74	0.05741	0.00123	0.61453	0.01382	0.07762	0.00107	507	26	486	9	482	6	0.83
XJ10-011-73	0.61	0.05296	0.00158	0.3784	0.01153	0.0518	0.00074	327	43	326	8	326	5	0
XJ10-011-74	1	0.05377	0.00158	0.42748	0.01283	0.05765	0.00082	361	42	361	9	361	5	0
XJ10-011-75	0.96	0.05334	0.00149	0.40429	0.0116	0.05496	0.00077	343	40	345	8	345	5	0
XJ10-011-76	0.66	0.05676	0.00136	0.56593	0.01407	0.0723	0.00101	482	31	455	9	450	6	1.11
XJ10-011-77	0.62	0.05305	0.00163	0.38083	0.01186	0.05205	0.00076	331	44	328	9	327	5	0.31
XJ10-011-78	0.43	0.05276	0.00233	0.36571	0.01615	0.05026	0.00077	318	72	316	12	316	5	0
XJ10-011-79	1.01	0.05245	0.00136	0.36793	0.00981	0.05086	0.00071	305	36	318	7	320	4	-0.62
XJ10-011-80	0.6	0.0525	0.00263	0.3505	0.01761	0.04841	0.00073	307	87	305	13	305	4	0
XJ10-011-81	1.6	0.05492	0.00132	0.49829	0.01244	0.06579	0.00092	409	32	411	8	411	6	0
XJ10-011-82	0.62	0.05477	0.00151	0.48464	0.01371	0.06416	0.00091	403	38	401	9	401	6	0
XJ10-011-83	0.69	0.05664	0.00138	0.56398	0.01421	0.0722	0.00101	478	32	454	9	449	6	1.11
XJ10-011-84	0.58	0.05311	0.00149	0.3891	0.01116	0.05313	0.00076	333	39	334	8	334	5	0
XJ10-011-85	1	0.05308	0.00143	0.38494	0.01065	0.05258	0.00075	332	37	331	8	330	5	0.3
XJ10-011-86	0.42	0.05465	0.00162	0.48038	0.0145	0.06374	0.00092	398	42	398	10	398	6	0
XJ10-011-87	0.76	0.05335	0.00198	0.39845	0.01492	0.05415	0.00079	344	58	341	11	340	5	0.29

XJ10-011-88	0.78	0.0532	0.00123	0.3916	0.00945	0.05338	0.00074	337	30	336	7	335	5	0.3
XJ10-011-89	0.62	0.05425	0.00146	0.44555	0.01229	0.05955	0.00085	381	37	374	9	373	5	0.27
XJ10-011-90	0.8	0.10791	0.00235	4.68608	0.10683	0.31489	0.00442	1764	22	1765	19	1765	22	-0.06
XJ10-011-91	0.53	0.05693	0.00145	0.58147	0.01528	0.07406	0.00104	489	34	465	10	461	6	0.87
XJ10-011-92	0.33	0.05582	0.00208	0.48551	0.01668	0.06308	0.0009	445	85	402	11	394	5	2.03
XJ10-011-93	2.09	0.05252	0.00196	0.35255	0.0133	0.04867	0.0007	308	60	307	10	306	4	0.33
XJ10-011-94	0.27	0.05574	0.00129	0.54729	0.01317	0.0712	0.00099	442	30	443	9	443	6	0
XJ10-011-95	0.88	0.05295	0.00214	0.379	0.0154	0.0519	0.00076	327	65	326	11	326	5	0
XJ10-011-96	0.64	0.05318	0.00229	0.35828	0.01547	0.04885	0.00074	336	70	311	12	307	5	1.3
XJ10-011-97	0.74	0.05576	0.00132	0.54889	0.01349	0.07139	0.001	443	31	444	9	445	6	-0.22
XJ10-011-98	0.86	0.0567	0.00153	0.59158	0.01632	0.07565	0.00108	480	36	472	10	470	6	0.43
XJ10-011-99	0.44	0.0521	0.00142	0.31855	0.00892	0.04433	0.00063	290	38	281	7	280	4	0.36
XJ10-011-100	0.78	0.05278	0.0019	0.36154	0.01316	0.04967	0.00072	319	56	313	10	312	4	0.32
XJ09-097														
XJ09-097-1	0.57	0.04963	0.00306	0.31624	0.01935	0.04623	0.00073	178	110	279	15	291	4	-4.12
XJ09-097-2	0.85	0.05157	0.00119	0.37295	0.00873	0.05247	0.00066	266	31	322	6	330	4	-2.42
XJ09-097-3	0.71	0.05199	0.00142	0.39628	0.01091	0.0553	0.00072	285	39	339	8	347	4	-2.31
XJ09-097-4	0.42	0.05296	0.00286	0.34647	0.01854	0.04746	0.00072	327	94	302	14	299	4	1

XJ09-097-5	0.43	0.05536	0.00239	0.36467	0.01559	0.04778	0.0007	427	69	316	12	301	4	4.98
XJ09-097-6	0.99	0.05445	0.00143	0.37367	0.00987	0.04978	0.00064	390	36	322	7	313	4	2.88
XJ09-097-7	0.33	0.05463	0.00121	0.55732	0.0126	0.074	0.00093	397	29	450	8	460	6	-2.17
XJ09-097-8	0.4	0.05594	0.00172	0.58492	0.01796	0.07585	0.00101	450	45	468	12	471	6	-0.64
XJ09-097-9	0.68	0.05253	0.00159	0.36822	0.01115	0.05084	0.00067	309	45	318	8	320	4	-0.62
XJ09-097-10	0.85	0.04978	0.00245	0.32973	0.01611	0.04804	0.0007	185	86	289	12	302	4	-4.3
XJ09-097-11	0.41	0.05197	0.00274	0.33748	0.01762	0.0471	0.00071	284	92	295	13	297	4	-0.67
XJ09-097-12	0.38	0.05818	0.00169	0.5944	0.01732	0.07411	0.00098	537	41	474	11	461	6	2.82
XJ09-097-13	0.19	0.05934	0.00236	0.67238	0.02654	0.08219	0.00118	580	61	522	16	509	7	2.55
XJ09-097-14	0.63	0.05613	0.0012	0.48999	0.01066	0.06331	0.00079	458	27	405	7	396	5	2.27
XJ09-097-15	0.53	0.052	0.0013	0.34571	0.00875	0.04822	0.00061	285	35	301	7	304	4	-0.99
XJ09-097-16	0.37	0.05376	0.00152	0.35803	0.01016	0.0483	0.00063	361	41	311	8	304	4	2.3
XJ09-097-17	0.51	0.05119	0.00258	0.28262	0.01411	0.04004	0.00059	249	88	253	11	253	4	0
XJ09-097-18	0.49	0.04906	0.00156	0.26165	0.00831	0.03868	0.00051	151	50	236	7	245	3	-3.67
XJ09-097-19	0.38	0.05674	0.00169	0.58588	0.01748	0.07488	0.00099	481	43	468	11	465	6	0.65
XJ09-097-20	0.4	0.05722	0.00181	0.60419	0.01906	0.07658	0.00103	500	46	480	12	476	6	0.84
XJ09-097-21	0.25	0.05375	0.00283	0.51712	0.02691	0.06977	0.00111	361	89	423	18	435	7	-2.76
XJ09-097-22	1.04	0.05272	0.00248	0.49239	0.02292	0.06773	0.00101	317	79	407	16	422	6	-3.55

XJ09-097-23	0.63	0.05194	0.00144	0.38346	0.01068	0.05354	0.00069	283	40	330	8	336	4	-1.79
XJ09-097-24	0.68	0.0575	0.00235	0.4223	0.01714	0.05327	0.00076	511	64	358	12	335	5	6.87
XJ09-097-25	0.78	0.05161	0.00196	0.37639	0.01419	0.05289	0.00072	268	61	324	10	332	4	-2.41
XJ09-097-26	0.46	0.05013	0.00272	0.32176	0.01728	0.04655	0.0007	201	96	283	13	293	4	-3.41
XJ09-097-27	0.24	0.05288	0.00229	0.35798	0.01535	0.04909	0.0007	324	71	311	11	309	4	0.65
XJ09-097-28	0.18	0.05227	0.00125	0.33423	0.00808	0.04637	0.00058	297	33	293	6	292	4	0.34
XJ09-097-29	0.73	0.05812	0.00154	0.38201	0.01014	0.04767	0.00061	534	36	329	7	300	4	9.67
XJ09-097-30	0.35	0.05278	0.00121	0.34524	0.00804	0.04743	0.00059	319	31	301	6	299	4	0.67
XJ09-097-31	0.52	0.0517	0.00116	0.35436	0.00804	0.0497	0.00062	272	30	308	6	313	4	-1.6
XJ09-097-32	1.13	0.05478	0.00175	0.38505	0.01229	0.05097	0.00068	403	48	331	9	320	4	3.44
XJ09-097-33	0.29	0.05047	0.00146	0.32729	0.0095	0.04703	0.00061	217	43	287	7	296	4	-3.04
XJ09-097-34	0.32	0.05306	0.00175	0.36815	0.01207	0.05031	0.00067	331	50	318	9	316	4	0.63
XJ09-097-35	0.53	0.05652	0.00155	0.64114	0.0176	0.08225	0.00106	473	38	503	11	510	6	-1.37
XJ09-097-36	0.54	0.05203	0.00125	0.32928	0.00801	0.04589	0.00057	287	33	289	6	289	4	0
XJ09-097-37	0.77	0.052	0.00177	0.37309	0.01263	0.05203	0.0007	285	53	322	9	327	4	-1.53
XJ09-097-38	0.42	0.05863	0.002	0.58455	0.01984	0.0723	0.00099	553	50	467	13	450	6	3.78
XJ09-097-39	0.78	0.04769	0.0029	0.33428	0.02014	0.05083	0.00077	84	105	293	15	320	5	-8.44
XJ09-097-40	0.33	0.05197	0.00219	0.33673	0.01407	0.04698	0.00066	284	70	295	11	296	4	-0.34

XJ09-097-41	0.66	0.05205	0.00168	0.35258	0.01137	0.04912	0.00065	288	49	307	9	309	4	-0.65
XJ09-097-42	0.8	0.05064	0.0022	0.35731	0.01538	0.05116	0.00072	224	73	310	12	322	4	-3.73
XJ09-097-43	0.39	0.05455	0.00154	0.36365	0.01024	0.04834	0.00062	394	40	315	8	304	4	3.62
~~**XJ09-097-44**~~	~~0.32~~	~~0.04647~~	~~0.00234~~	~~0.31782~~	~~0.0159~~	~~0.04959~~	~~0.0007~~	~~22~~	~~80~~	~~280~~	~~12~~	~~312~~	~~4~~	~~-10.26~~
XJ09-097-45	0.58	0.05733	0.0016	0.6606	0.01839	0.08355	0.00108	504	39	515	11	517	6	-0.39
XJ09-097-46	0.32	0.05447	0.00307	0.59565	0.0332	0.0793	0.00123	391	97	474	21	492	7	-3.66
XJ09-097-47	0.61	0.05323	0.00145	0.38582	0.01053	0.05256	0.00067	339	39	331	8	330	4	0.3
XJ09-097-48	1.34	0.05737	0.00167	0.38521	0.0112	0.04868	0.00064	506	41	331	8	306	4	8.17
XJ09-097-49	0.41	0.05378	0.00179	0.35481	0.01175	0.04783	0.00064	362	50	308	9	301	4	2.33
XJ09-097-50	1.02	0.05344	0.00208	0.37329	0.0144	0.05065	0.0007	348	62	322	11	319	4	0.94
XJ09-097-51	0.7	0.05365	0.00201	0.35141	0.01305	0.04749	0.00065	356	59	306	10	299	4	2.34
XJ09-097-52	1.08	0.05083	0.00218	0.35084	0.0149	0.05005	0.00072	233	71	305	11	315	4	-3.17
XJ09-097-53	0.49	0.04977	0.0025	0.33951	0.01685	0.04946	0.00073	184	88	297	13	311	4	-4.5
XJ09-097-54	0.85	0.05222	0.00168	0.37301	0.01193	0.0518	0.00068	295	49	322	9	326	4	-1.23
XJ09-097-55	1.06	0.05325	0.00201	0.34876	0.01302	0.04749	0.00065	339	60	304	10	299	4	1.67
XJ09-097-56	0.71	0.05524	0.00143	0.52584	0.01358	0.06902	0.00087	422	35	429	9	430	5	-0.23
XJ09-097-57	1.19	0.05217	0.00328	0.37915	0.02356	0.0527	0.00082	293	114	326	17	331	5	-1.51
XJ09-097-58	0.52	0.05277	0.00231	0.36413	0.01578	0.05003	0.00071	319	73	315	12	315	4	0

XJ09-097-59	0.09	0.0527	0.00147	0.33551	0.00934	0.04616	0.00059	316	40	294	7	291	4	1.03
XJ09-097-60	0.8	0.05454	0.00215	0.38312	0.01496	0.05093	0.00071	393	62	329	11	320	4	2.81
XJ09-097-61	0.97	0.04821	0.00215	0.33479	0.01477	0.05035	0.00072	110	74	293	11	317	4	-7.57
XJ09-097-62	0.51	0.05821	0.00183	0.57224	0.01779	0.07129	0.00094	538	45	459	11	444	6	3.38
XJ09-097-63	0.2	0.05608	0.00162	0.48886	0.01403	0.06321	0.00081	456	41	404	10	395	5	2.28
XJ09-097-64	0.8	0.052	0.00214	0.35444	0.01444	0.04942	0.00069	285	67	308	11	311	4	-0.96
XJ09-097-65	0.49	0.05552	0.00255	0.36436	0.01652	0.04759	0.00069	433	75	315	12	300	4	5
XJ09-097-66	0.5	0.05307	0.00223	0.35236	0.01464	0.04814	0.00068	332	68	306	11	303	4	0.99
XJ09-097-67	0.29	0.05534	0.00183	0.50005	0.01638	0.06553	0.00087	426	49	412	11	409	5	0.73
XJ09-097-68	0.9	0.05367	0.00186	0.36414	0.01244	0.0492	0.00066	357	53	315	9	310	4	1.61
XJ09-097-69	0.81	0.05388	0.00243	0.38965	0.01731	0.05244	0.00076	366	74	334	13	329	5	1.52
XJ09-097-70	0.32	0.05434	0.00294	0.35133	0.01873	0.04688	0.00073	385	92	306	14	295	4	3.73
XJ09-097-71	0.91	0.05226	0.00189	0.35614	0.01271	0.04942	0.00067	297	57	309	10	311	4	-0.64
XJ09-097-72	0.41	0.05601	0.00251	0.39121	0.01729	0.05065	0.00073	453	72	335	13	319	4	5.02
XJ09-097-73	1.18	0.05424	0.00299	0.37187	0.02019	0.04972	0.00077	381	94	321	15	313	5	2.56
XJ09-097-74	0.71	0.04992	0.00362	0.25707	0.01842	0.03734	0.00061	191	132	232	15	236	4	-1.69
XJ09-097-75	0.5	0.05804	0.0022	0.67058	0.02499	0.08379	0.00117	531	57	521	15	519	7	0.39
XJ09-097-76	0.74	0.05809	0.00332	0.42468	0.02386	0.05302	0.00088	533	94	359	17	333	5	7.81

XJ09-097-77	0.57	0.05348	0.00199	0.40602	0.01486	0.05506	0.00075	349	58	346	11	346	5	0
XJ09-097-78	0.48	0.05006	0.00226	0.31195	0.01386	0.0452	0.00065	198	76	276	11	285	4	-3.16
XJ09-097-79	0.57	0.05641	0.00544	0.48148	0.04587	0.06191	0.00093	468	220	399	31	387	6	3.1
XJ09-097-80	0.65	0.05447	0.00249	0.39176	0.01762	0.05217	0.00077	391	74	336	13	328	5	2.44
XJ09-097-81	0.6	0.05751	0.00183	0.58541	0.01836	0.07383	0.00097	511	46	468	12	459	6	1.96
XJ09-097-82	0.77	0.05319	0.00226	0.3834	0.016	0.05228	0.00075	337	68	330	12	329	5	0.3
XJ09-097-83	0.72	0.05374	0.00202	0.498	0.01838	0.06722	0.00092	360	58	410	12	419	6	-2.15
XJ09-097-84	0.79	0.05555	0.00275	0.43262	0.02101	0.05649	0.00086	434	81	365	15	354	5	3.11
~~**XJ09-097-85**~~	~~0.58~~	~~0.06028~~	~~0.00302~~	~~0.40204~~	~~0.01974~~	~~0.04838~~	~~0.00076~~	~~614~~	~~79~~	~~343~~	~~14~~	~~305~~	~~5~~	~~12.46~~
XJ09-097-86	0.71	0.05067	0.00309	0.35483	0.0213	0.0508	0.00081	226	109	308	16	319	5	-3.45
XJ09-097-87	0.44	0.05753	0.00444	0.38657	0.02941	0.04874	0.00088	512	136	332	22	307	5	8.14
XJ09-097-88	1	0.05365	0.00266	0.37943	0.01847	0.0513	0.00077	356	83	327	14	322	5	1.55
XJ09-097-89	0.55	0.05382	0.00191	0.35659	0.01242	0.04806	0.00064	364	54	310	9	303	4	2.31
XJ09-097-90	1.03	0.05546	0.00267	0.3753	0.01777	0.04909	0.00072	431	79	324	13	309	4	4.85
XJ09-097-91	0.54	0.05261	0.00217	0.32529	0.01313	0.04485	0.00063	312	66	286	10	283	4	1.06
XJ09-097-92	0.84	0.05621	0.00224	0.40963	0.01598	0.05287	0.00073	461	62	349	12	332	4	5.12
XJ09-097-93	0.55	0.05671	0.00252	0.53552	0.02334	0.0685	0.00099	480	71	435	15	427	6	1.87
XJ09-097-94	0.56	0.05921	0.00209	0.85129	0.02947	0.1043	0.0014	575	52	625	16	640	8	-2.34

XJ09-097-95	0.44	0.05398	0.00359	0.4199	0.0271	0.05642	0.00089	370	154	356	19	354	5	0.56
XJ09-097-96	0.7	0.07508	0.00317	1.88992	0.07807	0.18262	0.0027	1071	59	1078	27	1081	15	-0.93
XJ09-097-97	0.72	0.0539	0.00404	0.33579	0.02482	0.0452	0.00076	367	137	294	19	285	5	3.16
XJ09-097-98	0.8	0.05308	0.00247	0.27883	0.0127	0.03811	0.00055	332	77	250	10	241	3	3.73
XJ09-097-99	0.46	0.05501	0.00232	0.34316	0.01417	0.04526	0.00065	413	66	300	11	285	4	5.26
XJ09-097-100	0.58	0.0571	0.00258	0.51381	0.02273	0.06529	0.00095	495	72	421	15	408	6	3.19
XJ10-018														
XJ10-018-1	0.57	0.05341	0.00143	0.40595	0.01119	0.05511	0.00078	346	37	346	8	346	5	0
XJ10-018-2	0.55	0.05309	0.00165	0.38647	0.01229	0.05278	0.00075	333	46	332	9	332	5	0
XJ10-018-3	0.67	0.05306	0.00169	0.37475	0.01223	0.05122	0.00072	331	49	323	9	322	4	0.31
XJ10-018-4	0.28	0.05156	0.00187	0.27851	0.01019	0.03917	0.00058	266	57	249	8	248	4	0.4
XJ10-018-5	1.15	0.04926	0.00156	0.17063	0.00552	0.02512	0.00036	160	49	160	5	160	2	0
XJ10-018-6	0.33	0.05267	0.00119	0.36014	0.00858	0.04958	0.00068	315	30	312	6	312	4	0
XJ10-018-7	1.05	0.04934	0.00126	0.17711	0.00469	0.02603	0.00036	164	37	166	4	166	2	0
XJ10-018-8	0.49	0.05335	0.00142	0.40751	0.01123	0.05539	0.00078	344	37	347	8	348	5	-0.29
XJ10-018-9	0.95	0.15654	0.00235	9.8267	0.1669	0.45517	0.00614	2419	13	2419	16	2418	27	0.04
XJ10-018-10	0.94	0.05085	0.00215	0.25808	0.01102	0.0368	0.00053	234	72	233	9	233	3	0
XJ10-018-11	0.68	0.05104	0.00153	0.25641	0.00791	0.03643	0.00051	243	45	232	6	231	3	0.43

XJ10-018-12	0.67	0.05157	0.00186	0.29327	0.01077	0.04124	0.00059	266	58	261	8	261	4	0
XJ10-018-13	0.86	0.04953	0.00206	0.18659	0.00785	0.02731	0.00039	173	71	174	7	174	2	0
XJ10-018-14	0.53	0.05306	0.00168	0.37765	0.01222	0.05161	0.00073	331	48	325	9	324	4	0.31
XJ10-018-15	0.5	0.05332	0.00188	0.40013	0.01435	0.05441	0.00078	342	55	342	10	342	5	0
XJ10-018-16	0.46	0.0521	0.00297	0.32758	0.0187	0.04559	0.00069	290	103	288	14	287	4	0.35
XJ10-018-17	0.65	0.05278	0.00161	0.36936	0.01148	0.05075	0.00073	319	45	319	9	319	4	0
XJ10-018-18	0.71	0.05309	0.00126	0.38617	0.00954	0.05274	0.00074	333	31	332	7	331	5	0.3
XJ10-018-19	0.46	0.05525	0.00128	0.51601	0.01247	0.06772	0.00095	422	30	422	8	422	6	0
XJ10-018-20	1.19	0.04941	0.00143	0.17912	0.00533	0.02629	0.00037	167	43	167	5	167	2	0
XJ10-018-21	0.65	0.04944	0.00247	0.17538	0.00877	0.02572	0.00041	169	86	164	8	164	3	0
XJ10-018-22	0.55	0.05542	0.00132	0.52631	0.01311	0.06886	0.00097	429	31	429	9	429	6	0
XJ10-018-23	0.51	0.05822	0.00122	0.69837	0.01555	0.08698	0.00121	538	26	538	9	538	7	0
XJ10-018-24	0.61	0.05429	0.00141	0.4599	0.01234	0.06142	0.00087	383	35	384	9	384	5	0
XJ10-018-25	0.46	0.0523	0.00159	0.34104	0.01057	0.04728	0.00068	299	45	298	8	298	4	0
XJ10-018-26	1.11	0.04918	0.00206	0.17005	0.00715	0.02507	0.00039	156	69	159	6	160	2	-0.62
XJ10-018-27	0.61	0.04941	0.00203	0.18094	0.00754	0.02655	0.00038	167	70	169	6	169	2	0
XJ10-018-28	1.11	0.04944	0.00155	0.17704	0.00564	0.02596	0.00038	169	47	166	5	165	2	0.61
XJ10-018-29	0.87	0.05193	0.00165	0.326	0.01055	0.04552	0.00065	282	48	287	8	287	4	0

XJ10-018-30	0.92	0.0541	0.00379	0.19042	0.01333	0.02552	0.00042	375	129	177	11	162	3	9.26
XJ10-018-31	0.8	0.04935	0.00157	0.17392	0.00563	0.02555	0.00037	164	49	163	5	163	2	0
XJ10-018-32	0.56	0.04935	0.0018	0.1755	0.00648	0.02579	0.00038	164	59	164	6	164	2	0
XJ10-018-33	0.79	0.04939	0.00158	0.17911	0.00583	0.02629	0.00038	166	49	167	5	167	2	0
XJ10-018-34	0.63	0.0505	0.00132	0.24272	0.00661	0.03485	0.00049	218	37	221	5	221	3	0
XJ10-018-35	0.27	0.05598	0.00114	0.56093	0.01221	0.07266	0.001	452	25	452	8	452	6	0
XJ10-018-36	0.96	0.05307	0.00148	0.38765	0.01115	0.05296	0.00075	332	40	333	8	333	5	0
XJ10-018-37	1.22	0.04929	0.00144	0.17295	0.0052	0.02544	0.00036	162	44	162	5	162	2	0
XJ10-018-38	1.66	0.05085	0.00183	0.17819	0.00649	0.02541	0.00037	234	57	167	6	162	2	3.09
XJ10-018-39	0.45	0.04934	0.00175	0.1707	0.00616	0.02509	0.00036	164	57	160	5	160	2	0
XJ10-018-40	1.03	0.05092	0.00172	0.26358	0.00903	0.03754	0.00055	237	52	238	7	238	3	0
XJ10-018-41	0.71	0.05214	0.00144	0.33819	0.00961	0.04703	0.00067	292	39	296	7	296	4	0
XJ10-018-42	0.68	0.053	0.00105	0.38126	0.00807	0.05216	0.00072	329	25	328	6	328	4	0
XJ10-018-43	0.44	0.05288	0.00153	0.37605	0.01117	0.05156	0.00074	324	42	324	8	324	5	0
XJ10-018-44	1.06	0.05309	0.00157	0.38968	0.01183	0.05322	0.00076	333	43	334	9	334	5	0
XJ10-018-45	1.13	0.04933	0.00485	0.17178	0.01686	0.02525	0.00041	164	190	161	15	161	3	0
XJ10-018-46	0.63	0.0524	0.00169	0.34443	0.01134	0.04766	0.00069	303	49	301	9	300	4	0.33
XJ10-018-47	0.39	0.05763	0.00143	0.66296	0.01708	0.08342	0.00117	516	33	516	10	517	7	-0.19

XJ10-018-48	1.27	0.05293	0.00139	0.37699	0.01024	0.05164	0.00073	326	36	325	8	325	4	0
XJ10-018-49	0.44	0.05217	0.00132	0.33591	0.00882	0.04668	0.00066	293	35	294	7	294	4	0
XJ10-018-50	1.03	0.0514	0.00139	0.2676	0.00748	0.03775	0.00054	259	38	241	6	239	3	0.84
XJ10-018-51	0.52	0.05271	0.00137	0.33727	0.00909	0.0464	0.00064	316	37	295	7	292	4	1.03
XJ10-018-52	0.96	0.05282	0.00132	0.38573	0.00996	0.05295	0.00075	321	34	331	7	333	5	-0.6
XJ10-018-53	0.12	0.05726	0.00092	0.64233	0.01148	0.08134	0.0011	502	18	504	7	504	7	0
XJ10-018-54	0.59	0.04938	0.00337	0.17955	0.01222	0.02637	0.00043	166	123	168	11	168	3	0
XJ10-018-55	0.25	0.04962	0.00144	0.1783	0.0053	0.02606	0.00037	177	43	167	5	166	2	0.6
XJ10-018-56	0.56	0.05203	0.00136	0.34107	0.00921	0.04754	0.00067	287	36	298	7	299	4	-0.33
XJ10-018-57	0.87	0.05251	0.00148	0.36732	0.01062	0.05072	0.00072	308	40	318	8	319	4	-0.31
XJ10-018-58	1.01	0.05268	0.00086	0.36834	0.00665	0.0507	0.00068	315	19	318	5	319	4	-0.31
XJ10-018-59	0.6	0.0494	0.00133	0.18037	0.005	0.02647	0.00037	167	39	168	4	168	2	0
XJ10-018-60	0.61	0.0566	0.00108	0.6568	0.01351	0.08415	0.00116	476	23	513	8	521	7	-1.54
XJ10-018-61	0.7	0.05952	0.00158	0.75533	0.02063	0.09202	0.00131	586	35	571	12	567	8	0.71
XJ10-018-62	1.06	0.05276	0.00516	0.34966	0.03357	0.04806	0.00121	318	171	304	25	303	7	0.33
XJ10-018-63	0.78	0.05246	0.001	0.35799	0.00735	0.04948	0.00068	306	24	311	5	311	4	0
XJ10-018-64	1.89	0.04908	0.00173	0.1743	0.00624	0.02575	0.00037	152	57	163	5	164	2	-0.61
XJ10-018-65	0.37	0.0526	0.0018	0.37888	0.01316	0.05223	0.00077	312	52	326	10	328	5	-0.61

XJ10-018-66	0.78	0.05381	0.0017	0.39678	0.01278	0.05346	0.00076	363	47	339	9	336	5	0.89
XJ10-018-67	0.45	0.05399	0.00155	0.40233	0.01185	0.05404	0.00078	371	41	343	9	339	5	1.18
XJ10-018-68	0.94	0.05281	0.00141	0.34889	0.00961	0.04791	0.00068	321	37	304	7	302	4	0.66
XJ10-018-69	0.33	0.05225	0.00176	0.36875	0.0126	0.05118	0.00075	296	51	319	9	322	5	-0.93
XJ10-018-70	1.39	0.04988	0.00474	0.19838	0.01875	0.02884	0.00054	189	178	184	16	183	3	0.55
XJ10-018-71	0.35	0.05391	0.00515	0.45338	0.04252	0.06098	0.00155	367	166	380	30	382	9	-0.52
XJ10-018-72	1.05	0.0513	0.00132	0.27493	0.00733	0.03886	0.00054	254	36	247	6	246	3	0.41
XJ10-018-73	0.94	0.05308	0.00203	0.37087	0.01437	0.05066	0.00073	332	62	320	11	319	4	0.31
XJ10-018-74	0.24	0.05699	0.00096	0.64291	0.01192	0.0818	0.00111	491	20	504	7	507	7	-0.59
XJ10-018-75	0.54	0.05402	0.00136	0.4157	0.01085	0.0558	0.00078	372	34	353	8	350	5	0.86
XJ10-018-76	0.66	0.05355	0.00095	0.3846	0.00744	0.05208	0.00071	352	21	330	5	327	4	0.92
XJ10-018-77	0.48	0.04936	0.0011	0.17021	0.00402	0.025	0.00034	165	31	160	3	159	2	0.63
~~**XJ10-018-78**~~	~~1.17~~	~~0.06889~~	~~0.00205~~	~~0.37762~~	~~0.01155~~	~~0.03975~~	~~0.00056~~	~~895~~	~~40~~	~~325~~	~~9~~	~~251~~	~~3~~	~~29.48~~
XJ10-018-79	0.4	0.05332	0.00159	0.39691	0.01211	0.05398	0.00078	342	43	339	9	339	5	0
XJ10-018-80	0.57	0.05206	0.00271	0.34205	0.01782	0.04764	0.00074	288	91	299	13	300	5	-0.33
XJ10-018-81	0.35	0.05192	0.00097	0.32498	0.00656	0.04539	0.00062	282	23	286	5	286	4	0
XJ10-018-82	1.07	0.0509	0.0016	0.27668	0.00882	0.03941	0.00058	236	47	248	7	249	4	-0.4
XJ10-018-83	0.48	0.05363	0.00183	0.39462	0.01374	0.05336	0.00076	356	53	338	10	335	5	0.9

XJ10-018-84	0.75	0.0521	0.00159	0.33393	0.01045	0.04648	0.00066	290	46	293	8	293	4	0
~~**XJ10-018-85**~~	~~0.49~~	~~0.10401~~	~~0.00252~~	~~0.89696~~	~~0.0223~~	~~0.06254~~	~~0.00092~~	~~1697~~	~~25~~	~~650~~	~~12~~	~~391~~	~~6~~	~~66.24~~
XJ10-018-86	0.97	0.04985	0.00121	0.1907	0.00483	0.02774	0.00039	188	34	177	4	176	2	0.57
XJ10-018-87	1.02	0.05831	0.00179	0.67702	0.02109	0.08419	0.00124	541	43	525	13	521	7	0.77
XJ10-018-88	0.22	0.06544	0.00093	1.13144	0.01847	0.12537	0.00168	789	16	768	9	761	10	0.92
XJ10-018-89	0.37	0.04909	0.00191	0.17389	0.00683	0.02569	0.00038	152	64	163	6	164	2	-0.61
XJ10-018-90	0.73	0.04963	0.00099	0.17654	0.0038	0.02579	0.00035	178	26	165	3	164	2	0.61
XJ10-018-91	0.51	0.05273	0.00102	0.36111	0.00752	0.04966	0.00068	317	24	313	6	312	4	0.32
XJ10-018-92	0.86	0.05286	0.00657	0.35749	0.04435	0.04904	0.00089	323	247	310	33	309	5	0.32
XJ10-018-93	0.77	0.04939	0.00141	0.16913	0.00496	0.02483	0.00036	166	42	159	4	158	2	0.63
XJ10-018-94	0.69	0.06003	0.00101	0.79853	0.01482	0.09646	0.00131	605	19	596	8	594	8	0.34
XJ10-018-95	1.63	0.05282	0.00108	0.38088	0.00827	0.05229	0.00072	321	26	328	6	329	4	-0.3
XJ10-018-96	0.99	0.04948	0.00155	0.17134	0.00549	0.02511	0.00036	171	48	161	5	160	2	0.63
XJ10-018-97	0.86	0.04959	0.00259	0.17502	0.00918	0.02559	0.00038	176	93	164	8	163	2	0.61
XJ10-018-98	0.36	0.05596	0.00099	0.5695	0.01099	0.07379	0.001	451	21	458	7	459	6	-0.22
~~**XJ10-018-99**~~	~~0.84~~	~~0.07091~~	~~0.00269~~	~~0.5392~~	~~0.02049~~	~~0.05514~~	~~0.00086~~	~~955~~	~~52~~	~~438~~	~~14~~	~~346~~	~~5~~	~~26.59~~
XJ10-018-100	0.42	0.05297	0.00116	0.35697	0.00825	0.04886	0.00068	328	28	310	6	308	4	0.65
XJ09-100														

XJ09-100-1	0.65	0.05349	0.00158	0.39803	0.0118	0.05396	0.00071	350	43	340	9	339	4	0.29
XJ09-100-2	0.79	0.05211	0.00118	0.34314	0.0079	0.04775	0.0006	290	30	300	6	301	4	-0.33
XJ09-100-3	1.03	0.05353	0.00451	0.25962	0.0217	0.03517	0.00062	351	158	234	17	223	4	4.93
XJ09-100-4	0.63	0.05376	0.00121	0.35195	0.00808	0.04747	0.0006	361	30	306	6	299	4	2.34
XJ09-100-5	0.63	0.05308	0.00169	0.4038	0.01291	0.05516	0.00073	332	48	344	9	346	4	-0.58
XJ09-100-6	0.33	0.05164	0.00182	0.31197	0.01023	0.04382	0.00055	269	83	276	8	276	3	0
XJ09-100-7	0.45	0.05267	0.00133	0.34179	0.00872	0.04706	0.0006	315	35	299	7	296	4	1.01
XJ09-100-8	1.02	0.04655	0.00574	0.16253	0.01992	0.02532	0.00047	26	218	153	17	161	3	-4.97
XJ09-100-9	0.69	0.05661	0.00145	0.33905	0.00875	0.04343	0.00056	476	35	296	7	274	3	8.03
XJ09-100-10	0.1	0.09545	0.0019	3.42682	0.0551	0.26038	0.00307	1537	38	1511	13	1492	16	3.02
XJ09-100-11	0.89	0.0524	0.00322	0.35333	0.02155	0.04889	0.00075	303	111	307	16	308	5	-0.32
XJ09-100-12	0.45	0.05473	0.00181	0.36898	0.01218	0.04888	0.00066	401	50	319	9	308	4	3.57
XJ09-100-13	1.54	0.04786	0.00246	0.16451	0.00842	0.02492	0.00036	92	87	155	7	159	2	-2.52
XJ09-100-14	0.79	0.05382	0.00264	0.26337	0.01284	0.03548	0.00051	364	84	237	10	225	3	5.33
XJ09-100-15	1.36	0.04727	0.00139	0.16511	0.00488	0.02533	0.00033	63	44	155	4	161	2	-3.73
XJ09-100-16	0.64	0.05085	0.00118	0.3172	0.00747	0.04524	0.00057	234	32	280	6	285	4	-1.75
XJ09-100-17	0.87	0.05176	0.00347	0.18711	0.01245	0.02622	0.00041	275	124	174	11	167	3	4.19
XJ09-100-18	0.52	0.04904	0.00153	0.23041	0.00723	0.03407	0.00044	150	49	211	6	216	3	-2.31

XJ09-100-19	0.65	0.05359	0.00114	0.35793	0.00776	0.04844	0.0006	354	27	311	6	305	4	1.97
XJ09-100-20	0.53	0.05505	0.00158	0.51867	0.01493	0.06832	0.00089	414	41	424	10	426	5	-0.47
XJ09-100-21	0.94	0.07398	0.00201	1.55757	0.04241	0.15267	0.00203	1041	34	954	17	916	11	4.15
XJ09-100-22	1.06	0.05444	0.00295	0.42446	0.02283	0.05654	0.00085	389	94	359	16	355	5	1.13
XJ09-100-23	0.8	0.0565	0.00464	0.38538	0.03134	0.04946	0.00087	472	150	331	23	311	5	6.43
XJ09-100-24	1.06	0.04657	0.00244	0.15956	0.0081	0.02485	0.00033	27	114	150	7	158	2	-5.06
XJ09-100-25	1.05	0.05677	0.00237	0.30926	0.01278	0.0395	0.00058	483	65	274	10	250	4	9.6
XJ09-100-26	0.36	0.05133	0.00121	0.32618	0.00777	0.04608	0.00058	256	32	287	6	290	4	-1.03
XJ09-100-27	0.21	0.05125	0.00101	0.36736	0.00746	0.05198	0.00064	252	25	318	6	327	4	-2.75
XJ09-100-28	0.18	0.05861	0.00126	0.68546	0.01497	0.08481	0.00106	553	27	530	9	525	6	0.95
XJ09-100-29	0.79	0.04882	0.00171	0.2199	0.00768	0.03266	0.00044	139	57	202	6	207	3	-2.42
XJ09-100-30	0.48	0.05268	0.0013	0.34539	0.00863	0.04754	0.0006	315	34	301	7	299	4	0.67
XJ09-100-31	0.83	0.05352	0.00349	0.18628	0.01204	0.02524	0.0004	351	118	173	10	161	3	7.45
XJ09-100-32	0.7	0.05357	0.00141	0.38145	0.01012	0.05164	0.00066	353	37	328	7	325	4	0.92
XJ09-100-33	0.58	0.11392	0.00191	5.16068	0.09032	0.32849	0.00403	1863	15	1846	15	1831	20	1.75
XJ09-100-34	0.93	0.04857	0.0018	0.18516	0.00684	0.02764	0.00037	127	61	172	6	176	2	-2.27
XJ09-100-35	1.19	0.05424	0.00326	0.19043	0.0113	0.02546	0.00042	381	104	177	10	162	3	9.26
XJ09-100-36	0.5	0.05332	0.00247	0.18887	0.00868	0.02569	0.00037	342	78	176	7	164	2	7.32

XJ09-100-37	1.74	0.05035	0.00139	0.16864	0.00468	0.02429	0.00031	211	41	158	4	155	2	1.94
XJ09-100-38	0.68	0.0514	0.00134	0.35433	0.00928	0.04999	0.00064	259	37	308	7	314	4	-1.91
XJ09-100-39	0.98	0.05224	0.00158	0.29297	0.00887	0.04067	0.00054	296	45	261	7	257	3	1.56
XJ09-100-40	0.72	0.05015	0.0024	0.18202	0.00863	0.02632	0.00039	202	82	170	7	167	2	1.8
XJ09-100-41	0.73	0.0506	0.00164	0.34942	0.01134	0.05008	0.00066	223	51	304	9	315	4	-3.49
XJ09-100-42	0.46	0.05517	0.00217	0.35848	0.014	0.04712	0.00066	419	62	311	10	297	4	4.71
XJ09-100-43	1.81	0.05427	0.0022	0.37188	0.01496	0.04969	0.0007	382	65	321	11	313	4	2.56
XJ09-100-44	0.78	0.04882	0.00361	0.15929	0.0116	0.02366	0.00044	139	128	150	10	151	3	-0.66
XJ09-100-45	0.71	0.10825	0.00192	4.62037	0.08454	0.30952	0.00381	1770	17	1753	15	1738	19	1.84
XJ09-100-46	0.57	0.05243	0.00267	0.37674	0.01849	0.05211	0.00072	304	119	325	14	327	4	-0.61
XJ09-100-47	0.54	0.0575	0.00215	0.49052	0.01824	0.06186	0.00086	511	57	405	12	387	5	4.65
XJ09-100-48	0.49	0.05781	0.00479	0.37293	0.03055	0.04678	0.00085	523	149	322	23	295	5	9.15
XJ09-100-49	0.77	0.10219	0.00183	4.11983	0.076	0.29235	0.0036	1664	17	1658	15	1653	18	0.67
XJ09-100-50	0.39	0.05617	0.00195	0.65941	0.02274	0.08513	0.00116	459	52	514	14	527	7	-2.47
XJ09-100-51	0.8	0.05199	0.00127	0.29858	0.00733	0.04165	0.00053	285	33	265	6	263	3	0.76
XJ09-100-52	0.91	0.04722	0.00217	0.29736	0.01362	0.04567	0.00064	60	75	264	11	288	4	-8.33
XJ09-100-53	0.52	0.05524	0.00161	0.52328	0.0152	0.0687	0.00091	422	41	427	10	428	5	-0.23
XJ09-100-54	0.95	0.05832	0.00305	0.40992	0.02124	0.05097	0.00077	542	87	349	15	320	5	9.06

XJ09-100-55	0.49	0.05578	0.00157	0.43259	0.01218	0.05623	0.00074	444	39	365	9	353	5	3.4
XJ09-100-56	0.69	0.05384	0.00325	0.25754	0.0154	0.03468	0.00054	364	107	233	12	220	3	5.91
XJ09-100-57	0.75	0.05215	0.00195	0.344	0.01281	0.04783	0.00066	292	60	300	10	301	4	-0.33
XJ09-100-58	0.67	0.05183	0.00179	0.35366	0.01217	0.04948	0.00067	278	54	307	9	311	4	-1.29
XJ09-100-59	1.22	0.0461	0.00305	0.15678	0.01013	0.02466	0.00036	3	146	148	9	157	2	-5.73
XJ09-100-60	0.82	0.05468	0.00288	0.42623	0.02223	0.05652	0.00086	399	90	360	16	354	5	1.69
XJ09-100-61	0.57	0.05435	0.00214	0.41897	0.01635	0.05589	0.00078	386	62	355	12	351	5	1.14
XJ09-100-62	0.18	0.07025	0.00141	1.46824	0.02993	0.15156	0.00189	936	22	917	12	910	11	0.77
XJ09-100-63	0.81	0.04861	0.00185	0.36384	0.01375	0.05428	0.00074	129	63	315	10	341	5	-7.62
XJ09-100-64	1.71	0.04625	0.00478	0.16977	0.0174	0.02662	0.0005	11	190	159	15	169	3	-5.92
XJ09-100-65	1.11	0.05062	0.00247	0.25788	0.01247	0.03694	0.00054	224	85	233	10	234	3	-0.43
XJ09-100-66	0.93	0.05476	0.00166	0.38702	0.01168	0.05124	0.00068	402	44	332	9	322	4	3.11
XJ09-100-67	0.43	0.05233	0.00278	0.35612	0.01877	0.04935	0.00074	300	93	309	14	311	5	-0.64
XJ09-100-68	0.63	0.05427	0.00505	0.35665	0.03288	0.04765	0.00088	382	175	310	25	300	5	3.33
XJ09-100-69	0.77	0.04915	0.00181	0.24734	0.00904	0.03649	0.0005	155	60	224	7	231	3	-3.03
XJ09-100-70	2.06	0.05105	0.00216	0.1691	0.00712	0.02402	0.00034	243	71	159	6	153	2	3.92
XJ09-100-71	0.39	0.05549	0.00173	0.44048	0.01363	0.05756	0.00077	432	45	371	10	361	5	2.77
XJ09-100-72	0.84	0.04892	0.00399	0.16707	0.01349	0.02477	0.00042	144	149	157	12	158	3	-0.63

XJ09-100-73	0.38	0.0521	0.00225	0.33593	0.01435	0.04676	0.00067	290	71	294	11	295	4	-0.34
XJ09-100-74	0.76	0.05245	0.00138	0.40289	0.01061	0.0557	0.00072	305	37	344	8	349	4	-1.43
XJ09-100-75	0.26	0.05562	0.00169	0.37482	0.01132	0.04886	0.00065	437	44	323	8	308	4	4.87
XJ09-100-76	0.63	0.05944	0.00171	0.46431	0.01332	0.05664	0.00075	583	39	387	9	355	5	9.01
XJ09-100-77	0.64	0.05502	0.00158	0.37743	0.01081	0.04974	0.00066	413	40	325	8	313	4	3.83
XJ09-100-78	0.96	0.05656	0.00191	0.37849	0.01266	0.04852	0.00067	474	49	326	9	305	4	6.89
XJ09-100-79	0.81	0.05474	0.00202	0.38941	0.01425	0.05159	0.00072	402	57	334	10	324	4	3.09
XJ09-100-80	0.53	0.05054	0.002	0.19642	0.00772	0.02818	0.0004	220	65	182	7	179	3	1.68
XJ09-100-81	0.5	0.0534	0.00234	0.33285	0.01447	0.04519	0.00065	346	72	292	11	285	4	2.46
XJ09-100-82	0.44	0.05387	0.00167	0.34941	0.01079	0.04703	0.00063	366	45	304	8	296	4	2.7
XJ09-100-83	1.33	0.05296	0.00274	0.17847	0.00911	0.02444	0.00039	327	87	167	8	156	2	7.05
XJ09-100-84	1.45	0.05438	0.00313	0.28932	0.01646	0.03858	0.0006	387	100	258	13	244	4	5.74
XJ09-100-85	0.63	0.05555	0.00154	0.37364	0.01029	0.04877	0.00064	434	38	322	8	307	4	4.89
XJ09-100-86	1.15	0.05168	0.00164	0.25657	0.0081	0.036	0.00049	271	47	232	7	228	3	1.75
XJ09-100-87	0.77	0.04968	0.00222	0.36294	0.01607	0.05297	0.00077	180	76	314	12	333	5	-5.71
XJ09-100-88	0.66	0.05366	0.0017	0.38911	0.01225	0.05258	0.00071	357	47	334	9	330	4	1.21
XJ09-100-89	0.4	0.05396	0.00213	0.38251	0.01497	0.0514	0.00073	369	62	329	11	323	4	1.86
XJ09-100-90	0.68	0.05398	0.0018	0.38927	0.0129	0.05229	0.00071	370	50	334	9	329	4	1.52

XJ09-100-91	0.56	0.04605	0.01251	0.29815	0.08051	0.04696	0.00141	—	442	265	63	296	9	-10.47
XJ09-100-92	0.44	0.04877	0.0022	0.34489	0.01541	0.05128	0.00074	137	76	301	12	322	5	-6.52
XJ09-100-93	0.63	0.05155	0.00177	0.3326	0.01131	0.04678	0.00064	266	53	292	9	295	4	-1.02
XJ09-100-94	0.44	0.05159	0.00145	0.31071	0.00866	0.04367	0.00058	267	40	275	7	276	4	-0.36
XJ09-100-95	0.59	0.05532	0.0025	0.35183	0.01569	0.04611	0.00069	425	73	306	12	291	4	5.15
XJ09-100-96	0.61	0.05295	0.00242	0.39227	0.01775	0.05371	0.00079	327	76	336	13	337	5	-0.3
XJ09-100-97	0.87	0.05689	0.0037	0.36948	0.02367	0.04709	0.0008	487	112	319	18	297	5	7.41
XJ09-100-98	0.66	0.05448	0.00291	0.35538	0.01873	0.0473	0.00074	391	90	309	14	298	5	3.69
XJ09-100-99	0.43	0.05486	0.00223	0.43974	0.01764	0.05812	0.00084	407	64	370	12	364	5	1.65
XJ09-100-100	0.5	0.05451	0.00155	0.50461	0.01421	0.06712	0.00089	392	40	415	10	419	5	-0.95
XJ10-016														
XJ10-016-1	0.77	0.0557	0.00108	0.54233	0.0113	0.0706	0.00096	440	24	440	7	440	6	0
XJ10-016-2	0.44	0.05477	0.00123	0.48545	0.0115	0.06427	0.00087	403	30	402	8	402	5	0
XJ10-016-3	0.62	0.05223	0.0013	0.3424	0.00885	0.04753	0.00065	295	35	299	7	299	4	0
XJ10-016-4	0.66	0.05161	0.00125	0.33774	0.00852	0.04745	0.00065	268	33	295	6	299	4	-1.34
XJ10-016-5	0.66	0.05618	0.00148	0.54142	0.01478	0.06988	0.00096	459	37	439	10	435	6	0.92
XJ10-016-6	0.65	0.05174	0.00298	0.30963	0.01789	0.04339	0.00066	274	105	274	14	274	4	0
XJ10-016-7	0.61	0.05262	0.00133	0.36413	0.00957	0.05018	0.00069	312	35	315	7	316	4	-0.32

XJ10-016-8	0.55	0.08431	0.00109	2.52235	0.03823	0.21693	0.00287	1300	13	1278	11	1266	15	2.69
XJ10-016-9	0.28	0.05222	0.00113	0.33682	0.0077	0.04677	0.00064	295	28	295	6	295	4	0
XJ10-016-10	0.54	0.05236	0.00206	0.34467	0.01376	0.04773	0.00066	301	66	301	10	301	4	0
XJ10-016-11	0.56	0.05239	0.00132	0.34447	0.00901	0.04768	0.00065	302	35	301	7	300	4	0.33
XJ10-016-12	0.43	0.05283	0.00269	0.36971	0.01885	0.05074	0.00078	322	88	319	14	319	5	0
XJ10-016-13	0.4	0.05229	0.00103	0.33935	0.00715	0.04706	0.00063	298	25	297	5	296	4	0.34
XJ10-016-14	0.49	0.05406	0.00161	0.43661	0.01336	0.05856	0.00081	374	44	368	9	367	5	0.27
XJ10-016-15	0.48	0.05275	0.00121	0.36542	0.00876	0.05023	0.00069	318	30	316	7	316	4	0
XJ10-016-16	0.45	0.05269	0.00132	0.36879	0.00959	0.05076	0.0007	315	35	319	7	319	4	0
XJ10-016-17	0.52	0.05227	0.00133	0.33117	0.00875	0.04595	0.00063	297	36	290	7	290	4	0
XJ10-016-18	0.87	0.04954	0.00154	0.18799	0.00599	0.02752	0.00039	173	48	175	5	175	2	0
XJ10-016-19	0.39	0.05229	0.0015	0.34094	0.01009	0.04728	0.00065	298	43	298	8	298	4	0
XJ10-016-20	0.33	0.05233	0.00116	0.33872	0.00791	0.04694	0.00064	300	29	296	6	296	4	0
XJ10-016-21	0.56	0.05239	0.00204	0.34624	0.01363	0.04792	0.00069	302	63	302	10	302	4	0
XJ10-016-22	0.57	0.05175	0.00154	0.315	0.00963	0.04414	0.00062	274	44	278	7	278	4	0
XJ10-016-23	0.84	0.05476	0.001	0.49592	0.00978	0.06567	0.00089	402	22	409	7	410	5	-0.24
XJ10-016-24	0.5	0.05227	0.00135	0.34065	0.0091	0.04726	0.00065	297	36	298	7	298	4	0
XJ10-016-25	0.52	0.05226	0.00096	0.31648	0.00629	0.04391	0.00059	297	23	279	5	277	4	0.72

XJ10-016-26	0.46	0.05245	0.00127	0.34862	0.00877	0.0482	0.00067	305	33	304	7	303	4	0.33
XJ10-016-27	1.29	0.05487	0.00151	0.49299	0.01397	0.06515	0.00092	407	38	407	10	407	6	0
XJ10-016-28	0.44	0.0555	0.00123	0.49559	0.01158	0.06475	0.00089	432	29	409	8	404	5	1.24
XJ10-016-29	0.73	0.05463	0.00101	0.481	0.00958	0.06385	0.00086	397	22	399	7	399	5	0
XJ10-016-30	0.56	0.05212	0.0012	0.32777	0.0079	0.0456	0.00063	291	31	288	6	287	4	0.35
XJ10-016-31	0.52	0.05216	0.00092	0.33194	0.0064	0.04615	0.00062	292	22	291	5	291	4	0
XJ10-016-32	0.51	0.05235	0.00105	0.34706	0.00746	0.04807	0.00065	301	26	303	6	303	4	0
XJ10-016-33	0.76	0.05881	0.00132	0.44917	0.0106	0.05538	0.00077	560	28	377	7	347	5	8.65
XJ10-016-34	0.36	0.05228	0.00095	0.34244	0.00674	0.0475	0.00064	298	22	299	5	299	4	0
XJ10-016-35	0.47	0.05483	0.00128	0.48479	0.01187	0.06411	0.00088	405	31	401	8	401	5	0
XJ10-016-36	0.32	0.05207	0.0013	0.33854	0.00876	0.04714	0.00065	288	34	296	7	297	4	-0.34
XJ10-016-37	0.47	0.05241	0.00131	0.34821	0.00906	0.04818	0.00066	303	35	303	7	303	4	0
XJ10-016-38	0.28	0.07864	0.0012	2.14005	0.03668	0.19734	0.00265	1163	16	1162	12	1161	14	0.17
XJ10-016-39	0.64	0.05473	0.00159	0.48177	0.0144	0.06383	0.00089	401	42	399	10	399	5	0
XJ10-016-40	0.45	0.05182	0.0016	0.31629	0.00995	0.04426	0.00063	277	46	279	8	279	4	0
XJ10-016-41	0.68	0.05236	0.00163	0.3441	0.01092	0.04765	0.00068	301	46	300	8	300	4	0
XJ10-016-42	1	0.05145	0.00116	0.26946	0.00642	0.03798	0.00052	261	30	242	5	240	3	0.83
XJ10-016-43	1.25	0.04943	0.00143	0.17473	0.0052	0.02563	0.00036	168	43	164	4	163	2	0.61

XJ10-016-44	0.25	0.05644	0.00094	0.54588	0.01	0.07013	0.00094	470	19	442	7	437	6	1.14
XJ10-016-45	0.74	0.07232	0.00107	1.62341	0.02722	0.16278	0.00218	995	16	979	11	972	12	0.72
XJ10-016-46	0.92	0.05231	0.00135	0.3539	0.00943	0.04906	0.00069	299	36	308	7	309	4	-0.32
XJ10-016-47	0.36	0.05602	0.00174	0.58438	0.01846	0.07564	0.00109	453	45	467	12	470	7	-0.64
XJ10-016-48	0.51	0.05395	0.00106	0.40407	0.00852	0.05431	0.00074	369	25	345	6	341	5	1.17
XJ10-016-49	0.47	0.05258	0.00176	0.3381	0.01154	0.04663	0.00065	311	52	296	9	294	4	0.68
XJ10-016-50	0.68	0.05288	0.00156	0.34278	0.01037	0.047	0.00067	324	43	299	8	296	4	1.01
XJ10-016-51	0.44	0.05576	0.0012	0.53808	0.01229	0.06998	0.00095	443	28	437	8	436	6	0.23
XJ10-016-52	1.67	0.05043	0.00134	0.23421	0.0064	0.03367	0.00047	215	38	214	5	213	3	0.47
XJ10-016-53	1.01	0.05233	0.00109	0.3365	0.00746	0.04663	0.00063	300	27	295	6	294	4	0.34
XJ10-016-54	0.58	0.0535	0.00111	0.40591	0.00897	0.05502	0.00075	350	27	346	6	345	5	0.29
XJ10-016-55	0.77	0.05324	0.00125	0.3867	0.00951	0.05266	0.00072	339	32	332	7	331	4	0.3
XJ10-016-56	0.46	0.05234	0.0019	0.35427	0.01308	0.04908	0.00069	300	58	308	10	309	4	-0.32
XJ10-016-57	1.41	0.04937	0.00129	0.17811	0.00481	0.02616	0.00037	165	37	166	4	166	2	0
XJ10-016-58	0.35	0.05354	0.00158	0.40749	0.01227	0.05518	0.0008	352	42	347	9	346	5	0.29
XJ10-016-59	0.63	0.05412	0.00133	0.47035	0.01205	0.06302	0.00088	376	33	391	8	394	5	-0.76
XJ10-016-60	0.35	0.05577	0.00099	0.546	0.01063	0.07099	0.00095	443	21	442	7	442	6	0
XJ10-016-61	1.08	0.05321	0.00096	0.39409	0.00771	0.05371	0.00072	338	22	337	6	337	4	0

XJ10-016-62	0.47	0.05238	0.00122	0.3455	0.00841	0.04783	0.00066	302	31	301	6	301	4	0
XJ10-016-63	0.4	0.05212	0.00103	0.33144	0.00701	0.04611	0.00063	291	25	291	5	291	4	0
XJ10-016-64	0.45	0.05477	0.00114	0.48706	0.0108	0.06448	0.00088	403	26	403	7	403	5	0
XJ10-016-65	0.42	0.04969	0.0043	0.19195	0.01657	0.02801	0.00048	181	162	178	14	178	3	0
XJ10-016-66	0.69	0.05229	0.00099	0.32869	0.0067	0.04558	0.00062	298	24	289	5	287	4	0.7
XJ10-016-67	0.66	0.05477	0.00142	0.48329	0.01298	0.06399	0.00089	403	36	400	9	400	5	0
XJ10-016-68	0.46	0.05224	0.00156	0.34792	0.0106	0.0483	0.00069	296	44	303	8	304	4	-0.33
XJ10-016-69	0.37	0.06539	0.0012	1.16179	0.02317	0.12884	0.00175	787	21	783	11	781	10	0.26
XJ10-016-70	0.54	0.05227	0.00212	0.33784	0.01385	0.04686	0.00067	297	67	296	11	295	4	0.34
XJ10-016-71	0.42	0.05211	0.00141	0.33054	0.00922	0.04599	0.00064	290	39	290	7	290	4	0
XJ10-016-72	0.44	0.0523	0.00122	0.34207	0.00832	0.04743	0.00066	299	31	299	6	299	4	0
XJ10-016-73	0.69	0.17681	0.00245	12.25387	0.196	0.50253	0.00675	2623	12	2624	15	2625	29	-0.08
XJ10-016-74	0.61	0.05235	0.00107	0.34577	0.00755	0.04789	0.00066	301	26	302	6	302	4	0
XJ10-016-75	0.66	0.05216	0.00126	0.33308	0.00838	0.04631	0.00064	292	33	292	6	292	4	0
XJ10-016-76	0.85	0.05291	0.00265	0.37777	0.01899	0.05177	0.00076	325	87	325	14	325	5	0
XJ10-016-77	1.54	0.05268	0.00201	0.36434	0.01404	0.05015	0.00074	315	61	315	10	315	5	0
XJ10-016-78	0.43	0.05216	0.00194	0.33683	0.01275	0.04682	0.00066	292	61	295	10	295	4	0
XJ10-016-79	1.07	0.04938	0.00264	0.17532	0.00937	0.02575	0.00041	166	93	164	8	164	3	0

XJ10-016-80	0.38	0.05212	0.00102	0.33183	0.00699	0.04616	0.00063	291	25	291	5	291	4	0
XJ10-016-81	0.8	0.05461	0.00121	0.47155	0.01103	0.06261	0.00086	396	29	392	8	391	5	0.26
XJ10-016-82	0.51	0.05242	0.00252	0.34795	0.0168	0.04813	0.00072	304	83	303	13	303	4	0
XJ10-016-83	0.34	0.05211	0.00111	0.33802	0.00763	0.04704	0.00065	290	28	296	6	296	4	0
XJ10-016-84	0.48	0.05237	0.00174	0.34839	0.01174	0.04824	0.0007	302	50	304	9	304	4	0
XJ10-016-85	0.36	0.06794	0.00118	1.11552	0.02128	0.11906	0.00161	867	19	761	10	725	9	4.97
XJ10-016-86	0.93	0.05259	0.00181	0.35752	0.01249	0.04929	0.0007	311	54	310	9	310	4	0
XJ10-016-87	0.67	0.0499	0.00281	0.19521	0.01101	0.02836	0.00044	190	101	181	9	180	3	0.56
XJ10-016-88	1.06	0.05256	0.00402	0.33287	0.02541	0.04592	0.00074	310	145	292	19	289	5	1.04
XJ10-016-89	0.28	0.05256	0.00131	0.35736	0.00927	0.0493	0.00069	310	34	310	7	310	4	0
XJ10-016-90	0.66	0.05841	0.00222	0.71337	0.02718	0.08856	0.00138	545	56	547	16	547	8	0
XJ10-016-91	0.31	0.05197	0.00105	0.32842	0.00708	0.04582	0.00063	284	26	288	5	289	4	-0.35
XJ10-016-92	0.38	0.05085	0.0016	0.25991	0.00839	0.03706	0.00052	234	49	235	7	235	3	0
XJ10-016-93	0.43	0.05216	0.00108	0.334	0.00736	0.04643	0.00064	292	27	293	6	293	4	0
XJ10-016-94	0.71	0.05537	0.00155	0.52249	0.015	0.06843	0.00097	427	39	427	10	427	6	0
XJ10-016-95	0.47	0.05234	0.00166	0.34606	0.0112	0.04794	0.00068	300	48	302	8	302	4	0
XJ10-016-96	0.45	0.0522	0.00179	0.33644	0.01171	0.04673	0.00067	294	53	294	9	294	4	0
XJ10-016-97	0.94	0.05647	0.001	0.58544	0.01133	0.07517	0.00102	471	21	468	7	467	6	0.21

XJ10-016-98	0.34	0.05231	0.00141	0.34137	0.00949	0.04732	0.00067	299	38	298	7	298	4	0
XJ10-016-99	0.77	0.05214	0.0027	0.33576	0.01744	0.04669	0.0007	292	91	294	13	294	4	0
XJ10-016-100	0.75	0.05196	0.00154	0.32398	0.00985	0.04521	0.00063	284	44	285	8	285	4	0
XJ10-015														
XJ10-015-1	0.45	0.05243	0.00115	0.33426	0.00772	0.04623	0.00064	304	29	293	6	291	4	0.69
XJ10-015-2	0.3	0.05952	0.00104	0.73628	0.01411	0.0897	0.00122	586	20	560	8	554	7	1.08
XJ10-015-3	0.75	0.04875	0.00121	0.14418	0.00373	0.02145	0.0003	136	35	137	3	137	2	0
XJ10-015-4	0.51	0.05273	0.0026	0.34631	0.01712	0.04762	0.00073	317	84	302	13	300	4	0.67
XJ10-015-5	0.48	0.05176	0.00164	0.32654	0.01058	0.04575	0.00066	275	48	287	8	288	4	-0.35
XJ10-015-6	0.81	0.05268	0.00228	0.36145	0.01576	0.04976	0.00073	315	72	313	12	313	4	0
XJ10-015-7	0.95	0.05235	0.00106	0.31536	0.00681	0.04368	0.0006	301	26	278	5	276	4	0.72
XJ10-015-8	0.18	0.0519	0.00089	0.32412	0.00611	0.04529	0.00061	281	21	285	5	286	4	-0.35
XJ10-015-9	0.85	0.04899	0.00164	0.15041	0.00512	0.02226	0.00032	147	53	142	5	142	2	0
XJ10-015-10	0.85	0.05443	0.00233	0.46762	0.02024	0.0623	0.00091	389	71	390	14	390	6	0
XJ10-015-11	1.59	0.04924	0.00285	0.16074	0.00934	0.02367	0.00036	159	104	151	8	151	2	0
XJ10-015-12	0.98	0.04937	0.00492	0.17268	0.01707	0.02536	0.00052	165	184	162	15	161	3	0.62
XJ10-015-13	0.68	0.05324	0.0012	0.37724	0.00894	0.05138	0.00071	339	30	325	7	323	4	0.62
XJ10-015-14	0.4	0.04902	0.00155	0.15222	0.0049	0.02252	0.00033	149	48	144	4	144	2	0

XJ10-015-15	0.26	0.05598	0.00094	0.55742	0.01037	0.07221	0.00098	452	20	450	7	449	6	0.22
XJ10-015-16	0.99	0.04871	0.00165	0.14524	0.005	0.02162	0.00032	134	53	138	4	138	2	0
XJ10-015-17	1.07	0.05224	0.00145	0.34225	0.00979	0.04751	0.00068	296	40	299	7	299	4	0
XJ10-015-18	0.65	0.05217	0.00152	0.34411	0.01033	0.04783	0.00067	293	43	300	8	301	4	-0.33
XJ10-015-19	0.64	0.05182	0.00212	0.32655	0.01347	0.04569	0.00067	277	67	287	10	288	4	-0.35
XJ10-015-20	0.79	0.05192	0.00147	0.32228	0.0094	0.04501	0.00064	282	41	284	7	284	4	0
XJ10-015-21	0.68	0.05336	0.00208	0.37367	0.01471	0.05078	0.00075	344	62	322	11	319	5	0.94
XJ10-015-22	0.38	0.05189	0.00122	0.33989	0.00839	0.0475	0.00066	281	32	297	6	299	4	-0.67
XJ10-015-23	0.48	0.0488	0.00146	0.13565	0.00416	0.02016	0.00029	138	45	129	4	129	2	0
XJ10-015-24	0.84	0.05494	0.00143	0.49288	0.01331	0.06506	0.00091	410	36	407	9	406	6	0.25
XJ10-015-25	0.73	0.04876	0.00127	0.14681	0.00397	0.02183	0.00031	136	37	139	4	139	2	0
XJ10-015-26	0.55	0.04875	0.00143	0.14115	0.00426	0.021	0.00029	136	45	134	4	134	2	0
XJ10-015-27	0.69	0.05274	0.00116	0.3587	0.00829	0.04932	0.00068	318	29	311	6	310	4	0.32
XJ10-015-28	1.29	0.04887	0.0024	0.15139	0.00748	0.02246	0.00033	142	86	143	7	143	2	0
XJ10-015-29	0.18	0.07622	0.00126	1.76816	0.03237	0.16822	0.00229	1101	17	1034	12	1002	13	9.88
XJ10-015-30	0.39	0.05201	0.00117	0.33942	0.00802	0.04732	0.00066	286	30	297	6	298	4	-0.34
XJ10-015-31	0.79	0.04867	0.00119	0.13729	0.00349	0.02046	0.00029	132	34	131	3	131	2	0
XJ10-015-32	1.04	0.04865	0.00311	0.15105	0.00958	0.02251	0.00039	131	110	143	8	143	2	0

XJ10-015-33	0.66	0.05339	0.00153	0.40101	0.01185	0.05446	0.00077	345	41	342	9	342	5	0
XJ10-015-34	0.37	0.05299	0.00116	0.37682	0.00873	0.05157	0.00071	328	29	325	6	324	4	0.31
XJ10-015-35	0.75	0.049	0.00308	0.155	0.00967	0.02294	0.00041	148	108	146	9	146	3	0
XJ10-015-36	0.72	0.04885	0.00118	0.14848	0.00374	0.02204	0.00031	141	34	141	3	141	2	0
XJ10-015-37	0.45	0.05352	0.00145	0.3965	0.01115	0.05372	0.00075	351	39	339	8	337	5	0.59
XJ10-015-38	0.8	0.04939	0.00148	0.17477	0.00536	0.02566	0.00037	166	45	164	5	163	2	0.61
XJ10-015-39	0.95	0.05329	0.00127	0.36679	0.00912	0.04991	0.00069	341	32	317	7	314	4	0.96
XJ10-015-40	0.57	0.05188	0.0016	0.30946	0.00976	0.04325	0.00061	280	46	274	8	273	4	0.37
XJ10-015-41	0.64	0.04851	0.0013	0.1326	0.00367	0.01982	0.00028	124	39	126	3	127	2	-0.79
XJ10-015-42	0.67	0.05284	0.00189	0.34207	0.01241	0.04694	0.00068	322	56	299	9	296	4	1.01
XJ10-015-43	0.32	0.10338	0.00179	4.25931	0.08072	0.29875	0.00411	1686	17	1686	16	1685	20	0.06
XJ10-015-44	0.55	0.05264	0.00125	0.35442	0.00884	0.04882	0.00068	313	32	308	7	307	4	0.33
XJ10-015-45	0.47	0.05213	0.00155	0.33528	0.01023	0.04664	0.00067	291	44	294	8	294	4	0
XJ10-015-46	0.71	0.04884	0.00115	0.1557	0.00383	0.02312	0.00032	140	33	147	3	147	2	0
XJ10-015-47	0.9	0.04905	0.00172	0.15215	0.00539	0.02249	0.00033	150	55	144	5	143	2	0.7
XJ10-015-48	0.43	0.05508	0.00154	0.52154	0.01497	0.06866	0.00098	415	39	426	10	428	6	-0.47
XJ10-015-49	0.78	0.05339	0.00147	0.3778	0.01074	0.05131	0.00072	345	39	325	8	323	4	0.62
XJ10-015-50	0.76	0.05631	0.00139	0.58584	0.01502	0.07544	0.00107	465	32	468	10	469	6	-0.21

XJ10-015-51	0.68	0.05352	0.00279	0.40988	0.02137	0.05553	0.00086	351	90	349	15	348	5	0.29
XJ10-015-52	1.16	0.04879	0.00304	0.15194	0.00944	0.02258	0.00036	138	110	144	8	144	2	0
XJ10-015-53	0.81	0.04899	0.00365	0.15499	0.01153	0.02294	0.00036	147	138	146	10	146	2	0
XJ10-015-54	0.26	0.07033	0.00114	1.53802	0.02785	0.15857	0.00216	938	17	946	11	949	12	-0.32
~~**XJ10-015-55**~~	~~1.12~~	~~0.07359~~	~~0.00459~~	~~0.56157~~	~~0.03374~~	~~0.05534~~	~~0.00093~~	~~1030~~	~~130~~	~~453~~	~~22~~	~~347~~	~~6~~	~~30.55~~
XJ10-015-56	1.28	0.04899	0.00269	0.14925	0.00821	0.02209	0.00034	147	97	141	7	141	2	0
XJ10-015-57	0.38	0.05336	0.00161	0.39084	0.01209	0.05311	0.00076	344	44	335	9	334	5	0.3
XJ10-015-58	0.73	0.04889	0.00252	0.16559	0.00854	0.02456	0.00038	143	89	156	7	156	2	0
XJ10-015-59	0.56	0.05302	0.00108	0.39518	0.0086	0.05405	0.00074	330	26	338	6	339	5	-0.29
XJ10-015-60	0.43	0.05185	0.00213	0.33087	0.0137	0.04627	0.00069	279	67	290	10	292	4	-0.68
XJ10-015-61	0.78	0.04877	0.00404	0.1414	0.0117	0.02102	0.00034	137	155	134	10	134	2	0
XJ10-015-62	0.53	0.05234	0.00186	0.35653	0.01287	0.04939	0.00072	300	56	310	10	311	4	-0.32
XJ10-015-63	0.72	0.05279	0.00318	0.3653	0.02189	0.05018	0.00085	320	106	316	16	316	5	0
XJ10-015-64	0.34	0.05344	0.0012	0.40564	0.00962	0.05504	0.00077	348	29	346	7	345	5	0.29
XJ10-015-65	0.82	0.05271	0.00118	0.34659	0.00821	0.04768	0.00066	316	30	302	6	300	4	0.67
XJ10-015-66	0.98	0.06745	0.00117	1.20884	0.02304	0.12995	0.00178	852	19	805	11	788	10	2.16
XJ10-015-67	0.93	0.05311	0.00191	0.36056	0.01318	0.04923	0.00071	333	57	313	10	310	4	0.97
XJ10-015-68	0.47	0.0527	0.00182	0.3564	0.01242	0.04904	0.00074	316	52	310	9	309	5	0.32

XJ10-015-69	0.47	0.05201	0.00215	0.33095	0.01379	0.04614	0.00068	286	68	290	11	291	4	-0.34
XJ10-015-70	0.47	0.05269	0.00135	0.35834	0.00954	0.04932	0.00069	315	36	311	7	310	4	0.32
XJ10-015-71	0.66	0.04892	0.00322	0.14873	0.0098	0.02204	0.00034	144	120	141	9	141	2	0
XJ10-015-72	0.92	0.05266	0.00237	0.37078	0.01677	0.05105	0.00079	314	75	320	12	321	5	-0.31
XJ10-015-73	0.62	0.05312	0.00221	0.36172	0.01516	0.04938	0.00075	334	67	313	11	311	5	0.64
XJ10-015-74	0.28	0.05637	0.00124	0.57871	0.01349	0.07444	0.00104	467	28	464	9	463	6	0.22
XJ10-015-75	0.95	0.04906	0.00157	0.16121	0.00525	0.02383	0.00035	151	49	152	5	152	2	0
XJ10-015-76	0.4	0.05199	0.00101	0.33653	0.00704	0.04693	0.00065	285	24	295	5	296	4	-0.34
XJ10-015-77	0.7	0.04882	0.00228	0.14547	0.00683	0.02161	0.00032	139	81	138	6	138	2	0
XJ10-015-78	1.05	0.05267	0.00115	0.35888	0.00832	0.04941	0.00068	315	29	311	6	311	4	0
XJ10-015-79	0.47	0.05304	0.00163	0.37619	0.0118	0.05143	0.00074	331	45	324	9	323	5	0.31
XJ10-015-80	0.36	0.05562	0.00141	0.53145	0.01399	0.06929	0.00097	437	34	433	9	432	6	0.23
XJ10-015-81	1.43	0.05077	0.00223	0.24897	0.01102	0.03556	0.00052	230	75	226	9	225	3	0.44
XJ10-015-82	0.19	0.05546	0.00106	0.53089	0.01099	0.06942	0.00096	431	23	432	7	433	6	-0.23
XJ10-015-83	0.78	0.0546	0.00181	0.47615	0.01607	0.06323	0.00092	396	50	395	11	395	6	0
XJ10-015-84	0.78	0.05242	0.00131	0.35481	0.00925	0.04908	0.00069	304	34	308	7	309	4	-0.32
XJ10-015-85	0.94	0.05286	0.00164	0.36663	0.01167	0.05029	0.00072	323	46	317	9	316	4	0.32
XJ10-015-86	0.61	0.05251	0.00206	0.32391	0.01283	0.04473	0.00066	308	63	285	10	282	4	1.06

XJ10-015-87	1.86	0.07027	0.00134	1.5804	0.03253	0.16309	0.00226	936	21	963	13	974	13	-1.13
XJ10-015-88	0.65	0.04882	0.00144	0.14029	0.00426	0.02083	0.00029	139	45	133	4	133	2	0
XJ10-015-89	0.76	0.05315	0.0014	0.38587	0.01054	0.05264	0.00074	335	37	331	8	331	5	0
XJ10-015-90	0.69	0.05398	0.00148	0.42573	0.01203	0.05719	0.00082	370	38	360	9	359	5	0.28
XJ10-015-91	0.69	0.05746	0.00125	0.63066	0.0145	0.07958	0.00111	509	27	497	9	494	7	0.61
XJ10-015-92	0.73	0.04942	0.0016	0.17183	0.00568	0.02521	0.00037	168	50	161	5	160	2	0.63
XJ10-015-93	0.57	0.05844	0.00129	0.70762	0.01652	0.0878	0.00123	546	28	543	10	543	7	0
XJ10-015-94	0.15	0.0569	0.00134	0.5725	0.01415	0.07295	0.00103	488	30	460	9	454	6	1.32
XJ10-015-95	0.96	0.04972	0.00201	0.18793	0.00758	0.02741	0.00044	182	64	175	6	174	3	0.57
XJ10-015-96	0.43	0.05303	0.00153	0.38811	0.01152	0.05307	0.00076	330	42	333	8	333	5	0
XJ10-015-97	0.27	0.05458	0.00144	0.48101	0.01313	0.06391	0.00091	395	36	399	9	399	6	0
XJ10-015-98	0.73	0.04605	0.00204	0.12805	0.00536	0.02017	0.00029		95	122	5	129	2	-5.43
XJ10-015-99	0.43	0.05618	0.00149	0.55299	0.01509	0.07138	0.00103	459	35	447	10	444	6	0.68
XJ10-015-100	0.16	0.05292	0.00157	0.37785	0.01148	0.05177	0.00075	325	43	325	8	325	5	0
XJ09-010														
XJ09-010-1	0.77	0.05453	0.00181	0.38912	0.01283	0.05173	0.00069	393	50	334	9	325	4	2.77
XJ09-010-2	0.48	0.05342	0.00162	0.31026	0.0094	0.04211	0.00055	347	45	274	7	266	3	3.01
XJ09-010-3	0.42	0.05669	0.00222	0.35615	0.01383	0.04555	0.00064	479	61	309	10	287	4	7.67

XJ09-010-4	0.99	0.05652	0.0037	0.38051	0.0246	0.04881	0.00081	473	114	327	18	307	5	6.51
XJ09-010-5	1.55	0.06493	0.00129	1.08148	0.02192	0.12075	0.0015	772	23	744	11	735	9	1.22
XJ09-010-6	0.28	0.05259	0.00167	0.35167	0.01112	0.04848	0.00064	311	48	306	8	305	4	0.33
XJ09-010-7	0.67	0.0573	0.00304	0.40274	0.02116	0.05096	0.00079	503	88	344	15	320	5	7.5
XJ09-010-8	0.54	0.05434	0.00237	0.32352	0.014	0.04317	0.00062	385	71	285	11	272	4	4.78
XJ09-010-9	0.89	0.05329	0.00137	0.37425	0.00971	0.05092	0.00065	341	36	323	7	320	4	0.94
XJ09-010-10	0.35	0.05323	0.00337	0.39247	0.02461	0.05346	0.00086	339	113	336	18	336	5	0
XJ09-010-11	0.93	0.0509	0.0022	0.36696	0.01578	0.05227	0.00074	236	73	317	12	328	5	-3.35
XJ09-010-12	0.97	0.0527	0.00143	0.35224	0.00956	0.04846	0.00063	316	38	306	7	305	4	0.33
XJ09-010-13	1.11	0.05392	0.00125	0.35577	0.00835	0.04783	0.0006	368	31	309	6	301	4	2.66
XJ09-010-14	0.84	0.05662	0.00219	0.36431	0.014	0.04665	0.00066	477	60	315	10	294	4	7.14
XJ09-010-15	0.86	0.05371	0.00215	0.42097	0.01674	0.05683	0.0008	359	64	357	12	356	5	0.28
XJ09-010-16	1.61	0.04663	0.00296	0.1636	0.01032	0.02544	0.00039	30	108	154	9	162	2	-4.94
XJ09-010-17	0.62	0.05184	0.00151	0.3136	0.00916	0.04386	0.00058	278	43	277	7	277	4	0
XJ09-010-18	0.78	0.05221	0.00159	0.37258	0.01136	0.05174	0.00069	295	45	322	8	325	4	-0.92
XJ09-010-19	0.88	0.07011	0.00156	1.51348	0.03408	0.15651	0.00199	932	26	936	14	937	11	-0.11
XJ09-010-20	0.55	0.05353	0.00253	0.36455	0.01653	0.04939	0.00067	351	110	316	12	311	4	1.61
XJ09-010-21	0.56	0.05255	0.00208	0.31932	0.01254	0.04406	0.00063	309	63	281	10	278	4	1.08

XJ09-010-22	0.46	0.05151	0.00196	0.34375	0.01298	0.04839	0.00067	264	61	300	10	305	4	-1.64
~~**XJ09-010-23**~~	~~0.78~~	~~0.14717~~	~~0.00468~~	~~7.27084~~	~~0.20738~~	~~0.35832~~	~~0.00502~~	~~2313~~	~~56~~	~~2145~~	~~25~~	~~1974~~	~~24~~	~~17.17~~
~~**XJ09-010-24**~~	~~0.64~~	~~0.09313~~	~~0.00282~~	~~0.34941~~	~~0.0099~~	~~0.0272~~	~~0.00047~~	~~1491~~	~~29~~	~~304~~	~~7~~	~~173~~	~~3~~	~~75.72~~
XJ09-010-25	0.95	0.05198	0.00171	0.37779	0.01242	0.0527	0.00071	285	50	325	9	331	4	-1.81
XJ09-010-26	0.33	0.05282	0.00138	0.3863	0.01019	0.05302	0.00069	321	37	332	7	333	4	-0.3
XJ09-010-27	0.73	0.05689	0.00129	0.54412	0.01251	0.06935	0.00088	487	29	441	8	432	5	2.08
XJ09-010-28	0.37	0.05717	0.0014	0.55951	0.01387	0.07096	0.00091	498	32	451	9	442	5	2.04
XJ09-010-29	1.35	0.05382	0.00205	0.38535	0.0146	0.05191	0.00073	364	60	331	11	326	4	1.53
XJ09-010-30	0.88	0.05203	0.00428	0.31848	0.02567	0.04439	0.00075	287	188	281	20	280	5	0.36
XJ09-010-31	0.67	0.04814	0.0027	0.30101	0.0168	0.04534	0.00068	106	97	267	13	286	4	-6.64
XJ09-010-32	0.47	0.05371	0.0025	0.37489	0.01733	0.05061	0.00075	359	77	323	13	318	5	1.57
XJ09-010-33	0.74	0.0568	0.00156	0.5548	0.01528	0.07083	0.00094	484	38	448	10	441	6	1.59
XJ09-010-34	0.66	0.0558	0.00142	0.5263	0.01351	0.06839	0.00089	444	34	429	9	426	5	0.7
XJ09-010-35	0.68	0.05317	0.00207	0.33399	0.01296	0.04555	0.00064	336	62	293	10	287	4	2.09
XJ09-010-36	0.68	0.05455	0.00176	0.33516	0.01079	0.04455	0.0006	394	48	293	8	281	4	4.27
XJ09-010-37	0.75	0.05289	0.00218	0.32146	0.01319	0.04407	0.00062	324	67	283	10	278	4	1.8
XJ09-010-38	1.15	0.05673	0.00316	0.38839	0.02139	0.04964	0.0008	481	93	333	16	312	5	6.73
XJ09-010-39	0.48	0.05252	0.00243	0.31861	0.01462	0.04399	0.00065	308	77	281	11	278	4	1.08

XJ09-010-40	0.8	0.0561	0.00173	0.38041	0.01173	0.04917	0.00067	456	44	327	9	309	4	5.83
XJ09-010-41	0.82	0.05322	0.00173	0.38458	0.01249	0.0524	0.00072	338	49	330	9	329	4	0.3
XJ09-010-42	0.63	0.05543	0.00264	0.51518	0.02431	0.06739	0.00101	430	78	422	16	420	6	0.48
XJ09-010-43	0.38	0.05347	0.00152	0.36683	0.01049	0.04974	0.00066	349	41	317	8	313	4	1.28
XJ09-010-44	0.82	0.0566	0.00211	0.4081	0.01514	0.05229	0.00074	476	57	348	11	329	5	5.78
XJ09-010-45	0.87	0.05609	0.00152	0.56053	0.01535	0.07246	0.00096	456	37	452	10	451	6	0.22
XJ09-010-46	0.61	0.0541	0.00261	0.34678	0.01658	0.04648	0.00071	375	80	302	13	293	4	3.07
XJ09-010-47	0.34	0.05621	0.00183	0.55818	0.01814	0.072	0.00099	461	48	450	12	448	6	0.45
XJ09-010-48	0.51	0.05319	0.00215	0.39935	0.01605	0.05445	0.00078	337	65	341	12	342	5	-0.29
XJ09-010-49	0.76	0.05054	0.00144	0.31445	0.00902	0.04512	0.0006	220	42	278	7	284	4	-2.11
XJ09-010-50	0.58	0.05229	0.0017	0.39398	0.0128	0.05464	0.00075	298	49	337	9	343	5	-1.75
XJ09-010-51	0.78	0.05369	0.00163	0.38973	0.01187	0.05263	0.00071	358	44	334	9	331	4	0.91
XJ09-010-52	0.6	0.05722	0.00186	0.5877	0.01908	0.07448	0.00103	500	47	469	12	463	6	1.3
XJ09-010-53	0.66	0.05127	0.00149	0.38378	0.01125	0.05428	0.00073	253	43	330	8	341	4	-3.23
XJ09-010-54	0.66	0.05549	0.00138	0.56477	0.01425	0.0738	0.00097	432	33	455	9	459	6	-0.87
XJ09-010-55	0.62	0.05381	0.00181	0.37459	0.01259	0.05048	0.0007	363	51	323	9	317	4	1.89
XJ09-010-56	0.38	0.053	0.00157	0.33723	0.01004	0.04614	0.00062	329	43	295	8	291	4	1.37
XJ09-010-57	0.59	0.05321	0.0021	0.36997	0.01457	0.05042	0.00072	338	63	320	11	317	4	0.95

XJ09-010-58	0.45	0.05495	0.00164	0.49282	0.0148	0.06504	0.00088	410	43	407	10	406	5	0.25
XJ09-010-59	1.84	0.12776	0.00295	6.79866	0.16015	0.38589	0.00512	2067	23	2086	21	2104	24	-1.76
XJ09-010-60	0.6	0.05415	0.0026	0.33525	0.01598	0.0449	0.00068	377	80	294	12	283	4	3.89
XJ09-010-61	0.61	0.05329	0.00239	0.4024	0.01798	0.05476	0.00081	341	74	343	13	344	5	-0.29
XJ09-010-62	1.01	0.0577	0.00172	0.57701	0.01726	0.07252	0.00099	518	42	463	11	451	6	2.66
XJ09-010-63	0.89	0.05766	0.00198	0.42422	0.01459	0.05336	0.00075	517	51	359	10	335	5	7.16
XJ09-010-64	0.62	0.05187	0.0022	0.40405	0.01708	0.05649	0.00083	280	70	345	12	354	5	-2.54
XJ09-010-65	0.97	0.05496	0.00223	0.36067	0.01458	0.04759	0.0007	411	64	313	11	300	4	4.33
XJ09-010-66	0.57	0.05505	0.00197	0.40868	0.01456	0.05384	0.00077	414	54	348	10	338	5	2.96
XJ09-010-67	0.61	0.05479	0.00163	0.51439	0.01537	0.06809	0.00093	404	43	421	10	425	6	-0.94
XJ09-010-68	0.66	0.0527	0.00339	0.333	0.02125	0.04583	0.00075	316	116	292	16	289	5	1.04
XJ09-010-69	0.51	0.0524	0.00155	0.41432	0.01238	0.05734	0.00078	303	43	352	9	359	5	-1.95
XJ09-010-70	0.52	0.05143	0.00171	0.32884	0.01095	0.04637	0.00065	260	51	289	8	292	4	-1.03
XJ09-010-71	1.75	0.05348	0.00257	0.36454	0.01738	0.04944	0.00076	349	80	316	13	311	5	1.61
XJ09-010-72	0.52	0.05503	0.00183	0.41282	0.01374	0.0544	0.00077	413	49	351	10	341	5	2.93
XJ09-010-73	0.7	0.05309	0.00225	0.3244	0.01369	0.04431	0.00066	333	69	285	10	279	4	2.15
XJ09-010-74	1.11	0.05154	0.00299	0.36281	0.02088	0.05105	0.00082	265	103	314	16	321	5	-2.18
XJ09-010-75	0.47	0.05643	0.00169	0.54169	0.01634	0.06962	0.00096	469	42	440	11	434	6	1.38

XJ09-010-76	0.66	0.05006	0.00174	0.35242	0.01227	0.05105	0.00072	198	55	307	9	321	4	-4.36
XJ09-010-77	0.62	0.05227	0.00272	0.40036	0.02067	0.05555	0.00087	297	89	342	15	349	5	-2.01
XJ09-010-78	0.49	0.05263	0.00172	0.38814	0.01277	0.05349	0.00075	313	49	333	9	336	5	-0.89
XJ09-010-79	0.49	0.05154	0.00154	0.3526	0.01061	0.04962	0.00068	265	44	307	8	312	4	-1.6
XJ09-010-80	0.75	0.05136	0.00189	0.341	0.01256	0.04815	0.00069	257	58	298	10	303	4	-1.65
XJ09-010-81	1.1	0.07131	0.00191	1.74839	0.04768	0.17781	0.00243	966	34	1027	18	1055	13	-8.44
XJ09-010-82	1.28	0.05288	0.00149	0.36055	0.01031	0.04945	0.00068	324	40	313	8	311	4	0.64
XJ09-010-83	0.96	0.05618	0.00264	0.41638	0.01946	0.05375	0.00083	459	76	353	14	338	5	4.44
XJ09-010-84	1.5	0.0573	0.002	0.38791	0.01356	0.0491	0.00071	503	51	333	10	309	4	7.77
XJ09-010-85	0.98	0.05248	0.00285	0.37983	0.02047	0.05249	0.00085	306	93	327	15	330	5	-0.91
XJ09-010-86	0.68	0.16976	0.00443	11.66535	0.31074	0.4984	0.00683	2555	27	2578	25	2607	29	-1.99
XJ09-010-87	0.4	0.05642	0.00191	0.55424	0.01889	0.07125	0.00102	469	50	448	12	444	6	0.9
XJ09-010-88	0.36	0.0547	0.00183	0.5087	0.0171	0.06746	0.00097	400	50	418	12	421	6	-0.71
XJ09-010-89	1.51	0.05123	0.01311	0.2878	0.07331	0.04074	0.00097	251	459	257	58	257	6	0
XJ09-010-90	0.71	0.05152	0.00273	0.32952	0.01739	0.04639	0.00074	264	92	289	13	292	5	-1.03
XJ09-010-91	0.53	0.05021	0.00285	0.31241	0.01765	0.04513	0.00073	205	100	276	14	285	5	-3.16
XJ09-010-92	0.67	0.0529	0.0021	0.4076	0.01618	0.05589	0.00083	325	63	347	12	351	5	-1.14
XJ09-010-93	0.68	0.05319	0.00191	0.36904	0.01327	0.05032	0.00074	337	55	319	10	316	5	0.95

XJ09-010-94	0.84	0.05588	0.00183	0.53133	0.01759	0.06896	0.00099	448	48	433	12	430	6	0.7
XJ09-010-95	0.98	0.05589	0.00203	0.42752	0.0156	0.05548	0.00082	448	55	361	11	348	5	3.74
XJ09-010-96	0.91	0.093	0.00277	3.44541	0.10405	0.26872	0.00384	1488	36	1515	24	1534	20	-3
XJ09-010-97	0.64	0.05574	0.00198	0.41962	0.01501	0.0546	0.0008	442	53	356	11	343	5	3.79
XJ09-010-98	0.43	0.05677	0.00175	0.56463	0.01762	0.07215	0.00103	483	44	455	11	449	6	1.34
XJ09-010-99	0.42	0.05586	0.00206	0.48335	0.01791	0.06277	0.00093	447	56	400	12	392	6	2.04
XJ09-010-100	0.85	0.05616	0.00194	0.46028	0.01599	0.05945	0.00087	459	51	384	11	372	5	3.23
XJ09-011														
XJ09-011-1	0.45	0.05532	0.00232	0.37434	0.0156	0.04907	0.0007	425	67	323	12	309	4	4.53
XJ09-011-2	0.89	0.05972	0.00182	0.83152	0.02534	0.10097	0.00137	593	43	614	14	620	8	-0.97
XJ09-011-3	0.47	0.05155	0.00158	0.35126	0.01079	0.04942	0.00066	266	46	306	8	311	4	-1.61
XJ09-011-4	0.47	0.05277	0.00251	0.35047	0.01658	0.04816	0.00071	319	81	305	12	303	4	0.66
XJ09-011-5	0.43	0.05287	0.00285	0.3559	0.019	0.04882	0.00075	323	93	309	14	307	5	0.65
XJ09-011-6	0.88	0.05446	0.00239	0.44184	0.01926	0.05884	0.00086	390	71	372	14	369	5	0.81
XJ09-011-7	0.63	0.05408	0.00147	0.49152	0.0134	0.06591	0.00087	374	38	406	9	411	5	-1.22
XJ09-011-8	0.4	0.05296	0.00179	0.35375	0.01193	0.04844	0.00066	327	52	308	9	305	4	0.98
XJ09-011-9	0.48	0.05308	0.00248	0.35948	0.01666	0.04911	0.00072	332	78	312	12	309	4	0.97
XJ09-011-10	0.49	0.05445	0.00256	0.48087	0.02155	0.06406	0.00089	390	108	399	15	400	5	-0.25

XJ09-011-11	0.65	0.05528	0.0026	0.38092	0.01778	0.04997	0.00074	424	78	328	13	314	5	4.46
XJ09-011-12	0.45	0.05466	0.00231	0.35939	0.01507	0.04767	0.00069	398	68	312	11	300	4	4
XJ09-011-13	0.48	0.05303	0.00228	0.36251	0.01548	0.04957	0.00073	330	70	314	12	312	4	0.64
XJ09-011-14	0.8	0.05245	0.00168	0.36099	0.01153	0.04991	0.00068	305	48	313	9	314	4	-0.32
XJ09-011-15	0.49	0.05125	0.00223	0.3475	0.01506	0.04917	0.0007	252	73	303	11	309	4	-1.94
XJ09-011-16	0.5	0.04813	0.00209	0.3693	0.01597	0.05564	0.0008	106	72	319	12	349	5	-8.6
XJ09-011-17	0.44	0.05489	0.00292	0.36416	0.01915	0.04811	0.00077	408	89	315	14	303	5	3.96
XJ09-011-18	0.44	0.05343	0.00198	0.36481	0.01348	0.04951	0.00069	347	58	316	10	312	4	1.28
XJ09-011-19	0.63	0.05206	0.00219	0.35324	0.01481	0.04921	0.0007	288	70	307	11	310	4	-0.97
XJ09-011-20	0.7	0.05152	0.00312	0.35341	0.02124	0.04974	0.00077	264	110	307	16	313	5	-1.92
XJ09-011-21	0.89	0.05493	0.00203	0.34508	0.01269	0.04555	0.00063	409	57	301	10	287	4	4.88
XJ09-011-22	0.76	0.05604	0.00215	0.4626	0.01761	0.05986	0.00084	454	59	386	12	375	5	2.93
XJ09-011-25	0.45	0.05664	0.00304	0.4067	0.02162	0.05207	0.00082	478	90	346	16	327	5	5.81
XJ09-011-26	0.59	0.05679	0.00186	0.3952	0.01289	0.05046	0.00069	483	48	338	9	317	4	6.62
XJ09-011-27	0.98	0.05424	0.00149	0.52221	0.01439	0.06982	0.00091	381	39	427	10	435	5	-1.84
XJ09-011-28	0.5	0.0516	0.00252	0.35528	0.01723	0.04993	0.00073	268	84	309	13	314	4	-1.59
XJ09-011-29	0.63	0.05326	0.00223	0.37297	0.01549	0.05078	0.00073	340	68	322	11	319	4	0.94
XJ09-011-30	0.43	0.05787	0.00306	0.57279	0.02925	0.07179	0.00101	525	119	460	19	447	6	2.91

XJ09-011-31	0.44	0.0517	0.00169	0.3492	0.0114	0.04898	0.00066	272	50	304	9	308	4	-1.3
XJ09-011-32	1.34	0.05172	0.00163	0.36465	0.01148	0.05113	0.00069	273	47	316	9	321	4	-1.56
XJ09-011-33	0.62	0.0535	0.00166	0.39721	0.01234	0.05384	0.00072	350	46	340	9	338	4	0.59
XJ09-011-34	0.55	0.05695	0.00309	0.39853	0.02127	0.05075	0.00084	490	88	341	15	319	5	6.9
XJ09-011-35	0.44	0.07745	0.00184	2.09768	0.05037	0.19639	0.00257	1133	27	1148	17	1156	14	-1.99
XJ09-011-36	0.54	0.05152	0.00131	0.34789	0.0089	0.04896	0.00063	264	35	303	7	308	4	-1.62
XJ09-011-37	0.55	0.05161	0.00129	0.36321	0.00914	0.05103	0.00066	268	34	315	7	321	4	-1.87
XJ09-011-38	0.87	0.05107	0.00136	0.34942	0.00933	0.04961	0.00065	244	38	304	7	312	4	-2.56
XJ09-011-39	0.49	0.05207	0.00249	0.36009	0.01706	0.05015	0.00074	288	81	312	13	315	5	-0.95
XJ09-011-40	0.55	0.0552	0.0022	0.39683	0.01572	0.05213	0.00074	420	63	339	11	328	5	3.35
XJ09-011-41	1.01	0.05484	0.00151	0.43557	0.01202	0.05759	0.00076	406	38	367	9	361	5	1.66
XJ09-011-42	0.54	0.05202	0.00197	0.4725	0.0178	0.06586	0.00091	286	61	393	12	411	6	-4.38
XJ09-011-43	0.7	0.05146	0.00165	0.35025	0.01122	0.04936	0.00067	261	49	305	8	311	4	-1.93
XJ09-011-44	0.62	0.05072	0.00162	0.32282	0.01028	0.04615	0.00062	228	49	284	8	291	4	-2.41
XJ09-011-45	0.41	0.04946	0.00267	0.34623	0.01852	0.05076	0.00076	170	95	302	14	319	5	-5.33
XJ09-011-46	0.54	0.05103	0.00276	0.35806	0.01917	0.05088	0.00077	242	96	311	14	320	5	-2.81
XJ09-011-47	0.63	0.05226	0.00202	0.36109	0.01387	0.0501	0.0007	297	62	313	10	315	4	-0.63
XJ09-011-48	0.5	0.05193	0.00128	0.35605	0.00883	0.04971	0.00064	282	34	309	7	313	4	-1.28

XJ09-011-49	0.53	0.04742	0.00215	0.33084	0.01493	0.05059	0.00073	70	73	290	11	318	4	-8.81
XJ09-011-50	0.42	0.04984	0.00173	0.34816	0.01202	0.05065	0.00069	188	55	303	9	319	4	-5.02
XJ09-011-51	0.79	0.05141	0.00252	0.39483	0.01919	0.05569	0.00083	259	84	338	14	349	5	-3.15
XJ09-011-52	0.25	0.05021	0.00136	0.30936	0.00842	0.04468	0.00058	205	39	274	7	282	4	-2.84
XJ09-011-53	0.81	0.05465	0.00149	0.47156	0.0129	0.06257	0.00082	398	38	392	9	391	5	0.26
XJ09-011-54	0.39	0.05325	0.00209	0.3632	0.01416	0.04946	0.0007	339	63	315	11	311	4	1.29
XJ09-011-55	0.52	0.05031	0.0019	0.34655	0.013	0.04995	0.00069	209	61	302	10	314	4	-3.82
XJ09-011-56	0.98	0.05333	0.00225	0.3856	0.01613	0.05243	0.00076	343	68	331	12	329	5	0.61
XJ09-011-57	0.48	0.04771	0.00393	0.3423	0.02794	0.05203	0.00094	85	147	299	21	327	6	-8.56
XJ09-011-58	0.64	0.0557	0.00258	0.4751	0.02179	0.06185	0.00092	440	75	395	15	387	6	2.07
XJ09-011-59	0.65	0.05205	0.00168	0.35873	0.01156	0.04998	0.00068	288	49	311	9	314	4	-0.96
XJ09-011-60	0.88	0.06882	0.00163	1.42549	0.03407	0.15019	0.00194	893	29	900	14	902	11	-0.22
XJ09-011-61	0.54	0.05334	0.00143	0.35342	0.00947	0.04805	0.00063	343	37	307	7	303	4	1.32
XJ09-011-62	1.03	0.05471	0.00235	0.39896	0.01697	0.05288	0.00077	400	69	341	12	332	5	2.71
XJ09-011-63	0.53	0.05394	0.00252	0.37023	0.01715	0.04977	0.00074	369	77	320	13	313	5	2.24
XJ09-011-64	0.48	0.04966	0.00191	0.34366	0.0131	0.05018	0.0007	179	63	300	10	316	4	-5.06
XJ09-011-65	0.54	0.05246	0.00166	0.35919	0.01135	0.04964	0.00067	306	47	312	8	312	4	0
XJ09-011-66	0.37	0.05509	0.00422	0.40714	0.03088	0.05359	0.00093	416	140	347	22	337	6	2.97

XJ09-011-67	0.52	0.05629	0.00297	0.4312	0.0225	0.05555	0.00087	464	88	364	16	349	5	4.3
XJ09-011-68	0.89	0.04999	0.00198	0.3391	0.01331	0.04919	0.00069	195	65	296	10	310	4	-4.52
XJ09-011-69	0.89	0.04994	0.00217	0.33307	0.01436	0.04836	0.0007	192	73	292	11	304	4	-3.95
XJ09-011-70	0.59	0.05492	0.00199	0.50893	0.01826	0.06719	0.00094	409	55	418	12	419	6	-0.24
XJ09-011-71	0.71	0.04839	0.00219	0.32651	0.01467	0.04893	0.00071	118	76	287	11	308	4	-6.82
XJ09-011-72	0.58	0.05118	0.00178	0.34994	0.01207	0.04958	0.00068	249	54	305	9	312	4	-2.24
XJ09-011-73	0.82	0.05251	0.00248	0.38069	0.01776	0.05257	0.00079	308	79	328	13	330	5	-0.61
XJ09-011-74	0.65	0.05198	0.00182	0.34191	0.01188	0.04769	0.00066	285	54	299	9	300	4	-0.33
XJ09-011-75	0.71	0.04968	0.0038	0.35194	0.02657	0.05137	0.00094	180	136	306	20	323	6	-5.26
XJ09-011-76	0.6	0.05021	0.00247	0.34229	0.01661	0.04943	0.00075	205	84	299	13	311	5	-3.86
XJ09-011-77	0.49	0.05169	0.00322	0.34229	0.02112	0.04802	0.00077	272	112	299	16	302	5	-0.99
XJ09-011-78	0.46	0.05817	0.00345	0.37975	0.02219	0.04734	0.00081	536	98	327	16	298	5	9.73
XJ09-011-79	0.65	0.04833	0.00244	0.32715	0.01634	0.04909	0.00073	115	86	287	13	309	4	-7.12
XJ09-011-80	0.79	0.04826	0.00306	0.33494	0.02101	0.05033	0.00081	112	110	293	16	317	5	-7.57
XJ09-011-81	0.87	0.05268	0.00251	0.24657	0.01161	0.03394	0.00051	315	80	224	9	215	3	4.19
XJ09-011-82	0.64	0.05131	0.00227	0.36339	0.01588	0.05135	0.00076	255	73	315	12	323	5	-2.48
XJ09-011-83	0.51	0.05585	0.00269	0.49517	0.02281	0.06431	0.0009	446	110	408	15	402	5	1.49
XJ09-011-84	0.74	0.05866	0.00292	0.53683	0.02634	0.06635	0.00104	555	80	436	17	414	6	5.31

XJ09-011-85	0.63	0.05116	0.00315	0.35802	0.02178	0.05074	0.00081	248	111	311	16	319	5	-2.51
XJ09-011-86	0.45	0.05186	0.00171	0.35515	0.01161	0.04966	0.00068	279	50	309	9	312	4	-0.96
XJ09-011-87	0.44	0.0572	0.00199	0.46773	0.01608	0.05929	0.00083	499	51	390	11	371	5	5.12
XJ09-011-88	0.52	0.05278	0.00152	0.34763	0.00992	0.04776	0.00064	319	41	303	7	301	4	0.66
XJ09-011-89	0.64	0.05293	0.00286	0.3811	0.02032	0.05221	0.00082	326	93	328	15	328	5	0
XJ09-011-90	0.56	0.05347	0.0029	0.37455	0.02008	0.05079	0.00079	349	93	323	15	319	5	1.25
XJ09-011-91	0.91	0.0541	0.00256	0.3623	0.01693	0.04856	0.00073	375	78	314	13	306	4	2.61
XJ09-011-92	1.17	0.04976	0.00368	0.31123	0.02271	0.04535	0.00082	184	131	275	18	286	5	-3.85
XJ09-011-93	0.65	0.05551	0.00314	0.36984	0.02064	0.04831	0.00079	433	95	320	15	304	5	5.26
XJ09-011-94	0.84	0.0544	0.00174	0.37511	0.01189	0.05	0.00069	388	46	323	9	315	4	2.54
XJ09-011-95	1.14	0.05318	0.00178	0.45626	0.01513	0.06221	0.00086	336	50	382	11	389	5	-1.8
XJ09-011-96	0.66	0.05747	0.00405	0.4093	0.02839	0.05164	0.00095	510	121	348	20	325	6	7.08
XJ09-011-97	0.43	0.0582	0.00217	0.58528	0.0215	0.07292	0.00105	537	55	468	14	454	6	3.08
XJ09-011-98	0.62	0.08362	0.00383	2.43553	0.10601	0.21125	0.00303	1284	92	1253	31	1235	16	3.97
XJ09-011-99	0.64	0.05019	0.00345	0.33416	0.02272	0.04828	0.0008	204	124	293	17	304	5	-3.62
XJ09-011-100	0.91	0.0571	0.00236	0.40971	0.01669	0.05203	0.00077	495	64	349	12	327	5	6.73
XJ09-003														
XJ09-003-1	0.59	0.12602	0.00203	6.48303	0.10944	0.37298	0.00448	2043	15	2044	15	2043	21	0

XJ09-003-2	0.3	0.05527	0.00153	0.51534	0.01434	0.0676	0.00087	423	39	422	10	422	5	0
~~**XJ09-003-3**~~	~~0.22~~	~~0.15882~~	~~0.0033~~	~~8.23784~~	~~0.14032~~	~~0.37619~~	~~0.00447~~	~~2443~~	~~36~~	~~2258~~	~~15~~	~~2058~~	~~21~~	~~18.71~~
XJ09-003-4	0.54	0.05549	0.00125	0.52919	0.01214	0.06915	0.00086	432	29	431	8	431	5	0
XJ09-003-5	0.69	0.05356	0.00277	0.3865	0.01986	0.05232	0.00075	353	90	332	15	329	5	0.91
XJ09-003-6	0.4	0.05701	0.00124	0.63493	0.014	0.08076	0.001	492	27	499	9	501	6	-0.4
XJ09-003-7	0.13	0.05044	0.00108	0.23409	0.00511	0.03365	0.00041	215	29	214	4	213	3	0.47
XJ09-003-8	1.02	0.05426	0.00457	0.48785	0.04068	0.06519	0.00114	382	157	403	28	407	7	-0.98
XJ09-003-9	0.98	0.05213	0.00252	0.35807	0.01721	0.04981	0.0007	291	84	311	13	313	4	-0.64
XJ09-003-10	0.4	0.05697	0.00629	0.47988	0.05284	0.06108	0.00095	490	219	398	36	382	6	4.19
XJ09-003-11	0.54	0.05536	0.00136	0.52243	0.01296	0.06843	0.00086	427	33	427	9	427	5	0
XJ09-003-12	0.72	0.05139	0.00141	0.30591	0.00846	0.04317	0.00054	258	41	271	7	272	3	-0.37
XJ09-003-13	1.83	0.04909	0.00259	0.17094	0.00897	0.02525	0.00036	152	93	160	8	161	2	-0.62
XJ09-003-14	0.29	0.05622	0.00136	0.58714	0.01438	0.07572	0.00095	461	32	469	9	471	6	-0.42
XJ09-003-15	0.78	0.05226	0.00129	0.33685	0.00837	0.04674	0.00058	297	34	295	6	294	4	0.34
XJ09-003-16	0.55	0.04605	0.00584	0.27319	0.03448	0.04303	0.00057		243	245	27	272	4	-9.93
XJ09-003-17	0.11	0.06936	0.00127	1.43934	0.02722	0.15047	0.00182	909	20	905	11	904	10	0.11
XJ09-003-18	0.03	0.05031	0.00135	0.23697	0.00638	0.03416	0.00043	209	39	216	5	217	3	-0.46
XJ09-003-19	0.69	0.05001	0.00473	0.17449	0.01644	0.0253	0.00039	195	184	163	14	161	2	1.24

XJ09-003-20	0.52	0.05427	0.00138	0.46369	0.01184	0.06195	0.00078	382	35	387	8	387	5	0
XJ09-003-21	0.52	0.05269	0.00315	0.35619	0.02121	0.04902	0.0007	315	110	309	16	309	4	0
XJ09-003-22	0.71	0.05297	0.00283	0.34783	0.01855	0.04762	0.00064	328	97	303	14	300	4	1
XJ09-003-23	0.87	0.04887	0.0018	0.16651	0.00615	0.02471	0.00031	142	63	156	5	157	2	-0.64
XJ09-003-24	0.52	0.05187	0.00165	0.31034	0.00986	0.04339	0.00055	280	49	274	8	274	3	0
XJ09-003-25	0.6	0.05894	0.00352	0.52145	0.03107	0.06416	0.00085	565	107	426	21	401	5	6.23
XJ09-003-26	0.63	0.05256	0.00277	0.34491	0.01806	0.04759	0.00067	310	94	301	14	300	4	0.33
XJ09-003-27	0.71	0.05415	0.00199	0.43241	0.01587	0.05791	0.00076	377	59	365	11	363	5	0.55
XJ09-003-28	0.6	0.05287	0.00163	0.3757	0.01163	0.05154	0.00065	323	47	324	9	324	4	0
XJ09-003-29	0.58	0.05234	0.00254	0.35484	0.01711	0.04916	0.00069	300	84	308	13	309	4	-0.32
XJ09-003-30	0.94	0.04948	0.00591	0.1744	0.0207	0.02556	0.00047	171	230	163	18	163	3	0
XJ09-003-31	0.49	0.05248	0.00181	0.34979	0.01204	0.04834	0.00064	306	54	305	9	304	4	0.33
XJ09-003-32	0.27	0.05519	0.00168	0.50183	0.01529	0.06595	0.00085	420	45	413	10	412	5	0.24
XJ09-003-33	0.94	0.05611	0.0016	0.57761	0.01646	0.07466	0.00095	457	41	463	11	464	6	-0.22
XJ09-003-34	0.68	0.0516	0.00736	0.30809	0.0438	0.0433	0.00076	268	283	273	34	273	5	0
XJ09-003-35	0.38	0.05204	0.00275	0.33096	0.01743	0.04612	0.00064	287	95	290	13	291	4	-0.34
XJ09-003-36	0.58	0.05235	0.00274	0.33747	0.01764	0.04675	0.00063	301	95	295	13	295	4	0
XJ09-003-37	0.64	0.06656	0.00267	1.29068	0.04902	0.14063	0.00182	824	86	842	22	848	10	-0.71

XJ09-003-38	0.58	0.05436	0.00139	0.45609	0.01177	0.06085	0.00076	386	36	382	8	381	5	0.26
XJ09-003-39	1.14	0.06167	0.00212	0.55517	0.01905	0.06528	0.00086	663	51	448	12	408	5	9.8
XJ09-003-40	0.55	0.05664	0.00176	0.54079	0.01686	0.06925	0.00087	478	47	439	11	432	5	1.62
XJ09-003-41	0.79	0.05442	0.00142	0.46744	0.01229	0.06229	0.00078	388	37	389	9	390	5	-0.26
XJ09-003-42	0.73	0.05319	0.00165	0.39147	0.01209	0.05337	0.00069	337	46	335	9	335	4	0
XJ09-003-43	0.72	0.05341	0.0027	0.39368	0.01981	0.05346	0.00074	346	89	337	14	336	5	0.3
XJ09-003-44	1.15	0.05331	0.00498	0.40875	0.03799	0.05561	0.0009	342	181	348	27	349	5	-0.29
XJ09-003-45	0.46	0.05384	0.00173	0.40013	0.01284	0.0539	0.00069	364	49	342	9	338	4	1.18
XJ09-003-46	0.55	0.05424	0.00144	0.4762	0.01259	0.06367	0.00082	381	37	395	9	398	5	-0.75
XJ09-003-47	0.66	0.05197	0.00137	0.32787	0.00868	0.04576	0.00057	284	38	288	7	288	4	0
XJ09-003-48	0.62	0.05511	0.00138	0.54674	0.01372	0.07195	0.00091	417	34	443	9	448	5	-1.12
XJ09-003-49	0.72	0.05688	0.00316	0.62437	0.03455	0.07961	0.00108	487	98	493	22	494	6	-0.2
XJ09-003-50	0.65	0.05239	0.00175	0.34694	0.01157	0.04803	0.00063	302	52	302	9	302	4	0
XJ09-003-51	0.69	0.05291	0.00159	0.37539	0.01127	0.05146	0.00067	325	45	324	8	323	4	0.31
XJ09-003-52	0.87	0.05125	0.00179	0.30954	0.01078	0.04381	0.00057	252	56	274	8	276	4	-0.72
XJ09-003-53	1.3	0.04933	0.00283	0.16994	0.00967	0.02499	0.00037	164	102	159	8	159	2	0
XJ09-003-54	0.46	0.14108	0.00285	7.84373	0.16107	0.40324	0.00495	2241	19	2213	18	2184	23	2.61
XJ09-003-55	0.58	0.05215	0.00192	0.34267	0.01256	0.04766	0.00063	292	59	299	9	300	4	-0.33

XJ09-003-56	0.65	0.05581	0.00197	0.56212	0.01968	0.07305	0.00098	445	54	453	13	455	6	-0.44
XJ09-003-57	0.77	0.05373	0.00277	0.39453	0.02018	0.05326	0.00078	360	89	338	15	335	5	0.9
XJ09-003-58	0.68	0.05345	0.00171	0.37882	0.01207	0.0514	0.00066	348	49	326	9	323	4	0.93
XJ09-003-59	0.35	0.05402	0.00157	0.40413	0.01177	0.05426	0.00068	372	43	345	9	341	4	1.17
XJ09-003-60	0.47	0.05468	0.00439	0.47662	0.03808	0.06322	0.00096	399	153	396	26	395	6	0.25
~~**XJ09-003-61**~~	~~0.56~~	~~0.14168~~	~~0.00462~~	~~0.72261~~	~~0.02295~~	~~0.03699~~	~~0.00055~~	~~2248~~	~~34~~	~~552~~	~~14~~	~~234~~	~~3~~	~~135.9~~
XJ09-003-62	1.1	0.05233	0.00619	0.3392	0.03959	0.04701	0.00111	300	220	297	30	296	7	0.34
XJ09-003-63	0.59	0.07735	0.00288	2.07714	0.07658	0.19478	0.00275	1130	51	1141	25	1147	15	-1.48
XJ09-003-64	1.92	0.06529	0.00249	1.14758	0.04345	0.12748	0.00178	784	56	776	21	773	10	0.39
XJ09-003-65	0.41	0.06278	0.00214	0.99572	0.03371	0.11503	0.00155	701	49	702	17	702	9	0
XJ09-003-66	0.65	0.05227	0.00324	0.34141	0.021	0.04738	0.00071	297	113	298	16	298	4	0
XJ09-003-67	0.77	0.05262	0.00166	0.3583	0.01125	0.04939	0.00064	312	48	311	8	311	4	0
~~**XJ09-003-68**~~	~~2.47~~	~~0.04605~~	~~0.03212~~	~~0.37029~~	~~0.25786~~	~~0.05832~~	~~0.0024~~		~~1053~~	~~320~~	~~191~~	~~365~~	~~15~~	~~-12.33~~
XJ09-003-69	0.32	0.06848	0.00161	1.38789	0.03277	0.147	0.00182	883	29	884	14	884	10	0
XJ09-003-70	0.79	0.05241	0.00207	0.35099	0.01381	0.04858	0.00064	303	66	305	10	306	4	-0.33
XJ09-003-71	0.26	0.06559	0.00166	1.18482	0.0301	0.13103	0.00165	793	32	794	14	794	9	0
XJ09-003-72	0.67	0.05301	0.00326	0.38421	0.02323	0.05257	0.00089	329	107	330	17	330	5	0
XJ09-003-73	0.48	0.0534	0.00334	0.32687	0.0199	0.04439	0.00065	346	145	287	15	280	4	2.5

XJ09-003-74	0.96	0.0517	0.00136	0.30695	0.00809	0.04306	0.00055	272	37	272	6	272	3	0
~~**XJ09-003-75**~~	~~0.85~~	~~0.06332~~	~~0.00192~~	~~0.56438~~	~~0.01701~~	~~0.06465~~	~~0.00084~~	~~719~~	~~42~~	~~454~~	~~11~~	~~404~~	~~5~~	~~12.38~~
XJ09-003-76	0.52	0.05358	0.00138	0.41706	0.01077	0.05646	0.0007	353	36	354	8	354	4	0
~~**XJ09-003-77**~~	~~1.81~~	~~0.10894~~	~~0.01932~~	~~0.42955~~	~~0.07511~~	~~0.0286~~	~~0.00084~~	~~1782~~	~~350~~	~~363~~	~~53~~	~~182~~	~~5~~	~~99.45~~
XJ09-003-78	0.91	0.05479	0.00228	0.49015	0.02029	0.06488	0.00086	404	69	405	14	405	5	0
~~**XJ09-003-79**~~	~~0.99~~	~~0.07357~~	~~0.01157~~	~~0.47138~~	~~0.07343~~	~~0.04647~~	~~0.00102~~	~~1030~~	~~341~~	~~392~~	~~51~~	~~293~~	~~6~~	~~33.79~~
XJ09-003-80	0.42	0.05291	0.00157	0.37951	0.01126	0.05203	0.00067	325	44	327	8	327	4	0
XJ09-003-81	1.01	0.0521	0.00621	0.32927	0.03907	0.04584	0.00079	290	236	289	30	289	5	0
XJ09-003-82	0.56	0.05028	0.00145	0.346	0.00994	0.04991	0.00064	208	43	302	7	314	4	-3.82
~~**XJ09-003-83**~~	~~1.55~~	~~0.08017~~	~~0.00825~~	~~0.51617~~	~~0.0528~~	~~0.0467~~	~~0.00081~~	~~1201~~	~~177~~	~~423~~	~~35~~	~~294~~	~~5~~	~~43.88~~
~~**XJ09-003-84**~~	~~0.83~~	~~0.06494~~	~~0.00684~~	~~0.4594~~	~~0.04767~~	~~0.0513~~	~~0.00095~~	~~772~~	~~232~~	~~384~~	~~33~~	~~323~~	~~6~~	~~18.89~~
XJ09-003-85	0.61	0.05511	0.00151	0.50948	0.01388	0.06705	0.00085	417	38	418	9	418	5	0
XJ09-003-86	0.31	0.06416	0.00189	1.08429	0.03194	0.12259	0.00156	747	41	746	16	745	9	0.13
XJ09-003-87	1.1	0.05291	0.00212	0.37832	0.01497	0.05187	0.00072	325	64	326	11	326	4	0
XJ09-003-88	0.77	0.05156	0.01608	0.30012	0.09334	0.04222	0.00113	266	515	266	73	267	7	-0.37
XJ09-003-89	0.31	0.07278	0.00211	1.52978	0.04425	0.15246	0.00196	1008	38	942	18	915	11	2.95
~~**XJ09-003-90**~~	~~0.44~~	~~0.07955~~	~~0.00211~~	~~0.46923~~	~~0.0124~~	~~0.04278~~	~~0.00054~~	~~1186~~	~~32~~	~~391~~	~~9~~	~~270~~	~~3~~	~~44.81~~
XJ09-003-91	2.41	0.05418	0.00244	0.4542	0.02017	0.06081	0.00089	379	73	380	14	381	5	-0.26

XJ09-003-92	0.47	0.05647	0.00176	0.58917	0.01827	0.07567	0.00099	471	45	470	12	470	6	0
XJ09-003-93	0.46	0.052	0.00177	0.32325	0.01097	0.04509	0.00059	285	54	284	8	284	4	0
XJ09-003-94	0.47	0.05239	0.00239	0.34737	0.01575	0.04809	0.00065	302	79	303	12	303	4	0
XJ09-003-95	0.7	0.0534	0.00234	0.40825	0.01772	0.05545	0.00077	346	73	348	13	348	5	0
XJ09-003-96	0.63	0.05265	0.00224	0.36283	0.01528	0.04999	0.0007	314	70	314	11	314	4	0
XJ09-003-97	0.71	0.05399	0.00252	0.44069	0.02026	0.05921	0.0009	371	76	371	14	371	5	0
XJ09-003-98	0.63	0.0516	0.00249	0.30273	0.01446	0.04256	0.00061	268	83	269	11	269	4	0
XJ09-003-99	0.62	0.05195	0.00335	0.33059	0.02108	0.04616	0.00073	283	117	290	16	291	4	-0.34
XJ09-003-100	0.56	0.05659	0.00168	0.6015	0.01774	0.0771	0.00099	476	43	478	11	479	6	-0.21
XJ09-017														
XJ09-017-1	0.75	0.05459	0.00529	0.35962	0.03448	0.04777	0.00096	395	180	312	26	301	6	3.65
XJ09-017-2	0.4	0.04959	0.00311	0.31746	0.01971	0.04643	0.00073	176	112	280	15	293	4	-4.44
XJ09-017-3	0.82	0.05059	0.00284	0.36845	0.02051	0.05282	0.0008	222	101	319	15	332	5	-3.92
XJ09-017-4	0.62	0.05193	0.00225	0.1825	0.00784	0.02548	0.00037	282	72	170	7	162	2	4.94
XJ09-017-5	0.53	0.04854	0.00536	0.28117	0.03078	0.04201	0.00084	126	208	252	24	265	5	-4.91
XJ09-017-6	0.73	0.05458	0.00237	0.38235	0.01645	0.0508	0.00075	395	70	329	12	319	5	3.13
XJ09-017-7	0.95	0.05516	0.0035	0.40847	0.02554	0.0537	0.00092	419	109	348	18	337	6	3.26
XJ09-017-8	0.64	0.05805	0.00152	0.64861	0.0171	0.08103	0.00105	532	35	508	11	502	6	1.2

XJ09-017-9	0.59	0.05418	0.00132	0.56916	0.01403	0.07618	0.00097	379	33	457	9	473	6	-3.38
XJ09-017-10	0.6	0.05244	0.00166	0.3241	0.01025	0.04481	0.0006	305	48	285	8	283	4	0.71
XJ09-017-11	0.24	0.06877	0.00106	1.39086	0.02267	0.14667	0.00177	892	16	885	10	882	10	0.34
XJ09-017-12	0.73	0.05125	0.00295	0.35342	0.02015	0.05001	0.0008	252	102	307	15	315	5	-2.54
XJ09-017-13	0.47	0.04955	0.00179	0.34269	0.01231	0.05015	0.00068	174	58	299	9	315	4	-5.08
XJ09-017-14	0.58	0.0534	0.00195	0.36557	0.01331	0.04965	0.00069	346	57	316	10	312	4	1.28
XJ09-017-15	0.89	0.05053	0.00462	0.1835	0.01668	0.02633	0.00045	219	174	171	14	168	3	1.79
XJ09-017-16	0.82	0.05211	0.00182	0.36054	0.01256	0.05018	0.00068	290	55	313	9	316	4	-0.95
XJ09-017-17	0.6	0.05189	0.00137	0.346	0.00918	0.04835	0.00062	281	37	302	7	304	4	-0.66
XJ09-017-18	0.52	0.05236	0.00171	0.37609	0.01224	0.05209	0.0007	301	50	324	9	327	4	-0.92
XJ09-017-19	0.18	0.05512	0.00198	0.47447	0.01696	0.06242	0.00086	417	55	394	12	390	5	1.03
XJ09-017-20	0.84	0.05179	0.00161	0.37324	0.01155	0.05226	0.0007	276	46	322	9	328	4	-1.83
XJ09-017-21	0.57	0.05506	0.00134	0.51104	0.0126	0.06731	0.00086	415	33	419	8	420	5	-0.24
XJ09-017-22	0.62	0.05171	0.00128	0.49675	0.0124	0.06967	0.00089	273	34	410	8	434	5	-5.53
XJ09-017-23	0.83	0.04819	0.00262	0.17011	0.00918	0.0256	0.00038	109	93	160	8	163	2	-1.84
XJ09-017-24	0.63	0.05609	0.00175	0.62069	0.01936	0.08025	0.00109	456	45	490	12	498	7	-1.61
XJ09-017-25	0.55	0.04758	0.00269	0.29754	0.01666	0.04535	0.0007	78	95	264	13	286	4	-7.69
XJ09-017-26	0.3	0.06374	0.0019	1.18104	0.03523	0.13436	0.00182	733	40	792	16	813	10	-2.58

XJ09-017-27	0.92	0.05355	0.00137	0.47535	0.01228	0.06437	0.00083	352	35	395	8	402	5	-1.74
XJ09-017-28	0.6	0.05483	0.00243	0.41684	0.01829	0.05513	0.0008	405	72	354	13	346	5	2.31
XJ09-017-29	0.94	0.05526	0.00153	0.42208	0.01169	0.05539	0.00072	423	39	358	8	348	4	2.87
XJ09-017-30	0.92	0.05466	0.00343	0.41253	0.02568	0.05473	0.00088	398	111	351	18	343	5	2.33
XJ09-017-31	0.83	0.05785	0.00215	0.58362	0.02151	0.07315	0.00103	524	56	467	14	455	6	2.64
XJ09-017-32	0.72	0.05161	0.00154	0.46831	0.014	0.0658	0.00087	268	44	390	10	411	5	-5.11
XJ09-017-33	0.43	0.05249	0.0014	0.54684	0.01474	0.07555	0.00097	307	38	443	10	470	6	-5.74
XJ09-017-34	0.22	0.05461	0.00138	0.5584	0.0142	0.07415	0.00096	396	34	450	9	461	6	-2.39
XJ09-017-35	0.7	0.05003	0.00212	0.35032	0.01474	0.05077	0.00072	196	71	305	11	319	4	-4.39
XJ09-017-36	0.7	0.04826	0.00638	0.31401	0.04117	0.04719	0.00104	112	238	277	32	297	6	-6.73
XJ09-017-37	0.63	0.05089	0.00289	0.38242	0.02156	0.0545	0.00084	236	101	329	16	342	5	-3.8
XJ09-017-38	0.39	0.05289	0.00276	0.40974	0.02054	0.05619	0.0008	324	121	349	15	352	5	-0.85
XJ09-017-39	0.72	0.04688	0.00367	0.33784	0.02626	0.05226	0.00085	43	140	296	20	328	5	-9.76
XJ09-017-40	1.04	0.05135	0.00251	0.37542	0.0182	0.05301	0.00078	257	84	324	13	333	5	-2.7
XJ09-017-41	0.59	0.05138	0.00133	0.37774	0.00987	0.05331	0.00069	258	37	325	7	335	4	-2.99
XJ09-017-42	0.22	0.1234	0.00217	6.32766	0.11547	0.37184	0.0046	2006	16	2022	16	2038	22	-1.57
XJ09-017-43	0.86	0.04934	0.00187	0.34509	0.01303	0.05072	0.00071	164	62	301	10	319	4	-5.64
XJ09-017-44	0.66	0.04908	0.00685	0.31118	0.04315	0.04598	0.00097	152	254	275	33	290	6	-5.17

XJ09-017-45	0.09	0.14463	0.0029	8.97268	0.1834	0.44988	0.00585	2283	18	2335	19	2395	26	-4.68
XJ09-017-46	0.43	0.05185	0.00136	0.35301	0.00931	0.04937	0.00064	279	37	307	7	311	4	-1.29
XJ09-017-47	0.59	0.05346	0.00138	0.40938	0.01062	0.05553	0.00072	348	36	348	8	348	4	0
XJ09-017-48	0.42	0.05187	0.00339	0.32164	0.02085	0.04497	0.00073	280	119	283	16	284	5	-0.35
XJ09-017-49	0.49	0.05286	0.00187	0.39854	0.01402	0.05467	0.00076	323	55	341	10	343	5	-0.58
XJ09-017-50	0.75	0.05421	0.0037	0.40792	0.02757	0.05457	0.0009	380	123	347	20	343	6	1.17
XJ09-017-51	0.59	0.05161	0.00217	0.37148	0.01554	0.05219	0.00075	268	69	321	12	328	5	-2.13
XJ09-017-52	0.68	0.05435	0.00211	0.20065	0.00772	0.02677	0.00038	386	61	186	7	170	2	9.41
XJ09-017-53	0.72	0.0534	0.00243	0.32435	0.01462	0.04405	0.00065	346	75	285	11	278	4	2.52
XJ09-017-54	0.28	0.06856	0.00146	1.38704	0.03005	0.1467	0.00186	886	25	883	13	882	10	0.11
XJ09-017-55	0.9	0.05009	0.00454	0.32474	0.02911	0.04701	0.0009	199	166	286	22	296	6	-3.38
XJ09-017-56	0.46	0.05432	0.00263	0.35631	0.01653	0.04757	0.00067	384	112	309	12	300	4	3
XJ09-017-57	0.02	0.05638	0.00147	0.64926	0.01707	0.08351	0.00109	467	35	508	11	517	6	-1.74
XJ09-017-58	0.57	0.05654	0.00143	0.56397	0.01435	0.07233	0.00094	474	34	454	9	450	6	0.89
XJ09-017-59	0.65	0.05694	0.00306	0.43221	0.02293	0.05504	0.00088	489	89	365	16	345	5	5.8
XJ09-017-60	0.71	0.05041	0.00175	0.19796	0.00686	0.02848	0.00039	214	55	183	6	181	2	1.1
XJ09-017-61	0.67	0.05142	0.00304	0.37495	0.02201	0.05288	0.00082	260	107	323	16	332	5	-2.71
XJ09-017-62	0.5	0.05002	0.00193	0.35172	0.01352	0.05099	0.00071	196	63	306	10	321	4	-4.67

XJ09-017-63	1.08	0.17529	0.00342	11.04381	0.2215	0.45686	0.00575	2609	18	2527	19	2426	25	7.54
XJ09-017-64	1.09	0.05234	0.00195	0.33214	0.01232	0.04602	0.00064	300	59	291	9	290	4	0.34
XJ09-017-65	0.59	0.05324	0.00181	0.37084	0.01257	0.05051	0.00069	339	52	320	9	318	4	0.63
XJ09-017-66	0.53	0.0532	0.00247	0.27894	0.01285	0.03802	0.00057	337	77	250	10	241	4	3.73
XJ09-017-67	0.54	0.05299	0.00623	0.37609	0.04394	0.05147	0.00101	328	227	324	32	324	6	0
XJ09-017-68	0.88	0.06718	0.0019	1.30772	0.03703	0.14115	0.0019	843	37	849	16	851	11	-0.24
XJ09-017-69	0.77	0.05264	0.0013	0.35244	0.0088	0.04855	0.00063	313	34	307	7	306	4	0.33
XJ09-017-70	0.53	0.05401	0.0016	0.48331	0.01431	0.06489	0.00087	371	43	400	10	405	5	-1.23
XJ09-017-71	0.69	0.05419	0.00182	0.48745	0.01629	0.06523	0.00089	379	51	403	11	407	5	-0.98
XJ09-017-72	0.86	0.05299	0.00309	0.34694	0.02004	0.04748	0.00075	328	103	302	15	299	5	1
XJ09-017-73	1	0.05391	0.00243	0.19739	0.0088	0.02655	0.0004	367	73	183	7	169	3	8.28
XJ09-017-74	0.9	0.05111	0.00166	0.24707	0.008	0.03505	0.00048	246	49	224	7	222	3	0.9
XJ09-017-75	0.79	0.0529	0.00642	0.18719	0.02257	0.02566	0.00051	325	236	174	19	163	3	6.75
XJ09-017-76	1.12	0.05514	0.0014	0.56175	0.01438	0.07388	0.00097	418	34	453	9	459	6	-1.31
XJ09-017-77	0.55	0.05666	0.00188	0.50118	0.01653	0.06414	0.00089	478	48	413	11	401	5	2.99
XJ09-017-78	1.1	0.04874	0.00352	0.31143	0.02235	0.04633	0.00076	135	130	275	17	292	5	-5.82
XJ09-017-79	0.53	0.05991	0.00211	0.69642	0.02435	0.0843	0.00119	600	51	537	15	522	7	2.87
XJ09-017-80	0.47	0.05358	0.00205	0.391	0.0149	0.05292	0.00075	353	60	335	11	332	5	0.9

XJ09-017-81	0.94	0.04929	0.00251	0.3779	0.01908	0.05559	0.00083	162	89	325	14	349	5	-6.88
XJ09-017-82	1.06	0.05203	0.00189	0.30857	0.01116	0.043	0.0006	287	57	273	9	271	4	0.74
XJ09-017-83	0.5	0.19992	0.00446	15.36561	0.34798	0.55734	0.00721	2826	21	2838	22	2856	30	-1.05
XJ09-017-84	0.68	0.05309	0.00151	0.39577	0.01126	0.05406	0.00072	333	40	339	8	339	4	0
XJ09-017-85	0.53	0.05025	0.00285	0.21545	0.0121	0.03109	0.0005	207	100	198	10	197	3	0.51
XJ09-017-86	0.54	0.05414	0.00181	0.39697	0.01321	0.05317	0.00073	377	50	339	10	334	4	1.5
XJ09-017-87	0.18	0.05373	0.00162	0.34437	0.0104	0.04648	0.00063	360	44	300	8	293	4	2.39
XJ09-017-88	0.95	0.04766	0.00324	0.301	0.02032	0.04579	0.00073	82	119	267	16	289	4	-7.61
XJ09-017-89	0.77	0.0554	0.00182	0.34777	0.0114	0.04552	0.00063	428	48	303	9	287	4	5.57
XJ09-017-90	0.61	0.05477	0.00248	0.50517	0.02273	0.06689	0.00099	403	74	415	15	417	6	-0.48
XJ09-017-91	1.07	0.05635	0.00246	0.3718	0.01608	0.04785	0.00071	466	69	321	12	301	4	6.64
XJ09-017-92	0.73	0.05927	0.00269	0.52259	0.02342	0.06394	0.00099	577	70	427	16	400	6	6.75
XJ09-017-93	1.36	0.05631	0.00197	0.41005	0.01426	0.0528	0.00074	465	52	349	10	332	5	5.12
XJ09-017-94	0.64	0.05424	0.00196	0.35128	0.01263	0.04696	0.00067	381	55	306	9	296	4	3.38
XJ09-017-95	0.55	0.05666	0.00259	0.42141	0.01905	0.05393	0.00081	478	73	357	14	339	5	5.31
XJ09-017-96	0.72	0.05721	0.00264	0.40625	0.01853	0.05149	0.00079	500	73	346	13	324	5	6.79
XJ09-017-97	0.67	0.05622	0.002	0.59134	0.02097	0.07628	0.00108	461	53	472	13	474	6	-0.42
XJ09-017-98	0.44	0.05653	0.00197	0.47624	0.01652	0.06109	0.00086	473	52	395	11	382	5	3.4

XJ09-017-99	0.77	0.05602	0.0022	0.40478	0.01574	0.0524	0.00076	453	60	345	11	329	5	4.86
XJ09-017-100	0.88	0.0542	0.00172	0.37319	0.01178	0.04993	0.00069	379	46	322	9	314	4	2.55
XJ09-021														
XJ09-021-1	0.2	0.09382	0.00176	3.74334	0.0713	0.28953	0.00355	1504	19	1581	15	1639	18	-8.24
XJ09-021-2	0.46	0.04721	0.00187	0.30555	0.01196	0.04696	0.00066	60	61	271	9	296	4	-8.45
XJ09-021-3	0.36	0.06282	0.00206	0.65956	0.02138	0.07619	0.00105	702	46	514	13	473	6	8.67
XJ09-021-4	0.53	0.04763	0.00164	0.31987	0.01092	0.04873	0.00065	81	54	282	8	307	4	-8.14
XJ09-021-5	1.24	0.04776	0.0014	0.33275	0.00973	0.05055	0.00065	87	45	292	7	318	4	-8.18
XJ09-021-6	0.68	0.04992	0.00122	0.41456	0.01014	0.06026	0.00075	191	34	352	7	377	5	-6.63
XJ09-021-7	0.37	0.04891	0.00211	0.32597	0.01395	0.04836	0.00068	144	74	286	11	304	4	-5.92
XJ09-021-8	1.98	0.05021	0.00273	0.30918	0.01658	0.04468	0.0007	205	95	274	13	282	4	-2.84
XJ09-021-9	0.33	0.04768	0.00344	0.31307	0.02237	0.04765	0.0008	83	126	277	17	300	5	-7.67
XJ09-021-10	0.63	0.05171	0.00152	0.34127	0.00996	0.04789	0.00062	273	43	298	8	302	4	-1.32
XJ09-021-11	0.7	0.05007	0.0021	0.30409	0.01256	0.04406	0.00063	198	69	270	10	278	4	-2.88
XJ09-021-12	0.52	0.04966	0.00158	0.3176	0.01002	0.0464	0.00061	179	49	280	8	292	4	-4.11
XJ09-021-13	0.5	0.05199	0.00153	0.48116	0.01411	0.06715	0.00088	285	43	399	10	419	5	-4.77
XJ09-021-14	0.37	0.05137	0.00134	0.54792	0.01424	0.07739	0.00098	257	37	444	9	481	6	-7.69
XJ09-021-15	0.96	0.05279	0.00242	0.4471	0.02018	0.06145	0.00091	320	76	375	14	384	6	-2.34

XJ09-021-16	0.7	0.05224	0.00141	0.37142	0.00997	0.05158	0.00066	296	38	321	7	324	4	-0.93
XJ09-021-17	0.59	0.05608	0.00357	0.36213	0.02272	0.04685	0.00077	456	110	314	17	295	5	6.44
XJ09-021-18	0.49	0.05479	0.00311	0.33883	0.01898	0.04487	0.00071	404	97	296	14	283	4	4.59
XJ09-021-19	1.46	0.0506	0.0014	0.35131	0.00968	0.05037	0.00064	223	40	306	7	317	4	-3.47
XJ09-021-20	0.73	0.07251	0.00326	1.4932	0.06386	0.14936	0.0021	1000	94	928	26	897	12	3.46
XJ09-021-21	0.52	0.05078	0.0016	0.46716	0.0146	0.06674	0.00087	231	48	389	10	416	5	-6.49
XJ09-021-22	1.13	0.04915	0.00507	0.33109	0.03379	0.04887	0.00095	155	192	290	26	308	6	-5.84
XJ09-021-23	1.1	0.05843	0.00491	0.39875	0.0329	0.04951	0.00102	546	145	341	24	312	6	9.29
XJ09-021-24	0.55	0.05487	0.00166	0.43706	0.01316	0.0578	0.00076	407	44	368	9	362	5	1.66
XJ09-021-25	0.6	0.05161	0.00261	0.36976	0.01847	0.05198	0.00078	268	87	319	14	327	5	-2.45
XJ09-021-26	0.74	0.0485	0.00265	0.32251	0.01739	0.04824	0.00075	124	93	284	13	304	5	-6.58
XJ09-021-27	1.07	0.05101	0.00198	0.34056	0.01309	0.04844	0.00067	241	63	298	10	305	4	-2.3
XJ09-021-28	0.53	0.0512	0.00218	0.34121	0.01435	0.04835	0.00068	250	71	298	11	304	4	-1.97
XJ09-021-29	0.97	0.05559	0.00314	0.36466	0.02032	0.04759	0.00075	436	96	316	15	300	5	5.33
XJ09-021-30	0.39	0.07159	0.0015	1.3522	0.02854	0.13704	0.00168	974	24	869	12	828	10	4.95
XJ09-021-31	0.64	0.05054	0.00167	0.34995	0.01146	0.05023	0.00067	220	51	305	9	316	4	-3.48
XJ09-021-32	0.48	0.05411	0.00207	0.35678	0.01347	0.04783	0.00067	376	60	310	10	301	4	2.99
XJ09-021-33	1.06	0.04992	0.00203	0.30724	0.01241	0.04465	0.00061	191	68	272	10	282	4	-3.55

XJ09-021-34	0.7	0.05528	0.00328	0.48658	0.02854	0.06386	0.00102	424	103	403	19	399	6	1
XJ09-021-35	0.7	0.05051	0.00206	0.37028	0.01495	0.05318	0.00074	219	68	320	11	334	5	-4.19
XJ09-021-36	1.24	0.05375	0.0015	0.52533	0.01463	0.0709	0.00091	361	40	429	10	442	5	-2.94
XJ09-021-37	0.51	0.05038	0.00259	0.3542	0.01798	0.05101	0.00076	213	90	308	13	321	5	-4.05
XJ09-021-38	0.66	0.08503	0.00211	2.95258	0.0733	0.25191	0.00326	1316	28	1396	19	1448	17	-9.12
XJ09-021-39	1.07	0.10488	0.00221	4.54301	0.09668	0.31425	0.0039	1712	22	1739	18	1762	19	-2.84
XJ09-021-40	0.43	0.05391	0.00285	0.58466	0.0305	0.07868	0.00121	367	90	467	20	488	7	-4.3
XJ09-021-41	0.38	0.07406	0.00762	1.72491	0.17473	0.16896	0.00406	1043	167	1018	65	1006	22	3.68
XJ09-021-42	0.51	0.05026	0.00233	0.33804	0.01552	0.04879	0.0007	207	80	296	12	307	4	-3.58
XJ09-021-43	0.41	0.05075	0.00147	0.3194	0.00925	0.04565	0.00059	229	43	281	7	288	4	-2.43
XJ09-021-44	0.84	0.05228	0.00183	0.34471	0.01197	0.04783	0.00065	298	54	301	9	301	4	0
XJ09-021-45	0.35	0.04914	0.00253	0.3001	0.01527	0.0443	0.00065	155	90	266	12	279	4	-4.66
XJ09-021-46	0.97	0.05155	0.00206	0.31726	0.01252	0.04464	0.00062	266	65	280	10	282	4	-0.71
XJ09-021-47	0.78	0.06576	0.00161	1.33823	0.03287	0.14762	0.00186	799	31	862	14	888	10	-2.93
XJ09-021-48	0.99	0.05196	0.00188	0.45909	0.01647	0.06409	0.00087	284	57	384	11	400	5	-4
XJ09-021-49	0.49	0.05183	0.00204	0.34991	0.01359	0.04897	0.00068	278	63	305	10	308	4	-0.97
XJ09-021-50	0.76	0.05406	0.00208	0.3758	0.0143	0.05042	0.0007	374	61	324	11	317	4	2.21
XJ09-021-51	0.63	0.05657	0.00163	0.49594	0.01423	0.06359	0.00082	475	41	409	10	397	5	3.02

XJ09-021-52	0.82	0.05146	0.00349	0.40499	0.0271	0.05709	0.00099	261	122	345	20	358	6	-3.63
XJ09-021-53	0.55	0.05329	0.00327	0.36048	0.0218	0.04907	0.00081	341	107	313	16	309	5	1.29
XJ09-021-54	1.64	0.05251	0.00228	0.4044	0.01739	0.05587	0.0008	308	72	345	13	350	5	-1.43
XJ09-021-55	0.77	0.05419	0.00224	0.59928	0.02454	0.08022	0.00114	379	66	477	16	497	7	-4.02
XJ09-021-56	0.6	0.05316	0.00394	0.34942	0.02564	0.04768	0.00081	336	136	304	19	300	5	1.33
XJ09-021-57	1.22	0.04587	0.00375	0.22141	0.01791	0.03501	0.00061	-9	144	203	15	222	4	-8.56
XJ09-021-58	0.56	0.05296	0.00194	0.48914	0.01774	0.067	0.00092	327	57	404	12	418	6	-3.35
XJ09-021-59	0.52	0.07296	0.00171	1.60463	0.03773	0.15952	0.00198	1013	28	972	15	954	11	1.89
XJ09-021-60	1.97	0.04971	0.00295	0.19104	0.01123	0.02787	0.00043	181	106	178	10	177	3	0.56
XJ09-021-61	0.54	0.05537	0.00239	0.41553	0.01775	0.05444	0.00079	427	69	353	13	342	5	3.22
XJ09-021-62	0.53	0.0571	0.00155	0.54844	0.01483	0.06966	0.00089	495	37	444	10	434	5	2.3
XJ09-021-63	0.54	0.05647	0.00266	0.50698	0.02289	0.06512	0.00089	471	107	416	15	407	5	2.21
XJ09-021-64	0.88	0.05323	0.002	0.36519	0.01357	0.04976	0.00069	339	59	316	10	313	4	0.96
XJ09-021-65	1.06	0.05462	0.00212	0.40252	0.01545	0.05345	0.00075	397	61	343	11	336	5	2.08
XJ09-021-66	1.03	0.05234	0.00192	0.36395	0.01323	0.05043	0.00069	300	58	315	10	317	4	-0.63
XJ09-021-67	0.59	0.05766	0.00204	0.54379	0.01903	0.0684	0.00093	517	53	441	13	427	6	3.28
XJ09-021-68	0.95	0.05743	0.0022	0.53758	0.02037	0.0679	0.00095	508	59	437	13	423	6	3.31
XJ09-021-69	0.87	0.05544	0.00326	0.39216	0.02275	0.0513	0.00082	430	101	336	17	322	5	4.35

XJ09-021-70	0.88	0.05335	0.00258	0.35681	0.01702	0.04851	0.00072	344	81	310	13	305	4	1.64
XJ09-021-71	0.75	0.05355	0.00413	0.35815	0.0273	0.04851	0.00086	352	141	311	20	305	5	1.97
XJ09-021-72	0.44	0.05645	0.00276	0.3776	0.01815	0.04852	0.00075	470	79	325	13	305	5	6.56
XJ09-021-73	0.81	0.08955	0.0028	3.03392	0.09398	0.24574	0.00339	1416	38	1416	24	1416	18	0
XJ09-021-74	0.97	0.05114	0.00784	0.18264	0.02774	0.02591	0.00064	247	284	170	24	165	4	3.03
XJ09-021-75	1.24	0.05226	0.00315	0.36489	0.02165	0.05064	0.00083	297	106	316	16	318	5	-0.63
XJ09-021-76	0.52	0.07495	0.00229	1.7531	0.05313	0.16965	0.00226	1067	40	1028	20	1010	12	5.64
XJ09-021-77	0.89	0.0547	0.00274	0.62238	0.03081	0.08252	0.00127	400	83	491	19	511	8	-3.91
XJ09-021-78	0.7	0.05431	0.00222	0.36922	0.01494	0.04931	0.0007	384	65	319	11	310	4	2.9
XJ09-021-79	0.93	0.05185	0.00255	0.36033	0.01748	0.0504	0.00076	279	83	312	13	317	5	-1.58
XJ09-021-80	0.76	0.05374	0.00245	0.44822	0.02018	0.06049	0.00087	360	76	376	14	379	5	-0.79
~~**XJ09-021-81**~~	~~1.03~~	~~0.06621~~	~~0.00319~~	~~0.39099~~	~~0.01858~~	~~0.04283~~	~~0.00065~~	~~813~~	~~74~~	~~335~~	~~14~~	~~270~~	~~4~~	~~24.07~~
XJ09-021-82	0.71	0.06564	0.00334	0.77809	0.03893	0.08597	0.00141	795	77	584	22	532	8	9.77
XJ09-021-83	1.25	0.05544	0.00332	0.4904	0.02893	0.06415	0.00106	430	102	405	20	401	6	1
XJ09-021-84	1.67	0.05211	0.00266	0.37092	0.01873	0.05163	0.00077	290	88	320	14	325	5	-1.54
XJ09-021-85	0.14	0.06908	0.00196	1.4508	0.04113	0.15232	0.00196	901	37	910	17	914	11	-0.44
XJ09-021-86	0.39	0.05948	0.00336	0.46429	0.02584	0.05661	0.00092	585	93	387	18	355	6	9.01
XJ09-021-87	0.28	0.0573	0.00263	0.53634	0.02422	0.06788	0.00102	503	73	436	16	423	6	3.07

XJ09-021-88	0.8	0.05589	0.00391	0.41211	0.0284	0.05348	0.00094	448	122	350	20	336	6	4.17
XJ09-021-89	0.82	0.05459	0.00284	0.40939	0.02102	0.05439	0.00083	395	88	348	15	341	5	2.05
XJ09-021-90	0.98	0.05397	0.00242	0.37428	0.01654	0.05029	0.00074	370	73	323	12	316	5	2.22
XJ09-021-91	0.85	0.10804	0.00379	4.65251	0.16099	0.31228	0.00454	1767	42	1759	29	1752	22	0.86
XJ09-021-92	0.48	0.05521	0.00235	0.5454	0.02301	0.07164	0.00102	421	69	442	15	446	6	-0.9
XJ09-021-93	0.63	0.05445	0.00272	0.361	0.0178	0.04808	0.00074	390	83	313	13	303	5	3.3
XJ09-021-94	0.61	0.05491	0.00275	0.47423	0.02346	0.06263	0.00094	409	84	394	16	392	6	0.51
XJ09-021-95	0.98	0.05937	0.00244	0.44606	0.01814	0.05448	0.00078	581	63	375	13	342	5	9.65
XJ09-021-96	0.64	0.05562	0.0022	0.51427	0.02017	0.06705	0.00094	437	62	421	14	418	6	0.72
XJ09-021-97	1.13	0.05127	0.003	0.18949	0.01092	0.0268	0.00043	253	103	176	9	170	3	3.53
XJ09-021-98	1.29	0.06733	0.00413	1.09893	0.06655	0.11836	0.00199	848	98	753	32	721	11	4.44
XJ09-021-99	0.91	0.05081	0.00238	0.29527	0.01369	0.04214	0.00062	232	80	263	11	266	4	-1.13
XJ09-021-100	0.53	0.05316	0.00245	0.37092	0.01691	0.0506	0.00074	336	77	320	13	318	5	0.63

APPENDIX 2

Analysis number	*Th/U*	Isotopic ratios and erros						Ages and errors(Ma)						*Disc.%*
		$^{207}Pb/^{206}Pb$	1σ	$^{207}Pb/^{235}U$	1σ	$^{206}Pb/^{238}U$	1σ	$^{207}Pb/^{206}Pb$	1σ	$^{207}Pb/^{235}U$	1σ	$^{206}Pb/^{238}U$	1σ	
UC01														
UC01-01	0.12	0.12212	0.00457	5.90337	0.22289	0.35048	0.00473	1987	48	1962	33	1937	23	2.6
UC01-02	0.25	0.08812	0.00343	2.87619	0.11254	0.23666	0.00322	1385	54	1376	29	1369	17	1.2
UC01-03	0.56	0.05603	0.00338	0.56961	0.03437	0.0737	0.00106	454	109	458	22	458	6	0.0
UC01-04	0.08	0.05161	0.00303	0.30517	0.0179	0.04287	0.00061	268	109	270	14	271	4	-0.4
UC01-06	0.21	0.05712	0.00232	0.6296	0.02567	0.07992	0.00109	496	66	496	16	496	7	0.0
UC01-08	1.64	0.05784	0.003	0.65051	0.03364	0.08154	0.00119	524	88	509	21	505	7	0.8
UC01-09	0.21	0.06775	0.00295	1.41277	0.06158	0.15119	0.00216	861	67	894	26	908	12	-1.5
UC01-10	0.29	0.08533	0.00329	2.64501	0.1026	0.22477	0.00304	1323	54	1313	29	1307	16	1.2
UC01-12	0.11	0.06578	0.00272	1.20123	0.0498	0.13242	0.00184	799	63	801	23	802	10	-0.1
UC01-13	0.42	0.05704	0.01596	0.60354	0.16794	0.07672	0.00261	493	482	479	106	477	16	0.4
UC01-14	0.74	0.10675	0.00986	4.59099	0.41882	0.31185	0.00792	1745	131	1748	76	1750	39	-0.3
UC01-15	0.65	0.06734	0.00326	1.2932	0.06255	0.13926	0.00198	848	77	843	28	840	11	0.4
UC01-16	0.42	0.05783	0.00307	0.67641	0.03583	0.08481	0.00125	523	90	525	22	525	7	0.0
UC01-17	2.44	0.05167	0.01608	0.06882	0.02134	0.00966	0.00028	271	510	68	20	62	2	9.7

UC01-19	1.43	0.05785	0.00313	0.67097	0.03615	0.0841	0.00129	524	91	521	22	521	8	0.0
UC01-20	0.44	0.05555	0.00334	0.53465	0.03198	0.0698	0.00108	434	106	435	21	435	7	0.0
UC01-21	0.45	0.0593	0.00315	0.74548	0.0395	0.09116	0.00135	578	89	566	23	562	8	0.7
UC01-22	1	0.15657	0.00691	9.83989	0.43356	0.45571	0.00672	2419	55	2420	41	2421	30	-0.1
UC01-24	0.73	0.0567	0.02826	0.5594	0.27796	0.07154	0.00299	480	883	451	181	445	18	1.3
UC01-25	0.48	0.06433	0.00292	1.09471	0.04968	0.1234	0.00174	752	72	751	24	750	10	0.1
UC01-26	0.79	0.05657	0.00274	0.59909	0.02889	0.0768	0.0011	475	81	477	18	477	7	0.0
UC01-27	1.47	0.07185	0.00382	1.63274	0.08638	0.16478	0.00249	982	83	983	33	983	14	0.0
UC01-28	2.94	0.07554	0.00361	1.95788	0.09341	0.18795	0.00278	1083	72	1101	32	1110	15	-2.4
UC01-29	0.79	0.06699	0.0034	1.27747	0.0646	0.13829	0.00204	837	81	836	29	835	12	0.1
UC01-31	0.39	0.16454	0.00778	10.81686	0.50973	0.47671	0.00688	2503	60	2508	44	2513	30	-0.4
UC01-34	0.7	0.05626	0.0034	0.58114	0.03489	0.0749	0.00117	463	106	465	22	466	7	-0.2
UC01-35	0.59	0.0547	0.00387	0.48201	0.03386	0.0639	0.00103	400	129	399	23	399	6	0.0
UC01-36	1.75	0.05784	0.00326	0.67591	0.0378	0.08474	0.00131	524	96	524	23	524	8	0.0
UC01-37	0.49	0.07806	0.004	2.05485	0.10464	0.1909	0.00283	1148	78	1134	35	1126	15	2
UC01-39	0.73	0.08301	0.00618	2.39654	0.17617	0.20934	0.00419	1269	113	1242	53	1225	22	3.6
UC01-40	0.65	0.05582	0.0032	0.55048	0.03129	0.07152	0.00109	445	99	445	20	445	7	0.0
UC01-41	0.22	0.07011	0.00381	1.51592	0.08179	0.15679	0.00238	932	86	937	33	939	13	-0.2

UC01-43	0.57	0.07609	0.00433	1.95345	0.11031	0.18617	0.00291	1097	88	1100	38	1101	16	-0.4
UC01-47	0.16	0.06933	0.00393	1.45146	0.08157	0.15181	0.00233	909	91	910	34	911	13	-0.1
UC01-49	1.75	0.07088	0.01153	1.63913	0.26553	0.1677	0.00469	954	298	985	102	999	26	-1.4
UC01-50	1.37	0.05225	0.01478	0.32739	0.09205	0.04543	0.0016	296	459	288	70	286	10	0.7
UC01-51	1.03	0.10336	0.01492	4.27523	0.60893	0.29993	0.01049	1685	216	1689	117	1691	52	-0.4
UC01-53	0.63	0.05581	0.00415	0.55547	0.0409	0.07217	0.00121	445	135	449	27	449	7	0.0
UC01-57	0.57	0.05478	0.00369	0.48496	0.03227	0.0642	0.00106	403	120	401	22	401	6	0.0
UC01-58	1.43	0.0554	0.00388	0.52604	0.03638	0.06885	0.00116	428	125	429	24	429	7	0.0
UC02														
UC02-01	0.39	0.05178	0.00371	0.3072	0.02188	0.043	0.00068	276	134	272	17	271	4	0.4
UC02-02	0.63	0.05237	0.00595	0.35212	0.03983	0.04874	0.00085	302	224	306	30	307	5	-0.3
UC02-03	0.6	0.05188	0.00509	0.30654	0.02995	0.04283	0.00072	280	190	271	23	270	4	0.4
UC02-04	0.86	0.05236	0.00443	0.33936	0.02856	0.04698	0.00078	301	161	297	22	296	5	0.3
UC02-05	0.53	0.12501	0.00426	6.3921	0.21748	0.37066	0.00522	2029	40	2031	30	2033	25	-0.2
UC02-06	0.47	0.11252	0.00373	5.22196	0.17279	0.33642	0.00464	1841	40	1856	28	1869	22	-1.5
UC02-07	1.59	0.05489	0.00307	0.49374	0.02741	0.06521	0.00102	408	96	407	19	407	6	0.0
UC02-08	0.92	0.05302	0.005	0.38473	0.03612	0.0526	0.00087	330	183	331	26	330	5	0.3
UC02-09	0.43	0.05714	0.00353	0.62588	0.03848	0.0794	0.00118	497	110	494	24	493	7	0.2

UC02-10	0.71	0.0514	0.00292	0.27839	0.01575	0.03927	0.00057	259	104	249	13	248	4	0.4
UC02-11	0.71	0.05645	0.00289	0.57633	0.02936	0.07401	0.00109	470	87	462	19	460	7	0.4
UC02-12	0.72	0.0557	0.00248	0.5454	0.02418	0.07099	0.00102	440	73	442	16	442	6	0.0
UC02-13	0.85	0.14201	0.00491	8.09307	0.28002	0.41317	0.00597	2252	40	2241	31	2229	27	1
UC02-14	0.74	0.05524	0.00425	0.47487	0.03623	0.06233	0.00105	422	141	395	25	390	6	1.3
UC02-15	0.58	0.05525	0.00404	0.51478	0.03746	0.06755	0.00108	422	135	422	25	421	7	0.2
UC02-16	0.6	0.19274	0.00634	14.3373	0.47274	0.53933	0.0075	2766	36	2772	31	2781	31	-0.5
UC02-17	0.38	0.05184	0.01214	0.30822	0.07203	0.04311	0.00091	278	405	273	56	272	6	0.4
UC02-18	1.32	0.06394	0.0044	1.0679	0.07323	0.12109	0.00187	740	120	738	36	737	11	0.1
UC02-19	0.39	0.14836	0.00597	8.86696	0.35831	0.43336	0.00742	2327	46	2324	37	2321	33	0.3
UC02-20	0.3	0.05558	0.00315	0.54028	0.03049	0.07048	0.00107	436	99	439	20	439	6	0.0
UC02-21	1.12	0.05589	0.0071	0.56272	0.07118	0.07301	0.00132	448	252	453	46	454	8	-0.2
UC02-22	0.22	0.07475	0.00301	1.7847	0.07167	0.17313	0.00253	1062	57	1040	26	1029	14	3.2
UC02-23	0.56	0.05939	0.00304	0.76703	0.03904	0.09365	0.00141	581	84	578	22	577	8	0.2
UC02-24	1.16	0.05155	0.0058	0.29921	0.03358	0.04209	0.0007	266	223	266	26	266	4	0.0
UC02-25	0.15	0.11364	0.00388	5.24364	0.17959	0.33459	0.00463	1858	42	1860	29	1861	22	-0.2
UC02-26	1.15	0.05223	0.0098	0.33503	0.06269	0.04652	0.00094	295	344	293	48	293	6	0.0
UC02-27	0.05	0.05435	0.00239	0.4634	0.02028	0.06183	0.00091	386	72	387	14	387	6	0.0

UC02-28	0.41	0.05575	0.00321	0.58241	0.03343	0.07576	0.00113	442	101	466	21	471	7	-1.1
UC02-29	0.64	0.05361	0.0038	0.42146	0.02982	0.05701	0.00086	355	134	357	21	357	5	0.0
UC02-30	0.09	0.06801	0.0024	1.34476	0.04759	0.14339	0.00198	869	50	865	21	864	11	0.1
UC02-31	0.87	0.0511	0.00265	0.26889	0.01392	0.03816	0.00056	245	92	242	11	241	3	0.4
UC02-32	0.61	0.15673	0.00575	9.82636	0.36071	0.45465	0.00658	2421	43	2419	34	2416	29	0.2
UC02-33	1	0.16325	0.00611	10.51725	0.39379	0.4672	0.00686	2490	43	2481	35	2471	30	0.8
UC02-34	0.63	0.05146	0.00284	0.29738	0.01637	0.04191	0.00063	261	99	264	13	265	4	-0.4
UC02-35	0.47	0.09787	0.00724	3.54897	0.26095	0.26297	0.00456	1584	112	1538	58	1505	23	5.2
UC02-36	0.32	0.13971	0.00519	7.93118	0.29533	0.4117	0.00591	2224	45	2223	34	2223	27	0.0
UC02-37	1.43	0.05209	0.0044	0.33669	0.02836	0.04688	0.00077	289	161	295	22	295	5	0.0
UC02-38	0.53	0.09838	0.0192	3.74392	0.72597	0.276	0.0078	1594	340	1581	155	1571	39	1.5
UC02-39	0.38	0.14698	0.00552	8.86996	0.33362	0.43766	0.00631	2311	45	2325	34	2340	28	-1.2
UC02-40	1.02	0.14865	0.00549	8.98188	0.33307	0.43822	0.00619	2330	44	2336	34	2343	28	-0.6
UC02-41	0.59	0.05245	0.00344	0.35084	0.02296	0.04852	0.00074	305	122	305	17	305	5	0.0
UC02-42	0.64	0.05581	0.00576	0.55423	0.05699	0.07202	0.00124	445	201	448	37	448	7	0.0
UC02-43	0.34	0.11683	0.00555	5.58129	0.26402	0.34646	0.00541	1908	62	1913	41	1918	26	-0.5
UC02-44	2.08	0.12522	0.00624	6.42582	0.31791	0.37217	0.00624	2032	64	2036	43	2040	29	-0.4
UC02-45	0.62	0.05587	0.00357	0.55081	0.03502	0.07151	0.00112	447	114	446	23	445	7	0.2

UC02-46	0.97	0.05611	0.00342	0.56491	0.03434	0.07303	0.00111	457	108	455	22	454	7	0.2
UC02-47	0.34	0.07066	0.00312	1.56306	0.06906	0.16044	0.00236	948	66	956	27	959	13	-0.3
UC02-48	0.47	0.0512	0.00511	0.27769	0.02764	0.03934	0.00065	250	194	249	22	249	4	0.0
UC02-49	0.47	0.05199	0.0042	0.31993	0.02573	0.04463	0.00075	285	152	282	20	281	5	0.4
UC02-50	1.04	0.05231	0.00689	0.34703	0.04557	0.04812	0.00088	299	264	302	34	303	5	-0.3
UC02-51	0.17	0.08915	0.0038	3.04759	0.13018	0.24792	0.00369	1407	59	1420	33	1428	19	-1.5
UC02-52	0.49	0.11995	0.00507	5.86143	0.24821	0.3544	0.00523	1955	54	1956	37	1956	25	-0.1
UC02-53	1.41	0.11262	0.0051	5.13606	0.23219	0.33076	0.0051	1842	59	1842	38	1842	25	0.0
UC02-54	0.45	0.05116	0.00317	0.27118	0.01677	0.03845	0.0006	248	114	244	13	243	4	0.4
UC02-55	1.05	0.05536	0.00426	0.5154	0.03953	0.06752	0.00109	427	144	422	26	421	7	0.2
UC02-56	0.35	0.05595	0.00272	0.554	0.02693	0.07182	0.00108	450	81	448	18	447	6	0.2
UC02-57	1.06	0.05388	0.01635	0.42801	0.12958	0.05761	0.00147	366	519	362	92	361	9	0.3
UC02-58	0.62	0.12515	0.00567	6.57635	0.29831	0.38113	0.006	2031	58	2056	40	2082	28	-2.4
UC02-59	1.41	0.24916	0.01063	21.89561	0.93732	0.63736	0.00956	3179	49	3179	42	3179	38	0.0
UC02-60	0.71	0.05287	0.00291	0.37694	0.02073	0.0517	0.00079	323	97	325	15	325	5	0.0
UC02-61	0.5	0.05227	0.00773	0.35159	0.0518	0.04878	0.00096	297	291	306	39	307	6	-0.3
UC02-62	1.41	0.06736	0.00929	1.29288	0.17773	0.1392	0.0027	849	263	843	79	840	15	0.4
UC02-63	0.62	0.0537	0.00496	0.42884	0.03948	0.05792	0.001	358	177	362	28	363	6	-0.3

UC02-64	0.23	0.0564	0.00393	0.57332	0.03988	0.07373	0.0012	468	126	460	26	459	7	0.2
UC02-65	0.54	0.07374	0.00398	1.77706	0.09594	0.17478	0.00279	1034	83	1037	35	1038	15	-0.4
UC02-66	1.05	0.05562	0.00329	0.53925	0.03181	0.07031	0.00114	437	103	438	21	438	7	0.0
UC02-67	0.01	0.05524	0.00276	0.52153	0.02614	0.06847	0.00104	422	85	426	17	427	6	-0.2
UC02-68	0.37	0.14609	0.00664	8.69024	0.39686	0.43144	0.0065	2301	58	2306	42	2312	29	-0.5
UC02-69	0.74	0.05257	0.0033	0.35349	0.02216	0.04877	0.00078	310	114	307	17	307	5	0.0
UC02-70	0.79	0.14047	0.00683	7.54212	0.3671	0.38942	0.00619	2233	62	2178	44	2120	29	5.3
UC02-71	0.64	0.13407	0.00638	7.3115	0.34967	0.3955	0.00609	2152	62	2150	43	2148	28	0.2
UC02-72	0.64	0.05576	0.00378	0.54566	0.037	0.07098	0.00115	443	123	442	24	442	7	0.0
UC02-73	0.99	0.05575	0.00497	0.54469	0.04847	0.07086	0.00119	442	170	442	32	441	7	0.2
UC02-74	0.32	0.07095	0.00384	1.57349	0.08527	0.16083	0.00256	956	85	960	34	961	14	-0.1
UC02-75	0.64	0.0544	0.00948	0.45889	0.07979	0.06118	0.00121	388	336	383	56	383	7	0.0
UC02-76	0.55	0.05569	0.00384	0.53599	0.03698	0.0698	0.00113	440	125	436	24	435	7	0.2
UC02-77	0.97	0.1605	0.00796	10.13099	0.50489	0.45777	0.00721	2461	63	2447	46	2430	32	1.3
UC02-78	0.65	0.05631	0.00366	0.58656	0.03807	0.07554	0.00124	465	115	469	24	469	7	0.0
UC02-79	0.36	0.05616	0.00392	0.56107	0.03911	0.07245	0.0012	459	126	452	25	451	7	0.2
UC02-80	0.45	0.04882	0.00775	0.14165	0.02244	0.02104	0.00041	139	283	135	20	134	3	0.7
UC02-81	0.58	0.11188	0.00968	5.06182	0.43539	0.32809	0.00678	1830	127	1830	73	1829	33	0.1

UC02-82	0.09	0.15566	0.00796	9.35302	0.48209	0.43574	0.00699	2409	66	2373	47	2332	31	3.3
UC02-83	0.98	0.05154	0.00323	0.30256	0.01898	0.04257	0.00069	265	114	268	15	269	4	-0.4
UC02-84	0.7	0.05635	0.0041	0.58377	0.04248	0.07513	0.00127	466	132	467	27	467	8	0.0
UC02-85	1.09	0.11434	0.00625	5.28392	0.29029	0.33513	0.00546	1870	76	1866	47	1863	26	0.4
UC02-86	0.95	0.05564	0.00399	0.54202	0.03888	0.07064	0.0012	438	130	440	26	440	7	0.0
UC02-87	0.57	0.08542	0.01228	2.69537	0.3834	0.22881	0.00729	1325	232	1327	105	1328	38	-0.2
UC02-88	1.14	0.05257	0.00889	0.35339	0.05963	0.04875	0.00099	310	320	307	45	307	6	0.0
UC02-89	2.94	0.12484	0.00707	6.37302	0.36207	0.37018	0.00625	2027	77	2029	50	2030	29	-0.1
UC02-90	0.81	0.06836	0.01205	1.34684	0.23634	0.14286	0.00352	879	340	866	102	861	20	0.6
UC02-91	0.89	0.16761	0.00921	11.10701	0.61478	0.4805	0.0078	2534	71	2532	52	2529	34	0.2
UC02-92	0.45	0.05595	0.00349	0.55026	0.03447	0.07131	0.00119	450	110	445	23	444	7	0.2
UC02-93	2.08	0.14996	0.00843	9.01364	0.51057	0.43582	0.00716	2345	74	2339	52	2332	32	0.6
UC02-94	0.41	0.05578	0.01527	0.55134	0.15056	0.07167	0.00195	444	480	446	99	446	12	0.0
UC02-95	0.58	0.16712	0.01024	11.40715	0.70116	0.49492	0.00907	2529	79	2557	57	2592	39	-2.4
UC02-96	0.61	0.05655	0.00414	0.5992	0.04399	0.07682	0.00133	474	133	477	28	477	8	0.0
UC02-97	0.65	0.11935	0.00738	5.81102	0.36083	0.35301	0.00612	1947	86	1948	54	1949	29	-0.1
UC02-98	0.13	0.11746	0.00676	5.62761	0.32662	0.34736	0.00572	1918	81	1920	50	1922	27	-0.2
UC02-99	0.81	0.14567	0.00838	8.58115	0.49821	0.42709	0.00698	2296	77	2295	53	2293	32	0.1

UC02-100	0.37	0.12608	0.00741	6.49001	0.38468	0.3732	0.00622	2044	81	2045	52	2044	29	0.0
UC03														
UC03-01	1	0.16807	0.00884	11.31819	0.5899	0.48842	0.00733	2539	67	2550	49	2564	32	-1
UC03-02	0.51	0.05611	0.00581	0.57208	0.05884	0.07395	0.00127	457	201	459	38	460	8	-0.2
UC03-03	1.02	0.0527	0.00494	0.36233	0.03377	0.04986	0.00082	316	181	314	25	314	5	0.0
UC03-04	0.68	0.05899	0.00619	0.74811	0.07779	0.09198	0.00179	567	196	567	45	567	11	0.0
UC03-05	0.49	0.05558	0.00511	0.54529	0.04977	0.07116	0.00119	436	176	442	33	443	7	-0.2
UC03-06	1.56	0.05747	0.00366	0.65047	0.04104	0.08209	0.00127	510	112	509	25	509	8	0.0
UC03-07	0.21	0.15707	0.00849	9.908	0.52937	0.45749	0.00677	2424	71	2426	49	2428	30	-0.2
UC03-09	0.61	0.11805	0.00657	5.68105	0.31221	0.34899	0.00527	1927	77	1928	47	1930	25	-0.2
UC03-10	0.32	0.07201	0.00416	1.6491	0.09396	0.16608	0.00252	986	91	989	36	990	14	-0.1
UC03-11	0.92	0.05523	0.00444	0.51215	0.04078	0.06725	0.00109	422	150	420	27	420	7	0.0
UC03-12	0.87	0.05608	0.00391	0.5928	0.0408	0.07665	0.00126	456	124	473	26	476	8	-0.6
UC03-13	1.18	0.05573	0.00449	0.54053	0.04312	0.07034	0.00115	442	150	439	28	438	7	0.2
UC03-14	0.96	0.16642	0.00968	10.91522	0.62503	0.47563	0.00736	2522	75	2516	53	2508	32	0.6
UC03-15	0.45	0.05543	0.00422	0.53596	0.04021	0.07011	0.0012	430	138	436	27	437	7	-0.2
UC03-16	0.62	0.05597	0.0038	0.56341	0.03774	0.073	0.00117	451	121	454	25	454	7	0.0
UC03-17	0.7	0.08071	0.00676	2.35357	0.19467	0.21146	0.00373	1214	136	1229	59	1237	20	-1.9

UC03-18	0.54	0.05663	0.00667	0.59482	0.06948	0.07616	0.00142	477	229	474	44	473	9	0.2
UC03-20	0.74	0.05215	0.06239	0.35396	0.42284	0.04922	0.0032	292	1380	308	317	310	20	-0.6
UC03-21	0.15	0.10402	0.00632	4.32481	0.25782	0.30147	0.00467	1697	87	1698	49	1699	23	-0.1
UC03-22	0.96	0.06274	0.00456	0.98672	0.07066	0.11404	0.00189	699	125	697	36	696	11	0.1
UC03-23	0.52	0.05636	0.0047	0.58017	0.04772	0.07463	0.00127	467	154	465	31	464	8	0.2
UC03-24	0.5	0.05666	0.00385	0.5991	0.03996	0.07666	0.00123	478	120	477	25	476	7	0.2
UC03-25	0.98	0.05315	0.01046	0.38719	0.07572	0.05282	0.00127	335	355	332	55	332	8	0.0
UC03-26	0.52	0.05598	0.00401	0.57807	0.04068	0.07487	0.00123	452	128	463	26	465	7	-0.4
UC03-27	0.54	0.05759	0.00641	0.6543	0.07208	0.08236	0.00154	514	213	511	44	510	9	0.2
UC03-28	0.48	0.05622	0.00488	0.54174	0.04639	0.06986	0.0012	461	161	440	31	435	7	1.1
UC03-29	0.48	0.05617	0.00518	0.56226	0.05115	0.07257	0.00129	459	172	453	33	452	8	0.2
UC03-30	0.65	0.05551	0.00413	0.52861	0.03858	0.06904	0.00115	433	134	431	26	430	7	0.2
UC03-32	1.22	0.05962	0.00858	0.74548	0.10577	0.09065	0.0025	590	266	566	62	559	15	1.3
UC03-33	0.34	0.05542	0.0039	0.52248	0.03599	0.06834	0.00113	429	125	427	24	426	7	0.2
UC03-34	0.5	0.05833	0.01456	0.70706	0.17575	0.08786	0.00207	542	461	543	105	543	12	0.0
UC03-35	0.56	0.05218	0.00718	0.32925	0.04491	0.04573	0.00086	293	270	289	34	288	5	0.3
UC03-36	0.81	0.05596	0.00444	0.5584	0.04341	0.07233	0.00124	451	143	450	28	450	7	0.0
UC03-37	1.08	0.05396	0.00465	0.43663	0.03691	0.05865	0.00103	369	160	368	26	367	6	0.3

UC03-39	0.55	0.06658	0.0047	1.25687	0.08656	0.13682	0.00228	825	116	827	39	827	13	0.0
UC03-40	0.84	0.05585	0.00632	0.55648	0.06213	0.07221	0.00136	446	217	449	41	449	8	0.0
UC03-41	0.93	0.10869	0.00788	4.76612	0.33697	0.3178	0.00546	1778	104	1779	59	1779	27	-0.1
UC03-42	0.39	0.05254	0.00467	0.35275	0.03074	0.04865	0.00087	309	165	307	23	306	5	0.3
UC03-43	1.12	0.17287	0.01229	11.66861	0.8074	0.48915	0.00834	2586	93	2578	65	2567	36	0.7
UC03-44	1.23	0.0542	0.01104	0.43304	0.08722	0.0579	0.0018	379	361	365	62	363	11	0.6
UC03-45	0.57	0.0557	0.00467	0.53961	0.04425	0.0702	0.00123	440	153	438	29	437	7	0.2
UC03-46	0.13	0.16639	0.01189	11.24981	0.78157	0.48992	0.00822	2522	95	2544	65	2570	36	-1.9
UC03-47	0.88	0.09026	0.00667	3.15626	0.22694	0.2534	0.00436	1431	112	1447	55	1456	22	-1.7
UC03-49	0.57	0.05553	0.00421	0.53726	0.03959	0.0701	0.0012	434	135	437	26	437	7	0.0
UC03-50	0.68	0.05218	0.0063	0.33898	0.04037	0.04707	0.00089	293	234	296	31	297	5	-0.3
UC03-53	0.5	0.05573	0.00477	0.54915	0.04581	0.07139	0.00129	442	155	444	30	445	8	-0.2
UC03-54	0.52	0.05776	0.00743	0.68142	0.08631	0.08547	0.00195	521	242	528	52	529	12	-0.2
UC03-55	0.72	0.05555	0.00498	0.53717	0.04703	0.07005	0.00128	434	164	437	31	436	8	0.2
UC04														
UC04-01	0.61	0.05541	0.00639	0.53223	0.06118	0.06966	0.00117	429	228	433	41	434	7	-0.2
UC04-02	0.28	0.05568	0.00437	0.5334	0.04174	0.06948	0.00104	440	149	434	28	433	6	0.2
UC04-03	0.65	0.05579	0.01085	0.56375	0.1089	0.07329	0.00215	444	360	454	71	456	13	-0.4

UC04-04	0.61	0.05176	0.00408	0.30656	0.02398	0.04295	0.00071	275	148	272	19	271	4	0.4
UC04-05	0.89	0.05408	0.00864	0.45648	0.07267	0.06121	0.00114	374	320	382	51	383	7	-0.3
UC04-06	0.34	0.07924	0.00354	2.12918	0.0949	0.19487	0.0027	1178	66	1158	31	1148	15	2.6
UC04-07	0.45	0.0512	0.0082	0.29265	0.0467	0.04145	0.0008	250	299	261	37	262	5	-0.4
UC04-08	0.83	0.05266	0.00314	0.34614	0.02056	0.04767	0.00069	314	109	302	16	300	4	0.7
UC04-09	0.28	0.0562	0.00264	0.57545	0.02698	0.07425	0.00104	460	79	462	17	462	6	0
UC04-10	0.32	0.07398	0.00363	1.79267	0.08762	0.17571	0.00255	1041	75	1043	32	1043	14	-0.2
UC04-11	0.22	0.05499	0.00319	0.48603	0.02815	0.0641	0.00092	412	104	402	19	401	6	0.2
UC04-12	0.62	0.05324	0.01478	0.38509	0.10666	0.05245	0.00124	339	473	331	78	330	8	0.3
UC04-13	0.68	0.07094	0.00347	1.49255	0.07286	0.15258	0.00215	956	77	927	30	915	12	1.3
UC04-14	0.65	0.05591	0.00425	0.55128	0.04168	0.0715	0.00116	449	140	446	27	445	7	0.2
UC04-15	0.67	0.05567	0.00318	0.50466	0.02865	0.06573	0.00099	439	100	415	19	410	6	1.2
UC04-16	0.68	0.05562	0.00333	0.53749	0.03208	0.07007	0.00103	437	107	437	21	437	6	0
UC04-17	0.04	0.07102	0.01252	1.50718	0.26342	0.15389	0.00524	958	315	933	107	923	29	1.1
UC04-18	1.2	0.12311	0.00631	6.06203	0.30941	0.35706	0.00543	2002	69	1985	44	1968	26	1.7
UC04-19	0.48	0.05438	0.01201	0.49506	0.1091	0.06602	0.00142	387	399	408	74	412	9	-1
UC04-20	0.6	0.08263	0.00412	2.36335	0.11771	0.20739	0.00302	1260	75	1232	36	1215	16	3.7
UC04-21	0.53	0.11252	0.0054	5.11026	0.24484	0.3293	0.00477	1841	66	1838	41	1835	23	0.3

UC04-22	0.59	0.05195	0.0052	0.32332	0.03228	0.04513	0.00072	283	196	284	25	285	4	-0.4
UC04-23	0.57	0.11431	0.00524	5.19766	0.23834	0.32967	0.00465	1869	62	1852	39	1837	23	1.7
UC04-24	0.46	0.05176	0.00386	0.30192	0.02244	0.04229	0.00066	275	141	268	18	267	4	0.4
UC04-25	0.73	0.05264	0.00422	0.36662	0.02936	0.0505	0.00077	313	154	317	22	318	5	-0.3
UC04-26	0.88	0.11604	0.00535	5.44165	0.25108	0.34002	0.00478	1896	63	1891	40	1887	23	0.5
UC04-27	0.33	0.05172	0.00366	0.30967	0.02179	0.04341	0.00071	273	131	274	17	274	4	0
UC04-28	0.63	0.11202	0.00591	5.11169	0.26919	0.33085	0.0051	1832	73	1838	45	1843	25	-0.6
UC04-29	0.14	0.06738	0.00329	1.26747	0.06187	0.13637	0.00196	850	78	831	28	824	11	0.8
UC04-30	1.35	0.09285	0.01144	3.34112	0.40912	0.2609	0.00685	1485	196	1491	96	1494	35	-0.6
UC04-31	0.53	0.12328	0.00636	6.24018	0.32115	0.36698	0.00561	2004	70	2010	45	2015	26	-0.5
UC04-32	0.47	0.05592	0.00475	0.57464	0.0486	0.0745	0.00124	449	160	461	31	463	7	-0.4
UC04-33	1.41	0.05129	0.01267	0.29412	0.07247	0.04157	0.00098	254	413	262	57	263	6	-0.4
UC04-34	1.04	0.05181	0.00524	0.32216	0.03246	0.04508	0.00076	277	196	284	25	284	5	0
UC04-35	0.79	0.05134	0.00582	0.29811	0.03371	0.0421	0.00068	256	226	265	26	266	4	-0.4
UC04-36	0.33	0.17524	0.00841	12.02079	0.57849	0.49732	0.00711	2608	61	2606	45	2602	31	0.2
UC04-37	0.63	0.05245	0.00426	0.34658	0.02812	0.04791	0.00074	305	157	302	21	302	5	0
UC04-38	0.68	0.05258	0.0047	0.35653	0.03178	0.04916	0.0008	311	172	310	24	309	5	0.3
UC04-39	0.55	0.05427	0.00877	0.45666	0.07356	0.061	0.00122	382	321	382	51	382	7	0

UC04-40	0.6	0.12643	0.0094	6.70538	0.49805	0.38449	0.0073	2049	105	2073	66	2097	34	-2.3
UC04-41	0.26	0.05648	0.00685	0.58153	0.07026	0.07464	0.00133	471	239	465	45	464	8	0.2
UC04-42	0.61	0.05513	0.00389	0.50086	0.03531	0.06587	0.00103	417	130	412	24	411	6	0.2
UC04-43	0.92	0.11395	0.00586	5.27519	0.27154	0.3356	0.00501	1863	71	1865	44	1865	24	-0.1
UC04-44	0.69	0.05614	0.00316	0.57521	0.03237	0.07428	0.00112	458	98	461	21	462	7	-0.2
UC04-45	0.72	0.05192	0.01628	0.31361	0.09806	0.04379	0.00124	282	517	277	76	276	8	0.4
UC04-46	0.66	0.05555	0.0037	0.53775	0.03582	0.07018	0.00108	434	122	437	24	437	7	0
UC04-47	0.44	0.05054	0.00479	0.24462	0.02313	0.03509	0.00058	220	183	222	19	222	4	0
UC04-48	0.61	0.05153	0.00948	0.30248	0.05556	0.04256	0.00082	265	338	268	43	269	5	-0.4
UC04-49	0.88	0.05415	0.00464	0.45108	0.03854	0.0604	0.00101	377	163	378	27	378	6	0
UC04-50	0.32	0.05264	0.00485	0.37065	0.03404	0.05105	0.00086	313	177	320	25	321	5	-0.3
UC04-51	0.82	0.05296	0.00383	0.37677	0.02724	0.05157	0.00081	327	136	325	20	324	5	0.3
UC04-52	0.72	0.05079	0.00815	0.2619	0.04179	0.03738	0.00086	231	291	236	34	237	5	-0.4
UC04-53	0.55	0.07047	0.00427	1.53933	0.09319	0.15835	0.00251	942	98	946	37	948	14	-0.2
UC04-54	0.5	0.0706	0.00431	1.52217	0.09289	0.15632	0.00248	946	99	939	37	936	14	0.3
UC04-55	0.64	0.05555	0.00362	0.5284	0.03445	0.06896	0.00108	434	118	431	23	430	7	0.2
UC04-56	0.96	0.0546	0.00466	0.45824	0.039	0.06085	0.00106	396	161	383	27	381	6	0.5
UC04-57	0.77	0.05247	0.0153	0.33932	0.09878	0.04689	0.00111	306	491	297	75	295	7	0.7

UC04-58	0.21	0.0572	0.00685	0.64253	0.07671	0.08144	0.0015	499	235	504	47	505	9	-0.2
UC04-59	0.83	0.05115	0.00983	0.283	0.05429	0.04011	0.0008	248	340	253	43	254	5	-0.4
UC04-60	0.91	0.05615	0.00401	0.57508	0.04106	0.07425	0.0012	458	131	461	26	462	7	-0.2
UC04-61	1.06	0.10452	0.00656	4.35247	0.27313	0.30191	0.00503	1706	91	1703	52	1701	25	0.3
UC04-62	0.63	0.0559	0.0033	0.56105	0.03322	0.07277	0.00114	448	104	452	22	453	7	-0.2
UC04-63	0.52	0.14914	0.00891	8.88874	0.53215	0.43209	0.00711	2336	80	2327	55	2315	32	0.9
UC04-64	1.12	0.05128	0.00858	0.28139	0.04697	0.03978	0.0008	253	307	252	37	251	5	0.4
UC04-65	0.45	0.05547	0.00404	0.53497	0.03896	0.06993	0.00116	431	134	435	26	436	7	-0.2
UC04-66	0.38	0.0594	0.00456	0.79866	0.06119	0.09747	0.0017	582	137	596	35	600	10	-0.7
UC04-67	0.58	0.05519	0.00376	0.50765	0.03456	0.06669	0.0011	420	123	417	23	416	7	0.2
UC04-68	0.5	0.05353	0.00557	0.40815	0.04231	0.05529	0.00106	351	199	348	31	347	6	0.3
UC04-69	0.6	0.05588	0.00359	0.55498	0.03575	0.072	0.00117	448	115	448	23	448	7	0
UC04-70	0.63	0.15326	0.00923	8.59883	0.51947	0.40678	0.00669	2383	81	2296	55	2200	31	8.3
UC04-71	0.67	0.05088	0.01556	0.28411	0.08668	0.04049	0.00111	235	497	254	69	256	7	-0.8
UC04-72	0.52	0.05804	0.00387	0.69021	0.04611	0.08622	0.00142	531	118	533	28	533	8	0
UC04-73	1.35	0.05184	0.009	0.31154	0.054	0.04358	0.0009	278	320	275	42	275	6	0
UC04-74	0.58	0.10827	0.00731	4.74049	0.32061	0.31744	0.00545	1771	99	1774	57	1777	27	-0.3
UC04-75	0.72	0.05182	0.00407	0.31836	0.02503	0.04454	0.00076	277	147	281	19	281	5	0

UC04-76	3.03	0.05054	0.00596	0.25227	0.02969	0.03619	0.00067	220	232	228	24	229	4	-0.4
UC04-77	0.8	0.06643	0.00587	1.26603	0.11167	0.13819	0.00257	820	155	831	50	834	15	-0.4
UC04-78	0.74	0.05556	0.00369	0.56971	0.038	0.07435	0.00122	435	120	458	25	462	7	-0.9
UC04-79	1.22	0.051	0.01058	0.27099	0.05612	0.03852	0.00083	241	357	243	45	244	5	-0.4
UC04-80	0.78	0.05635	0.00573	0.57043	0.05792	0.0734	0.0014	466	194	458	37	457	8	0.2
UC04-81	0.23	0.0555	0.00636	0.53457	0.0612	0.06984	0.00129	432	224	435	40	435	8	0
UC04-82	0.71	0.05632	0.00619	0.57978	0.06368	0.07465	0.00143	465	212	464	41	464	9	0
UC04-83	0.51	0.11792	0.0079	5.80377	0.39064	0.35691	0.00609	1925	96	1947	58	1968	29	-2.2
UC04-84	0.64	0.146	0.00957	8.91955	0.5881	0.443	0.00745	2300	90	2330	60	2364	33	-2.7
UC04-85	0.63	0.05598	0.00445	0.56451	0.04497	0.07313	0.00128	452	147	454	29	455	8	-0.2
UC04-86	0.59	0.066	0.00483	1.20589	0.08858	0.13249	0.00232	806	125	803	41	802	13	0.1
UC04-87	0.6	0.05081	0.01179	0.25682	0.05947	0.03666	0.00087	232	392	232	48	232	5	0
UC04-88	0.39	0.06429	0.00812	1.12209	0.14121	0.12657	0.00279	751	235	764	68	768	16	-0.5
UC04-89	1.39	0.11769	0.00806	5.85719	0.40354	0.36091	0.0063	1921	99	1955	60	1986	30	-3.3
UC04-90	0.03	0.05695	0.0039	0.63272	0.04362	0.08057	0.00137	490	123	498	27	500	8	-0.4
UC04-91	2.04	0.05487	0.00488	0.50057	0.04458	0.06616	0.00121	407	168	412	30	413	7	-0.2
UC04-92	0.85	0.0519	0.0067	0.32706	0.04224	0.0457	0.00088	281	257	287	32	288	5	-0.3
UC04-93	0.19	0.12794	0.00905	6.73382	0.47943	0.38172	0.00681	2070	101	2077	63	2084	32	-0.7

UC04-94	2.5	0.05825	0.00692	0.70802	0.08401	0.08815	0.00184	539	228	544	50	545	11	-0.2
UC04-95	0.12	0.08066	0.02362	2.28572	0.66663	0.20552	0.00716	1213	564	1208	206	1205	38	0.7
UC04-96	0.47	0.06376	0.00462	1.0744	0.07841	0.12221	0.00216	734	125	741	38	743	12	-0.3
UC04-97	0.32	0.05487	0.00431	0.51842	0.04096	0.06853	0.00122	407	146	424	27	427	7	-0.7
UC04-98	0.39	0.05166	0.00724	0.30542	0.04277	0.04288	0.00091	270	274	271	33	271	6	0
UC04-99	0.67	0.05419	0.02722	0.45651	0.22884	0.0611	0.00235	379	874	382	160	382	14	0
UC04-100	0.78	0.05204	0.01148	0.33748	0.07435	0.04704	0.00113	287	378	295	56	296	7	-0.3
UC05														
UC05-01	0.77	0.1057	0.00539	4.48529	0.2267	0.30751	0.00459	1727	71	1728	42	1728	23	-0.1
UC05-02	1.05	0.10135	0.00777	4.05064	0.30776	0.28965	0.00504	1649	116	1644	62	1640	25	0.5
UC05-03	0.07	0.05181	0.00402	0.41497	0.03164	0.05805	0.00112	277	138	352	23	364	7	-3.3
UC05-04	1.2	0.0509	0.00816	0.25134	0.04006	0.03579	0.00076	236	294	228	33	227	5	0.4
UC05-05	0.37	0.06935	0.00275	1.59144	0.0626	0.16633	0.00231	909	58	967	25	992	13	-2.5
UC05-06	1.33	0.05123	0.00473	0.29148	0.0268	0.04123	0.00064	251	179	260	21	260	4	0
UC05-07	0.92	0.05141	0.00355	0.29078	0.01999	0.041	0.00058	259	131	259	16	259	4	0
UC05-08	0.24	0.05335	0.00402	0.39516	0.02965	0.05369	0.00079	344	144	338	22	337	5	0.3
UC05-09	1.02	0.05088	0.006	0.26511	0.03115	0.03777	0.00061	235	236	239	25	239	4	0
UC05-10	1.27	0.05594	0.00483	0.58009	0.04978	0.07516	0.00119	450	165	465	32	467	7	-0.4

UC05-11	0.59	0.05071	0.00415	0.24547	0.02	0.03509	0.00051	228	157	223	16	222	3	0.5
UC05-12	0.86	0.11425	0.0037	5.83337	0.18839	0.37011	0.00494	1868	39	1951	28	2030	23	-8
UC05-13	0.86	0.05289	0.00322	0.37029	0.02244	0.05075	0.00072	324	112	320	17	319	4	0.3
UC05-14	0.38	0.14363	0.00448	8.45786	0.26317	0.42688	0.00561	2271	35	2281	28	2292	25	-0.9
UC05-15	0.79	0.11318	0.00343	5.32058	0.16123	0.34076	0.0044	1851	36	1872	26	1890	21	-2.1
UC05-16	0.48	0.06954	0.00236	1.46916	0.04961	0.15314	0.00202	915	48	918	20	919	11	-0.1
UC05-17	0.22	0.10788	0.00328	4.69199	0.14275	0.31529	0.00408	1764	37	1766	25	1767	20	-0.2
UC05-18	0.49	0.05503	0.00428	0.5115	0.03962	0.06738	0.00101	413	148	419	27	420	6	-0.2
UC05-19	0.58	0.14453	0.00434	8.46793	0.25463	0.42474	0.00548	2282	34	2282	27	2282	25	0
UC05-20	0.92	0.05207	0.00603	0.32283	0.03726	0.04495	0.00076	288	230	284	29	283	5	0.4
UC05-21	0.16	0.15717	0.00467	10.12131	0.3014	0.46686	0.00596	2425	33	2446	28	2470	26	-1.8
UC05-22	0.52	0.05594	0.00456	0.55916	0.04528	0.07246	0.00113	450	154	451	29	451	7	0
UC05-23	1.18	0.05213	0.00278	0.34106	0.01816	0.04744	0.00065	291	97	298	14	299	4	-0.3
UC05-24	1.14	0.16802	0.00523	11.40166	0.35463	0.49198	0.00652	2538	34	2557	29	2579	28	-1.6
UC05-25	0.27	0.0552	0.00354	0.51273	0.03272	0.06735	0.00099	420	117	420	22	420	6	0
UC05-26	0.63	0.10606	0.00323	4.50506	0.13768	0.30796	0.00396	1733	37	1732	25	1731	20	0.1
UC05-27	0.93	0.06776	0.0277	1.34428	0.54715	0.14383	0.00612	861	756	865	237	866	34	-0.1
UC05-28	0.47	0.05505	0.00235	0.49128	0.02093	0.06471	0.00087	414	71	406	14	404	5	0.5

UC05-29	1.64	0.05794	0.02401	0.70546	0.29148	0.08828	0.00313	527	724	542	174	545	19	-0.6
UC05-30	0.72	0.05115	0.01714	0.27484	0.09191	0.03896	0.00101	248	544	247	73	246	6	0.4
UC05-31	0.93	0.07791	0.00623	2.12394	0.16899	0.19768	0.0032	1145	134	1157	55	1163	17	-1.5
UC05-32	0.01	0.12502	0.00475	6.37632	0.24071	0.36981	0.00533	2029	46	2029	33	2029	25	0
UC05-33	0.63	0.15367	0.00475	9.45208	0.29306	0.44601	0.00574	2387	35	2383	28	2377	26	0.4
UC05-34	0.72	0.09489	0.00493	3.51605	0.18166	0.26869	0.00394	1526	75	1531	41	1534	20	-0.5
UC05-35	0.66	0.05604	0.0038	0.57213	0.03857	0.07403	0.00109	454	124	459	25	460	7	-0.2
UC05-36	0.4	0.11267	0.00361	5.10202	0.16381	0.32835	0.00431	1843	39	1836	27	1830	21	0.7
UC05-37	0.83	0.05163	0.01044	0.30044	0.06058	0.0422	0.0009	269	353	267	47	266	6	0.4
UC05-38	0.65	0.07048	0.00267	1.52833	0.05788	0.15725	0.00211	942	55	942	23	941	12	0.1
UC05-39	1.67	0.05276	0.04176	0.34364	0.27147	0.04723	0.00248	318	1186	300	205	297	15	1
UC05-40	0.38	0.05098	0.00344	0.27664	0.01858	0.03935	0.00058	240	127	248	15	249	4	-0.4
UC05-41	0.83	0.06759	0.00351	1.33921	0.06928	0.14368	0.00204	856	84	863	30	865	11	-0.2
UC05-42	0.31	0.05535	0.00276	0.52823	0.02623	0.06921	0.00096	426	86	431	17	431	6	0
UC05-43	0.47	0.05159	0.00619	0.30147	0.03606	0.04237	0.00069	267	241	268	28	268	4	0
UC05-44	0.48	0.05493	0.00974	0.51025	0.09009	0.06737	0.00147	409	338	419	61	420	9	-0.2
UC05-45	0.35	0.14633	0.00473	8.677	0.28145	0.43001	0.00558	2303	38	2305	30	2306	25	-0.1
UC05-46	1.3	0.072	0.00292	1.6518	0.0668	0.16638	0.0023	986	60	990	26	992	13	-0.2

UC05-47	0.7	0.05169	0.01328	0.30338	0.07771	0.04256	0.00101	272	431	269	61	269	6	0
UC05-48	0.44	0.05546	0.00403	0.53123	0.03848	0.06946	0.00104	431	136	433	26	433	6	0
UC05-49	0.77	0.05437	0.00234	0.45854	0.0197	0.06116	0.00085	386	71	383	14	383	5	0
UC05-50	0.89	0.11415	0.00411	5.33476	0.1919	0.33893	0.00465	1867	45	1874	31	1882	22	-0.8
UC05-51	1.28	0.0515	0.00875	0.29433	0.04987	0.04145	0.00079	263	314	262	39	262	5	0
UC05-52	0.72	0.05586	0.00367	0.5421	0.03552	0.07039	0.00103	447	120	440	23	439	6	0.2
UC05-53	0.28	0.05327	0.00302	0.40919	0.02311	0.05571	0.0008	340	102	348	17	349	5	-0.3
UC05-54	0.05	0.0562	0.00258	0.56756	0.02599	0.07324	0.00103	460	77	456	17	456	6	0
UC05-55	0.16	0.13969	0.00519	7.12582	0.26471	0.36995	0.0052	2223	45	2127	33	2029	24	9.6
UC05-56	1.75	0.0639	0.00652	1.13209	0.11502	0.1285	0.00213	738	191	769	55	779	12	-1.3
UC05-57	0.99	0.0547	0.00373	0.49337	0.03347	0.06541	0.001	400	125	407	23	408	6	-0.2
UC05-58	0.35	0.17525	0.00605	12.0162	0.4167	0.49728	0.00658	2608	40	2606	33	2602	28	0.2
UC05-59	0.96	0.07423	0.00874	1.81712	0.21286	0.17754	0.00346	1048	210	1052	77	1054	19	-0.6
UC05-60	0.69	0.0562	0.00248	0.57588	0.0254	0.07431	0.00102	460	73	462	16	462	6	0
UC05-61	0.68	0.05175	0.0028	0.30591	0.0165	0.04287	0.00062	274	97	271	13	271	4	0
UC05-62	0.26	0.05453	0.00255	0.48022	0.02244	0.06387	0.0009	393	79	398	15	399	5	-0.3
UC05-63	0.14	0.06629	0.0024	1.34729	0.04901	0.14742	0.00196	816	54	866	21	886	11	-2.3
UC05-64	0.46	0.05274	0.01615	0.37059	0.1132	0.05096	0.00131	318	513	320	84	320	8	0

UC05-65	0.36	0.06023	0.00304	0.83884	0.0423	0.10101	0.00144	612	84	619	23	620	8	-0.2
UC05-66	0.18	0.16196	0.00588	10.12807	0.36952	0.45357	0.00613	2476	43	2447	34	2411	27	2.7
UC05-67	0.36	0.12303	0.00469	6.14882	0.2352	0.36248	0.00498	2001	48	1997	33	1994	24	0.4
UC05-68	1.27	0.05199	0.00576	0.33493	0.03696	0.04673	0.00079	285	218	293	28	294	5	-0.3
UC05-69	0.47	0.05554	0.00334	0.52664	0.03159	0.06878	0.00101	434	108	430	21	429	6	0.2
UC05-70	0.88	0.0553	0.00886	0.51131	0.08171	0.06707	0.00127	424	323	419	55	418	8	0.2
UC05-71	0.16	0.06487	0.00404	1.03106	0.06376	0.11528	0.0019	770	103	719	32	703	11	2.3
UC05-72	0.55	0.05595	0.0035	0.5511	0.03439	0.07144	0.00106	450	113	446	23	445	6	0.2
UC05-73	0.81	0.12324	0.00499	6.20945	0.25211	0.36543	0.00513	2004	52	2006	36	2008	24	-0.2
UC05-74	0.72	0.16259	0.00618	10.47823	0.40026	0.46743	0.00637	2483	46	2478	35	2472	28	0.4
UC05-75	0.25	0.11341	0.00435	5.20247	0.20061	0.33271	0.00452	1855	50	1853	33	1852	22	0.2
UC05-76	0.09	0.06093	0.00408	0.87175	0.05818	0.10377	0.00157	637	118	637	32	636	9	0.2
UC05-77	0.46	0.0597	0.00283	0.79209	0.03758	0.09624	0.00136	593	78	592	21	592	8	0
UC05-78	0.38	0.05543	0.00277	0.52712	0.02633	0.06897	0.001	430	85	430	18	430	6	0
UC05-79	1.06	0.05559	0.00705	0.54297	0.06872	0.07085	0.00121	436	255	440	45	441	7	-0.2
UC05-80	0.34	0.0706	0.00326	1.53467	0.07088	0.15767	0.00224	946	71	944	28	944	12	0
UC05-81	0.12	0.06136	0.00278	0.84815	0.03848	0.10026	0.00143	652	73	624	21	616	8	1.3
UC05-82	0.64	0.0558	0.00334	0.55664	0.03334	0.07236	0.00106	444	108	449	22	450	6	-0.2

UC05-83	0.71	0.06908	0.00285	1.43144	0.05941	0.1503	0.00207	901	63	902	25	903	12	-0.1
UC05-84	0.76	0.07024	0.00514	1.55898	0.11385	0.16097	0.00248	935	126	954	45	962	14	-0.8
UC05-85	0.5	0.09641	0.00458	3.58142	0.17048	0.26945	0.00392	1556	67	1545	38	1538	20	1.2
UC05-86	0.3	0.05642	0.0028	0.56517	0.02808	0.07266	0.00104	469	85	455	18	452	6	0.7
UC05-87	0.52	0.05576	0.00308	0.54966	0.03035	0.0715	0.00104	443	97	445	20	445	6	0
UC05-88	0.8	0.05645	0.00293	0.58636	0.03044	0.07534	0.00109	470	89	469	19	468	7	0.2
UC05-89	0.89	0.10177	0.00464	4.08906	0.18688	0.29143	0.00426	1657	63	1652	37	1649	21	0.5
UC05-90	0.45	0.05599	0.00281	0.56398	0.02838	0.07306	0.00106	452	86	454	18	455	6	-0.2
UC05-91	0.32	0.07568	0.00348	1.83456	0.08454	0.17583	0.00255	1087	69	1058	30	1044	14	4.1
UC05-92	0.84	0.06543	0.00444	1.18577	0.08025	0.13144	0.00208	788	116	794	37	796	12	-0.3
UC05-93	0.74	0.05134	0.00607	0.28973	0.03416	0.04093	0.0007	256	235	258	27	259	4	-0.4
UC05-94	0.36	0.11341	0.00485	5.3008	0.22826	0.33901	0.00476	1855	57	1869	37	1882	23	-1.4
UC05-95	1.35	0.05279	0.0101	0.34704	0.06627	0.04768	0.00095	320	353	302	50	300	6	0.7
UC05-96	1.18	0.07249	0.00352	1.67726	0.08171	0.1678	0.00245	1000	75	1000	31	1000	14	0
UC05-97	1.41	0.11702	0.00524	5.76589	0.25977	0.35735	0.00521	1911	60	1941	39	1970	25	-3
UC05-98	0.47	0.05259	0.00349	0.36076	0.02393	0.04975	0.00075	311	124	313	18	313	5	0
UC05-99	0.92	0.05879	0.00356	0.7368	0.04471	0.0909	0.00136	559	107	561	26	561	8	0
UC05-100	0.91	0.06463	0.00353	1.12968	0.06173	0.12677	0.00191	762	90	768	29	769	11	-0.1

UC06

UC06-01	1.19	0.16488	0.0044	10.7797	0.2906	0.47411	0.0063	2506	28	2504	25	2502	28	0.2
UC06-02	0.49	0.06694	0.00196	1.2345	0.03646	0.13373	0.00175	836	40	816	17	809	10	0.9
UC06-03	1.05	0.11177	0.00297	4.96932	0.13339	0.32241	0.00419	1828	30	1814	23	1801	20	1.5
UC06-04	0.02	0.10543	0.00288	4.56323	0.12598	0.31388	0.00415	1722	31	1743	23	1760	20	-2.2
UC06-05	0.32	0.10893	0.003	4.78555	0.13311	0.31859	0.00419	1782	32	1782	23	1783	20	-0.1
UC06-06	0.73	0.05371	0.00456	0.4214	0.0357	0.0569	0.00086	359	165	357	26	357	5	0.0
UC06-07	0.48	0.0514	0.00882	0.29571	0.05061	0.04172	0.0008	259	318	263	40	263	5	0.0
UC06-08	0.2	0.12203	0.00335	6.08633	0.16878	0.36167	0.00478	1986	31	1988	24	1990	23	-0.2
UC06-09	0.48	0.05127	0.00281	0.28241	0.01541	0.03994	0.00057	253	99	253	12	252	4	0.4
UC06-10	0.83	0.11265	0.0031	5.12934	0.14243	0.33019	0.00436	1843	31	1841	24	1839	21	0.2
UC06-11	1.37	0.11779	0.00306	5.61142	0.14787	0.34546	0.00445	1923	29	1918	23	1913	21	0.5
UC06-12	0.61	0.055	0.00461	0.50939	0.04247	0.06717	0.00107	412	160	418	29	419	6	-0.2
UC06-13	0.66	0.11074	0.00446	4.97987	0.19962	0.32609	0.00484	1812	51	1816	34	1819	24	-0.4
UC06-14	0.91	0.05663	0.00186	0.59766	0.01976	0.07654	0.001	477	50	476	13	475	6	0.2
UC06-15	0.93	0.05399	0.00214	0.44626	0.01768	0.05994	0.00081	371	65	375	12	375	5	0.0
UC06-16	0.29	0.0558	0.00491	0.54288	0.04754	0.07055	0.00117	444	167	440	31	439	7	0.2
UC06-17	0.93	0.05265	0.00649	0.3568	0.04377	0.04914	0.00091	314	244	310	33	309	6	0.3

UC06-18	0.39	0.12302	0.00331	6.17712	0.16813	0.36411	0.00479	2000	30	2001	24	2002	23	-0.1
UC06-19	0.68	0.05252	0.00325	0.36025	0.02224	0.04974	0.00071	308	115	312	17	313	4	-0.3
UC06-20	0.57	0.05202	0.01059	0.32203	0.06537	0.04489	0.00091	286	363	283	50	283	6	0.0
UC06-21	0.29	0.07864	0.00223	2.14811	0.06156	0.19808	0.0026	1163	36	1164	20	1165	14	-0.2
UC06-22	0.87	0.0543	0.0046	0.45482	0.03837	0.06074	0.00097	384	163	381	27	380	6	0.3
UC06-23	0.83	0.1117	0.00298	5.00462	0.13526	0.32491	0.00422	1827	30	1820	23	1814	21	0.7
UC06-24	0.72	0.05618	0.00343	0.56834	0.03467	0.07336	0.00105	459	110	457	22	456	6	0.2
UC06-25	0.8	0.1082	0.01031	4.73101	0.44737	0.31707	0.00635	1769	145	1773	79	1775	31	-0.3
UC06-26	0.5	0.05529	0.00496	0.51898	0.04641	0.06807	0.00108	424	174	424	31	425	7	-0.2
UC06-27	1.41	0.05766	0.00244	0.65863	0.02791	0.08284	0.00111	517	69	514	17	513	7	0.2
UC06-28	0.49	0.05535	0.00306	0.52692	0.02903	0.06903	0.00098	426	98	430	19	430	6	0.0
UC06-29	1.35	0.15143	0.00793	9.17294	0.47669	0.43928	0.00741	2362	66	2355	48	2347	33	0.6
UC06-30	0.5	0.0678	0.00273	1.34998	0.05418	0.1444	0.00202	862	60	868	23	869	11	-0.1
UC06-31	0.02	0.05527	0.00167	0.515	0.01571	0.06757	0.00088	423	45	422	11	421	5	0.2
UC06-32	0.55	0.05536	0.00772	0.51903	0.07213	0.06799	0.00123	427	281	425	48	424	7	0.2
UC06-33	0.57	0.05521	0.00246	0.51182	0.02283	0.06722	0.00091	421	75	420	15	419	5	0.2
UC06-34	0.66	0.10903	0.00503	4.80911	0.22052	0.31986	0.005	1783	61	1786	39	1789	24	-0.3
UC06-35	0.81	0.05219	0.00504	0.35205	0.0339	0.04892	0.00078	294	189	306	25	308	5	-0.6

UC06-36	0.69	0.05836	0.01487	0.7235	0.18314	0.0899	0.00353	543	453	553	108	555	21	-0.4
UC06-37	1.54	0.09803	0.00531	3.78611	0.20329	0.28006	0.00468	1587	75	1590	43	1592	24	-0.3
UC06-38	0.7	0.05541	0.00447	0.52643	0.0423	0.0689	0.00107	429	153	429	28	430	6	-0.2
UC06-39	0.84	0.05146	0.00806	0.30179	0.0471	0.04253	0.00083	261	296	268	37	268	5	0.0
UC06-40	0.42	0.11591	0.00374	5.46122	0.17682	0.34165	0.00471	1894	38	1895	28	1895	23	-0.1
UC06-41	1.28	0.05481	0.00426	0.49326	0.03817	0.06525	0.00099	404	148	407	26	407	6	0.0
UC06-42	0.41	0.0753	0.00224	1.89095	0.05656	0.1821	0.00241	1077	39	1078	20	1078	13	-0.1
UC06-43	0.63	0.0558	0.00312	0.55193	0.03078	0.07172	0.00101	444	99	446	20	447	6	-0.2
UC06-44	0.68	0.10573	0.00376	4.48271	0.15883	0.30745	0.00446	1727	44	1728	29	1728	22	-0.1
UC06-45	0.64	0.0585	0.01975	0.70957	0.23897	0.08796	0.00243	549	601	544	142	543	14	0.2
UC06-46	0.49	0.11268	0.00345	5.15687	0.15874	0.33188	0.00452	1843	36	1846	26	1847	22	-0.2
UC06-47	0.66	0.05139	0.00213	0.29322	0.01217	0.04138	0.00057	258	70	261	10	261	4	0.0
UC06-48	0.47	0.10618	0.00451	4.52314	0.19075	0.3089	0.00475	1735	55	1735	35	1735	23	0.0
UC06-49	0.61	0.0567	0.0021	0.60643	0.02247	0.07756	0.00106	480	58	481	14	482	6	-0.2
UC06-50	0.98	0.0509	0.011	0.25645	0.05531	0.03653	0.00073	236	370	232	45	231	5	0.4
UC06-51	0.79	0.05233	0.00707	0.34009	0.04583	0.04713	0.00081	300	270	297	35	297	5	0.0
UC06-52	0.09	0.05555	0.0024	0.52959	0.02289	0.06914	0.00096	434	71	432	15	431	6	0.2
UC06-53	0.63	0.05126	0.00592	0.27758	0.03192	0.03927	0.00068	253	228	249	25	248	4	0.4

UC06-54	0.69	0.1664	0.00491	11.51406	0.34187	0.50176	0.00678	2522	32	2566	28	2621	29	-3.8
UC06-55	0.62	0.11381	0.00342	5.36014	0.16213	0.34153	0.00461	1861	35	1879	26	1894	22	-1.7
UC06-56	1.3	0.12129	0.00351	5.98248	0.17449	0.35766	0.00472	1975	33	1973	25	1971	22	0.2
UC06-57	0.8	0.05632	0.00649	0.59056	0.06768	0.07604	0.00141	465	224	471	43	472	8	-0.2
UC06-58	1.39	0.11834	0.00398	5.71482	0.19219	0.3502	0.00501	1931	40	1934	29	1936	24	-0.3
UC06-59	0.46	0.0549	0.00459	0.51124	0.04258	0.06752	0.00103	408	161	419	29	421	6	-0.5
UC06-60	0.71	0.10773	0.004	4.68566	0.17368	0.31541	0.00453	1761	47	1765	31	1767	22	-0.3
UC06-61	0.37	0.12174	0.00362	6.04732	0.18121	0.36022	0.00482	1982	34	1983	26	1983	23	-0.1
UC06-62	0.76	0.05677	0.00283	0.60895	0.03031	0.07779	0.00111	483	85	483	19	483	7	0.0
UC06-63	0.69	0.05533	0.00522	0.51791	0.04862	0.06788	0.00112	426	182	424	33	423	7	0.2
UC06-64	0.63	0.05704	0.00242	0.6328	0.02683	0.08044	0.00114	493	68	498	17	499	7	-0.2
UC06-65	0.61	0.05604	0.00291	0.56604	0.02934	0.07324	0.00104	454	90	455	19	456	6	-0.2
UC06-66	0.87	0.05599	0.00237	0.56307	0.02382	0.07293	0.00101	452	69	454	15	454	6	0.0
UC06-67	0.67	0.14815	0.00459	8.85738	0.27587	0.43355	0.00595	2325	35	2323	28	2322	27	0.1
UC06-68	0.72	0.0514	0.00289	0.28295	0.01589	0.03992	0.00057	259	103	253	13	252	4	0.4
UC06-69	0.4	0.14221	0.00474	8.08421	0.26991	0.41223	0.00594	2254	38	2240	30	2225	27	1.3
UC06-70	0.53	0.11953	0.01184	5.82504	0.57093	0.35339	0.00789	1949	145	1950	85	1951	38	-0.1
UC06-71	1.09	0.14486	0.00511	8.51597	0.29985	0.4263	0.00621	2286	40	2288	32	2289	28	-0.1

UC06-72	0.48	0.05946	0.0088	0.7722	0.11362	0.09418	0.00232	584	283	581	65	580	14	0.2
UC06-73	0.99	0.05352	0.00735	0.41335	0.0564	0.056	0.00125	351	268	351	41	351	8	0.0
UC06-74	0.44	0.11822	0.00377	5.68806	0.18204	0.34889	0.00476	1929	38	1930	28	1929	23	0.0
UC06-75	1.02	0.05304	0.00918	0.3808	0.06562	0.05206	0.00112	331	329	328	48	327	7	0.3
UC06-76	0.75	0.05695	0.02791	0.60457	0.29541	0.07698	0.0032	490	866	480	187	478	19	0.4
UC06-77	0.08	0.12481	0.00407	6.27092	0.20511	0.36433	0.00501	2026	38	2014	29	2003	24	1.1
UC06-78	0.42	0.05679	0.00249	0.6127	0.02673	0.07824	0.00113	483	71	485	17	486	7	-0.2
UC06-79	0.57	0.05373	0.00508	0.42094	0.0397	0.05681	0.00091	360	184	357	28	356	6	0.3
UC06-80	0.55	0.05561	0.00239	0.53146	0.02278	0.06931	0.00097	437	70	433	15	432	6	0.2
UC06-81	0.39	0.12212	0.00406	6.08185	0.2028	0.36113	0.00499	1987	40	1988	29	1988	24	-0.1
UC06-82	0.46	0.05638	0.00428	0.57075	0.0432	0.0734	0.00111	467	142	458	28	457	7	0.2
UC06-83	0.32	0.11134	0.00381	4.99966	0.17124	0.32562	0.00452	1821	42	1819	29	1817	22	0.2
UC06-84	0.65	0.05206	0.0089	0.34451	0.05873	0.04798	0.00092	288	319	301	44	302	6	-0.3
UC06-85	0.58	0.10669	0.00463	4.57963	0.19771	0.31125	0.00467	1744	57	1746	36	1747	23	-0.2
UC06-86	0.85	0.15351	0.00514	9.50428	0.31953	0.44896	0.00629	2385	38	2388	31	2391	28	-0.3
UC06-87	0.87	0.05404	0.00722	0.44468	0.05922	0.05967	0.00101	373	270	374	42	374	6	0.0
UC06-88	0.29	0.11805	0.00386	5.65582	0.18572	0.34743	0.0047	1927	39	1925	28	1922	22	0.3
UC06-89	0.87	0.10837	0.00421	4.74239	0.18323	0.31732	0.00475	1772	49	1775	32	1777	23	-0.3

UC06-90	0.5	0.11114	0.00369	4.99371	0.16669	0.32583	0.00443	1818	41	1818	28	1818	22	0.0
UC06-91	0.55	0.10843	0.00421	4.71597	0.18266	0.3154	0.00456	1773	49	1770	32	1767	22	0.3
UC06-92	0.98	0.05556	0.00487	0.54557	0.04769	0.07121	0.00112	435	169	442	31	443	7	-0.2
UC06-93	0.88	0.05649	0.00261	0.5857	0.02696	0.07518	0.00108	472	76	468	17	467	6	0.2
UC06-94	1.25	0.12501	0.00437	6.38037	0.22361	0.37011	0.00517	2029	42	2030	31	2030	24	0.0
UC06-95	0.69	0.05535	0.00334	0.52035	0.03121	0.06817	0.00104	426	107	425	21	425	6	0.0
UC06-96	0.4	0.11185	0.00381	5.06133	0.17328	0.32815	0.00449	1830	42	1830	29	1829	22	0.1
UC06-97	0.95	0.1121	0.00394	5.02967	0.17711	0.32536	0.00452	1834	44	1824	30	1816	22	1
UC06-98	0.56	0.05275	0.03178	0.33771	0.20308	0.04642	0.00188	318	1008	295	154	293	12	0.7
UC06-99	0.55	0.05137	0.0254	0.27289	0.13466	0.03852	0.00138	257	830	245	107	244	9	0.4
UC06-100	0.63	0.11193	0.00437	5.14369	0.20033	0.33325	0.0049	1831	49	1843	33	1854	24	-1.2
UC07														
UC07-01	1.03	0.05158	0.01626	0.305	0.09589	0.04287	0.00119	267	518	270	75	271	7	0.4
UC07-02	0.42	0.11031	0.00267	4.92265	0.12146	0.32358	0.00407	1805	27	1806	21	1807	20	-0.1
UC07-03	0.74	0.05144	0.0017	0.29277	0.0097	0.04127	0.00054	261	52	261	8	261	3	0.0
UC07-04	0.7	0.10753	0.00276	4.41026	0.1146	0.2974	0.00383	1758	29	1714	22	1678	19	4.8
UC07-05	0.63	0.05176	0.00491	0.31032	0.02932	0.04348	0.00068	275	185	274	23	274	4	0.0
UC07-06	0.16	0.18822	0.00457	13.77511	0.34093	0.53067	0.00671	2727	24	2734	23	2744	28	-0.6

UC07-07	0.69	0.07114	0.00205	1.59525	0.04624	0.1626	0.00213	961	38	968	18	971	12	-0.3
UC07-08	0.4	0.17082	0.00415	11.52404	0.28565	0.48918	0.00617	2566	25	2567	23	2567	27	0.0
UC07-09	0.46	0.05658	0.00249	0.58953	0.02593	0.07555	0.00103	475	73	471	17	470	6	0.2
UC07-10	0.44	0.20889	0.00594	15.47079	0.44176	0.53702	0.00764	2897	28	2845	27	2771	32	4.5
UC07-11	0.26	0.05628	0.00364	0.5906	0.03811	0.0761	0.00107	463	119	471	24	473	6	-0.4
UC07-12	0.44	0.11504	0.00298	5.41051	0.14207	0.34103	0.00439	1881	29	1887	23	1892	21	-0.6
UC07-13	0.33	0.05516	0.00176	0.51633	0.0166	0.06788	0.00088	419	49	423	11	423	5	0.0
UC07-14	0.52	0.06609	0.00184	1.21367	0.03425	0.13316	0.00172	809	38	807	16	806	10	0.1
UC07-15	1.01	0.05187	0.00388	0.31728	0.02359	0.04435	0.00069	280	141	280	18	280	4	0.0
UC07-16	0.56	0.05292	0.00243	0.37814	0.01739	0.05182	0.00071	325	79	326	13	326	4	0.0
UC07-17	1.41	0.11275	0.00322	5.17485	0.14907	0.33281	0.0044	1844	33	1848	25	1852	21	-0.4
UC07-18	0.39	0.05566	0.00168	0.53385	0.01625	0.06955	0.00091	439	44	434	11	433	5	0.2
UC07-19	0.6	0.0531	0.00859	0.40296	0.06499	0.05503	0.00109	333	315	344	47	345	7	-0.3
UC07-20	0.96	0.0554	0.00379	0.53587	0.0365	0.07014	0.00104	428	126	436	24	437	6	-0.2
UC07-21	0.97	0.10071	0.00609	3.82931	0.23017	0.27572	0.00454	1637	87	1599	48	1570	23	4.3
UC07-22	0.71	0.05185	0.00487	0.31277	0.0293	0.04374	0.00069	279	183	276	23	276	4	0.0
UC07-23	0.79	0.05571	0.0036	0.53818	0.03459	0.07005	0.00106	441	117	437	23	436	6	0.2
UC07-25	0.81	0.05199	0.00677	0.32166	0.04175	0.04487	0.00075	285	259	283	32	283	5	0.0

UC07-26	0.7	0.05509	0.00265	0.51615	0.0248	0.06794	0.00097	416	82	423	17	424	6	-0.2
UC07-27	0.12	0.18013	0.00484	12.28944	0.33543	0.49474	0.00642	2654	28	2627	26	2591	28	2.4
UC07-28	0.42	0.05486	0.0026	0.52013	0.02456	0.06875	0.00098	407	80	425	16	429	6	-0.9
UC07-29	1.61	0.11309	0.00318	4.89705	0.13939	0.31402	0.00412	1850	33	1802	24	1760	20	5.1
UC07-30	0.57	0.14768	0.00405	8.69097	0.24161	0.42677	0.00554	2319	30	2306	25	2291	25	1.2
UC07-31	0.8	0.05151	0.00255	0.28443	0.01401	0.04004	0.00059	264	86	254	11	253	4	0.4
UC07-32	0.93	0.0669	0.00233	1.27678	0.04461	0.13839	0.0019	835	50	835	20	836	11	-0.1
UC07-33	0.15	0.05492	0.00229	0.48909	0.02044	0.06458	0.00088	409	69	404	14	403	5	0.2
UC07-34	0.96	0.07034	0.0029	1.52393	0.0628	0.15712	0.00219	938	61	940	25	941	12	-0.1
UC07-35	1.03	0.05206	0.00542	0.32753	0.03393	0.04563	0.00079	288	202	288	26	288	5	0.0
UC07-36	0.93	0.16169	0.00463	10.46338	0.30378	0.46927	0.00616	2473	31	2477	27	2480	27	-0.3
UC07-37	0.3	0.0667	0.00346	1.25531	0.06498	0.13648	0.00195	828	84	826	29	825	11	0.1
UC07-38	0.62	0.11514	0.00395	5.18922	0.17815	0.32682	0.00465	1882	41	1851	29	1823	23	3.2
UC07-39	0.49	0.12745	0.00367	6.62241	0.19361	0.37681	0.0049	2063	33	2062	26	2061	23	0.1
UC07-40	0.63	0.05276	0.0039	0.35384	0.0261	0.04864	0.00074	318	141	308	20	306	5	0.7
UC07-41	0.6	0.10605	0.00522	4.70157	0.23017	0.32148	0.00508	1733	67	1768	41	1797	25	-3.6
UC07-42	0.81	0.14358	0.00429	8.36603	0.25318	0.42254	0.00558	2271	34	2272	27	2272	25	0.0
UC07-43	0.29	0.06974	0.00218	1.57	0.04958	0.16325	0.00216	921	43	958	20	975	12	-1.7

UC07-44	0.78	0.0525	0.00517	0.34705	0.03404	0.04793	0.00078	307	192	302	26	302	5	0.0
UC07-45	0.46	0.05605	0.00202	0.55852	0.02022	0.07227	0.00099	454	56	451	13	450	6	0.2
UC07-46	0.41	0.05661	0.00194	0.61312	0.02109	0.07854	0.00106	476	52	486	13	487	6	-0.2
UC07-47	0.54	0.05249	0.00721	0.33911	0.04643	0.04685	0.00088	307	272	296	35	295	5	0.3
UC07-48	1.19	0.05245	0.00247	0.35823	0.01689	0.04953	0.0007	305	82	311	13	312	4	-0.3
UC07-49	0.48	0.0521	0.00249	0.33533	0.01605	0.04667	0.00066	290	83	294	12	294	4	0.0
UC07-50	0.92	0.06966	0.00796	1.48586	0.16883	0.15469	0.00309	918	205	925	69	927	17	-0.2
UC07-51	0.35	0.05704	0.00207	0.62874	0.02298	0.07993	0.00109	493	56	495	14	496	7	-0.2
UC07-52	0.95	0.05299	0.00479	0.37492	0.03376	0.05131	0.00081	328	175	323	25	323	5	0.0
UC07-53	0.5	0.11292	0.00372	5.17072	0.17193	0.33205	0.00448	1847	41	1848	28	1848	22	-0.1
UC07-54	1.37	0.05218	0.00288	0.33972	0.01869	0.04721	0.00069	293	99	297	14	297	4	0.0
UC07-55	0.39	0.05619	0.00234	0.57603	0.02402	0.07434	0.00103	460	68	462	15	462	6	0.0
UC07-56	0.43	0.07081	0.00276	1.54744	0.06047	0.15848	0.00221	952	57	949	24	948	12	0.1
UC07-57	2.7	0.05606	0.00544	0.55812	0.05396	0.07219	0.00118	455	189	450	35	449	7	0.2
UC07-58	0.68	0.10633	0.00411	4.51098	0.175	0.30766	0.00437	1737	50	1733	32	1729	22	0.5
UC07-59	1.14	0.12257	0.00456	6.14975	0.22936	0.36383	0.00525	1994	46	1997	33	2000	25	-0.3
UC07-60	0.37	0.11863	0.00413	5.72589	0.20093	0.35001	0.00481	1936	43	1935	30	1935	23	0.1
UC07-61	0.83	0.09845	0.00525	3.79806	0.20196	0.27976	0.0043	1595	76	1592	43	1590	22	0.3

UC07-62	0.85	0.05045	0.01357	0.25242	0.06762	0.03629	0.00103	216	436	229	55	230	6	-0.4
UC07-63	1.12	0.06753	0.00415	1.29784	0.07948	0.13936	0.00215	854	102	845	35	841	12	0.5
UC07-64	1.19	0.05384	0.01088	0.43799	0.08808	0.05899	0.00155	364	363	369	62	369	9	0.0
UC07-65	0.74	0.05236	0.00454	0.35219	0.03044	0.04877	0.0008	301	166	306	23	307	5	-0.3
UC07-66	0.71	0.05224	0.00557	0.34237	0.03641	0.04753	0.00078	296	210	299	28	299	5	0.0
UC07-67	0.32	0.14835	0.00531	9.01656	0.32545	0.44073	0.00606	2327	43	2340	33	2354	27	-1.1
UC07-68	0.52	0.12305	0.00484	6.13842	0.24238	0.36175	0.00524	2001	49	1996	34	1990	25	0.6
UC07-69	0.58	0.05589	0.00332	0.55641	0.03295	0.07219	0.0011	448	105	449	21	449	7	0.0
UC07-70	0.79	0.07089	0.00312	1.55435	0.06836	0.15899	0.00233	954	66	952	27	951	13	0.1
UC07-71	0.48	0.05112	0.00392	0.27673	0.02122	0.03925	0.00059	246	147	248	17	248	4	0.0
UC07-72	0.34	0.05547	0.00261	0.53811	0.02536	0.07035	0.00101	431	79	437	17	438	6	-0.2
UC07-73	1.09	0.05593	0.00293	0.55852	0.02922	0.07241	0.00107	450	90	451	19	451	6	0.0
UC07-74	0.64	0.05238	0.00395	0.3358	0.02528	0.04649	0.0007	302	144	294	19	293	4	0.3
UC07-75	0.56	0.0554	0.00262	0.52376	0.02485	0.06855	0.00099	428	80	428	17	427	6	0.2
UC07-76	0.5	0.05644	0.00268	0.57657	0.02739	0.07408	0.00109	470	79	462	18	461	7	0.2
UC07-77	0.49	0.0559	0.0027	0.55078	0.02663	0.07145	0.00106	448	81	446	17	445	6	0.2
UC07-78	0.55	0.1204	0.0048	5.93682	0.23833	0.35754	0.00514	1962	51	1967	35	1971	24	-0.5
UC07-79	0.64	0.13963	0.00555	8.02631	0.32102	0.41683	0.00595	2223	49	2234	36	2246	27	-1

UC07-80	0.54	0.15775	0.00624	9.99023	0.39841	0.45921	0.0065	2432	48	2434	37	2436	29	-0.2
UC07-81	0.12	0.0705	0.003	1.52505	0.06526	0.15684	0.00227	943	64	941	26	939	13	0.2
UC07-82	0.83	0.05567	0.00332	0.54228	0.03234	0.07064	0.00106	439	106	440	21	440	6	0.0
UC07-83	0.43	0.11542	0.00482	5.36407	0.2251	0.33698	0.00489	1886	55	1879	36	1872	24	0.7
UC07-84	0.56	0.05222	0.00555	0.33997	0.03605	0.04721	0.00081	295	208	297	27	297	5	0.0
UC07-85	0.37	0.10359	0.00511	4.29909	0.21197	0.30093	0.00479	1689	67	1693	41	1696	24	-0.4
UC07-86	0.22	0.05521	0.00262	0.5166	0.02464	0.06784	0.00099	421	80	423	16	423	6	0.0
UC07-87	0.45	0.05631	0.00287	0.57868	0.02951	0.07451	0.00111	465	87	464	19	463	7	0.2
UC07-88	0.75	0.12293	0.00534	6.13256	0.2674	0.36171	0.00539	1999	56	1995	38	1990	26	0.5
UC07-89	0.57	0.05531	0.00867	0.51961	0.08108	0.06811	0.00144	425	310	425	54	425	9	0.0
UC07-90	0.39	0.0838	0.00427	2.43278	0.12383	0.21049	0.00351	1288	73	1252	37	1231	19	4.6
UC07-91	0.71	0.05216	0.01895	0.34808	0.12612	0.04839	0.00149	292	594	303	95	305	9	-0.7
UC07-92	0.35	0.07652	0.00344	1.97181	0.08917	0.18684	0.00275	1109	67	1106	30	1104	15	0.5
UC07-93	0.27	0.12534	0.00577	6.40354	0.29613	0.37042	0.00565	2034	60	2033	41	2031	27	0.1
UC07-94	1.05	0.0566	0.00275	0.5935	0.02898	0.07603	0.00113	476	82	473	18	472	7	0.2
UC07-95	1.11	0.05218	0.00294	0.3346	0.01885	0.04649	0.00072	293	101	293	14	293	4	0.0
UC07-96	1.25	0.1232	0.00547	6.19392	0.27719	0.36451	0.00531	2003	59	2004	39	2004	25	0.0
UC07-97	0.52	0.05696	0.00564	0.60499	0.05967	0.07701	0.00137	490	189	480	38	478	8	0.4

UC07-98	0.37	0.05628	0.00314	0.57697	0.03228	0.07433	0.00113	463	97	463	21	462	7	0.2
UC07-99	1.45	0.05676	0.01208	0.60486	0.12839	0.07727	0.00181	482	400	480	81	480	11	0.0
UC07-100	0.11	0.06883	0.00326	1.41139	0.06714	0.14867	0.00222	894	73	894	28	894	12	0.0
UC08														
UC08-01	0.4	0.05084	0.00237	0.25682	0.01202	0.03663	0.0005	234	83	232	10	232	3	0
UC08-02	0.53	0.07339	0.00489	1.73128	0.115	0.17107	0.00261	1025	110	1020	43	1018	14	0.7
UC08-03	0.61	0.07296	0.00301	1.71486	0.0709	0.17044	0.0024	1013	61	1014	27	1015	13	-0.2
UC08-04	0.25	0.17628	0.00519	12.3078	0.36752	0.50629	0.00683	2618	32	2628	28	2641	29	-0.9
UC08-05	0.83	0.05149	0.00408	0.29756	0.02354	0.0419	0.00063	263	152	264	18	265	4	-0.4
UC08-06	0.81	0.07362	0.00316	1.77861	0.07644	0.17519	0.00247	1031	64	1038	28	1041	14	-1
UC08-07	0.6	0.07435	0.00259	1.80397	0.06318	0.17594	0.00238	1051	49	1047	23	1045	13	0.6
UC08-08	0.48	0.06328	0.00331	1.02956	0.05379	0.11799	0.00171	718	86	719	27	719	10	0
UC08-09	0.18	0.06826	0.0053	1.31995	0.10207	0.14021	0.00227	876	134	854	45	846	13	0.9
UC08-10	0.19	0.06035	0.00269	0.83922	0.03742	0.10083	0.00139	616	72	619	21	619	8	0
UC08-11	0.86	0.06028	0.00203	0.81813	0.02779	0.09841	0.00131	614	50	607	16	605	8	0.3
UC08-12	0.78	0.06448	0.00418	1.12033	0.07245	0.12599	0.00191	757	111	763	35	765	11	-0.3
UC08-13	0.53	0.06682	0.00371	1.26177	0.07001	0.13692	0.00196	832	92	829	31	827	11	0.2
UC08-14	1.32	0.12351	0.0042	6.21777	0.21243	0.36504	0.00509	2008	41	2007	30	2006	24	0.1

UC08-15	0.34	0.05573	0.00402	0.55394	0.03994	0.07207	0.00105	442	136	448	26	449	6	-0.2
UC08-16	0.61	0.06361	0.00279	1.04792	0.04609	0.11945	0.00164	729	70	728	23	727	9	0.1
UC08-17	0.64	0.11417	0.00371	5.26345	0.17222	0.33429	0.00456	1867	39	1863	28	1859	22	0.4
UC08-18	0.86	0.07389	0.00344	1.77546	0.0826	0.17422	0.00248	1038	71	1037	30	1035	14	0.3
UC08-19	0.5	0.05887	0.00235	0.74831	0.02995	0.09217	0.00125	562	63	567	17	568	7	-0.2
UC08-20	1.11	0.06035	0.00315	0.83894	0.04381	0.1008	0.00143	616	88	619	24	619	8	0
UC08-21	0.19	0.06293	0.0022	1.00157	0.03515	0.11541	0.00154	706	52	705	18	704	9	0.1
UC08-22	0.93	0.07603	0.00422	1.91675	0.10578	0.1828	0.00282	1096	86	1087	37	1082	15	1.3
UC08-23	0.52	0.07583	0.00293	1.87995	0.07267	0.17976	0.00249	1091	55	1074	26	1066	14	2.3
UC08-24	1.06	0.05586	0.00512	0.55814	0.05106	0.07245	0.00114	447	178	450	33	451	7	-0.2
UC08-25	0.23	0.06112	0.00216	0.884	0.03143	0.10488	0.00141	643	53	643	17	643	8	0
UC08-26	0.52	0.06836	0.00426	1.39825	0.0869	0.14832	0.00222	879	104	888	37	892	12	-0.4
UC08-27	0.09	0.1275	0.00438	6.54412	0.22647	0.37215	0.00533	2064	41	2052	30	2040	25	1.2
UC08-28	0.7	0.07314	0.00268	1.72901	0.06355	0.17142	0.00232	1018	52	1019	24	1020	13	-0.2
UC08-29	0.23	0.06494	0.0027	1.14717	0.04758	0.12808	0.00182	772	63	776	23	777	10	-0.1
UC08-30	1.1	0.0748	0.0052	1.7954	0.12456	0.17403	0.00262	1063	116	1044	45	1034	14	2.8
UC08-31	0.19	0.06298	0.00314	1.0394	0.05173	0.11966	0.00168	708	82	724	26	729	10	-0.7
UC08-32	0.36	0.06532	0.00324	1.09702	0.05432	0.12178	0.00174	785	80	752	26	741	10	1.5

UC08-33	1.11	0.06055	0.01127	0.82315	0.15279	0.09857	0.0019	623	379	610	85	606	11	0.7
UC08-34	0.34	0.05992	0.00352	0.81276	0.04753	0.09835	0.00146	601	101	604	27	605	9	-0.2
UC08-35	0.11	0.06209	0.00248	0.92609	0.03706	0.10814	0.00148	677	62	666	20	662	9	0.6
UC08-36	1.41	0.06772	0.00558	1.3268	0.10867	0.14205	0.00245	860	143	857	47	856	14	0.1
UC08-37	0.44	0.07433	0.00298	1.84471	0.07389	0.17994	0.00248	1050	58	1062	26	1067	14	-1.6
UC08-38	0.9	0.05576	0.00546	0.55047	0.05376	0.07159	0.00112	443	192	445	35	446	7	-0.2
UC08-39	0.63	0.05328	0.00339	0.40986	0.02585	0.05577	0.00091	341	114	349	19	350	6	-0.3
UC08-40	0.42	0.06546	0.00277	1.16656	0.04929	0.12921	0.0018	789	65	785	23	783	10	0.3
UC08-41	0.2	0.06536	0.00248	1.13122	0.04283	0.12549	0.00171	786	56	768	20	762	10	0.8
UC08-42	0.92	0.11967	0.00477	5.89637	0.23468	0.35725	0.00516	1951	50	1961	35	1969	25	-0.9
UC08-43	1.06	0.10975	0.00474	4.86209	0.20878	0.32123	0.00486	1795	56	1796	36	1796	24	-0.1
UC08-44	0.41	0.072	0.00295	1.64982	0.06751	0.16614	0.00232	986	60	989	26	991	13	-0.2
UC08-45	0.75	0.06753	0.00268	1.28619	0.05098	0.1381	0.00191	854	59	840	23	834	11	0.7
UC08-46	0.69	0.17755	0.00661	12.45131	0.46316	0.50847	0.00704	2630	43	2639	35	2650	30	-0.8
UC08-47	2.78	0.06036	0.00654	0.86848	0.09363	0.10433	0.00189	617	206	635	51	640	11	-0.8
UC08-48	0.38	0.05986	0.0034	0.80084	0.04537	0.097	0.0014	599	98	597	26	597	8	0
UC08-49	0.72	0.07397	0.00299	1.77583	0.07151	0.17408	0.0024	1041	59	1037	26	1035	13	0.6
UC08-50	1.69	0.0757	0.00757	1.86566	0.18535	0.17869	0.0033	1087	172	1069	66	1060	18	2.5

UC08-51	1.09	0.0603	0.00411	0.83125	0.05631	0.09995	0.00154	614	120	614	31	614	9	0
UC08-52	0.15	0.077	0.00357	1.83396	0.08446	0.1727	0.0026	1121	68	1058	30	1027	14	9.2
UC08-53	1.43	0.05922	0.00462	0.75314	0.05834	0.09222	0.00153	575	141	570	34	569	9	0.2
UC08-54	0.73	0.06293	0.00342	0.99796	0.05391	0.11498	0.00171	706	90	703	27	702	10	0.1
UC08-55	0.74	0.0517	0.02408	0.3207	0.14898	0.04497	0.00165	272	770	282	115	284	10	-0.7
UC08-56	0.07	0.05528	0.00292	0.51481	0.02706	0.06752	0.00098	424	91	422	18	421	6	0.2
UC08-57	0.01	0.06576	0.00299	1.18616	0.05352	0.13078	0.00187	799	70	794	25	792	11	0.3
UC08-58	1.15	0.18346	0.00777	13.07211	0.5497	0.51665	0.00751	2684	50	2685	40	2685	32	0
UC08-59	0.64	0.06168	0.00614	0.91842	0.09085	0.10797	0.00185	663	186	662	48	661	11	0.2
UC08-60	0.95	0.06973	0.00516	1.448	0.10637	0.15057	0.00251	920	124	909	44	904	14	0.6
UC08-61	0.33	0.14358	0.00621	8.48119	0.36366	0.4283	0.00617	2271	54	2284	39	2298	28	-1.2
UC08-62	0.53	0.17536	0.00754	11.81932	0.50425	0.48873	0.00703	2609	52	2590	40	2565	30	1.7
UC08-63	0.07	0.0663	0.0034	1.21823	0.06196	0.13324	0.002	816	81	809	28	806	11	0.4
UC08-64	0.82	0.07098	0.00379	1.565	0.08289	0.15987	0.00237	957	84	956	33	956	13	0
UC08-65	0.51	0.07987	0.00394	2.13837	0.10452	0.19413	0.00285	1194	73	1161	34	1144	15	4.4
UC08-66	0.56	0.06265	0.00373	0.98416	0.05808	0.11391	0.00173	696	100	696	30	695	10	0.1
UC08-67	0.54	0.05723	0.00292	0.63685	0.03221	0.08069	0.00116	500	86	500	20	500	7	0
UC08-68	0.39	0.06181	0.00343	0.91655	0.05029	0.10752	0.00164	668	91	661	27	658	10	0.5

UC08-69	0.43	0.06106	0.00828	0.89772	0.12116	0.10661	0.002	641	266	651	65	653	12	-0.3
UC08-70	0.39	0.07576	0.00384	1.93923	0.09741	0.1856	0.00273	1089	77	1095	34	1097	15	-0.7
UC08-71	0.17	0.06055	0.00304	0.85802	0.04259	0.10275	0.0015	623	82	629	23	631	9	-0.3
UC08-72	0.32	0.06146	0.00328	0.90699	0.04782	0.10701	0.0016	655	87	655	25	655	9	0
UC08-73	0.7	0.07189	0.00686	1.63898	0.15534	0.16533	0.00286	983	167	985	60	986	16	-0.1
UC08-74	0.4	0.0554	0.00815	0.51741	0.07579	0.06772	0.00124	428	298	423	51	422	7	0.2
UC08-75	0.68	0.05638	0.00323	0.58122	0.03297	0.07476	0.00112	467	99	465	21	465	7	0
UC08-76	0.45	0.06425	0.00378	1.07782	0.06257	0.12165	0.00191	750	96	743	31	740	11	0.4
UC08-77	0.33	0.13037	0.00628	6.95086	0.3303	0.38662	0.00563	2103	63	2105	42	2107	26	-0.2
UC08-78	0.41	0.1262	0.00631	6.45497	0.31803	0.3709	0.00562	2046	66	2040	43	2034	26	0.6
UC08-79	0.98	0.07536	0.004	1.88852	0.09893	0.18172	0.00277	1078	81	1077	35	1076	15	0.2
UC08-80	0.65	0.10758	0.00572	4.49337	0.2354	0.30287	0.00488	1759	72	1730	44	1706	24	3.1
UC08-81	0.78	0.0612	0.00364	0.87815	0.05154	0.10406	0.00163	646	99	640	28	638	10	0.3
UC08-82	0.52	0.07511	0.00446	1.80445	0.10563	0.17421	0.0028	1071	92	1047	38	1035	15	3.5
UC08-83	1.61	0.07428	0.00488	1.73826	0.1126	0.16971	0.00279	1049	104	1023	42	1011	15	3.8
UC08-84	0.54	0.06461	0.00415	1.11916	0.07083	0.1256	0.00202	762	107	763	34	763	12	0
UC08-85	0.57	0.07147	0.00518	1.48363	0.10619	0.15053	0.00264	971	118	924	43	904	15	2.2
UC08-86	0.72	0.05939	0.0035	0.77323	0.04499	0.09441	0.00145	581	100	582	26	582	9	0

UC08-87	1.04	0.06071	0.00406	0.85278	0.05633	0.10187	0.00164	629	115	626	31	625	10	0.2
UC08-88	0.18	0.06028	0.08233	0.83815	1.1424	0.10083	0.00885	614	1648	618	631	619	52	-0.2
UC08-89	0.97	0.06758	0.00455	1.32997	0.08839	0.14272	0.00236	856	111	859	39	860	13	-0.1
UC08-90	1.43	0.05574	0.011	0.55393	0.10887	0.07207	0.00152	442	373	448	71	449	9	-0.2
UC08-91	1.12	0.06058	0.005	0.86149	0.07032	0.10313	0.00173	624	149	631	38	633	10	-0.3
UC08-92	1.06	0.05226	0.01523	0.33094	0.09606	0.04593	0.00136	297	483	290	73	289	8	0.3
UC08-93	0.3	0.10217	0.00571	4.13234	0.22666	0.29332	0.00454	1664	79	1661	45	1658	23	0.4
UC08-94	0.16	0.06449	0.00423	1.11643	0.072	0.12555	0.00208	758	108	761	35	762	12	-0.1
UC08-95	0.89	0.06488	0.00462	1.14373	0.08035	0.12785	0.00206	770	122	774	38	776	12	-0.3
UC08-96	0.17	0.06141	0.00405	0.91963	0.05962	0.10861	0.00172	654	112	662	32	665	10	-0.5
UC08-97	1.89	0.0602	0.0046	0.82342	0.06199	0.0992	0.00165	611	135	610	35	610	10	0
UC08-98	0.78	0.12883	0.00741	6.33357	0.35669	0.35653	0.00564	2082	77	2023	49	1966	27	5.9
UC08-99	0.76	0.13168	0.00775	7.01645	0.40427	0.38643	0.00627	2120	78	2114	51	2106	29	0.7
UC08-100	0.79	0.05531	0.01135	0.52557	0.10742	0.06892	0.00154	425	385	429	71	430	9	-0.2

APPENDIX 3

Mine Section

Sample	Level (m)	Declinaion IS (˚)	Inclination IS (˚)	Declinaion TC (˚)	Inclination TC (˚)	MAD (˚)	VGP latitude (˚)
ZB001	-69.00	24.7	-35.9	24.8	33.9	5.9	60.1
ZB002	-68.50	16.6	-21.7	11.8	46.3	4.2	74.6
ZB003	**-66.00**	**57.7**	**61.0**	**191.5**	**44.6**	**22.0**	**-23.4**
ZB004	**-65.00**	**11.0**	**42.8**	**240.8**	**62.2**	**7.9**	**9.5**
ZB005	**-58.00**	**293.1**	**-29.7**	**326.5**	**-15.5**	**25.1**	**33.4**
ZB006	**-51.50**	**306.1**	**80.2**	**220.4**	**20.7**	**6.7**	**-27.3**
ZB007	**-47.50**	**206.9**	**-33.5**	**40.9**	**-76.2**	**16.5**	**-18.3**
ZB008	**-43.50**	**121.6**	**68.4**	**187.2**	**18.0**	**36.5**	**-40.8**
ZB009	**-38.50**	**233.7**	**23.1**	**239.4**	**-41.1**	**16.4**	**-37.9**
ZB010	**-36.50**	**274.2**	**45.1**	**249.5**	**-2.7**	**16.3**	**-16.6**
ZB011	**-30.75**	**127.1**	**-7.9**	**114.9**	**-9.3**	**28.5**	**-22.1**
ZB012	**-27.25**	**264.0**	**50.4**	**241.2**	**-5.1**	**14.6**	**-23.6**
ZB013	**-23.50**	**236.8**	**-5.2**	**274.0**	**-60.0**	**23.7**	**-22.1**
ZB014	**-18.00**	**287.3**	**46.8**	**252.2**	**6.2**	**30.6**	**-11.6**
ZB015	**-14.50**	**237.8**	**44.9**	**230.6**	**-20.3**	**22.9**	**-36.7**
ZB016	**-11.00**	**88.7**	**0.4**	**108.7**	**29.4**	**7.2**	**-3.8**
ZB017	-8.00	212.5	56.1	211.4	-13.9	10.0	-47.0
ZB018	**-4.50**	**81.1**	**-65.5**	**48.9**	**-3.8**	**25.9**	**29.1**
ZB019	**-0.50**	**253.5**	**31.5**	**249.9**	**-23.7**	**25.4**	**-23.3**
ZB020	2.50	354.8	-1.0	327.2	49.6	26.8	61.8
ZB021	6.00	2.9	-32.3	3.1	31.6	3.4	67.4
ZB022	9.75	338.9	-13.1	329.1	29.8	12.3	54.3
ZB023	13.75	357.7	-7.3	337.5	48.1	9.1	68.8
ZB024	**16.25**	**310.3**	**38.1**	**265.5**	**20.1**	**40.2**	**3.1**
ZB025	19.25	165.6	62.6	191.2	-0.3	4.1	-49.3

ZB026	21.75	13.9	3.6	4.4	57.0	5.9	86.1
ZB027	25.25	9.9	10.0	352.5	61.5	3.6	83.5
ZB028	28.25	17.1	-9.8	14.0	44.6	18.8	72.3
ZB029	**28.75**	**9.6**	**39.7**	**269.4**	**76.9**	**17.3**	**35.0**
ZB030	35.75	351.5	-16.5	351.8	13.7	3.3	56.6
ZB031	**37.75**	**59.7**	**60.3**	**132.8**	**67.5**	**5.8**	**8.9**
ZB032	40.75	339.5	15.4	327.4	40.2	10.5	57.8
ZB033	43.25	348.7	36.5	322.7	62.6	5.0	62.1
ZB034	46.25	209.8	23.9	208.7	-8.3	4.0	-46.2
ZB035	49.85	183.9	-8.6	180.1	-40.7	3.4	-73.8
ZB036	52.65	183.1	31.6	185.0	-0.7	4.6	-50.6
ZB037	57.65	24.1	34.3	33.1	66.6	6.5	64.7
ZB038	62.25	356.3	-22.1	357.6	9.2	6.5	55.1
ZB039	66.05	341.0	36.6	312.2	59.1	4.5	53.7
ZB040	69.75	29.3	-21.7	30.5	28.0	4.7	53.7
ZB041	73.55	2.6	-27.0	2.7	25.8	4.9	64.0
ZB042	**76.35**	**243.9**	**38.3**	**228.5**	**1.2**	**17.7**	**-30.3**
ZB043	**81.35**	**21.7**	**23.5**	**52.9**	**72.1**	**9.2**	**51.9**
ZB044	85.35	352.6	-24.6	352.3	26.7	7.0	63.7
ZB045	88.15	343.3	3.2	328.2	49.3	5.1	62.5
ZB046	90.65	28.1	-21.5	29.3	28.5	6.3	54.7
ZB047	**93.65**	**55.5**	**18.2**	**86.9**	**44.5**	**22.3**	**18.5**
ZB048	99.90	183.0	39.1	184.0	-13.8	6.2	-57.3
ZB048A	**99.90**	**199.4**	**50.4**	**195.2**	**-2.0**	**8.2**	**-49.1**
ZB049	104.80	82.8	-6.4	83.6	8.1	22.2	7.5
ZB049B	104.80	346.8	38.1	267.8	73.2	24.8	32.0
ZB049A	**104.80**	**349.3**	**21.7**	**316.2**	**67.7**	**36.0**	**57.7**
ZB050	108.00	157.0	59.7	172.7	10.0	11.8	-45.0
ZB051	**110.50**	**269.3**	**3.7**	**269.8**	**-4.7**	**10.3**	**-1.7**
ZB052	**116.00**	**267.8**	**60.8**	**220.7**	**27.2**	**40.0**	**-24.1**
ZB053	118.80	16.7	14.5	29.3	66.2	6.1	67.2

ZB054	120.80	164.6	31.8	167.2	-17.8	7.9	-57.5
ZB055A	**123.80**	**338.4**	**63.8**	**212.2**	**57.8**	**19.8**	**-6.7**
ZB055	**123.80**	**18.7**	**21.3**	**41.6**	**71.8**	**15.2**	**58.0**
ZB056	**126.90**	**109.7**	**30.2**	**128.9**	**9.4**	**26.0**	**-25.5**
ZB057	**129.40**	**307.6**	**-6.2**	**301.8**	**19.1**	**25.4**	**30.6**
ZB058	132.90	165.9	55.5	175.7	4.4	20.2	-48.1
ZB058A	132.90	148.6	19.7	147.8	-22.2	12.2	-50.1
ZB059	**142.90**	**28.6**	**58.9**	**163.2**	**64.4**	**36.4**	**-3.0**
ZB060	**146.90**	**14.3**	**36.5**	**94.2**	**84.9**	**37.4**	**38.0**
ZB061	**149.90**	**339.2**	**67.2**	**207.3**	**55.7**	**21.3**	**-10.2**
ZB062	**154.90**	**287.4**	**-29.7**	**307.3**	**-10.7**	**27.7**	**23.9**
ZB063	160.90	130.8	23.8	136.9	-8.8	14.9	-37.6
ZB064	**164.40**	**308.2**	**-24.8**	**315.9**	**6.4**	**4.2**	**36.1**
ZB065	**166.40**	**47.2**	**7.5**	**68.3**	**43.8**	**25.7**	**32.2**
ZB066	169.90	240.8	63.8	209.8	19.1	17.5	-33.5
ZB067	172.90	185.9	26.7	185.9	-26.3	9.8	-63.9
ZB068	**176.65**	**346.6**	**29.6**	**294.3**	**70.7**	**6.6**	**44.7**
ZB069	180.15	20.6	-41.6	17.6	10.6	4.4	52.3
ZB070	183.15	26.9	31.2	83.2	73.3	4.6	36.3
ZB071	184.65	348.1	-14.9	344.4	34.8	5.5	65.6
ZB072	188.65	340.3	-37.2	345.8	11.5	6.0	54.0
ZB073	192.65	343.4	-40.8	349.4	9.0	2.8	53.7
ZB074	196.65	353.0	15.3	332.5	64.5	3.5	68.9
ZB075	**200.65**	**165.6**	**-30.6**	**110.4**	**-70.4**	**5.1**	**-42.4**
ZB076	**203.55**	**304.2**	**-6.1**	**299.4**	**16.7**	**16.5**	**28.0**
ZB077	**208.35**	**342.7**	**-46.4**	**350.8**	**3.6**	**21.1**	**51.4**
ZB078	211.85	19.7	4.5	29.1	55.8	29.2	66.9
ZB079	216.05	0.6	10.6	351.9	62.8	4.7	82.4
ZB080	**219.15**	**271.8**	**-57.3**	**327.9**	**-33.6**	**16.0**	**24.8**
ZB081	**221.25**	**327.3**	**-43.3**	**339.7**	**1.6**	**13.5**	**47.1**
ZB082	**232.05**	**306.8**	**4.4**	**292.6**	**25.5**	**9.2**	**25.8**

ZB083	233.75	335.6	-34.1	340.9	12.8	3.4	52.8
ZB084	236.75	14.9	-3.0	18.6	49.5	5.4	72.3
ZB085	**239.15**	**307.4**	**30.3**	**266.9**	**40.0**	**11.9**	**12.0**
ZB85.5	242.25	331.5	-17.1	328.8	25.9	2.3	52.3
ZB086	245.85	4.9	11.2	1.0	64.0	7.7	83.7
ZB86.5	247.05	358.1	-9.5	354.7	42.6	9.8	74.5
ZB087	247.95	1.5	-21.2	0.9	31.5	4.5	67.5
ZB088	251.55	8.5	-14.6	8.6	38.4	9.8	70.7
ZB88.5	**252.25**	**54.9**	**23.2**	**92.6**	**47.6**	**3.2**	**15.9**
ZB089	253.25	333.1	-13.3	328.0	29.9	6.3	53.6
ZB090	255.75	355.1	-25.6	355.0	26.2	8.2	63.9
ZB091	259.55	0.6	4.4	354.5	56.7	12.4	85.2
ZB092	**262.25**	**347.4**	**26.6**	**302.9**	**69.7**	**5.7**	**49.5**
ZB093	264.55	353.1	18.3	329.0	67.2	7.4	65.9
ZB094	**267.45**	**70.7**	**-2.9**	**78.4**	**19.6**	**24.6**	**15.3**
ZB095	**270.45**	**326.1**	**11.1**	**301.6**	**44.4**	**8.7**	**40.0**
ZB096	272.95	2.9	-8.1	0.9	44.6	8.5	76.7
ZB097	275.15	3.2	3.5	359.4	56.2	2.2	87.2
ZB098	**277.55**	**232.8**	**-19.6**	**266.6**	**-47.4**	**8.1**	**-20.1**
ZB099	**279.25**	**297.6**	**53.0**	**235.7**	**39.9**	**27.9**	**-9.0**
ZB100	282.05	167.7	15.8	164.3	-33.8	7.7	-65.0
ZB101	283.35	163.0	3.4	152.5	-43.4	6.1	-63.0
ZB102	285.95	143.1	27.1	147.8	-13.3	9.9	-46.3
ZB103	289.55	183.7	-15.8	176.7	-68.5	2.4	-77.5
ZB104	292.35	169.5	36.2	172.6	-14.8	2.4	-57.3
ZB105	**296.15**	**184.3**	**-36.2**	**112.0**	**-86.9**	**18.6**	**-41.6**
ZB106	298.75	176.4	18.2	174.7	-33.7	6.9	-68.4
ZB107	301.35	191.5	30.0	191.3	-22.9	4.2	-60.7
ZB108	303.35	195.8	24.6	196.0	-28.0	4.6	-61.7
ZB109	310.15	177.2	8.1	173.1	-43.8	3.4	-75.0
ZB110	**316.85**	**73.6**	**-12.3**	**73.1**	**11.2**	**9.7**	**16.6**

ZB111	321.75	8.6	-22.4	8.6	30.6	21.3	65.8
ZB112	325.35	358.9	-21.3	358.1	31.1	4.4	67.2
ZB113	328.85	345.3	1.3	332.3	48.6	11.3	65.2
ZB114	331.25	350.1	19.5	321.3	66.5	16.3	61.1
ZB115	336.25	13.5	-17.5	14.4	35.3	7.4	66.5
ZB116	339.35	9.1	-22.5	9.2	30.5	25.9	65.6
ZB117	343.25	21.5	-27.7	21.1	24.1	9.1	57.3
ZB118	**345.25**	**27.9**	**11.0**	**47.7**	**58.4**	**7.3**	**53.5**
ZB119	348.35	1.1	-3.0	344.5	43.8	5.1	71.0
ZB120	**350.25**	**334.6**	**39.7**	**276.5**	**40.4**	**17.6**	**19.2**
ZB121	355.45	11.0	-2.6	355.7	50.1	19.4	80.7
ZB122	**357.75**	**213.8**	**60.7**	**214.4**	**0.7**	**27.0**	**-39.3**
ZB123	360.65	30.7	-26.3	30.4	33.5	20.8	56.3
ZB124	**362.65**	**40.7**	**-4.8**	**44.9**	**54.8**	**5.5**	**54.5**
ZB125	365.75	23.3	-6.5	16.0	51.8	24.9	75.3
ZB126.5	367.05	18.1	-17.9	14.0	39.4	4.6	69.1
ZB126	367.95	7.0	-3.7	351.7	47.0	11.4	76.8
ZB127	371.45	2.8	-51.4	15.5	3.8	24.9	49.8
ZB128	373.65	7.1	11.8	334.1	58.4	26.5	70.0
ZB130	**379.05**	**353.6**	**27.7**	**298.1**	**53.9**	**7.4**	**41.3**
ZB131	383.65	116.1	48.3	167.2	27.5	4.5	-34.6
ZB131.5	384.05	16.6	-22.3	14.2	34.8	1.8	66.3
ZB132.5	386.65	205.9	9.8	201.2	-49.2	5.2	-70.3
ZB132	**387.85**	**42.3**	**-7.3**	**46.8**	**52.0**	**7.4**	**52.0**
ZB133	**394.95**	**348.4**	**30.3**	**292.4**	**50.0**	**5.9**	**35.3**
ZB134	397.35	344.4	-8.3	334.9	28.1	16.2	57.1
ZB135	400.65	16.3	-1.5	2.1	53.8	13.0	84.6
ZB136	**402.65**	**49.7**	**24.0**	**103.9**	**75.6**	**6.7**	**28.8**
ZB137	405.85	3.3	25.8	305.7	61.8	18.0	49.7
ZB138	408.95	16.2	-14.4	10.1	42.0	9.7	72.5
ZB139	411.35	343.7	-22.4	345.6	18.1	25.2	57.2

ZB140	413.45	4.9	-21.7	2.2	30.7	6.9	67.0
ZB141	415.45	15.1	-6.4	4.0	48.9	4.1	79.8
ZB142	419.95	20.0	-7.1	11.3	50.2	4.8	77.5
ZB143	423.15	334.3	10.1	310.9	30.3	12.7	41.6
ZB144	**426.45**	**313.0**	**18.9**	**292.1**	**16.0**	**22.8**	**22.2**
ZB145	429.15	349.5	-15.6	344.7	26.8	4.9	61.3
ZB146	431.55	345.8	-2.2	330.4	33.1	12.3	56.6
ZB146.5	431.75	355.1	-18.1	351.1	28.4	1.8	64.4
ZB147	434.55	346.1	-22.4	347.3	19.6	2.4	58.5
ZB148	439.15	34.8	-7.9	34.7	52.1	3.4	61.3
ZB148.5	439.55	24.8	-31.4	25.2	27.8	4.4	56.9
ZB149	441.95	12.1	-31.7	13.6	24.6	5.8	60.8
ZB150.5	**444.55**	**356.1**	**28.7**	**297.3**	**56.2**	**5.2**	**41.6**
ZB150	**444.85**	**357.8**	**32.2**	**291.3**	**58.2**	**4.7**	**38.1**
ZB151	447.65	201.0	36.8	202.9	-21.9	8.3	-55.3
ZB152	450.25	177.0	62.6	198.4	7.5	5.0	-43.5
ZB153	458.45	215.7	7.0	216.2	-53.0	5.5	-60.5
ZB154	462.45	224.3	38.0	222.9	-21.4	14.8	-42.6
ZB155	463.75	212.6	28.4	212.5	-31.6	2.2	-54.0
ZB156	**468.65**	**217.7**	**-26.5**	**249.8**	**-85.8**	**18.3**	**-41.9**
ZB157	471.95	201.2	0.8	189.4	-56.5	3.6	-82.2
ZB158	474.75	187.9	-11.0	156.3	-58.5	4.4	-71.7
ZB159	477.85	190.2	23.1	188.0	-31.8	4.1	-66.7
ZB160	481.55	193.6	37.5	197.1	-19.6	13.1	-56.9
ZB161	485.55	196.6	28.6	196.6	-28.8	3.2	-61.8
ZB162	487.15	185.8	8.3	174.1	-42.5	7.2	-74.3
ZB163	490.95	183.4	12.3	174.6	-37.9	4.7	-71.2
ZB164	493.05	182.7	2.9	166.1	-44.9	2.4	-72.6
ZB165	**495.45**	**218.1**	**-11.7**	**224.6**	**-71.5**	**5.8**	**-56.5**
ZB166	497.45	170.2	14.3	164.2	-28.2	4.4	-61.9
ZB167	501.15	176.5	14.6	169.7	-32.0	4.7	-66.1

ZB168	502.95	183.5	9.2	172.3	-40.5	3.0	-72.4
ZB587	**503.95**	**277.2**	**75.3**	**229.1**	**22.4**	**19.6**	**-21.5**
ZB169	506.85	203.2	18.5	201.5	-26.7	2.4	-58.4
ZB170	508.85	347.0	-4.2	341.1	18.2	3.5	55.4
ZB171	511.55	343.4	-18.0	348.5	5.9	29.9	52.0
ZB596	512.05	2.0	-19.6	3.2	16.1	11.8	58.6
ZB596A	**512.05**	**47.3**	**7.5**	**45.9**	**57.5**	**2.8**	**54.6**
ZB172	**514.15**	**61.0**	**2.9**	**68.4**	**51.3**	**24.9**	**35.3**
ZB173	517.75	155.1	-1.7	148.2	-13.4	4.2	-46.6
ZB603	519.35	174.0	-4.0	160.0	-28.9	3.9	-60.2
ZB174	522.85	174.5	-28.0	136.6	-44.0	5.5	-51.4
ZB175	526.25	181.8	-35.1	131.1	-52.7	12.8	-50.6
ZB176	**531.25**	**230.2**	**-33.6**	**237.9**	**-83.5**	**11.5**	**-45.3**
ZB177	**534.65**	**298.2**	**25.8**	**286.4**	**2.0**	**14.8**	**13.2**
ZB619	534.85	180.7	12.4	177.6	-21.1	7.6	-61.3
ZB619A	**534.85**	**195.6**	**-47.4**	**110.7**	**-65.0**	**3.7**	**-40.6**
ZB178	**537.65**	**7.2**	**62.5**	**262.9**	**56.5**	**8.4**	**17.9**
ZB179	539.65	26.3	2.3	14.5	47.0	7.7	73.5
ZB180	541.15	188.3	47.7	202.9	4.9	13.2	-43.1
ZB181	549.25	179.7	-17.7	152.0	-42.2	8.7	-62.0
ZB636A	**552.95**	**215.8**	**-34.0**	**164.5**	**-77.9**	**9.6**	**-61.4**
ZB636	**552.95**	**146.7**	**-16.1**	**131.2**	**-16.1**	**5.0**	**-36.4**
ZB182	555.25	151.3	-9.9	139.2	-15.7	20.3	-41.8
ZB183	558.35	173.8	7.5	168.7	-20.5	12.0	-59.4
ZB184	**561.15**	**27.8**	**-58.5**	**37.9**	**-10.1**	**22.1**	**33.4**
ZB185	568.25	357.5	0.4	345.8	28.8	3.6	62.9
ZB186	572.25	351.2	-3.6	343.8	21.5	14.0	58.2
ZB187	**574.45**	**66.1**	**11.0**	**81.3**	**57.3**	**25.2**	**28.9**
ZB188	576.45	18.0	3.7	3.2	44.2	8.7	76.2
ZB189	**579.15**	**130.2**	**-26.2**	**113.3**	**-10.3**	**14.5**	**-21.2**
ZB190	581.65	37.9	34.5	347.4	79.6	26.8	58.9

ZB191	583.65	14.1	-33.6	20.1	9.6	11.9	50.9
ZB219	**586.65**	**48.9**	**26.7**	**48.6**	**76.7**	**3.6**	**52.5**
ZB192	**586.65**	**39.6**	**67.3**	**236.8**	**62.2**	**15.8**	**7.5**
ZB220	591.35	168.0	68.9	195.5	28.5	5.8	-33.4
ZB221	595.85	347.0	21.9	319.0	46.7	4.8	54.3
ZB222	598.65	5.4	-26.9	7.7	14.1	2.3	56.9
ZB223	602.95	356.7	-1.9	348.1	33.6	4.0	66.5
ZB224	605.45	5.6	0.8	356.5	40.0	4.6	73.0
ZB225	608.55	3.5	8.2	349.4	45.7	6.3	74.8
ZB226	**611.25**	**27.6**	**38.6**	**3.4**	**82.8**	**7.4**	**53.6**
ZB227	615.35	1.9	4.1	350.2	41.4	6.4	72.2
ZB228	619.25	30.6	-29.8	30.7	15.2	9.1	48.0
ZB229	622.25	344.2	-26.2	350.0	6.5	4.9	52.6
ZB230	626.45	338.3	-7.8	334.6	18.6	11.9	52.5
ZB231	**628.35**	**170.0**	**-46.6**	**103.6**	**-61.0**	**28.8**	**-34.1**
ZB232	**630.35**	**277.9**	**70.0**	**234.2**	**34.5**	**18.0**	**-12.7**
ZB233	633.75	184.8	6.7	179.3	-32.8	9.9	-68.4
ZB234	636.95	176.0	12.3	173.0	-24.1	4.2	-62.4
ZB235	640.15	176.2	13.1	173.6	-23.5	5.8	-62.2
ZB236	643.55	205.9	-3.0	202.9	-47.7	6.8	-68.3
ZB237	645.45	162.9	-12.4	144.1	-37.2	29.4	-54.1
ZB238	649.95	183.4	1.7	175.3	-36.8	10.5	-70.6
ZB239	653.15	166.2	-1.8	155.3	-31.0	7.5	-58.7
ZB240	656.45	204.6	22.9	204.7	-21.8	11.2	-54.3
ZB241	659.45	174.4	24.6	177.4	-12.4	5.7	-56.7
ZB242	663.35	189.0	-13.4	173.0	-52.8	8.3	-81.7
ZB243	**666.65**	**46.3**	**49.6**	**152.5**	**79.3**	**7.4**	**20.7**
ZB244	669.65	181.9	4.4	175.0	-33.8	19.1	-68.6
ZB245	673.45	197.9	47.6	202.5	3.4	11.8	-43.9
ZB246	677.45	212.8	5.0	213.0	-40.0	5.7	-57.4
ZB247	**682.25**	**205.9**	**-31.9**	**190.0**	**-76.1**	**4.3**	**-65.1**

ZB248	685.25	191.0	13.1	188.5	-28.9	3.1	-64.8
ZB249	688.05	185.3	18.3	184.6	-22.2	5.8	-61.7
ZB250	694.25	182.2	18.6	181.7	-20.9	2.6	-61.3
ZB251	701.45	192.8	-7.5	182.2	-49.0	12.4	-80.2
ZB252	708.55	171.7	12.7	169.2	-21.8	3.5	-60.2
ZB253	716.25	168.8	8.3	164.1	-24.1	6.3	-59.7
ZB254	724.25	180.5	26.3	183.2	-13.1	3.4	-57.0
ZB255	727.55	187.4	-29.3	152.6	-65.1	9.2	-68.8
ZB256	**731.25**	**221.4**	**-14.8**	**229.7**	**-58.8**	**8.1**	**-52.2**
ZB257	737.65	209.9	21.2	209.9	-23.8	7.4	-52.2
ZB258	741.65	173.0	-4.7	160.0	-37.3	4.0	-64.7
ZB259	745.95	188.3	25.5	189.8	-16.3	1.6	-57.6
ZB260	754.75	203.6	19.9	203.3	-24.6	5.0	-56.4
ZB261	758.85	146.7	-7.0	134.9	-22.3	12.9	-41.4
ZB262	762.45	144.6	28.8	157.6	5.9	10.8	-42.8
ZB263	765.95	173.7	30.7	177.4	-15.3	10.3	-58.2
ZB264	771.35	351.8	27.5	305.9	60.4	11.6	49.5
ZB265	773.35	15.0	-4.6	10.5	46.4	5.3	75.3
ZB266	776.25	321.5	-0.7	312.6	20.1	13.8	38.9
ZB267	781.25	11.5	19.1	349.4	67.7	5.0	76.6
ZB268	**787.75**	**356.5**	**59.9**	**235.2**	**61.6**	**13.4**	**6.2**
ZB269	792.85	324.6	3.6	311.3	25.3	4.8	39.9
ZB270	**798.05**	**273.3**	**86.7**	**208.8**	**36.7**	**36.1**	**-24.3**
ZB271	**802.15**	**124.5**	**8.6**	**127.6**	**-2.1**	**8.3**	**-28.8**
ZB272	**808.05**	**147.6**	**-9.2**	**128.6**	**-31.2**	**3.1**	**-40.2**
ZB273	812.05	145.1	10.3	142.6	-16.2	3.9	-44.3
ZB274	821.05	189.3	22.9	188.7	-27.3	7.0	-63.8
ZB275	823.05	196.5	25.2	196.4	-26.3	14.8	-60.6
ZB276	832.05	171.1	37.9	178.6	-7.9	14.5	-54.4
ZB277	835.95	180.9	3.9	171.4	-42.5	8.5	-73.4
ZB278	838.75	203.7	14.4	203.4	-37.6	7.5	-62.8

ZB279	844.35	187.7	48.5	193.6	-2.1	10.6	-49.6
ZB280	**851.75**	**30.8**	**24.7**	**47.0**	**75.8**	**10.4**	**53.6**
ZB281	854.95	20.4	5.2	16.6	56.9	3.9	76.9
ZB282.5	862.05	180.9	2.4	170.5	-43.9	17.2	-74.1
ZB282	**862.95**	**234.5**	**24.9**	**233.6**	**-21.3**	**7.6**	**-34.8**
ZB282.5A	863.55	215.0	33.0	213.8	-18.4	8.2	-47.5
ZB283	872.95	10.2	-10.2	5.9	39.9	6.1	72.5
ZB283.5	**877.45**	**355.6**	**81.0**	**211.3**	**45.7**	**8.6**	**-17.3**
ZB283.5A	880.05	354.4	-42.8	3.0	4.6	4.4	52.7
ZB284.5	881.65	28.4	5.6	31.3	57.5	8.9	65.7
ZB284.5B	887.85	349.6	3.0	333.5	42.4	3.4	63.2
ZB284.5A	**887.85**	**307.8**	**2.6**	**300.9**	**11.7**	**1.3**	**27.4**
ZB285	889.05	154.9	-5.9	137.2	-34.5	4.7	-47.9
ZB285.5	890.25	353.1	18.6	321.0	56.1	15.6	59.4
ZB285.5A	**890.25**	**321.7**	**-21.9**	**328.6**	**5.7**	**22.1**	**43.6**
ZB286.5A	**893.65**	**323.8**	**41.3**	**270.7**	**43.8**	**4.1**	**16.5**
ZB286.5	**893.65**	**291.5**	**-74.2**	**5.0**	**-37.3**	**14.2**	**29.5**
ZB286.5C	**895.05**	**237.7**	**-1.9**	**252.7**	**-43.1**	**27.0**	**-28.5**
ZB286.5E	895.85	173.8	12.7	168.7	-31.5	5.0	-65.5
ZB286.5F	895.85	190.4	-4.0	180.0	-53.5	10.6	-84.5
ZB286.5D	**895.85**	**212.9**	**-16.1**	**224.8**	**-67.0**	**9.4**	**-57.1**
ZB288.5	911.95	12.6	0.8	5.0	51.1	10.0	81.3
ZB288.5A	**911.95**	**60.1**	**45.8**	**143.1**	**63.0**	**6.8**	**0.3**
ZB289A	**914.25**	**351.3**	**75.2**	**217.7**	**49.7**	**3.3**	**-11.7**
ZB289	914.55	13.7	18.9	354.6	68.5	8.1	77.2
ZB289B	918.35	350.2	-8.3	342.4	33.5	18.0	63.9
ZB290	**921.95**	**348.0**	**46.6**	**265.4**	**61.6**	**4.9**	**22.7**
ZB290A	922.45	31.3	-7.9	33.7	43.7	5.8	58.6
ZB291	927.65	2.6	7.4	345.8	53.3	3.3	77.3
ZB292	931.65	9.4	-15.8	6.8	34.2	7.8	68.5
ZB295	**942.05**	**142.9**	**-11.7**	**123.0**	**-29.1**	**10.5**	**-35.1**

ZB290B	946.45	349.4	-13.0	344.5	29.1	7.6	62.5
ZB296	**947.15**	**348.9**	**62.4**	**235.3**	**57.2**	**8.2**	**2.5**
ZB297	950.45	20.5	7.3	16.3	59.0	6.7	77.5
ZB291A	**955.85**	**241.3**	**24.1**	**239.9**	**-19.2**	**12.9**	**-29.4**
ZB298	957.75	27.3	-16.9	27.7	35.1	2.3	58.8
ZB292A	959.25	347.9	-27.0	350.9	16.3	6.1	57.8
ZB292B	961.45	351.4	-1.5	338.9	39.8	5.6	65.4
ZB300A	963.15	348.0	-2.0	335.8	37.4	3.0	62.2
ZB300	965.35	356.8	7.2	338.2	50.0	3.8	70.2
ZB302A	970.15	212.0	42.1	210.3	-9.6	5.4	-45.8
ZB302B	**970.15**	**231.3**	**37.9**	**225.8**	**-10.3**	**15.0**	**-36.4**
ZB301	**971.55**	**108.1**	**-28.8**	**87.9**	**-12.3**	**21.0**	**-2.3**
ZB302	**975.55**	**174.2**	**60.5**	**190.1**	**11.7**	**24.2**	**-43.6**
ZB303	979.75	204.9	28.7	204.9	-23.3	11.5	-54.9
ZB303A	**980.55**	**248.4**	**-55.7**	**340.9**	**-56.2**	**11.3**	**11.7**
ZB303B	983.15	176.8	15.8	173.3	-30.0	4.6	-65.9
ZB304	983.75	196.6	2.8	192.3	-48.5	6.7	-75.8
ZB305	986.55	192.1	-2.6	183.4	-52.7	5.9	-83.2
ZB304A	**988.55**	**217.3**	**-30.7**	**262.9**	**-77.5**	**4.9**	**-38.3**
ZB304B	991.55	199.2	13.4	197.8	-38.3	3.9	-66.5
ZB306	991.75	175.6	3.1	164.7	-40.7	11.8	-69.2
ZB307	998.05	131.6	42.2	157.9	14.3	6.5	-39.0
ZB308	1004.65	190.5	-6.2	178.9	-55.6	3.1	-86.5
ZB309	1008.85	184.8	20.9	183.5	-28.1	5.3	-65.3
ZB310	1012.85	181.8	8.4	175.0	-38.8	6.8	-71.9
ZB311	1017.55	186.2	25.1	186.3	-24.5	7.3	-62.8
ZB312	1025.85	190.6	0.8	182.7	-49.0	9.8	-80.2
ZB313	1030.15	191.6	46.4	195.8	-4.7	4.9	-50.2
ZB314	1036.85	199.1	9.0	197.1	-42.7	12.1	-69.4
ZB315	1041.05	166.3	12.0	161.0	-28.3	5.2	-60.4
ZB316	1046.85	174.3	-3.6	158.2	-45.6	14.0	-68.0

ZB317	**1050.15**	**22.0**	**-72.0**	**24.0**	**-20.0**	**19.7**	**35.4**
ZB318	**1054.25**	**156.6**	**-20.6**	**123.6**	**-44.9**	**14.7**	**-41.7**
ZB319A	**1057.25**	**152.8**	**-16.9**	**124.9**	**-39.9**	**6.1**	**-40.7**
ZB319	**1057.95**	**206.1**	**-23.8**	**209.1**	**-75.8**	**11.3**	**-60.7**
ZB320A	1063.55	187.5	3.6	179.7	-45.3	6.5	-77.3
ZB320	1064.15	182.0	-9.3	163.2	-54.6	2.7	-76.0
ZB321	1070.45	184.7	15.4	181.4	-33.3	11.7	-68.6
ZB322	**1075.05**	**310.7**	**-11.5**	**313.8**	**4.9**	**26.7**	**34.1**
ZB323	1079.05	186.5	-6.8	172.1	-54.6	12.3	-82.4
ZB323A	1079.45	146.5	10.5	143.7	-17.0	10.9	-45.3
ZB324	**1082.85**	**99.2**	**30.4**	**132.0**	**29.8**	**24.0**	**-18.7**
ZB324A	1083.85	181.6	6.3	173.7	-40.6	9.2	-72.8
ZB324B	1083.85	191.6	-8.9	179.0	-58.5	15.9	-89.2
ZB325	**1086.45**	**255.0**	**-8.9**	**275.4**	**-36.6**	**15.2**	**-8.8**
ZB326	**1089.35**	**277.5**	**75.6**	**221.3**	**32.5**	**14.5**	**-21.1**
ZB327	**1095.55**	**3.6**	**33.8**	**302.1**	**72.2**	**5.4**	**49.2**
ZB328	**1099.75**	**321.4**	**44.0**	**266.5**	**42.8**	**5.2**	**13.0**
ZB329	1104.45	210.9	37.9	209.8	-13.9	5.6	-48.0
ZB330	**1108.25**	**22.0**	**73.8**	**206.4**	**54.2**	**10.9**	**-11.9**
ZB330A	1109.25	204.9	-7.2	204.8	-59.2	23.4	-71.0
ZB330B	1109.25	204.0	-7.2	203.1	-59.2	9.9	-72.3
ZB331	**1113.65**	**241.5**	**-26.6**	**285.4**	**-57.4**	**29.6**	**-13.3**
ZB332	1120.45	177.2	20.5	175.9	-25.9	19.0	-63.9
ZB333A	1125.55	154.7	24.6	159.4	-11.6	9.4	-51.6
ZB333	**1125.85**	**298.4**	**40.8**	**262.2**	**26.0**	**8.1**	**2.8**
ZB334	**1132.05**	**348.0**	**71.7**	**222.7**	**51.5**	**5.3**	**-8.1**
ZB335	**1135.55**	**154.0**	**75.6**	**192.3**	**28.2**	**22.9**	**-34.3**
ZB335A	**1136.05**	**258.6**	**43.7**	**240.7**	**5.0**	**4.2**	**-20.5**
ZB336	**1145.45**	**130.5**	**60.6**	**173.3**	**25.7**	**14.1**	**-36.6**
ZB336A	1149.85	172.0	-0.5	158.1	-41.8	9.6	-66.0
ZB337	1150.75	345.4	-45.7	358.6	-0.9	17.9	50.0

ZB338	**1152.75**	**23.7**	**53.0**	**208.0**	**75.0**	**7.0**	**13.8**
ZB338A	1153.15	188.4	11.6	184.2	-38.0	3.5	-71.5
ZB339	**1156.65**	**313.0**	**39.4**	**269.3**	**35.4**	**26.8**	**11.8**
ZB339B	1159.05	149.8	5.0	142.1	-23.2	3.6	-46.8
ZB339A	1159.05	182.4	6.2	174.6	-41.1	2.8	-73.4
ZB340	**1160.25**	**342.9**	**51.1**	**257.2**	**57.8**	**4.5**	**15.2**
ZB341	1162.05	7.2	-34.3	9.8	15.8	8.0	57.3
ZB342	**1174.85**	**315.6**	**13.4**	**296.8**	**24.4**	**3.7**	**28.7**
ZB343	1181.05	351.7	-16.6	348.8	27.1	2.6	63.0
ZB343A	1181.05	338.2	-13.1	334.7	22.7	4.6	54.4
ZB344	**1191.65**	**158.4**	**-19.8**	**125.9**	**-45.9**	**10.0**	**-43.9**
ZB345	1200.25	184.9	20.4	184.2	-31.2	20.3	-67.1
ZB346A	1214.45	334.3	0.0	320.5	38.6	7.0	52.1
ZB346	**1214.45**	**346.7**	**7.4**	**328.7**	**51.8**	**7.1**	**63.8**
ZB347	1219.85	310.8	-11.3	309.4	14.6	29.2	34.6
ZB347A	**1219.85**	**307.3**	**-13.3**	**308.4**	**10.7**	**14.6**	**32.5**
ZB348	1229.25	354.4	-2.9	346.2	46.0	14.0	73.3
ZB348A	1229.25	27.3	5.6	39.1	54.7	12.6	58.9
ZB349	1238.65	359.6	-24.4	359.4	26.5	11.6	64.5
ZB349A	1238.65	21.9	10.1	32.2	60.7	6.8	65.6
ZB350	1244.85	187.9	28.2	188.1	-23.7	20.4	-61.9
ZB350A	**1244.85**	**146.2**	**-23.2**	**109.3**	**-48.4**	**17.5**	**-32.3**
ZB351	1248.45	156.8	10.0	150.1	-31.8	23.7	-55.8
ZB352	1264.70	190.7	-13.7	188.9	-65.7	4.5	-79.4
ZB353A	**1269.55**	**220.9**	**-11.4**	**243.8**	**-52.9**	**5.7**	**-39.4**
ZB353	**1269.55**	**259.2**	**-34.2**	**299.9**	**-36.8**	**12.0**	**7.9**
ZB354	1274.85	182.8	30.2	183.5	-21.3	14.8	-61.4
ZB354A	1276.30	175.2	23.1	174.7	-26.9	3.9	-64.3
ZB354.5	1280.85	172.8	11.0	167.9	-37.8	5.5	-69.0
ZB356	1289.65	353.2	3.4	341.0	51.4	14.3	72.9
ZB357A	1297.65	358.4	-10.4	354.4	40.0	8.0	72.6

ZB357	**1297.65**	**343.2**	**30.7**	**290.5**	**65.2**	**8.6**	**40.6**
ZB358	1302.35	355.6	4.5	343.9	53.3	8.0	75.9
ZB358A	1302.35	352.2	-8.6	346.1	39.9	8.9	69.5
ZB359A	1307.05	10.7	2.7	9.8	54.7	7.9	81.1
ZB359	1307.05	1.0	-17.7	359.4	33.3	7.1	68.7
ZB360A	1310.05	345.9	-6.8	337.8	39.0	4.5	64.3
ZB360	1310.05	337.1	-12.5	331.9	29.8	13.0	56.0
ZB361A	**1316.25**	**55.3**	**36.1**	**112.5**	**55.7**	**13.3**	**7.9**
ZB362	**1318.05**	**359.1**	**27.9**	**321.3**	**75.2**	**10.9**	**57.5**
ZB363A	1323.05	5.8	-29.5	6.2	22.3	9.1	61.6
ZB363	**1323.05**	**307.7**	**-6.4**	**303.5**	**15.7**	**9.5**	**30.7**
ZB364	1328.45	24.6	15.0	41.2	64.4	6.7	59.4
ZB364A	**1328.45**	**48.8**	**-13.3**	**53.4**	**28.2**	**14.0**	**37.5**
ZB365	1335.85	342.6	2.9	327.3	45.8	1.8	60.3
ZB365A	**1335.85**	**326.7**	**12.5**	**302.0**	**42.4**	**5.8**	**39.5**
ZB365.5	1337.25	13.3	23.8	16.8	75.8	16.5	64.3
ZB367	1347.65	321.3	-1.2	309.7	29.1	5.8	40.2
ZB368	1351.85	351.8	-5.4	344.1	42.7	12.8	70.1
ZB368A	1351.85	338.4	-17.8	336.1	25.9	9.7	56.7
ZB369A	1357.65	21.2	-40.9	19.1	10.7	4.1	51.8
ZB369	1357.65	24.1	-2.1	30.4	48.4	13.9	63.1
ZB370	1357.85	2.3	1.8	355.9	52.7	14.9	83.0
ZB370A	1359.45	343.5	22.3	306.5	61.0	9.7	50.1
ZB371	1365.25	352.3	2.5	340.3	50.2	7.9	71.8
ZB372	1371.00	1.6	10.0	350.8	60.5	8.7	82.7
ZB373	**1372.45**	**324.4**	**33.2**	**274.2**	**51.4**	**13.8**	**22.7**
ZB374	1375.45	353.4	22.8	320.3	68.0	10.3	60.2
ZB375	**1381.45**	**26.9**	**23.8**	**58.1**	**70.9**	**6.4**	**49.0**
ZB376	1387.45	182.0	32.4	183.1	-19.0	3.4	-60.1
ZB377	1391.05	190.6	33.3	190.8	-18.7	5.8	-58.6
ZB378	1398.05	182.8	17.5	181.4	-33.8	7.3	-69.0

ZB380	**1406.65**	**40.4**	**20.8**	**75.0**	**60.1**	**4.6**	**34.6**
ZB382A	1422.05	326.3	-11.2	321.3	24.9	23.9	46.9
ZB382	**1422.05**	**239.1**	**25.4**	**234.7**	**-12.7**	**2.9**	**-31.0**
ZB383	1432.25	325.2	-9.9	319.5	25.2	3.6	45.8
ZB384	1437.65	22.4	-7.7	26.2	43.3	11.1	63.8
ZB385	1445.05	5.2	8.7	358.4	60.1	12.7	88.1
ZB386	1448.85	11.0	-13.7	10.8	38.3	8.3	69.8
ZB387	1455.85	349.5	-18.2	347.2	30.0	10.2	64.1
ZB388	**1459.25**	**15.0**	**57.0**	**187.0**	**70.9**	**15.7**	**5.0**
ZB389	1465.25	346.2	-17.1	343.4	29.8	5.6	62.4
ZB390	1470.65	350.4	-3.0	341.0	44.4	6.5	69.2
ZB391	1471.85	337.2	-17.2	334.7	25.9	4.8	55.9
ZB392	1477.25	354.8	-9.3	349.6	40.0	8.3	71.1
ZB393	1480.25	6.1	-3.4	3.1	48.2	4.1	79.4
ZB394	1485.25	343.6	1.4	329.7	45.1	11.0	61.7
ZB395	**1489.41**	**313.6**	**0.3**	**302.5**	**24.6**	**8.4**	**33.1**
ZB396	**1494.45**	**327.2**	**16.7**	**297.9**	**45.4**	**6.3**	**37.6**
ZB397	1501.05	21.5	2.2	28.0	53.2	10.6	66.9
ZB398	**1505.05**	**249.7**	**39.7**	**232.7**	**4.0**	**19.6**	**-26.4**
ZB399	**1513.65**	**78.6**	**-9.3**	**79.9**	**12.1**	**3.1**	**11.7**
ZB400	**1518.80**	**289.9**	**3.4**	**284.2**	**8.3**	**7.2**	**13.6**
ZB401	1531.45	160.9	1.2	148.5	-41.4	12.1	-59.2
ZB401A	1531.45	164.3	2.6	153.3	-42.0	10.6	-62.8
ZB402A	1538.45	182.5	-1.9	176.1	-52.9	8.9	-83.2
ZB402	1538.45	174.5	19.2	172.8	-30.5	23.2	-66.1
ZB404	1559.45	5.5	-11.7	3.7	39.9	27.4	72.9
ZB404.5	1560.73	351.6	4.0	338.3	51.2	14.8	70.9
ZB405	1566.60	355.3	-3.6	347.8	45.6	8.7	73.9
ZB405A	1566.60	348.5	-14.6	344.6	33.0	14.5	64.7
ZB406	1573.85	332.1	-8.6	324.7	30.4	7.9	51.6
ZB408	**1583.21**	**36.4**	**-25.2**	**35.9**	**22.8**	**13.7**	**47.9**

ZB409	1587.65	347.1	17.1	318.9	59.8	8.9	58.8
ZB410	1594.75	326.7	-19.5	327.1	18.5	5.3	48.1
ZB411	1601.85	328.2	0.3	314.5	34.9	11.3	46.1
ZB412	**1608.25**	**18.4**	**52.7**	**177.2**	**74.6**	**12.0**	**10.7**
ZB413	1615.65	2.8	-5.3	358.8	45.9	13.0	77.8
ZB414	**1624.25**	**185.2**	**-34.8**	**130.3**	**-83.7**	**7.4**	**-46.8**
ZB415	1629.93	11.5	-24.8	11.5	27.2	19.5	63.0
ZB416	1632.65	314.6	-25.1	321.8	7.1	10.6	40.1
ZB417A	1636.05	4.0	-20.5	3.3	31.0	14.9	67.0
ZB417	1636.05	6.8	-22.2	6.5	29.6	7.4	65.7
ZB418	**1640.13**	**130.6**	**15.6**	**132.4**	**-11.4**	**10.4**	**-35.6**
ZB419	1645.25	196.3	4.7	198.3	-47.1	13.5	-71.2
ZB421	1658.25	27.0	-24.0	27.3	26.4	5.9	55.0
ZB422	1666.65	348.1	-14.5	344.1	32.9	14.6	64.4
ZB423	1672.05	5.6	-19.1	4.8	32.6	12.8	67.8
ZB424	1679.25	171.5	22.1	170.7	-26.9	12.5	-63.4
ZB425	1691.05	350.9	-17.0	348.2	31.5	5.7	65.3
ZB425A	**1691.05**	**214.4**	**11.9**	**219.4**	**-35.9**	**34.6**	**-51.0**
ZB426	**1700.85**	**31.6**	**31.2**	**85.0**	**72.5**	**15.9**	**35.0**
ZB426A	**1700.85**	**275.1**	**-42.8**	**315.4**	**-29.2**	**10.9**	**21.0**